Combustion characteristics of coal, biomass and their chars in air and oxy-fuel environments

Benjamin Dooley

Submitted in accordance with the requirements for the degree of Doctor of Philosophy as part of the integrated PhD with MSc in Low Carbon Technologies

Doctoral Training Centre in Low Carbon technologies, Energy Research Institute, School of Chemical and Process Engineering,

The University of Leeds

March 2017

"Insanity is doing something over and over again and expecting a different result"

Albert Einstein

The candidate confirms that the work submitted is his own and that appropriate credit has been given where reference has been made to the work of others.

Acknowledgements

Firstly I would like to thank my supervisors, Professor Jenny Jones, Dr Leilani Darvell, Professor Alan Williams and Professor Mohamed Pourkashanian for their support, guidance and patience throughout the last four years. Without them, and in particular Jenny and Leilani, I would not have undertaken a PhD.

I would also like to thank the Bio Cap UK team for their support throughout the project – Dr Karen Finney, Dr János Szuhánszki, Dr Hannah Chalmers, Dr Jim Swithenbank, Professor Patricia Thornley and the research hubs Supergen and the UKCCSRC.

My research group have been a tremendous source of advice, thanks to Dr Abby Samson, Dr Patrick Mason, Dr Bijal Gudka, Dr Femi Akinrinola, Dr. Eddy Mitchell, Douglas Phillips, Yee-Sing Chin, Dr Farooq Abubakar Atiku, Peinong Xing, Diarmaid Clery and especially Dr Paula McNamee for her friendship throughout the PhD.

I must also thank members of staff at the University of Leeds – Susanne Patel, Dr. Adrian Cunliffe, Karen Alves Thorne, James Mckay, Emily Bryan-Kinns, David Haynes, Simon Lloyd, Dr Patrick Biller and Ed Woodhouse and all of the academic staff for their continual advice and support during my time at Leeds.

The student cohorts in the low carbon technology and bioenergy doctoral training centres have been a continual welcome distraction and source of support, in particular, Dr Jamie Bright, Dr Dave Allen, Dr Josh Cottom, Dr Stephen Chilton, Dr Harriet Fletcher, Dr Lloyd Davies, Dr Morgan Thatchell-Evans, Laura Campbell, Dr Ray Edmunds, Dr Ramzi Cherad, Dr Ruth Bush, Dr David Jacques, Dr Richard Riley, Dr Andy Dixon, Dr Thom Best, Dr Zarashpe Kapadia, Dr Joel Millward-Hopkins, Arthur Goodland, Hana Mandová and Jo Robinson. In addition I am grateful for the support shown by friends outside of the energy building including Dr Laura Sellers, Dr Radka Jersákova and Dr Rebecca Sheridan, Neil O'Malley and Dr Marianne Mugabo.

Thanks to the Engineering and Physical Science research council (ESPRC) for my studentship and members of the Supergen and UKCCSRC I have worked with throughout my studies.

Finally, I would like to express deepest gratitude to my family, my mum Kate, my stepdad Ant, my sisters Emma and Jess, my brother Sam and my nieces and nephew Faye, Violet and Liam and the dogs, Beck and Bella for giving me a reason to walk up a big hill and get away from my work.

Abstract

Carbon capture and storage (CCS) is expected to play an important role in mitigating the effects of climate change. The focus of this work is to determine how the change of combustion environment in an oxy-fuel CCS plant affects the combustion behaviour of coal, biomass and a torrefied biomass. The industrially relevant fuels selected were analysed to determine their fundamental composition and combusted in air and a range of oxy-fuel environments (5-30% O_2/CO_2) using a thermogravimetric analyser (TGA). The key temperatures and kinetic parameters of both the devolatilisation and char combustion stages were investigated to determine how the shift to an oxy-fuel combustion environment effects overall combustion behaviour.

The changes in devolatilisation behaviour were determined through the derivation of apparent first order kinetics and no noticeable difference between combustion in air and 21% O_2/CO_2 atmospheres were observed. The increase in oxygen concentration in the oxy-fuel environments resulted in linear increases in kinetic parameters which were then used to develop fuel specific empirical equations that relate the devolatilisation rate to the oxygen concentration. The devolatilisation of the biomass fuels were shown to be more sensitive to the change in combustion atmosphere than the coals.

Chars were produced using ballistic heating rates in a TGA (1000 K min^{-1}) and it was found that the coals exhibited similar mass loss behaviour in N_2 and CO_2 environments during char production. The biomass and torrefied biomass samples showed enhanced devolatilisation in CO_2 atmospheres which leads to differences in the char combustion behaviour between the coal and biomass fuels. The char combustion behaviour was determined through the determination of apparent m^{th} order kinetics, from which, fuel specific n^{th} order kinetic models were derived to describe char combustion accurately over the full range of oxy-fuel combustion atmospheres. The kinetic parameters determined highlighted the similarity between the N_2 and CO_2 produced coal chars and the difference between the biomass chars. The coal chars were found to be more sensitive to the change in combustion atmosphere.

The work in this thesis gives a good understanding of the differences between conventional air and oxy-fuel combustion atmospheres using industrially relevant fuels. Several useful kinetic models have been derived for both the devolatilisation and char combustion stages that lend themselves to computational fluid dynamics and process optimisation while the fundamental characterisation lends itself to life cycle analysis of CCS systems.

Table of Contents

List of Tables

List of Figures

Abbreviations and nomenclature

Abbreviations

A	Ash
ad	As determined
AFOLU	Agriculture Forestry and Other Land Use
ASA	Active Surface Area
ASU	Air Separation Unit
BECCS	Bio-energy Carbon Capture and Storage
BEIS	Department of Business, Energy and Industrial Strategy
BET	Brunauer- Emmett-Teller
BIGCC	Biomass Integrated Combined Cycle
CaL	Calcium Looping Technology
CCC	Committee on Climate Change
CCGT	Combined Cycle Gas Turbines
CCS	Carbon Capture and Storage
CDR	Carbon Dioxide Removal
CFB	Circulating Fluidised Bed
CfDs	Contracts for Difference
CLC	Chemical Looping Combustion
CLD	Chemoluminesence Detector
CO_{2eq}	Carbon dioxide equivalent
CPU	Compression and Purification Unit
db	Dry Basis
daf	Dry Ash Free
DEA	Diethanolamines
DECC	Department of Energy and Climate Change
DFT	Density Function Theory
DTG	Differential Thermogravimetric Curves
DTR	Drop Tube Reactor

ECCC	House of Commons Energy and Climate Change Committee
EMR	Electricity Market Reform
EOR	Enhanced Oil Recovery
ETI	Energy Technologies Institute
EU	European Union
EUTR	Eurpoean Timber Regulation
FBR	Fixed Bed Reactor
FC	Fixed Carbon
FGD	Flue Gas Desulphurisation
GHG	Greenhouse Gas
Gt	Giga tonnes
GW	Gigawatt
HGI	Hardgrove Grindability Index
HHV	High Heating Value
IAS	International Aviation and Shipping
IEA	International Energy Agency
IEAGHG	International Energy Agency Greenhouse Gas R and D Programme
IGCC	Integrated Gasification Combined Cycle
INDC	Intended National Determined Contributions
LCA	Life Cycle Assessment
LCPD	Large Combustion Plant Directive
M	Moisture
MEA	Monoethanolamine
Mt	Mega tonnes
MtO_e	Million Tonnes of Oil Equivalent
MWh	Megawatt Hour
OFC	Oxy-fuel Combustion
OFGEM	Office for Gas and Energy Market
PACT	Pilot Scale Advanced Capture Technology Facilities
PC	Pulverised Coal

PID	Proportional, Integral, Derivative
RO	Renewable Obligation
ROCs	Renewable Obligation Certificates
TGA	Thermogravimetric Analyser
TR	Tubular Furnace
SEM	Scanning Electron Microscopy
UK	United Kingdom
UNFCCC	United Nations Framework on Climate Change Committee
V	Volatile
VTF	Vertical Tube Furnace

Symbols

%RE	Relative error	(%)
a	Radius of particle	(m)
A	Pre exponential factor	(s^{-1})
A_{app}	Char apparent pre exponential factor	(s^{-1})
A_{BET}	Surface area	($m^2\ g^{-1}$)
A_E	Absolute error in ash	(wt%)
A_I	Char intrinsic pre exponential factor	($s^{-1}\ Pa^{-n}$)
a_m	Cross sectional area of a nitrogen molecule	(0.162 nm^2 @ 77 K)
A_n	Char n^{th} order pre exponential factor	($s^{-1}\ Pa^{-1}$)
A_O	Area of a single oxygen atom	(0.83 nm^2)
A_s	Particle surface area	(m^2)
ASA	Active surface area	($m^2\ g^{-1}$)
Bi	Biot number	
C	A constant that is dependent on the isotherm shape	-
C,H,N,S_{AE}	Absolute error in chemical analysis	(wt%)
Cp	Specific heat capacity	($W\ m^{-1}\ K^1$)
D	Particle diameter	(m)
D_g	Diffusion coefficient of O_2 in CO_2	($m^2\ s^{-1}$)
dm/dt_P	The maximum rate of mass loss at T_P	(wt % s^{-1})
dm/dt_V	The maximum rate of mass loss associated with the release of volatiles in the biomass fuels	(wt % s^{-1})
Ea	Activation energy	($kJ\ mol^{-1}$)
Ea_{app}	Char apparent activation energy	($kJ\ mol^{-1}$)

Ea_n	Char n^{th} order activation energy	(kJ mol^{-1})
E_x	Absolute error in relation to x	(wt%)
$_{exp}$	Experimental data	-
FC_E	Absolute error in fixed carbon	(wt%)
h	Heat transfer coefficient	(W m^{-2} K^{-1})
HGI_{Eq}	Hardgroves equivalent	-
HHV	Higher Heating Value	(MJ kg^{-1})
k	Rate constant	(s^{-1})
k_g	Mass transfer coefficient	(m s^{-1})
L	Avogadros constant	(6.022 x 10^{23} mol^{-1})
m	Initial mass of sample	(mg)
^{m}	Reaction order with respect to char conversion	-
m_1	Mass of sample passing through a 75µm sieve (HGI_{Eq})	(g)
m_2	Mass of sample collected on a 75µm sieve (HGI_{Eq})	(g)
m_∞	Terminal mass of sample	(mg)
M_E	Standard error in moisture	(wt%)
m_O	Mass gain related to low temperature oxygen chemisorption	(g)
m_v	Mass of 50 cm^3 of sample (HGI_{Eq})	(g)
M_{Wo}	Molecular weight of oxygen	(16 g mol^{-1})
n	Number of samples	-
^{n}	Reaction order with respect to oxygen	-
n_a	The amount adsorbed at the relative pressure p/p_o	(mL)
n_m	Monolayer capacity of the adsorbent	(mL)
Nu	Nusselt number	
O_{AE}	Absolute error in oxygen determination	(wt%)
P	Partial vapour pressure of the adsorbate gas	(Pa)
P_1	Ash in fuel (db)	(wt%)
P_2	Ash in char (db)	(wt%)
P_o	Saturation pressure of the adsorbate gas	(Pa)
P_{O2}	Partial pressure of oxygen	(Pa)
Pr	Prandtl number	(0.71)
$_{pre}$	Predicted data	-
R	Gas constant	(8314 kJ mol^{-1} K^{-1})
R_{app}	Char apparent reaction rate constant	(s^{-1})
Re	Reynolds number	
R_i	Intrinsic reactivity constant	(g m^{-2} s^{-1})/ (kg m^{-2} s^{-1})
R_n	Char n^{th} order reaction rate constant	(s^{-1})

ro_2	Mass transfer rate of oxygen	(mol s^{-1})
S	Char surface area	(m^2 g^{-1})
s	Standard deviation	-
Sh	Sherwood number	-
T	Temperature	(K)
t	Time	(s)
T_B	Burnout temperature defined as the point at which the mass loss rate slows to 1 wt% min^{-1}	(^oC)
T_C	The temperature at which the maximum rate of char combustion is seen in the biomass fuels	(^oC)
T_{Chem}	Temperature at which the maximum mass gain due to chemisorption of oxygen is seen in the coals	(^oC)
T_{IM}	Temperature at which the rate of mass loss reached (1 wt% min^{-1})	(^oC)
T_g	Gas temperature	(K)
T_{part}	Particle temperature	(K)
T_P	Temperature at which the maximum rate of mass loss was seen in coals	(^oC)
T_V	The temperature at which the maximum rate of volatile release is seen in the biomass fuels	(^oC)
T_w	Furnace wall temperature	(K)
u	Gas velocity	(m s^{-1})
V_E	Absolute error in volatile	(wt%)
w	Initial mass of char sample	(mg)
x	Fractional conversion	-
Y_c	Component x in the char (db)	(wt%)
Y_{char}	Char yield (db)	(wt%)
Y_f	Component x in fuel (db)	(wt%)
Y_x	Component x (db)	(wt%)
ΔW	Change in weight	(wt%)
ε	Emissivity of particle	(0.85)
σ	Stefan-Boltzmann constant	(5.67 x 10^{-8} W m^{-2} K^{-4})
κ	Thermal diffusivity	(m^2 s^{-1})
ρ	Density	(kg m^{-3})
$\tau_{heatint}$	Internal thermal conduction	(s^{-1})
$\tau_{heatint}$	External thermal conduction	(s^{-1})
ν	Kinematic viscosity	(m^2 s^{-1})
λ_s	Thermal conductivity fuel	(W m^{-1} K^{-1})
λ_s	Thermal conductivity gas	(W m^{-1} K^{-1})
$[O_2]_g$	Concentration of oxygen in combustion atmosphere	(mol m^{-3})
$[O_2]_p$	Concentration of oxygen at particle surface	(mol m^{-3})

Outline of thesis

Chapter 1 starts with a brief introduction to UK climate change policy and a discussion focusing on both UK and global emissions by sector. The Paris agreement, that is the agreement between 195 parties to reduce emissions, and the potential gap between the agreed emissions reductions and the levels needed for an average temperature rise of 2^{o}C are discussed. Two energy technologies and their potential for emissions reduction are introduced; the first, bioenergy and its role in the UK, the second, carbon capture and storage with coal and/or biomass combustion for energy production. As carbon capture and storage is a new technology, an overview of the technology options associated with each stage of the CCS process is given along with a more in depth assessment of a pulverised oxy-fuel plant. A review of the CCS plants currently in operation and plants that are planned for deployment in the 2020s is also given. This chapter finishes with a summary of several UK governmental departments calls for action and suggestions to what the UK government should do to implement the key emissions reduction technology of CCS.

Chapter 2 outlines the aims and objectives of the thesis.

Chapter 3 is a literature review giving an introduction to coal, biomass, torrefied biomass. A description of the general combustion process of solid fuels is given and differences between coal and biomass during the multiple stages of combustion are highlighted. The factors effecting each stage of solid fuel combustion, drying, devolatilisation and char combustion and the difference between air and oxy-fuel combustion is introduced. An introduction to reactivity of the fuels and the methods and description of reactivity during devolatilisation and char combustion stages are given. The fate of nitrogen present in the fuel and the different mechanisms in the formation of NO_x and the difference between air and oxy-fuel combustion is also introduced.

Chapter 4 provides a description of the methodology used in the experiments and analysis of results seen in this work. A description of the fuels, the reasoning for their selection and the fuel IDs is provided. In addition a description of the char production methodologies is given. At the end of the chapter an overview of which experiments were performed on each of the fuels and their chars derived is provided.

Chapter 5 focuses on the fundamental characteristics of the fuels and their chars. Proximate and ultimate analysis were performed on both the fuels and their chars and the change in char characteristics (yield, composition, surface area, morphology) as a result of char production atmosphere and methodology discussed. The effect of char production

atmosphere and production method on the nitrogen partitioning and its potential effect on NO_x emissions are discussed. The oxygen demand in the TGA and the particle heating rates in the TGA in CO_2 and N_2 atmospheres and in N_2 in DTR are estimated. Finally the milling trials of the TSP sample are presented to try and determine the degree of torrefaction that the raw spruce experienced. The particle heating rates of a coal and biomass particle are estimated in both the TGA and DTR.

Chapter 6 focuses on the overall combustion and pyrolysis behaviour of the raw fuels in air and oxy-fuel environments using a thermogravimetric analyser. The mass transfer rates of oxygen in a selection of the oxy-fuel combustion atmospheres are compared to the oxygen consumption rates are compared to ensure chemical control. The apparent first order devolatilisation kinetics are determined in the full range of combustion and pyrolysis atmospheres. In addition fuel specific models are developed to describe fuel devolatilsation reaction rates as a function of oxygen concentration for use in CFD models.

Chapter 7 focuses on the combustion behaviour of chars produced at ballistic heating rates using a TGA and combusted in air and the full range of oxy-fuel environments. Several reactivity models are used to describe char reactivity; firstly an m^{th} order reactivity model is used to determine the apparent reactivity and kinetic parameters of all chars. Secondly an n^{th} order model is developed to describe the combustion of all chars in oxy-fuel environments only. Finally the intrinsic reactivity of the coal chars produced in N_2 and combusted in air and chars produced in CO_2 and combusted in the full range of oxy-fuel environments is determined.

Chapter 8 investigates the difference in char combustion behaviour as a result of char production technique. The chars of a biomass fuel and a single coal are produced using a thermogravimetric analyser, at ballistic heating rates ($1000^oC\ min^{-1}$) and a drop tube reactor at high heating rates (10^4-$10^5\ ^oC\ min^{-1}$) in a nitrogen atmosphere. The chars are analysed based on the combustion behaviour in air, apparent kinetics and in the case of the coal chars their intrinsic reactivity.

Chapter 9 addresses the research questions identified in chapter 2.

Chapter 10 outlines the potential future research that is required to further understand the combustion of solid fuels in oxy-fuel environments.

1 Introduction

"Human influence on the climate system is clear and growing, with impacts observed across all continents and oceans. Many of the observed changes since the 1950's are unprecedented over decades to millennia"(1).

1.1 Climate change policy

It is widely accepted throughout the scientific community that the climate is changing as the result of anthropogenic emissions (2). This acceptance has spread to political leaders with 195 parties adopting the first ever universal, legally binding global climate deal in Paris at the COP21 climate conference. The Paris agreement aims to keep the global averaged temperature increase below 2^{o}C by the end of the century compared to pre-industrial levels, and if possible to no more than a 1.5^{o}C rise through the reduction in global emissions (3). Although the Paris agreement has not been ratified by all of the 195 parties, it came into force on the 4th November 2016 as countries responsible for 55% of emissions had already ratified the agreement (4). The participating parties submitted an Intended Nationally Determined Contributions (INDC) which outlined how each signatory is planning to meet the emission reduction targets. At this point in time the UK is still part of the EU and as a result must follow the INDC as outlined by the European Union which aims for at least a 40% reduction in greenhouse gas emissions by 2030 relative to levels seen in 1990.

1.1.1 UK climate change policy

The UK's main driver for emissions reduction is the 2008 Climate Change act that aims to reduce emissions by at least 34% by 2020 and 80% by 2050 relative to those levels seen in 1990. In addition to the UK targets, the EU has stated that 15% of the UK's energy should be sourced from renewable technologies by 2020 (5). The UK climate change act already exceeds the emissions reduction targets agreed upon in Paris and as a result the Committee on climate change (CCC), an independent statutory body, suggested that no further emission reduction commitments are required (6). To meet the targets outlined in the Climate Change act the UK Government implemented the Carbon Plan which sets 5 yearly carbon budgets to progressively reduce emissions up to 2050. The first five carbon budgets are now set in law covering UK emissions from 2008-2032 where a 57% reduction is expected by 2030 (significantly higher than the 40% agreed on in Paris). The emissions levels for the first two

carbon budgets (2008-2012 and 2013-2017) and the future targets of the next three carbon budgets can be seen in Figure 1.1 and Table 1.1.

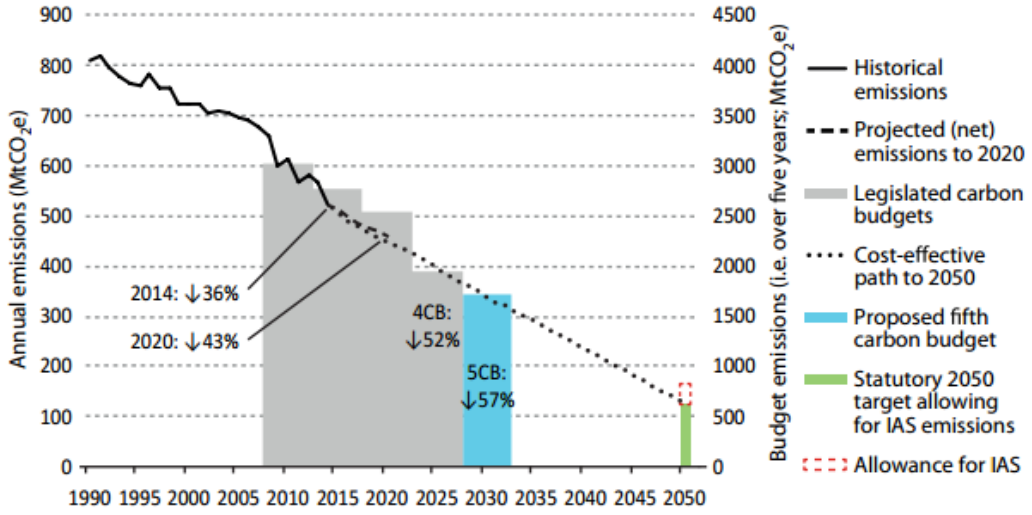

Figure 1.1: UK carbon budgets and projected emissions (IAS – international aviation and shipping) (7)

Table 1.1: Carbon budget levels covering 2008-2032

Budget	Carbon budget level (Mt CO_{2eq})	% Reduction below 1990
1st (2008-2012)	3018	23
2nd (2013-2017)	2782	29
3rd (2018-2022)	2544	35 by 2020
4th (2023-2027)	1950	50 by 2025
5th (2028-2032)	1725	57 by 2030

The UK was able to meet the first of the carbon budgets with emissions of carbon totalling 2,982 Mt CO_{2eq}, a reduction of 23.6% relative to the 1990 levels (8) and significant progress is being made towards meeting the second and third carbon budgets (9). The main driver in meeting the first three carbon budgets has been the reduction of emissions in the power sector (10). Progress towards the fourth and fifth carbon budget (post 2032) is expected to slow under existing UK policy with 10% excess expected in the fourth carbon budget period (9), and only half of the required emission reductions expected during the fifth carbon budget period (11). In response to the realisation of the shortfall in meeting emissions targets the Committee on Climate Change (CCC) set out a number of recommendations to Parliament through the carbon budget progress reports, issued at the end of each year. The

recommendations are split over several sectors; (i) power, (ii) buildings, (iii) industry, (iv) domestic transport, (v) agriculture, land use, land-use change and forestry, (vi) waste and (vii) fluorinated gases. In general the CCC recommended that policy changes are required now if the emissions targets throughout the 2020s are to be met due to the long lead times required for the development and implementation of emissions reduction technologies. As the work in this thesis is related to electricity production the recommendations suggested by the CCC in the power sector and the response from government are outlined below:

Recommendation 1: A strategic approach to carbon capture and storage deployment in the UK (new policy required).

Recommendation 2: A new approach to bring forward the cheapest low carbon generation (e.g. auctions for generation from onshore wind, solar and sustainable biomass) (new policy required).

Recommendation 3: Support for offshore wind costs are driven down, based on funding and cost goals announced in the 2016 budget (stronger implementation of existing policy required).

Recommendation 4: Plans for flexibility options (e.g. storage, interconnection, demand response) including rapid development of market rules to ensure that revenues available to these options reflect their full value to the electricity system (stronger implementation of existing policy required).

Recommendation 5: Contingency plans for delay or cancellation of planned projects, for example new nuclear power plants (new policy required).

(10)

The UK government provided a response to the above concerns of the CCC, the first point made in the response paper is that the current government is working towards its own emission reduction plan expected in 2017, focusing on decarbonisation throughout the 2020s whilst delivering secure and affordable electricity, also known as the energy trilemma (12). The delivery of low carbon, secure and affordable electricity will be driven in the UK by the Electricity Market Reform (EMR) policy which is outlined in the Energy Act 2013 (13). The Act contains two new market mechanisms: the first, Contracts for Difference (CfDs) aims to introduce low carbon technologies into the energy sector; the second, Capacity Markets to ensure security of supply.

The CfD replaces the existing Renewable Obligation scheme (RO), in which a generator is issued Renewable Obligation Certificates (ROCs) for each MWh of electricity generated. A generator under the RO scheme must meet a pre-agreed level of ROCs and if it does not then additional ROCs must be purchased at the current price of £44.77 per ROC. If a generator meets or exceeds the level of ROCs required, then the money acquired from suppliers buying ROCs, due to a shortfall in their own renewable generation, is redistributed to the generators who met the pre-agreed targets. The RO scheme is closed from 2017 to new applicants and support for renewable generation will be covered by the newly implemented CfD. The CfD provides support by guaranteeing a price (strike price) that a generator gets for electricity produced (MWh) which is dependent on the method of generation. The wholesale price of electricity if below the strike price is subsidised to the strike price level, if the cost of wholesale electricity exceeds the strike price the generator pays back the excess above the strike price. Biomass support under CfDs is set at £125/MWh when combined with CHP and £105/MWh for biomass conversion, compared to £92.50/MWh agreed for the new nuclear reactor at Hinkley Point C and £155/MWh for offshore wind generation. Currently 41 projects are listed on the CfD register, the majority of which are on and offshore wind with a total of 31 projects with the remainder either solar, waste or biomass with and without CHP (14).

The aim of the second market mechanism, the Capacity Market, is to provide a secure energy supply to the UK. The increase in the use of intermittent renewable technologies and inflexible nuclear generation make management of supply and demand difficult. In addition the closure of several oil and coal generating plants due to the introduction of the Large Combustion Plant Directive (LCPD) (EU legislation covering SOx, NOx and Particulate emissions replaced by the Industrial Emissions Directive) requires the availability of additional capacity in times of high demand and low generation from renewables (low wind). Suppliers are paid, through capacity auctions, based on operating costs, to maintain generating plant so it is available when needed at times of stress. If the generator does not make the plant available and therefore do not meet the contractual agreements they face financial penalties. Currently 46.35 GW of capacity have been contracted (~62% of current capacity) under the capacity market with a forecasted cost of ~£835 million. The capacity comprises of existing (42 GW) and refurbished (0.85 GW) plants as well as new build (2 GW) and existing interconnectors (2 GW) with combined cycle gas turbines (CCGT) providing ~47% of capacity. Coal and biomass plant have been awarded ~4.7 GW of capacity as of 2015. The lifespan for the contract is dependent on generation type with new builds

receiving contracts for up to 15 years and existing plant awarded 1 year rolling contracts (15).

The UK Governments principal tool to ensure security of electricity supply is the Capacity Market and in the response to the CCC the government suggested that an early auction should be held in 2017-18. The Government also stated that more capacity should be bought earlier and that stricter penalties should be applied to those companies that don't deliver their agreed capacities. In addition the government response outlined its continued support of nuclear energy and on and offshore wind as well as the move towards smart energy systems to ensure reductions in emissions. Carbon capture and storage (CCS), the focus of the work in this thesis is also mentioned in the response to the CCC and is discussed in section 1.6.2.

1.2 Emission sources current and future trends

In order to meet the <2^{o}C temperature rise target agreed on in the Paris Agreement, concentrations of CO_{2eq} must not exceed 450 ppm in the atmosphere and if the 1.5^{o}C target is to be met then concentrations must not exceed 430 ppm by 2100 (1). In 2015 the global average concentration of CO_2 exceeded 400 ppm for the first time which continued in to 2016 (16). In order to meet these targets, peak emissions must be reached as soon as possible in order to reduce long term climate change preferably by the mid-2020s (17).

1.2.1 Global emissions trends

The global greenhouse gas emissions trends (CO_{2eq}) by sector can be in Figure 1.2. The global emissions have continued to rise in all sectors with energy production (electricity and heat) the main source of emissions, accounting for ~36% of total emissions in 2010. An increase in energy demand is expected over the coming decades (30% increase by 2040 (18)) due to population growth and the electrification of the building and transport sectors (to reduce emissions by use of renewable electricity in those sectors) (17, 18) making a reduction in the carbon intensity of the energy sector of great importance. The need for the decarbonisation of the energy sector has been widely acknowledged and the International Energy Agency (IEA) stated that at least two thirds of the emission reductions set out in the Paris agreement comes from the transformation of the energy sector (18).

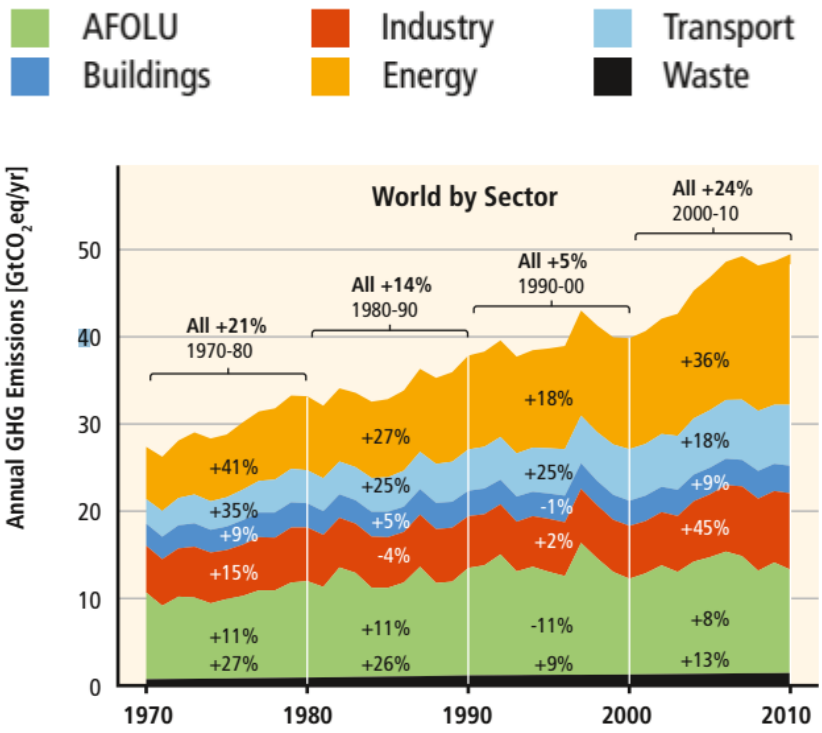

Figure 1.2: GHG global historical emissions trends (17) (AFOLU – Agriculture, Forestry and Other Land Use)

1.2.1.1 Global future emissions as a result of the Paris agreement

Figure 1.3 highlights the potential emissions gap between the targets required to limit the average global temperature rise to 2°C and the predicted emissions as a result of the Paris Agreement. The predicted emissions are derived from INDCs submitted by 187 of the 195 parties (including the major polluters USA, China and the EU). The unconditional and conditional agreements are country specific but essentially the best case scenario is the conditional agreement case which would result in a temperature rise of 2.9-3.4°C by 2100 (19) if further actions are not taken. A number of the parties included in the Paris agreement have current legislation that exceeds the targets set out by their INDCs submitted to UNFCCC (UK, Russia and Indonesia etc.) but the total emissions are still expected to exceed the 2°C temperature increase limit (19). If the trend seen in Figure 1.3 becomes reality then there may well be a greater need to remove emissions from the atmosphere post 2030, especially if the 1.5°C temperature increase limit is a serious proposal (19). One potential method for this is bio-energy carbon capture and storage (BECCS), the partial focus of this study.

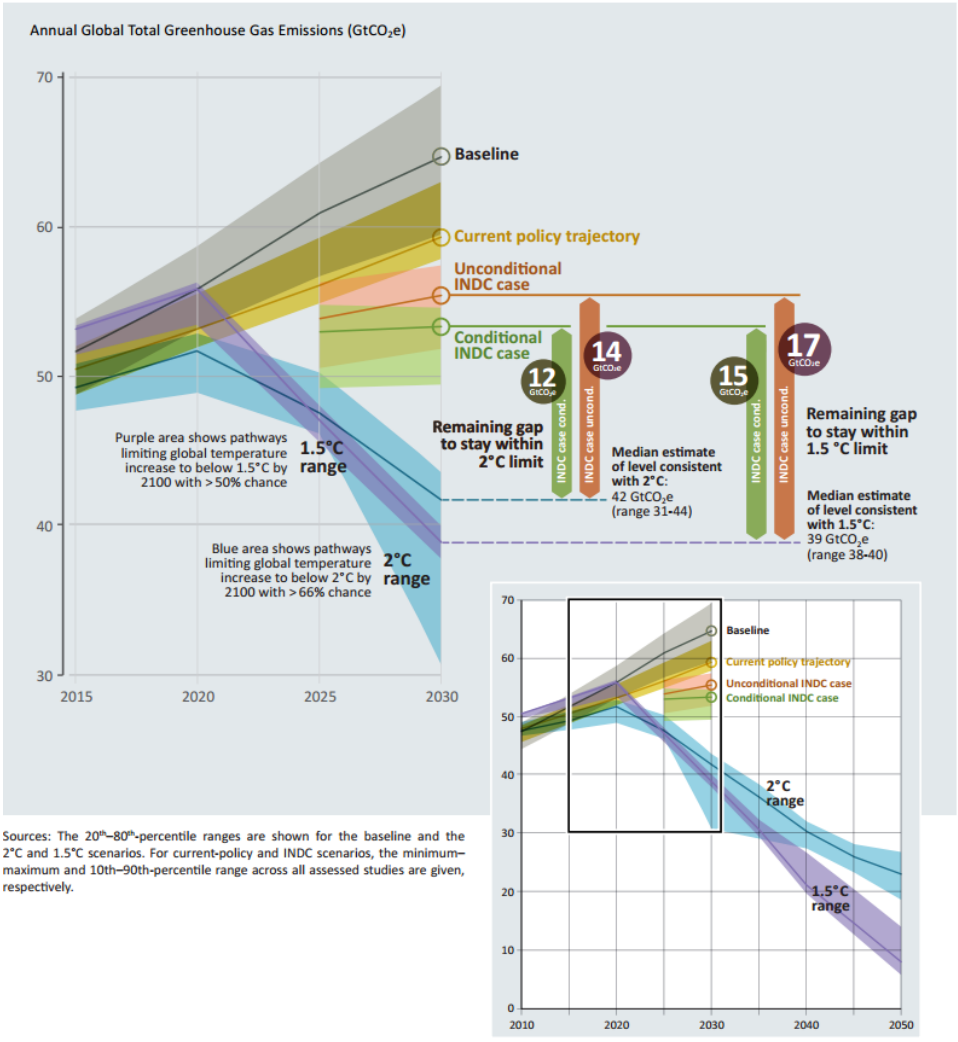

Figure 1.3: Global greenhouse gas emissions under different scenarios and the gap between the emissions gap in 2030 (19)

1.2.2 UK emissions and energy trends

In contrast to the global emissions, the overall UK emissions have continued to reduce since 1990 (Figure 1.1), the breakdown of emissions by sector can be seen in Figure 1.4. Emissions from the energy sector (electricity generation and other energy production) are consistently the highest contributor accounting for ~32-35% of all UK emissions. Although the percentage is stable, the actual emissions from the energy sector reduced by 41% from 278 $MtCO_{2eq}$ in 1990 to 164 $MtCO_{2eq}$ in 2014 (20), significantly higher than the 23% reduction target outlined in the first carbon budget. Emissions from power stations accounted for 75% of the emissions from the energy sector which equates to ~25% of the UKs total greenhouse gas emissions in 2014 (21).

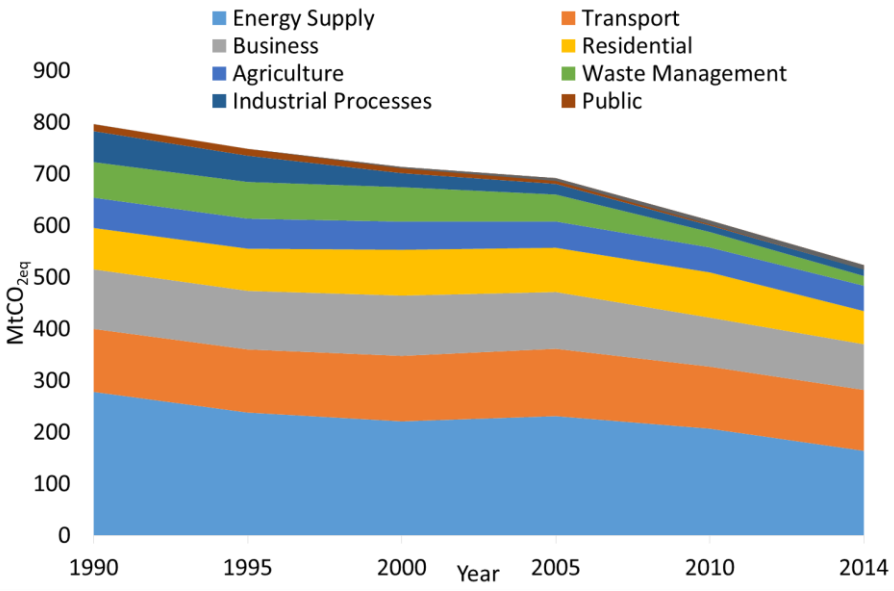

Figure 1.4: Sources of UK greenhouse gas emissions (adapted from (20))

The decline in emissions from the energy sector has be driven by the change in the fuel mix used for the generation of electricity, with a decline in coal use, which has been replaced by gas, the growth of renewable technology and the increase in plant efficiencies (20). The historical fuel mix and the shift away from coal can be seen in Figure 1.5. The decline of coal is set to continue over the coming decade due to closures of existing plant driven by the LCPD and in addition the speech in 2015 by the then Secretary of State for Energy and Climate Change Amber Rudd initiating a consultation on the closure of all unabated coal plants in the UK by 2025 (22).

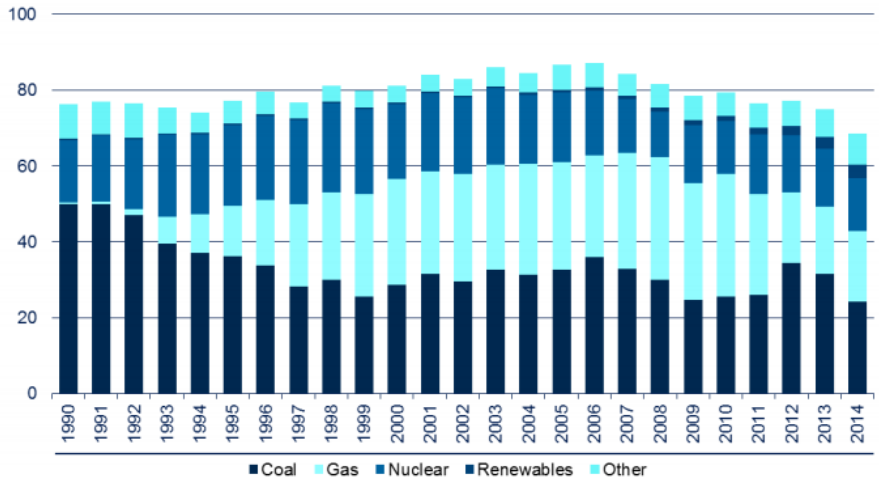

Figure 1.5: Fuels used for UK electricity generation (MtO_e) (20)

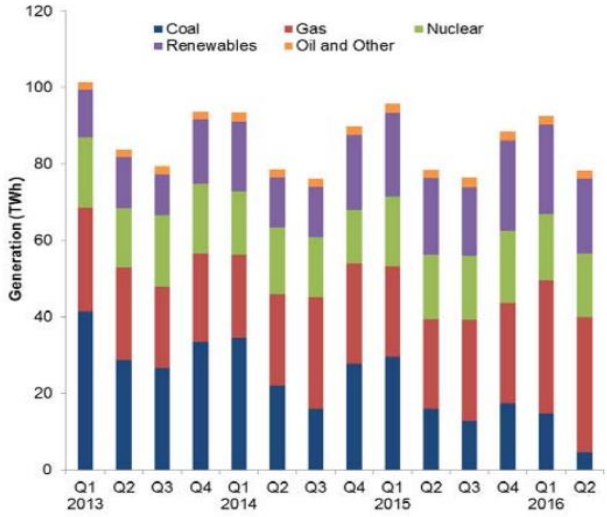

Figure 1.6: Electricity generation in the UK by fuel type (23)

The latest energy trends available for the UK (Figure 1.6) shows the continued decline in coal use for electricity generation, caused by the closure of Ferrybridge C and Longannet and the conversion from coal to biomass of a 660 MW unit at DRAX power station (23). The generation from coal reached a record low in Q2 of 2016 producing just 4.6TWh, a fall of 71% from the same quarter in 2015. The reduction in coal and a small reduction in renewable generation, due to lower wind speeds and low rainfall (hydro generation), resulted in the increase in use of gas which accounted for ~45% of the total electricity generated in Q2 of 2016 (23).

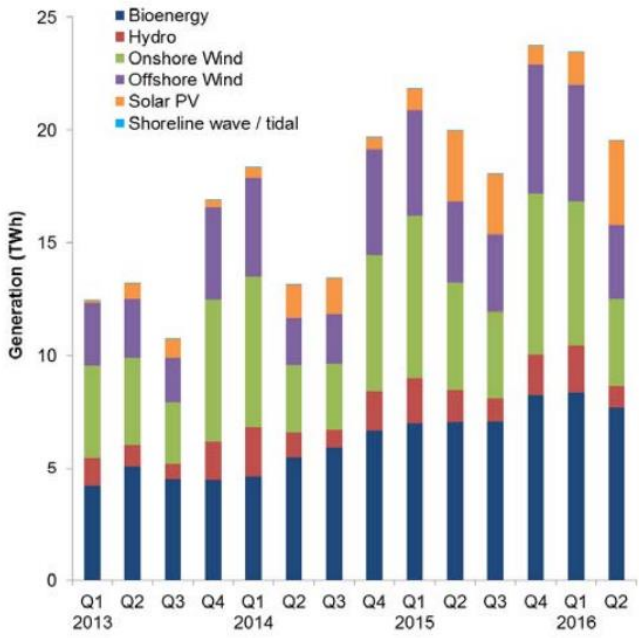

Figure 1.7: Renewable electricity generation in the UK (23).

The electricity generated by renewable sources in the UK can be seen in Figure 1.7 which accounted for ~25% of total generation in Q2 of 2016 the majority of which comes from bioenergy (~40% of all electricity generated from renewable sources). The term bioenergy covers landfill gas, sewage sludge, energy from waste, animal biomass, anaerobic digestion and finally plant biomass (large scale power generation). The majority of the remaining renewable generation came from solar PV (19.2%), offshore wind (16.6%) and onshore wind (19.9%). On and offshore wind generation decreased relative to Q2 in 2015 by 9 and 18% respectively despite an increase in capacity by 1.4 and 8.5% respectively (23) highlighting the need for a reliable, low carbon, renewable technology.

1.2.2.1 UK progress towards 2020 target

A report by the House of Commons Energy and Climate Change Committee (ECCC) suggested that the UKs target of 15% of its energy needs from renewable sources is unlikely to be met (24). The government proposed that to meet the renewable target, 30% of electricity, 12% of heat and 10% of transport would need to be from renewable sources by 2020. At the end of 2015, 22.31% of electricity, 5.64% of heat and 4.23% of transport fuel was from renewable sources, equating to 8.31% of the UKs energy needs. The success in the electricity sector is expected to continue, reaching ~35% by 2020 (25% Q2 2016), but is not expected to meet the shortfall in the transport and heat sectors, therefore, it is possible that the overall target of 15% renewable energy by 2020 may be missed (24). The report suggests that the reason for the failure to meet the 2020 target is the inconsistent approach taken by government and that the creation of the new Department of Business, Energy and Industrial Strategy (BEIS) is an opportunity for greater cooperation and consistency. The report also suggested that regardless of Brexit, the government must reassess and set replacement targets for both the EU legislated 2020 targets and the longer term decarbonisation targets laid out in the 2008 climate change act (24).

1.3 Biomass as a renewable energy source for the generation of electricity

The increase in generation from biomass has been driven by the need to replace unabated coal combustion with a reliable, renewable, sustainable technology. Biomass although a renewable fuel still has carbon emissions associated with cultivation, fuel processing, transport, any direct (and indirect) land use changes and the reduction in conversion efficiency of the plant. In order for biomass to be used in power generation in the UK and to qualify for government support strict sustainability criteria must be met (updated in March 2016) for generators with ≥1MW plant, including feedstocks sourced from both the UK and overseas (25). The sustainability criteria for biomass use in the UK power sector is split in two: the first section is related to land from which the biomass is sourced, which is dependent on the biomass type (woody, non-woody), the second is related to overall GHG emissions (26).

Woody biomass, i.e. that typically used in the production of white wood pellets (the biomass type used in this work) and combusted in large plants (27), has land criteria that require a minimum of 70% of all wood fuels meets the definition of legal and sustainable (28). The term legal means that the woody biomass must have been legally harvested and is covered by the EU timber regulation (EUTR) (29). This includes compliance in the country of origin with regards to harvesting rights and payments for those rights, environmental and forest management including biodiversity conservation and all trade and customs requirements. The sustainability criteria are focused on forest management and the balance between economic, environmental and social interests taking into account not just the health of the ecosystem and biodiversity but also the adherence to local labour, welfare and health and safety laws (30). In the UK sustainability of UK sourced woody biomass is enforced through the UK Forestry Standard (31). In order to ensure compliance and ensure an industry wide code of practice, a strategy for sourcing wood pellets has been agreed by the major European electricity generators (E.ON, DRAX, RWE, GDF, SUEZ, Dong, Vattenfall and Eggborough) (32).

The second section of the sustainability criteria is related to emissions levels of biomass plants. Emission savings must be determined by performing Life Cycle Assessments (LCAs) which take into account the cultivation, processing and transport and distribution of the solid bioenergy system under consideration (26). In order to determine compliance with the required sustainability a generator must commission an independent annual sustainability

audit report (33). In order to meet the emissions targets laid out in the biomass sustainability report the generator must meet emissions targets given in Table 1.2. The levels of GHG emissions are reduced over time and encompass an annually-averaged target and a maximum threshold. Data from OFGEM indicates that the targets laid out in Table 1.2 have been easily met by electricity generators using wood pellets with emissions ranging from 14.79 - 54.44 gCO_{2eq}/MJ in 2014 – 2015 dependent on the type of fuel used and the origin of the wood pellet (34).

Table 1.2: GHG targets and ceiling values for sustainable solid biomass (ROC compliance)

	Relevant target	Relevant ceiling
Definition	Threshold for which the average GHG emissions of all of the relevant biomass used in an obligation year should be met	Maximum threshold for which biomass can be issued ROCs
Post 2013 dedicated biomass stations before April 1st 2020	66.7 gCO_{2eq}/MJ electricity	79.2 gCO_{2eq}/MJ electricity
All solid biomass stations 1st April 2020 to 31st March 2025	55.6 gCO_{2eq}/MJ electricity	75 gCO_{2eq}/MJ electricity
All solid biomass stations post 2025	50 gCO_{2eq}/MJ electricity	72.2 gCO_{2eq}/MJ electricity

Note: GHG emissions coefficients - Coal ~113 g CO_{2eq}/MJ and Natural Gas ~67 g CO_{2eq}/MJ (26)

The method of determining the associated GHG emissions of bioenergy systems is outlined in the OFGEM sustainability report and includes emissions factors for many different land use changes, cultivation, processing and transport and distribution methods as well as conversion efficiencies. However the determination of GHG emissions associated with each of the above steps in a bioenergy system is extremely complex (35) and the use of emissions factors over measured emissions (due to the difficulty in determining real world emissions) may not accurately reflect real world emissions. Direct and indirect land-use changes are particularly difficult to determine and can have a significant effect on the total GHG emissions of a system (36). The use of carbon capture and storage in bioenergy systems allows for the capture of emitted CO_2 at the stack (which is not accounted in the RO emissions register since it is assumed to be utilised in plant photosynthesis) which would reduce overall emissions further (towards negative emissions) and would help to offset some of the uncertainty in GHG emissions determination.

1.4 Carbon capture and storage

Carbon capture and storage (CCS) has been identified as another potential emissions reduction technology. CCS is the process of capturing CO_2 emissions from large scale emitters such as electricity generation, oil, cement, chemical or steel production, transporting it via pipelines or ships and storing it to prevent emissions to atmosphere. The captured CO_2 may be stored in geological formations, used in enhanced oil recovery (EOR) or utilised which is known as carbon capture and utilisation (37). The CO_2 may be utilised in the chemical industry to produce polymers, fuels (kerosene, diesel etc.) syngas or intermediates such as formic acid and may also be utilised in the food industry , for use in accelerating food growth, carbonation of drinks (38).

In relation to the 2^oC target, the majority of climate change models incorporate some form of CCS (17) and the use of negative emissions technologies such as bioenergy CCS (BECCS) (19) for the reduction of emissions in the energy sector. Without CCS the cost of meeting the 450 ppm, 2^oC limit could be 1.5 to 4 times higher globally (17) and the CCC suggested that in the UK the cost of meeting the 2050 targets could almost double (7). As reducing the cost associated with emissions reduction is part of the energy trilemma (emissions reduction at low cost while maintaining a secure supply) then the use of CCS in the world wide energy sector is of great importance.

1.4.1 CCS technology

As mentioned above CCS comprises of three steps, capture, transport and storage, with many different individual technology options available in each step. The main technologies for each of the three steps are outlined in the following sections.

1.4.1.1 CCS – Capture

CCS is most suited to large scale CO_2 producers as capture and transport from small or mobile sources is both expensive and difficult and the removal of CO_2 directly from the atmosphere is discussed in section 1.5. As a result this section focuses on large scale emitters.

There are three options for capturing CO_2 from solid fuel processes:

- Pre-combustion capture
- Post-combustion capture
- Oxy-fuel combustion

Pre-combustion capture

The pre-combustion capture process involves the processing of the fuel to convert the fuel bound carbon to CO_2 and its removal before the final product is utilised. The main pre-combustion option available for solid fuels is gasification where the fuel is partially oxidised in mixture of air or oxygen and steam at elevated temperatures and pressures. The product of the gasification process are high value chemicals or a syngas comprising mainly of H_2, CO, CO_2 and H_2O and traces of N_2, COS, H_2S, HCN, NH_3 volatile species and H_g (39). The gasification step is followed by the water gas shift reaction to produce a hydrogen and carbon dioxide enriched syngas (40). The CO_2 is then separated, usually by physical or chemical absorption (discussed in section 1.4.1.2) resulting in a hydrogen rich fuel which can then be used in boilers, gas turbines, engines and fuel cells (39).

Post-combustion capture

Post combustion capture is the capture of CO_2 from flue gases generated from the combustion of fossil fuels or biomass in air. The preferred method of CO_2 removal in post-combustion capture is the use of a chemical sorbent (39, 41) rather than physical sorption due to the relatively low concentration of CO_2 in the nitrogen rich flue gas (10-15% volume). The low concentration of CO_2 and low pressure of a typical flue gas stream results in large volumes of gases that require the removal of CO_2, the increase in the associated energy penalty and the increase in both capital and operating costs (41, 42).

Oxy-fuel combustion

Oxy-fuel combustion is the capture of CO_2 post combustion from the flue gases, as in the previous case, however the use of pure oxygen rather than air in the combustion atmosphere results in a CO_2 rich flue gas (80-98% CO_2) (39). The use of a pure oxygen stream instead of air in the combustion chamber results in changes in the operating behaviour of a boiler. Elevated flame temperatures, flame stability issues and a decrease in gas volume in the system (due to the loss of N_2 in the flue gas stream) resulting in poor heat transfer properties (especially in boilers that are retrofitted with an oxy-fuel CCS system) can be expected. In order to manage these issues a percentage of the CO_2 rich flue gas is recycled back into the system and combustion takes place in a O_2/CO_2 atmosphere. The main disadvantage of an oxy-fuel system is the need for pure oxygen and the energy intensive air separation units required which may result in an energy penalty of ~7% - 10% (42, 43). A substantial reduction in NO_X emissions is an advantage of the oxy-fuel process due to the removal of N_2 in the combustion atmosphere (and therefore thermal NO_x (42)). Oxy-fuel

combustion of coal and biomass is the focus of this work and a more detailed explanation of the oxy-fuel plant layout can be seen in the section 1.4.1.3.

In addition to the oxy-fuel combustion outlined above, oxygen can be provided to the combustion system by the use of oxygen carriers such as metal oxides, rather than by an oxygen gas stream, a process known as chemical looping combustion (CLC). The reactor system is typically comprised of two interconnected fluidised beds, one containing air and the second the fuel. The fuel is introduced into the fuel reactor where it reacts with a metal oxide producing a gas stream containing CO_2 and H_2O which is then condensed resulting in a CO_2 rich flue gas. The reduced metal oxide is then transferred to the air containing reactor where it is oxidised before being recycled back into the fuel reactor. A second flue gas stream is generated in the air reactor comprising of mainly N_2 and some unused O_2. The heat generated by the CLC system is the same as in normal combustion where the oxygen is in direct contact with the fuel (44). The benefit of a CLC system is that an air separation unit is not required, reducing the efficiency penalty 3-4% in CLC compared to 10% in oxy-fuel systems (43). Additionally, as the flue gas streams are kept separate throughout the process an almost pure CO_2 stream is generated (after condensation of the moisture) removing the need for extra CO_2 separation equipment reducing the associated energy penalty and overall cost of the plant (39).

In addition to the three above capture options there are opportunities to capture CO_2 from industrial processes such as natural gas sweetening, cement and steel production and fermentation for food and drinks. The techniques that may be used to capture CO_2 from these processes (as outlined in 1.4.1.2) are common to the three methods outlined above (39).

Each of the above technologies have advantages and disadvantages associated with economics of both the building and operation, energy requirements of the systems and technological challenges that are specific to each raw fuel conversion process. The advantages and disadvantages of the above capture technologies are outlined in Table 1.3

Table 1.3: Advantages and disadvantages of the different CO_2 capture technologies

Capture Process	Advantages	Disadvantages
Pre-combustion	• High CO_2 concentrations increase sorption efficiency • Mature technology • Opportunity to retrofit to existing plant (42) • Energy penalty reduction compared to post-combustion due to increased pressure systems • Continued increase in efficiency of turbines improve overall efficiency of IGCC plants (45)	• Heat transfer problems and decay issues associated with a hydrogen rich gas • High parasitic energy requirement for sorbent regeneration • High capital and operating costs (42) • Associated energy penalty • IGCC not widely used in the power industry (45)
Post-combustion	• Easily retrofitted to existing plant • Mature technology (42)	• Low CO_2 concentration in the nitrogen rich flue gas affects the capture efficiency (42) • Associated energy penalty • Size of additional capture plant required • Potential reduction in turbine efficiency and turn down capability due to steam extraction for solvent regeneration (45)
Oxy-fuel combustion	• High CO_2 concentration in the flue gas stream increasing absorption efficiency • Air separation technologies needed to produce oxygen are mature • Gas volumes decreased requiring smaller boiler and other equipment (42)	• High efficiency and energy penalties • High cost of cryogenic air separation • Potential corrosion issues (42) • Retrofitting and integrating whole system in existing plant is difficult (45)
Chemical looping combustion	• CO_2 is the main combustion product • Air separation units not required (42)	• Immature technology with limited large scale experience (42)

1.4.1.2 CO_2 separation technologies

There are several different methods to remove the CO_2 from the flue gas streams of the capture technologies outlined in the previous sections. The separation techniques relevant to the capture technologies are outlined in the following sections.

Post combustion solvent scrubbing

Absorption involves the separation of the CO_2 containing flue gas using a liquid absorbent such as monoethanolamine (MEA), diethanolamines (DEA) or potassium carbonate (42). The flue gas emitted from the conversion process is first cooled and introduced in an absorber (at 40-60^oC) where the CO_2 in the flue gas is bound to the solvent. The flue gas is washed to remove any solvent droplets before leaving the absorber with a low CO_2 concentration, which is dependent on the on the height of the absorber. The solvent containing CO_2 is then sent to a stripper or regeneration vessel operating at 100-140^oC and near atmospheric pressures allowing desorption of the CO_2. The recovered solvent is then recycled for use in the absorber column (46) and CO_2 stream sent for further processing. This method is the most mature for CO_2 separation (42) and absorption using MEA is the preferred option for post combustion separation (47). There are several issues related to this type of CO_2 separation including solvent degradation, MEA can be degraded by both oxygen present in the flue stream (from excess air in the combustion chamber) and other flue gas contaminants. Amine based solvents can also have detrimental effects on health and the environment if not controlled correctly (47, 48) which would be of greater concern if post combustion capture is deployed at large scale (36).

Adsorption

Adsorption uses a solid sorbent such as activated carbon, zeolites, calcium oxides and lithium zirconate to separate CO_2 from the flue gas stream. The adsorbed CO_2 can be recovered by either reducing the pressure (Pressure swing adsorption) or by increasing the temperature (temperature swing adsorption). Recovery of CO_2 by this method is >85% compared to >90% if separation is performed by absorption using a solvent (42). A drawback of the adsorption method is that the adsorbents are not selective enough to only capture CO_2 and gases smaller than CO_2, such as N_2, can penetrate the pores filling the adsorbent and decreasing efficiency (49).

Membrane separation

Membranes, a composite polymer, can be used to allow only CO_2 through producing a CO_2 rich gas stream. The membrane technology has been successfully used in the separation of

CO_2 from natural gas and O_2 from air. This technology requires further development before being deployed at large scale for CCS (39).

Cryogenic distillation separation

The separation of CO_2 from the flue gas stream uses the same technology as the oxygen production step in oxy-fuel combustion. The flue gas stream is cooled to between -100 to -135^oC and then the solidified CO_2 is separated from other light gases and compressed. The main problem associated with this is the high energy penalty (49).

Calcium looping separation

Calcium looping technology (CaL) is similar to CLC systems except that instead of providing oxygen for combustion, CO_2 is removed from the flue gas (post-combustion) by reaction with calcium oxide. The CO_2 present in the flue gas reacts with CaO in the first reactor (the carbonator) to produce $CaCO_3$ which is then fed into a second reactor (the calciner) at higher temperatures to regenerate the CaO and produce a high purity CO_2 stream. The main drawback of this method is the degradation of the sorbent (CaO) (43).

Other methods of CO_2 separation such as electrical desorption, hydrate based separation and redox technologies are available but are not discussed in this work.

1.4.1.3 Pulverised fuel combustion plant layout using oxy-fuel technology

This section outlines the fundamental processes and equipment an oxy-fuel plant would require and gives a more in-depth description of the process during electricity production. A simplified typical oxy-fuel pulverised fuel plant with possible flue gas recycle systems can be seen in Figure 1.8.

Air separation unit

The first stage of the pulverised oxy-fuel combustion plant is the production of oxygen in the ASU (the main separation step of the process). The oxygen is separated from the air by cryogenic distillation which can produce oxygen with a purity of >95% (50). The energy penalty, a 7-10% reduction in plant efficiency (the majority of the energy penalty associated with the overall CCS process) (39, 43, 51) and the cost of air separation is the main criticism of oxy-fuel combustion (52).

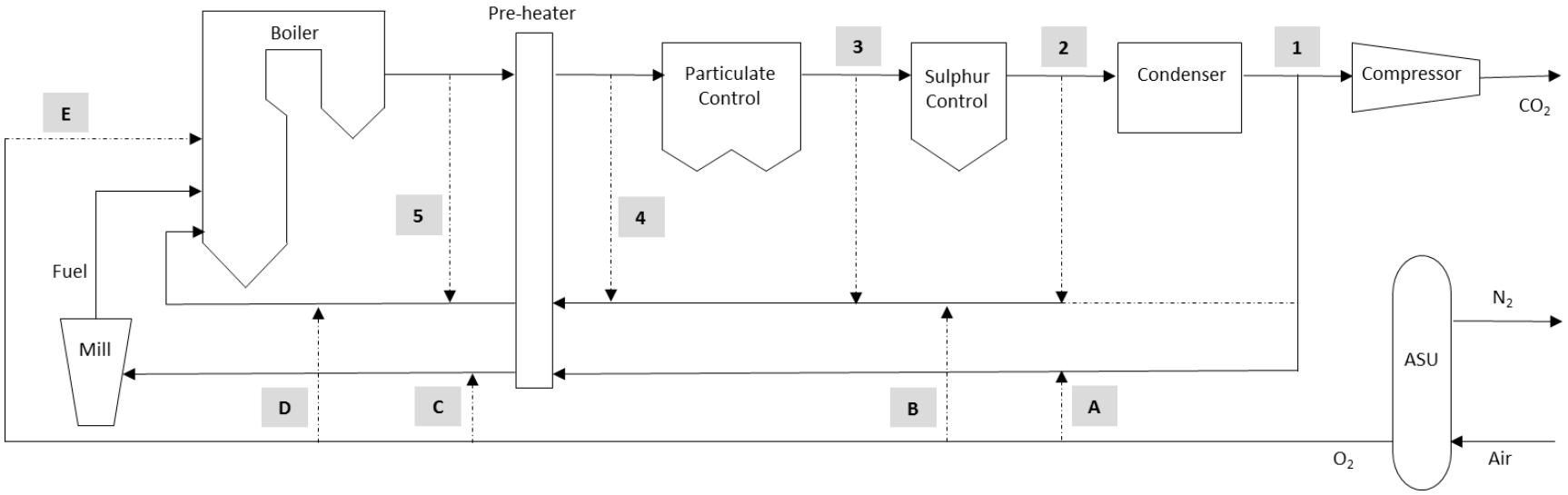

Figure 1.8: Simplified pulverised oxy-fuel plant layout with possible flue gas recycle options (adapted from (53))

In addition the continued availability of oxygen for plant operation (98-99% availability) and the ability of the ASU to respond to demand changes (as would be expected if CCS is deployed to mitigate intermittent renewables) are also of concern. Xu et al reported that the ramp rate of a pulverised coal plant is up to 6% min^{-1} where the ASU units are only able to achieve 3% min^{-1} and in addition the efficiencies of the ASU units are poor below 80% load (54). The introduction of additional oxygen storage capacity could help to mitigate this problem and additionally make use of renewable technologies at times of low demand making the oxygen production stage an energy storage technology (51, 52, 54, 55). A 500 MW_e coal plant would require 9000-10,000 tonnes of oxygen a day requiring 2-3 ASU units (51), if additional storage of O_2 is required then this may be more difficult in a retro-fitting scenario.

The energy penalty associated with the ASU (one of the main disadvantages of the oxy-fuel plant) is decreasing as the technology improves. First studies suggested the energy penalty would be ~220 kW h t/O_2 produced (39) but improvements in the ASU process have reduced the energy penalty to 140 kW h t/O_2 and with further improvements in heat integration the energy penalty is expected to be reduced to 120 kW h t/O_2 by 2020 (51, 55). The utilisation of the large amounts of almost pure nitrogen (31,000 t/day) and the increase in efficiency of the ASU help to decrease the cost implications and patristic load of the oxy-fuel plant (51).

Flue gas recycle

The flue gas containing mainly CO_2 and other gas species, NO_x, SO_x, N_2, Ar and H_2O (combustion products, impurities in the ASU process and due to air leakage) is recycled into the oxygen stream to moderate flame temperatures and to provide heat transfer properties similar to those seen in air combustion. As can be seen in Figure 1.8, two recycle streams are necessary, the primary recycle used to transport and dry the fuel from the mills to the boiler, and the secondary stream used to provide the remainder of the required combustion atmosphere.

The primary recycle stream accounts for ~20% of the total combustion atmosphere (51) and should be taken after the condensation of the flue gas [1] and is known as dry recycle flue gas. If taken before the condenser [2] the high levels of moisture may inhibit the drying of the fuel and also cause agglomeration problems. If the primary is taken before the flue gas desulphurisation [3] process (wet recycle flue gas) then the SO_x levels and the potential for low and high temperature corrosion is increased. As the primary recycle is taken after the condensation step the temperature is typically less than 30°C and the stream needs to be

reheated to 250-350°C in order to dry the fuels in the mill, increasing the energy penalty of the overall process (56). The oxygen separated in the ASU may then be added to the primary recycle stream either before or after the pre-heater [A,C]. However it has been suggested that the O_2 should not be added to the primary recycle (especially in the case of high rank coals) to prevent explosions in the mills that may arise from mismatches in recycle and oxygen flows when the plant responds to demand (51, 57, 58). Work by Trabadela et al (59) looked at the ignition behaviour of biomass in a 20L sphere and reported that at 21% O_2 levels in the primary recycle the milling safety is improved when compared to air combustion. This, although it does not take into account the possibility of mismatched in the system, suggests that the addition of oxygen into the primary recycle may be possible.

If the oxygen cannot be added to the primary recycle then it must be added to the secondary recycle and is supplied to the boiler to combust the pulverised fuel. Again several options are available to where the secondary recycle is taken and the problems outlined earlier (SOx and H_2O content etc.) are applicable here. The addition of the oxygen into the secondary recycle stream can again be added before or after the pre-heater [B, D] or may even be introduced into the furnace directly via the over-fire ports [E] (58). The addition of the oxygen into the secondary recycle stream after the pre-heater would result in a higher energy penalty due to the lower gas temperatures but may increase safety. The key concern in the addition of the oxygen into the recycle stream results in a well-mixed, homogeneous combustion gas to maintain burner stability and to prevent safety hazards due to the injection of large volumes of pure oxygen into the system (51).

Boiler

The use of oxygen and the recycled flue gas have a significant impact on the combustion and heat transfer properties of a pulverised fuel boiler. Burner stability, fuel combustion behaviour, heat transfer, pollutant formation, slagging and fouling and ash behaviour are potential issues (51, 60, 61). The use of CO_2 rather than N_2 in the combustion atmosphere results in the reduction of flame temperatures at the same oxygen conditions as air due to the higher heat capacity of CO_2 resulting in lower flame propagation speeds and flame stability. The higher heat capacity of CO_2 may also result in a delayed ignition relative to air (61). Chen et al. reported that higher oxygen concentrations (25-35% O_2) result in higher flame temperatures, broader flammability limits and laminar burning velocities providing more stability in the flame. In addition the ability to inject oxygen at different points in the boiler (primary, secondary and direct injection) allow for and should be selected for optimisation of burner stability (60). The effect of the change of combustion atmosphere on

the devolatilisation and char combustion stages are discussed in chapters 6 and 7 and this is a key area of the work in this thesis.

Heat transfer differences are particularly important in retrofitting applications and is effected by two main property changes, gas radiative properties and the gas thermal capacity. The majority of heat in the boiler system is transferred from the flame through thermal radiation, and the high proportions of CO_2 and H_2O result in high gas emissivity such that similar transfer properties in a coal oxy-fuel plant can be achieved with O_2 levels at 30%. The thermal capacities of CO_2 and H_2O are higher than that of N_2 which results in the heat transfer in the convective section of the boiler. However the reduction in gas volumes passing through the boiler and increased radiative heat transfer in the super-heater result in a cooler gas temperature and reduced convective heat transfer in the economiser (61, 62). The problem of heat transfer could be eradicated in new oxy-fuel systems by optimisation in boiler design.

Oxy-fuel combustion produces the same major pollutants as found in conventional air combustion, NO_x, SO_x, CO, trace metals including mercury and particulate matter and the fundamental mechanisms for formation appear to change little in oxy-fuel combustion environments (63). NO_x emissions are investigated in section 5.3.4. The concentration of SO_x and trace metals are expected to increase in the boiler due to the concentration in the recycled flue streams. Although the concentration of the species in the boiler is increased, the emissions to atmosphere of these species is expected to be similar to air (61).

The increase in sulphur concentration in the combustion gas can affect both the slagging and fouling behaviour and ash composition. A greater retention of sulphur in the fly ash decreases melting behaviour and potentially impairs fly ash utilisation in concrete production (51). The effects on the above properties as a result of change in combustion atmosphere are plant specific and more understanding will be gained through operation of large scale plant.

Particulate removal

Electrostatic precipitators (ESP) are the most common form of particulate removal in large scale pulverised fuel combustion plants and the main changes to the operation of the ESP in oxy-fuel combustion are related to the particulate sizes and flue gas composition. Oxy-fuel combustion has the potential to change the size distribution of particulate size with a greater proportion of smaller particulates when lower flame and particle temperatures are seen.

The flue gas composition could result in a change in ion production rate in the ESP and may result in a change in collection efficiency (51).

Desulphurisation unit (FGD)

There are some uncertainties in the operation of the FGD plant in oxy-fuel combustion systems. A series of reactions occur in a wet FGD, firstly SO_2 is dissolved in the aqueous phase producing hydrogen sulphite and at the same time limestone is dissolved releasing CO_2. The hydrogen sulphite is oxidised to sulphate using air and finally gypsum is produced by reaction of the sulphate with calcium. The high concentration of CO_2 in the flue gas stream may limit the CO_2 release from the limestone. Furthermore a pure oxygen stream (rather than air) would be required to oxidise the hydrogen sulphite to prevent dilution of the CO_2 rich stream with N_2. In addition, the high concentration of moisture in the flue gas stream could lead to the increase in equilibrium temperature of the gypsum/limestone suspension and influence the kinetics of the desulphurisation due to the decrease in solubility of SO_2. Issues surrounding gypsum purity and its utilisation may have a negative effect on the economics of the oxy-fuel plant (51).

CO_2 processing

The CO_2 processing step is the final stage in the capture process and is performed using a compression and purification unit (CPU). At this stage the flue gas is mainly CO_2 as the moisture and the majority of impurities have been removed in the previous steps. There are many different types and configurations of CPUs (56) but in general are comprised of multi-stage compression units with inter-stage coolers used to separate out any inert gases present in the flue stream (60). The remaining CO_2 rich stream is compressed which carries a significant energy penalty of ~7.5% and the reduction of this penalty is harder to achieve than that in the ASU (55, 56). When combined with the energy penalties associated with the ASU the total energy penalty is a considerable disadvantage of oxy-fuel systems. However optimisation of plant performance through heat integration, correct selection of oxygen concentrations and recycle scenarios can considerably reduce the associated energy penalty (55, 58).

1.4.2 CO_2 transport

Transport of CO_2 is the second stage of the CCS process and already occurs primarily in the food, oil and gas industry. In these industries CO_2 is transported by pipeline, ship and by road. However the amount of CO_2 that would require transportation from power plants is significantly greater than the existing transportation infrastructure capacity. Pipelines are widely considered to be the most reliable form of transportation for large amounts of CO_2 especially for the amounts that would be required if CCS was as widely deployed as climate models suggest. However the initial demand for the pipeline infrastructure will be low due to the low number and locations of CCS plants in operation. In order to mitigate the cost, the development of CCS hubs and networks that links point sources to a larger network of pipelines is expected. The EU developed the Europipe project looking at how to link Europe's large emitters to both onshore and offshore suitable storage sites (64). The Europipe project incorporated the political and public perception of CCS and in particular how this effects the selection of long term CO_2 storage sites (onshore and offshore geological formations). If the perception of CCS is negative and offshore storage sites are preferred then networks transporting large volumes of CO_2 linking Europe to the North Sea are required. In both cases regardless of public perception, the North Sea storage capacity plays an important role in the EU emissions reduction plans under the scenarios laid out in the Europipe project. This would suggest that the UK is in prime position to take advantage of the storage capacity available to us.

In order to transport the CO_2 over the long distances required to reach the storage sites the CO_2 will be transported under high pressure supercritical conditions at temperatures above 31^{o}C and pressures above 74bar. The purity of the CO_2 is also important and is required to be >90% to reduce the possibility of unwanted acid formation along the pipeline. High levels of moisture cause formation of Carbonic acid H_2CO_3 and sulphurous acid H_2SO_3 that cause corrosion to carbon steel pipes. The maximum water concentration is related to the solubility of CO_2 in water and levels of SO_2 and its solubility in water (65). These required operating conditions exceed those of the existing gas pipeline infrastructure (64). Pipeline leaks are also of concern due to the high purity and high pressure of the CO_2. In the UK the HSE are considering if CO_2 should be considered as a dangerous fluid in pipeline safety regulations due to the risk of asphyxiation if a large onshore pipe were to rupture (66). The development of a safe, large scale CO_2 transportation network is essential if CCS is to reach its full potential.

1.4.3 CO_2 storage

The final stage and the most important is the long term storage or in some cases the industrial use of the captured CO_2. There are several options for long term storage: geological storage; storage in the ocean; and mineral carbonation (39).

Geological storage

Suitable geological storage sites include depleted oil and gas reservoirs, potentially in coal formations and in deep underground porous rock formations. These geological storage sites are situated both onshore and offshore and require the CO_2 to be stored at depths below 800-1000m where CO_2 remains in a supercritical state (liquid like, density 500 kg m^{-3} (40)) allowing for sufficient use of the underground storage volume (39). Once injected the CO_2 may be retained through physical or chemical mechanisms:

- Physical trapping – stratigraphic and structural where the CO_2 is trapped below low permeability capping rocks such a sedimentary basins and stratigraphic traps (rock layers). Care must be taken to not over pressurise the well causing fractures and the loss of the integrity of the site (39).
- Physical trapping – hydrodynamic trapping can occur in saline formations that are not closed. When CO_2 is injected into a saline formation, water is displaced which migrates upwards due to its density. When the saline formation water reaches the top of the formation it is trapped in stratigraphic or structural formations capping the storage well (39)
- Geochemical trapping – the CO_2 undergoes a sequence of interactions with the rock and water that increase storage capacity. The CO_2 reacts with water, a process known as solubility trapping, producing a weak acid that then reacts with the metals to form carbonate minerals. The benefit of this process is that the CO_2 is permanently stored however the process may take several thousand years in some instances (39). A research project called CarbFix aimed at reducing the time required for this process to occur by injecting water containing dissolved CO_2 into a ultramafic and basaltic rock formation. The injection of water with CO_2 resulted in solubility storage within 5 minutes significantly shorter than the injection of supercritical CO_2. However this requires large amounts of water 5000 t of water to sequester 175 t of CO_2 (67). The increased reactivity and the composition (up to 25% by weight calcium, magnesium and iron) of the basaltic rocks resulted in the reaction of the dissolved CO_2 and metals present in the rock to form carbonates, this took only two years

rather than the thousands of years taken when supercritical CO_2 is injected directly into the storage site (68).

The CO_2 may also be used to extract oil from depleted oil wells, a process known as enhanced oil recovery (EOR) a mature technology (69). The mature technologies used in the oil and gas industry (drilling, capping and monitoring) lend themselves to long term CO_2 sequestration in geological storage sites making this a favoured technology (69). The depleted North Sea oil and gas reservoirs again provide an opportunity for the UK to become world leaders in CO_2 geological storage solutions. The UK storage is especially important when public opinion prevents onshore storage due to health and safety and environmental concerns (70). The main issue with geological storage is the potential for the failure of the storage system and the release of large amounts of CO_2 into the ocean in the case of offshore storage sites (the preferred option) and the potential damage to marine atmospheres and in onshore sites the contamination of fresh water aquifers (67). Work in this area is being widely undertaken to identify the most suitable storage sites and how these can be managed and monitored over their potentially long lifetimes (71-74).

Ocean Storage

The ocean currently plays an important part in the sequestration of CO_2 from the atmosphere via physical, chemical and biological processes during the carbon cycle. CO_2 is soluble and reacts with the oceans to form bicarbonate and carbonate ions known as dissolved inorganic carbons. The carbon is more soluble in colder waters and as colder water sinks the dissolved carbon is transported to the depths of the ocean (75). The CO_2 captured from industrial processes could be directly injected into the depths of the ocean by ships or pipelines where it would remain isolated from the atmosphere for centuries. Injections of CO_2 at the rates required (Gt CO_2 per year) would impact on the immediate injection points, with the reduction in oxygen supply and oxygen mobility, damage to marine life such as limited growth and reproduction and increased mortality over time. Higher levels of CO_2 injection over long periods of time would eventually spread the damaging effects over the entire ocean making this type of storage not a viable option for CO_2 storage at the volumes that may be required (39).

Mineral Carbonation

Mineral carbonation is the same process that occurs in geological storage but where large volumes of CO_2 are brought into contact with metal oxide bearing materials with the aim of fixing the CO_2 as carbonates. Silicate rocks, serpentine and olivine minerals are suitable for

mineral carbonation as well as industrial residues such as fly ash or slag from the steel industry. The resulting carbonates require disposal and it has been suggested that filling and reclaiming depleted mines is one option but there is potential for leakage to atmosphere, water and soil contamination. In addition the large amounts of carbonate that may be formed could result in land clearing for both the sourcing of raw material and the long term storage (39).

1.5 Bioenergy carbon capture and storage (BECCS)

Bioenergy CCS is the use of CCS technologies in conjunction with biomass to potentially provide negative emissions (removal of CO_2 from the atmosphere) an important technology if emissions targets are to be met (17, 76). The CCS process can be fitted to a range of biomass conversion technologies (combustion for electricity, gasification, chemical production etc.) using pre, post or oxy-fuel combustion capture technologies described earlier. The basic concept of a BECCS system is that the CO_2 is removed from the atmosphere by the growth of biomass and is released, captured and stored when the biomass is converted using CCS technology, thus removing emissions from atmosphere. The amount of negative emissions possible are dependent on many factors including the type and sustainability of the biomass used, as mentioned in section 1.3, the biomass conversion technology and the CCS conversion technology.

The International Energy Agency Greenhouse Gas research and development programme (IEAGHG) produced a report outlining the overall potential of six BECCS systems for emissions removal. The report considered the biomass supply and CCS chains alongside and a techno-economic assessment. Table 1.4 highlights the potential level of negative emissions for each technology based on the technical potential and the realisable potential. Technical potential, defined as "***the potential applying current or future technical constraints, which for BECCS is constrained by only resource availability, CO_2 storage capacity, and future technical performance of the technology"***. Realisable potential defined as ***" is technically feasible, determined by possible deployment rate and expected demand, hence increases in time with deployment rate (where deployment rate is dependent on the possibility of applying BECCS to existing energy conversion technologies and retirement rate of technologies it replaces). The realisable potential is hence a limitation applied to the technical rate by including capital stock turnover, final energy demand and deployment rate"*** (77).

Table 1.4: Greenhouse gas performance of BECCS technologies - technical potential and realisable potential (77)

BECCS Technology	Technical Potential Gt yr^{-1}		Realisable potential Gt yr^{-1}	
	2030	2050	2030	2050
PC- CCS Co-firing	-4.3	-9.9	-2.3	-3.2
CFB – CCS dedicated	-5.7	-10.4	-0.7	-1.3
IGCC – CCS co-firing	-4.3	-9.9	-1.1	-1.8
BIGCC – CCS dedicated	-5.7	-10.4	-0.3	-0.8

Note: Co-firing levels are 30% in 2030 and 50% in 2050

The technical potential for each of the BECCS routes for electricity generation is significant in both 2030 and 2050 and if reached could help to fill the gap between the required emissions reduction and the INDC's laid out in the Paris agreement (Figure 1.3). The realisable potential however indicates that co-firing in pulverised fuel plants has the largest potential for emissions reduction which would be increased in dedicated biomass pulverised fuel combustion systems. The continued growth in knowledge in dedicated biomass combustion since the IEAGHG report in 2011 due to stations like DRAX lends itself to dedicated BECCS systems.

The potential negative emissions of BECCS systems is shown in Figure 1.9 taken from the latest IPCC report (17) and the emissions compared to coal and gas used for electricity generation and coal to liquid processes. The use of bioenergy alone is shown to reduce emissions but when combined with CCS the potential negative emissions are clear.

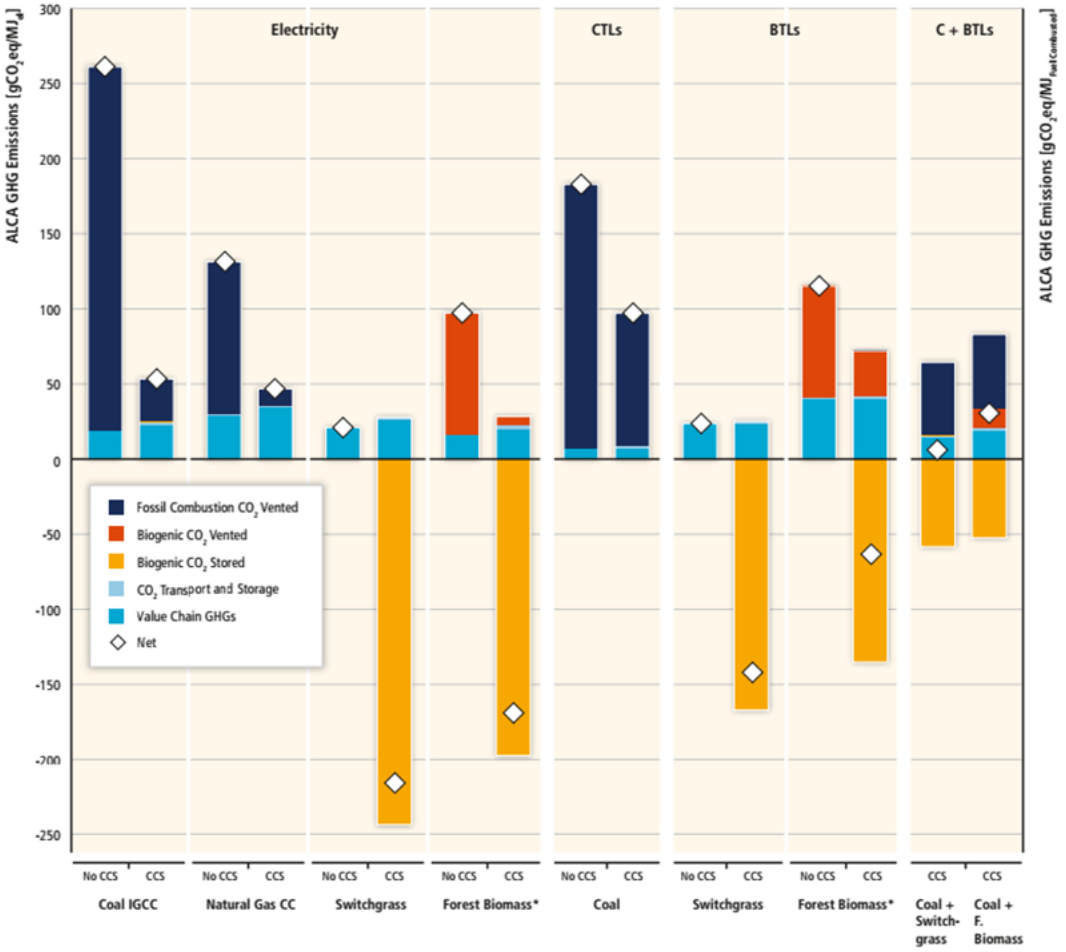

Figure 1.9: Comparison of emissions from electricity generation and alternative transport fuel technologies with and without CCS (17)

As outlined in the previous sections, the wide range of biomass conversion technologies and applicable capture and storage options make it difficult to determine the exact emissions reduction potential for a pulverised oxy-fuel plant, the focus of this work. However, Gladysz et al (78) investigated the emissions from a pulverised oxy-fuel plant using coal, co-firing with biomass (30%) and dedicated biomass. Although it is difficult to determine the exact boundary conditions, and therefore which emissions have been taken in to account, the author does give a comparative study of coal and biomass combustion compared to oxy-fuel with CCS emissions. It can again be seen in Figure 1.10 that the use of biomass alone in a standard combustion process lowers emissions compared to coal but when CCS is added then the reduction in emissions is significantly higher. The work also suggested that co-firing at levels of 30% biomass (the same levels as the IEAGHG proposed in 2030) are enough to generate negative emissions. However as would be expected the scenario with the largest potential for emissions reduction in an oxy-fuel environment is dedicated biomass systems.

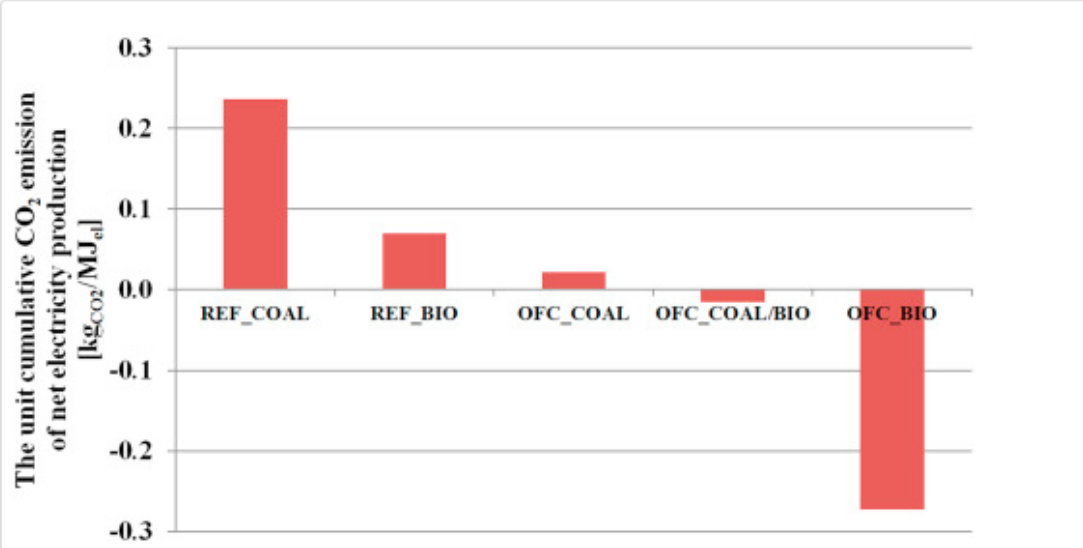

Figure 1.10: CO_2 emissions of net electricity production taken from (78) (OFC – oxy-fuel combustion)

However the author would again like to point out that the exact boundary systems are unknown and that this work displays the potential benefit of BECCS relative to coal CCS under the same boundary conditions rather than the exact expected emissions.

1.5.1 Competing carbon removal technologies

Alternative negative emissions and carbon dioxide removal technologies (CDR) are available including afforestation, reforestation, biochar, direct air capture and a number of geoengineering options such as ocean fertilisation. The benefit of these systems is that CO_2 emissions from non-stationary sources or sources where it is not economically viable to install CCS can be removed (79). Direct capture from air is an expensive technology due to the large gas volumes containing low levels of CO_2 and geoengineering options could have serious environmental risks (80).

Afforestation, reforestation and avoided deforestation have the potential to significantly reduce atmospheric CO_2 concentrations. A reduction in deforestation could remove 1.5-2.7 Gt CO_2 yr^{-1} but this would require a 50% reduction in the rate of deforestation (81). However the author noted that this scenario would be expensive and that a 10% reduction in deforestation that could remove 0.3-0.6 Gt CO_2 yr^{-1} is possible under current financial mechanisms. The use of afforestation and reforestation could potentially remove ~4Gt CO_2 yr^{-1} from the atmosphere (82) slightly less than suggested for the potential of BECCS.

Although reforestation and BECCS seem like fundamentally opposite options (plant trees rather than cut them down) BECCS requires a sustainable supply of biomass that could well

be provided by managed reforestation particularly in the case of pellet production for combustion in pulverised fuel plants (83).

1.6 CCS in operation today and what the future holds

1.6.1 CCS in operation today

According to the Global CCS institute there are currently 15 large scale projects in operation and 22 pilot and demonstration plants looking at all aspects of the CCS chain. A large scale project is defined as ***"at least 800,000 tonnes of CO_2 annually for a coal based power plant, or, at least 400,000 tonnes of CO_2 annually for other emissions-intensive industrial facilities (including natural gas-based power production"*** (84). In addition to the operating plants, six more are expected to become operational in 2017 making 21 operational plants with a capture capacity of 40 Mt yr^{-1}. Of the 15 plants currently in operation only 1 is for power generation (Boundary Dam project in Canada) and uses post combustion capture with the CO_2 used for enhanced oil recovery to capture up to 1Mt yr^{-1} of CO_2. The boundary dam power generation project in Canada commenced operation in October 2014, with CO_2 injection beginning in April 2015. In July 2016 the operators announced that over 1Mt of CO_2 had been captured since operations began in 2014. The majority of the remaining operating projects are in the gas industry, with eight in natural gas processing all with pre-combustion capture, two plants producing fertilizers, two plants producing hydrogen and one plant producing iron and steel, all with industrial separation (where CO_2 is removed in the actual process rather than an additional removal stage). Of the six plants expected to be operational at the end of 2017 two are for power generation, one with pre-combustion and one with post-combustion capture, both in America. In addition the first BECCS plant (the Illinois Carbon Capture and Storage Project) also in America and is due to come into operation in 2017 producing ethanol from corn using industrial separation technologies and onshore geological storage to capture 1Mt CO_2 yr^{-1} (84).

In addition to the 21 plants that are expected to be operational by the end of 2017 there are 27 others at various stages of planning with 11 in the power generation sector. China and America combined have plans to install 20 of the 27 projects, 7 of which are for power generation (84) suggesting that the pact made in 2014 between the two countries to collaborate in the development of CCS is being taken seriously. China is also at the initial stages of developing the only planned oxy-fuel power generation facility (Shanxi

International Energy Group CCUS Project) capable of capturing 2 Mt CO_2 yr^{-1} with an expected operational date in the 2020s (84).

1.6.2 Future of CCS

As mentioned earlier CCS is a fundamental set of technologies if we are to meet climate change targets and BECCS is set to become more and more important throughout the coming decades. The use of CCS in the UK is also seen as a crucial technology despite the withdrawal of a £1 billion UK government funded programme (85) in 2015 just days before the COP21 meeting in Paris. As a result of the cancellation of the four year funded programme, the two projects under consideration, Shell and SSE CCS project in Peterhead (Gas CCS) and the Capture Power project at DRAX, (Coal CCS) were immediately concluded (37). Since the initial announcement by DECC to withdraw the funding there has been considerable concern raised by a number of Government departments and bodies calling for more support to be given to the CCS industry. The ECCC called for stronger support for the industry as a whole and suggested that CCS capture plants, transportation and storage should receive separate support under a new funding mechanism alongside contracts for difference. The report also highlighted how CCS is integral in meeting emissions reduction in areas other than electricity generation and the possible wider implications the lack of CCS deployment may have in those sectors (10). A parliamentary advisory group went further and suggested that a "***CCS delivery company should be established that would be initially government owned but could then be subsequently privatised***" (86). This is particularly telling suggesting that a state owned company should be introduced under a conservative government at a time of austerity. In addition the report stated that:

- CCS is essential
- CCS works and can be deployed quickly at scale
- CCS in the power sector is an essential enabling technology
- CCS is the most cost effective method for the consumer to reduce emissions
- Heavy costs will be inherited by future consumers with any delay in CCS deployment
- There is no reason to delay the development of the UK offshore storage facilities
- An industrial capture contract providing financial incentives for the capture of CO_2 paid for by government is needed (86)

The government issued a response to the ECCC 2016 report on the future of CCS in the UK and reported that:

- A detailed reflection of the lessons learned during the four year CCS funding competition should be undertaken
- Discussions between the UK and the European commission and the European banking system to keep future financing options which were developed under the UK CCS funding competition open should be immediately facilitated (NER 300 – the world's largest funding programme for low carbon energy demonstration projects (87))
- The UK government should engage with the National Infrastructure Commission to explore options for CO_2 transport and storage development and to decide if the infrastructure should be of priority
- Clarification on the potential long term role of CCS and if this is needed in the 2020s, 2030s or if CCS is needed at all
- If new gas fired power stations are expected to be retrofitted with CCS and how this is to be achieved
- Clarification of the funding mechanisms for CCS
- Study of new the potential and existing storage sites in the North Sea
- Details of the requirements for the deployment of industrial CCS in the UK
- Potential development of a National Carbon Storage Authority in the UK (87)

The Energy Technologies Institute (ETI), a public-private partnership between industry and the UK government also highlighted the potential reduction in costs of CCS use for emissions reduction and that funding should be given for demonstration plants (88).

An additional report by the ETI solely focused on BECCS was also published in 2016 (89). The report suggested that:

- BECCS is a credible, scalable and efficient technology that is critical for the UK to meet emission targets
- There are no show stopping technical barriers to BECCS
- BECCS has the potential to deliver negative emissions
- The UK is particularly well placed to exploit the benefits of CCS due to storage availability, bioenergy expertise and the academic and industrial knowledge base in both bioenergy and CCS
- The UK is able to produce the majority of the required biomass with moderate imports needed to meet 2050 targets
- De-risking BECCS should be an integral part of the UK's future CCS strategy

- Deployment of BECCS is achievable by 2030
- Significant support is needed over the next 5-10 years to demonstrate a commercial deployment of BECCS technology and CO_2 storage supply chain (89)

As of yet the new UK government and the newly formed department of business, energy and industrial strategy have not yet clearly identified their technological routes to emissions reduction, however a new energy policy framework is expected from the current government sometime in 2017 (12). The government also stated in a 2016 response to the CCC progress on meeting carbon budgets, that CCS cost must be reduced if it is to play a part in the long term decarbonisation of the UKs economy but did also emphasise that this is before the findings in the report by the ECCC and Lord Oxburgh (86) were fully evaluated. The report also stated that the future approach to CCS in the UK will be set out in due course (12).

In contrast to the uncertainty in the UK the USA and China (the largest emission sources) agreed to expand joint research and development of advanced carbon capture systems as well as other low carbon technologies (90).

The IEA reported that CCS continues to be essential but is routinely overlooked in many main stream policy discussions as other low carbon technologies are preferred due to the rapid cost reductions and focus on energy efficiency. They stated that industrial CCS is one of the only options available for emissions reduction in that sector and that in the electricity sector CCS provides a solution to emissions reduction whilst using fossil fuels to increase energy security (76).

The reported concluded that:

- Long term commitment and stability in policy frameworks are critical
- Early opportunities for CCS deployment are available and must be cultivated
- Investment in storage must be a priority and the most significant impediment to large scale deployment of CCS is the geological storage
- Availability of CCS in the future is dependent on investment today and an expanded pipeline project allowing for integration in the future is required
- Community engagement is essential
- BECCS should be deployed as soon as possible to understand if negative emissions can be achieved allowing for the modification of climate change models and future emissions scenarios (76).

1.7 Conclusions

The consensus of scientists and the governments of the world regarding climate change is now clear through the agreement made in Paris. However if we are to meet the global averaged temperature targets decided upon in Paris then significant levels of renewable technologies must be deployed to reduce anthropogenic emissions. One of the most important technologies is CCS, which has the potential to reduce emissions from the power sector and the potential ability to achieve negative emissions if utilised alongside biomass. Although the technologies are widely utilised in climate change models there are only a limited number of CCS sites in operation today but more are set to come online over the coming decade. The importance of CCS in the UK meeting its own emissions targets has also been highlighted by a number of UK government departments.

The many different technology options and technology combinations associated with a complete CCS system offer a wide breadth of research opportunities. The work in this thesis is part of a wider research group that is focussing on oxy-fuel combustion. The project, called BIO-CAP UK comprises of both industrial partners and academic institutions and aims to better understand the operational behaviour of an oxy-fuel plant alongside the potential emissions reductions through LCA and a techno-economic analysis. The operational behaviour of the oxy-fuel plant is determined through laboratory scale work (the focus of this thesis), pilot scale experiments at the PACT facility in Sheffield and CFD modelling (incorporating the kinetic models derived in this work).

2 Aims and objectives of thesis

As can be seen from the previous chapter, carbon, capture and storage is a complex technology with many potential research areas. This work focuses on oxy-fuel combustion and in particular how the change in combustion atmosphere from conventional air to an O_2/CO_2 environment effects the combustion behaviour of a solid fuel. In order to investigate this, the combustion behaviour of six industrially relevant fuels, two North American white wood biomass pellets, a torrefied biomass pellet and three coals were investigated in air and oxy-fuel atmospheres ranging from 5-30% O_2/CO_2. The two main stages of combustion were analysed, the first the devolatilisation behaviour and the second char combustion, the rate limiting step of the overall combustion process.

In order to determine the combustion behaviour of fuels in air and oxy-fuel environments the following questions were asked:

1. How does the change in combustion atmosphere effect the overall combustion behaviour of the fuels?

2. How is the devolatilisation process affected by the change in combustion atmosphere and does this differ between biomass and coal samples?

3. What effect does the devolatilisation atmosphere have on the resulting char properties?

4. How is the char combustion process affected by the change in combustion atmosphere and does this differ between biomass and coal samples?

5. Are there any differences in the combustion behaviours of coal, biomass and torrefied biomass and are there any lessons that can be learnt by industry?

6. Can chars produced using a TGA replicate chars produced using a drop tube reactor and is this a reliable method for the investigation of char oxy-fuel combustion?

3 Literature review

3.1 Introduction

This chapter is a literature review relevant to the topics researched in the thesis and gives an introduction to coal, biomass and torrefied biomass and their composition. The focus then shifts to their decomposition pathways during both pyrolysis and combustion in air and oxy-fuel environments. The devolatilisation and char combustion behaviour is described and the identification of kinetic combustion regimes associated with the above combustion steps analysed. The chapter finishes with a discussion on the formation of nitrogen pollutants and this is effected by the change to oxy-fuel environments.

3.2 What is coal?

Coal is a solid fossil fuel utilised by humankind for thousands of years as a source of energy (91). The pressures of climate change are resulting in the overall decline of coal use but it is set to be utilised as an energy source for the foreseeable future, particularly in developing nations (18, 92).

Coal is found in seams in the Earth's crust and originated form deposited vegetation that underwent chemical and physical changes due to a process called coalification. The coalification process starts with the decaying of the deposited vegetation followed by burying due to sedimentation, compaction and finally transformation of the plant remains to organic rock. The deposited coal differs throughout the world due to the localised conditions at the seams at the time of coalification, the different organic material deposited (coal type), the degree of coalification, that is the extent of the chemical and physical processes (coal rank) and the range and amount of impurities present in the vegetation (coal grade) (93). Coal itself is composed of both organic constituents, mainly carbon, hydrogen and oxygen with small amounts of nitrogen and sulphur, and ash forming inorganic constituents typically silicon, aluminium, iron, magnesium, potassium, sodium, titanium, calcium and phosphorus (94). The organic fractions of the coal consist of macerals, microscopic components of coal (95) which can be linked to the type of plant material originally deposited (96). The macerals can be classified into three main categories, vitrinites, liptinites and intertinites. Vitrinite is formed from the woody tissue derived from lignin and cellulose (bark and roots) of the original biomass and tend to contain more oxygen than other macerals. Liptinites derive from plant resins, spores and algal remains and

contain higher levels of hydrogen than other macerals. Intertinites derive from the same source as vitrinites but have undergone thermal or biological oxidation (such as forest fires) resulting in a high inherent carbon content (93, 97).

3.2.1 The coalification process and coal classification system

Coalification the geochemical process that transforms deposited plant material into coal can be described by the following steps:

Peat → Lignite → Subbituminous coal →Bituminous coal →Anthracite

This overall coalification process can be split into three stages, the peat forming process which is the microbiological degradation of the cellulose present in the plant material, the conversion of the lignin into humic substances and the condensation of these substances to form larger coal molecules (93). The type of vegetation decaying and the decomposition environment are important factors in determining the nature and quality of the coal seams. The chemical and biological composition of the plant material differed over geological periods and the depth, temperature, acidity and movement of water differed between deposit sites all affecting the coal composition. The geochemical phase is the result of increased temperatures and high pressure over millions of years experienced, due to the burying of the vegetation, and is the most important factor in the coalification process. The greater the extent of the coalification process the less moisture, volatiles, hydrogen and oxygen are present in the coal while the carbon content is increased relative to the original vegetation deposited (93). The chemical processes that occur during each stage of coalification are outlined in Table 3.1.

Table 3.1: The coalification process (98)

Materials	**Partial Process**	**Main Chemical Reaction**
Vegetation	Peatification	Bacterial and fungal life cycles
Peat	Lignification	Air oxidation, followed by decarboxylation and dehydration
Lignite	Bituminization	Decarboxylation and hydrogen disproportioning
Bituminous Coal	Preanthracitization	Condensation to small aromatic ring systems
Semianthracite	Anthracitization	Condensation of small aromatic ring systems to larger ones; dehydrogenation
Anthracite	Graphitization	Complete carbonification

The extent of the coalification process and the conditions at the deposition sites result in coals with different measurable properties which are used to rank and classify coal types. The classifications of coals can be seen in Table 3.2 (91) with anthracite coals undergoing coalification to the greatest extent.

Table 3.2: Classification of coals

Coal Rank	Volatile Matter (%)	Hydrogen (wt%)	Carbon (wt%)	Oxygen (wt%)	Heating Value (MJ/kg)	$\frac{C}{H}$	$\frac{C+H}{O}$
Anthracite							
Meta	1.8	2.0	94.4	2.0	34.4	46.0	50.8
Anthracite	5.2	2.9	91.0	2.3	35.0	33.6	42.4
Semi	9.9	3.9	91.0	2.8	35.7	23.4	31.3
Bituminous							
Low–Vol	19.1	4.7	89.9	2.6	36.3	19.2	37.5
Med-Vol	26.9	5.2	88.4	4.2	35.9	16.9	25.1
High-Vol A	38.8	5.5	83.0	7.3	34.7	15.0	13.8
High-Vol B	43.6	5.6	80.7	10.8	33.3	14.4	8.1
High-Vol C	44.6	4.4	77.7	13.5	31.9	14.2	6.2
Subbituminous							
Sub A	44.7	5.3	76.0	16.4	30.7	14.3	5.0
Sub B	42.7	5.2	76.1	16.6	30.4	14.7	5.0
Sub C	44.2	5.1	73.9	19.2	29.1	14.6	4.2
Lignite							
Lignite A	46.7	4.9	71.2	21.9	28.3	14.5	3.6

Note: Values determined on a dry ash free basis

3.2.2 Chemical composition of coal

The structure of coal is complex (99) and a general structure of a bituminous coal as described by De Abreu et al (100) can be seen in Figure 3.1. The coal is presented as a polymeric matrix of cyclic aromatic carbon rings (benzene and polycyclic aromatic hydrocarbons) linked with other aromatic structures by bridges consisting of aliphatic groups, oxygen functional groups and oxygen or sulphur atoms (100). Nitrogen may also be present in forms such as amines but as the coal matures the nitrogen forms into more condensed structures (pyridines and pyrroles). Sulphur is present as sulphide, disulphide or mercaptan in both aliphatic and aromatic structures (101).

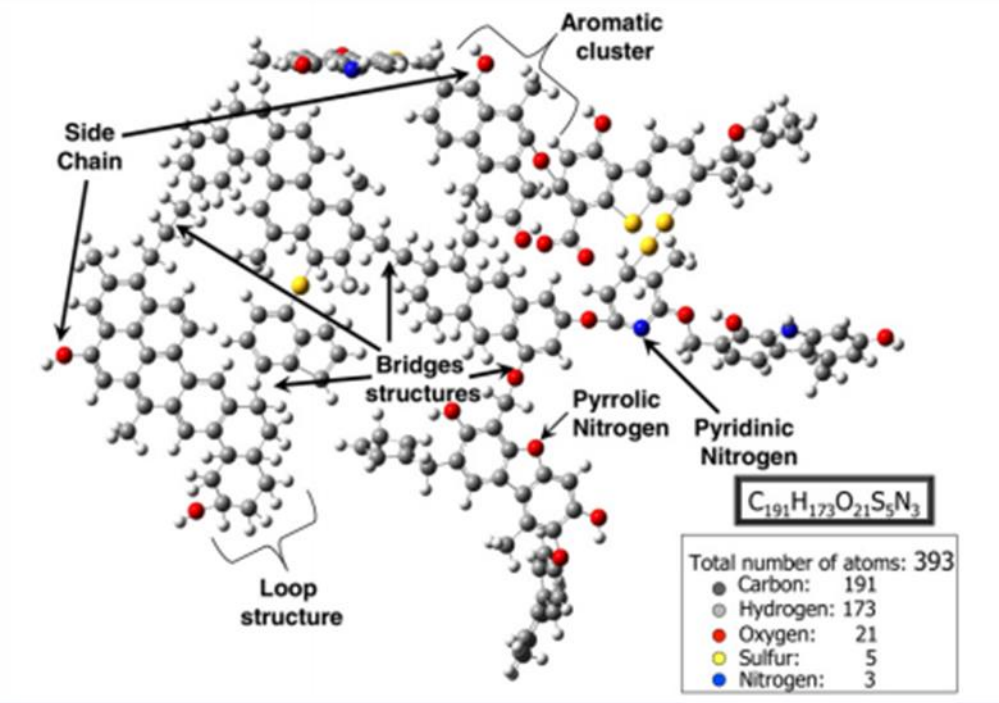

Figure 3.1: Chemical composition of bituminous coal (100)

3.3 What is biomass?

The term biomass can include a wide range of material that is directly or indirectly derived from photosynthesis reactions such as wood fuel, wood derived fuel, fuel crops, agricultural by-products or waste and animal by-products (102). In this work only woody biomass is investigated.

3.3.1 The structure of biomass

Wood is a complicated structure and comprised of three major organic compounds cellulose (40-50%), hemicellulose (15-30%), lignin (16-33%) and minor substances such as pectin, protein, extractives, starch and inorganics (ash) making up the remaining (103). An example of the structure of lignocellulosic biomass can be seen in Figure 3.2.

3.3.1.1 Cellulose

Cellulose, a fibrous material, provides strength to the biomass cell walls. Cellulose is a long chain, linear polymer molecules that contain 5000-10,000 glucose monomers, and has high molecular weight (10^6 or more). The individual cellulose molecules organise to form

cellobiose units consisting of two glucose anhydrite units. The decomposition of cellulose occurs at temperatures in the range of 240-350^{o}C (104).

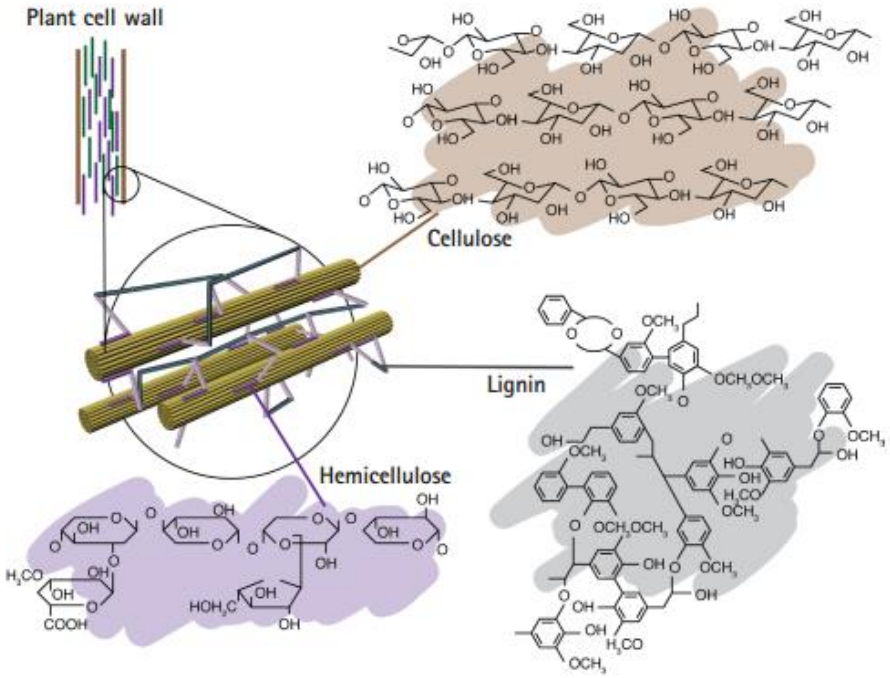

Figure 3.2: Plant cell wall and lignocellulosic biomass composition (105)

3.3.1.2 Hemicellulose

Hemicellulose molecules are less structured than cellulose and consist of only 100-200 sugar monomers resulting in a lower molecular weight (104) and the exact composition varies widely among different woody species (106). Hemicellulose molecules are a mixture of polysaccharides derived from glucose, galactose, mannose, xylose, arabinose and glucuronic acids. Decomposition of hemicellulose occurs at temperatures between 200-260^{o}C and produces more light volatiles and less tars and chars than a cellulose molecule (104).

3.3.1.3 Lignin

Lignin is a complex polymer that penetrates the spaces between cellulose and hemicellulose adding strength to the wall (105). Lignin has no exact structure and is mainly derived from three aromatic alcohols, p-coumaryl, coniferyl and sinapyl (106) which are connected in weakly linked branched structures (107). These units produce high molecular weight materials rich in carbon (108).

3.3.1.4 Inorganics

The inorganics found in biomass influence the combustion process and the composition of the ashes remaining. The main inorganic components can be split into two categories, the first ash forming components are Si, Ca, Mg, K, Na, P, S, Cl, Al, Fe and Mn and secondly the heavy metals Cu, Zn, Co, Mo, As, Ni, Cr, Pb, Cd, V, Hg (109). These elements act as nutrients during the plants growth and are present in the ash after combustion (110).

3.3.2 Introduction to white wood pellets

The main drawbacks of utilising biomass over coal and gas is the low energy density, high moisture content and high heterogeneity. These can be lessened with the production of pellets with consistent quality, low moisture, higher energy density and homogenous size and shape. Pellets can be produced from many materials and used in many different processes. In this work the focus is on pellets produced for energy production that are made from wood, but pellets may also be made from peat, herbaceous biomass or waste. This type of pellet can be split into three categories dependent on the type of biomass used to produce the pellet. White pellets are produced from wood without bark, brown pellets are produced from materials including the bark and black pellets are produced from steam exploded or torrefied wood (111). The white wood pellet is widely used in the energy sector and can again be split into three categories dependent on the measurable properties of the pellet, such as the elemental composition and the inorganic elements. The white wood pellet classification scheme can be seen in Table 12.3 in the Appendix. The biomass sample used in this work is a North American white wood pellet, made from Pine.

3.4 What is torrefied biomass?

Torrefaction is a pre-treatment process where biomass is heated in the absence of oxygen at temperatures between 200-300^{o}C to produce a material with improved chemical and physical properties relative to the original biomass material. The mild pyrolysis process reduces the moisture content and drives off oxygen rich volatiles that have a low calorific value. The loss of volatiles is associated with the decomposition of the hemicellulose component which binds the cellulose structures in the cell wall. The result is a more energy dense fuel that is easier to mill, transport and store that and has the potential to further decrease carbon emissions relative to the raw biomass sample (112). Although torrefied pellets are not as widely available as the white wood pellets in today's market the

improvement in properties such as milling behaviour and higher energy density, may make this type of fuel more favourable in the future (113).

3.5 Combustion of solid fuels

Solid fuels have been utilised for energy production through combustion in pulverised fuel power plants for decades. The fundamental combustion process of solid fuels whether coal, biomass or torrefied biomass is the same (114, 115) and can be described by the process outlined in Figure 3.3 and discussed in the following sections.

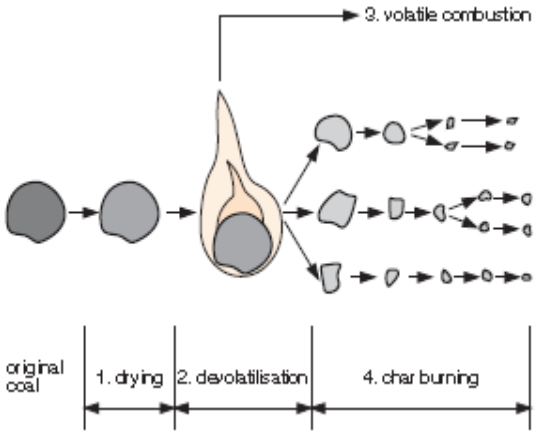

Figure 3.3: Overall combustion process of coal (116)

3.5.1 Heating and drying

In a combustion system the pulverised fuel (pf) particle enters a boiler at relatively low temperatures and are rapidly heated whereby the surface temperature increases and inherent moisture within the particles porous structure evaporates (117). High moisture content can delay particle heating, which in turn can increase the overall combustion time by a factor of 3 to 5 (118). This can be a problem in biomass fuels where moisture contents can be up to 50 wt% (119) compared to bituminous coals that contains 1-12 wt% (120). The evaporation of the moisture involves simultaneous heat and mass transfer processes which can be seen in Figure 3.4.

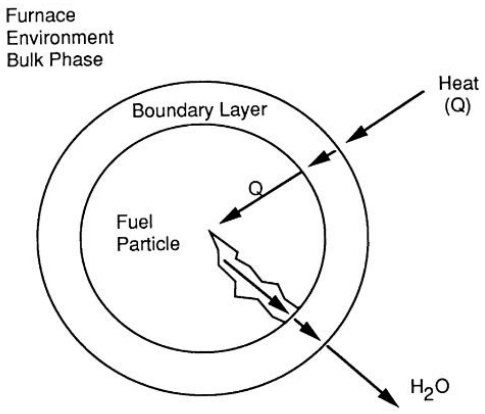

Figure 3.4: Schematic of the particle heating and drying process (114)

Heat is driven from the furnace environment to the particle surface by radiation and convection and then transferred to the centre of the particle by conduction through the particle. In order to remove all of the moisture present, the core of the particle must reach temperatures of 120°C. When the particle is heated sufficiently the moisture is converted to the vapour phase and is then able to move through the porous structure to the surface of the particle, through the boundary layer and into the furnace environment (120). The loss in moisture results in an overall reduction in the size of the particle and the internal pores may shrink. In high temperature environments the vaporised moisture may become trapped within the particles increasing internal pressure causing the particle to fracture (114).

The drying stage is a heat transfer-limited process and is influenced by the furnace temperature, particle size, porosity and the initial moisture content of the fuel and can be described by the following equation (114):

$$q = k_1 A_1 [\frac{T_1 - T_2}{x_1}] \quad \text{Eq 3.1}$$

Where q is the flow of heat, k_1 is the thermal conductivity of the fuel, A_1 is the surface area, T_1 is the temperature at the particle surface, T_2 is the temperature at the centre of the particle and x_1 is the radius of the particle.

3.5.2 Devolatilisation

The second step in the combustion process, outlined in Figure 3.3, is the devolatilisation step. This refers to the thermochemical conversion under external heating that results in a change in the chemical composition and physical characteristics of a fuel particle (118). As

the particle is heated (temperatures above 200°C) the fuel starts to decompose and light volatile gases are released. These volatiles are driven out of the fuel particle and prevent oxygen, present in the combustion environment, from penetrating the particle and oxidising the carbon, hydrogen, and sulphur present in the particle. As the thermal energy is able to penetrate the particle but the oxygen is not, the particle is heated in a pyrolysis environment (121). The escaping volatiles burn much more rapidly than the char, the remaining fraction after devolatilisation, and therefore play an important role in flame ignition, flame stability, flammability limits (122) and the formation of pollutants such as NO_x (107). The volatiles when combusted can account for up to 36% of the total heat output of coal and 70% for biomass (123) and the devolatilisation process determines the properties of the remaining char such as char yield, porosity and composition, all important factors in the overall char combustion properties (107).

The devolatilisation process can be divided into three physical processes, (i) pyrolysis or the decomposition chemistry, (ii) the transport of the volatiles through the porous network and (iii) the secondary reactions that change the chemical products and/or cause decomposition of the volatile products on the particle walls or pores (122).

The first physical process, pyrolysis, is similar in both coal and biomass. An overview of the pyrolysis process can be seen in Figure 3.5 and is described here. Pyrolysis involves a two stage mechanism; the first is the breaking of bridges between aromatic structures in coals and the breaking of long polymeric chains in biomass, producing tars and chars. The second stage is the formation of non-condensable volatile matter via the decomposition of functional groups. Typical volatiles produced from coal and biomass pyrolysis can be seen in Table 3.3 and the species produced and yields are fuel and devolatilisation condition dependent.

Table 3.3: Typical volatile species formed during pyrolysis of coal and biomass (124)

Coal	Biomass
Tar	Formaldehyde
H_2O	Acetaldehyde
CO_2	Formic Acid
CO	Acetic Acid
CH_4	Methanol
NH_3	Phenol
HCN	Acetone
COS	Levoglucosan
SO_2	-

NOTE: Biomass typically contain the species found in coal in addition to those listed above.

The tars produced as a result of the breaking of long chains are composed of high molecular weight molecules such as aromatic and phenolic hydrocarbons and aliphatic hydrocarbons which are liquids at room temperature. The tars are very reactive and may also undergo secondary reactions such as cracking and repolymerisation within the structure of the particle (125). The tars and non-condensable volatile species are mobile throughout the porous network and secondary reactions can occur between the, evolved species themselves, with the active sites present in the particle or with the combustion atmosphere surrounding the particle.

The process starts at the particle surface when the outside of the particle reaches the pyrolysis temperature (>200^{o}C). The volatiles are driven off at the surface and a layer of char (a carbon rich solid with minor fractions of oxygen and hydrogen (91)) is formed. This process is repeated as the inner layers of the particle reach the required pyrolysis temperature (121). Hence a particle undergoing devolatilisation has a char zone which has undergone pyrolysis, an active zone where pyrolysis is occurring within the particle and an unreacted internal zone (120, 126).

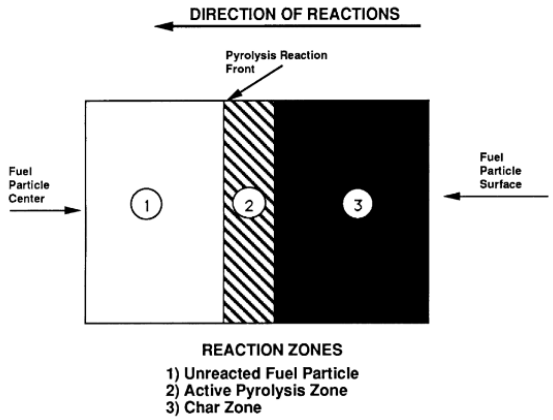

Figure 3.5: Solid particle pyrolysis process (114)

The devolatilisation behaviour of solid fuels is affected by the temperature of the combustion environment, the heating rate of the particle, particle size, moisture content and fuel type (122, 123, 125). The peak temperature, the time a particle is held at the peak temperature, and the heating rate are important factors in the devolatilisation stage. As the temperature, residence time and heating rates are increased, the yield of volatiles is also increased (117, 118, 121, 127, 128) and as a result char yield decreased. Increasing particle size generally results in larger char yields but the extent of the particle size on volatile yield is fuel dependent (122, 129, 130). The composition of the fuel plays an important role in

devolatilisation and the differences between coal and biomass devolatilisation behaviour are outlined in the following sections.

3.5.2.1 Devolatilisation of coal

The hypothetical structure of a coal macromolecule (part a of Figure 3.6) and the changes to it during pyrolysis can be seen in Figure 3.6. During pyrolysis of coal the weakest bridges break first, that is the aliphatic and functional groups, producing molecular fragments (depolymerisation) separate from the macromolecule (part b of Figure 3.6). These fragments are known as metaplast or liquid coal components and have fluid properties (122). The fluidity normally occurs in coals containing carbon contents of 81-92wt% (bituminous) but is also dependent on oxygen and hydrogen concentration and the heating rate of the coal at which devolatilisation occurs. At high heating rates plasticity is increased until heating rates become too high for coals to plasticise and instead crosslinking, the recombination of metaplast within the particle structure increasing stability, is the preferred route (122).

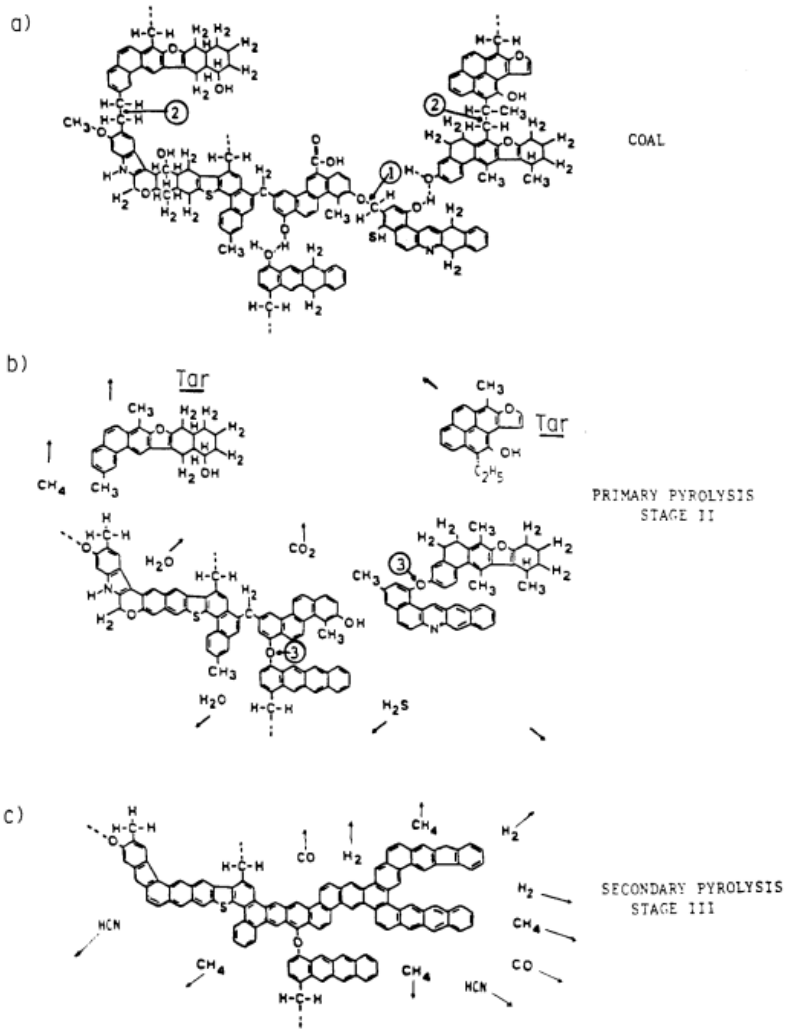

Figure 3.6: Hypothetical coal molecule during the stages of pyrolysis (131)

The metaplast fragments will either be released as tar or crosslink back into the macromolecular structure and stabilise the evolving char matrix (132). In order for the metaplast to be released as tar, the fragments must be small enough to vaporise under typical pyrolysis conditions (133). The tar can consist of hundreds of thousands of organic species with average molecular weights of 350 (132) and with a chemical structure that resembles the chemical structure of the parent coal (122).

Alongside the production, vaporisation, tar formation and crosslinking of the metaplast the functional groups decompose to release CO_2, aliphatic gases, CH_4 and H_2O. These light gases/vapours may be ignited causing flaming combustion, or aid in crosslinking, CH_4 by a substitution reaction with a larger molecule, CO_2 by condensation after a radical is formed when a carboxyl is removed and H_2O by the condensation of two OH groups to produce an ether link. The degree of cross-linking is important to determine the release of tar, volatiles and the properties of the char such as porosity and overall yield (133). The degree of crosslinking can be affected by the coal rank, the level of oxidation within the vicinity of the particle and the particle heating rate. As the rank of the coal increases (degree of coalification), the temperature at which crosslinking reactions occur is increased (134, 135). Work by Deshpande et al. (134) found that crosslinking occurs in lignites at 650K and in bituminous coals at 800K and attributed this to the lower carboxyl functional groups found in higher rank coals. The effect of the increased heating rate in an inert atmosphere was also studied in this work and found that crosslinking was decreased in a coal sample when heated at 20,000^{o}C min^{-1} compared to the same coal heated at 5^{o}C min^{-1} (134). This trend was also seen in work performed by Solomon et al. (135). The devolatilisation of coal in air was found to increase the degree of crosslinking at low temperatures and was attributed to the formation of oxygen containing functional groups that participate in the formation of crosslinks within the coal macromolecule (135).

During the secondary stage of devolatilisation (part c Figure 3.6) the char and tar formed during the primary stage decompose. This results in the formation of light gases CH_4, CO, H_2 as well as light nitrogen species, and ultimately soot, being released as the remaining aliphatic side chains are broken and ring condensation occurs in the solid matrix. Secondary pyrolysis occurs at temperatures above 1150K and is strongly temperature and rank dependent (136). The char, the remainder of the macromolecule, and its combustion properties are discussed in section 3.5.3.

3.5.2.2 Devolatilisation of biomass

The decomposition pathway of biomass differs from coal due to the composition of the fuel. As mentioned in section 3.3.1 biomass contains cellulose, hemicellulose and lignin and contains higher levels of volatiles resulting in much smaller char yields than those seen in coals (123, 137). Typically, the temperature at which pyrolysis starts in biomass is about 160-250°C compared to 350°C for bituminous coal. The amount and nature of the pyrolysis products is again dependent on heating rates and final temperatures, and the conditions seen in pulverised fuel combustion favour gaseous volatiles rather than tar formation (123).

The devolatilisation and pyrolysis mechanisms of a biomass can be seen if Figure 3.7. A wide range of gaseous products are released during the devolatilisation stage and are dependent on which part of the biomass is undergoing pyrolysis.

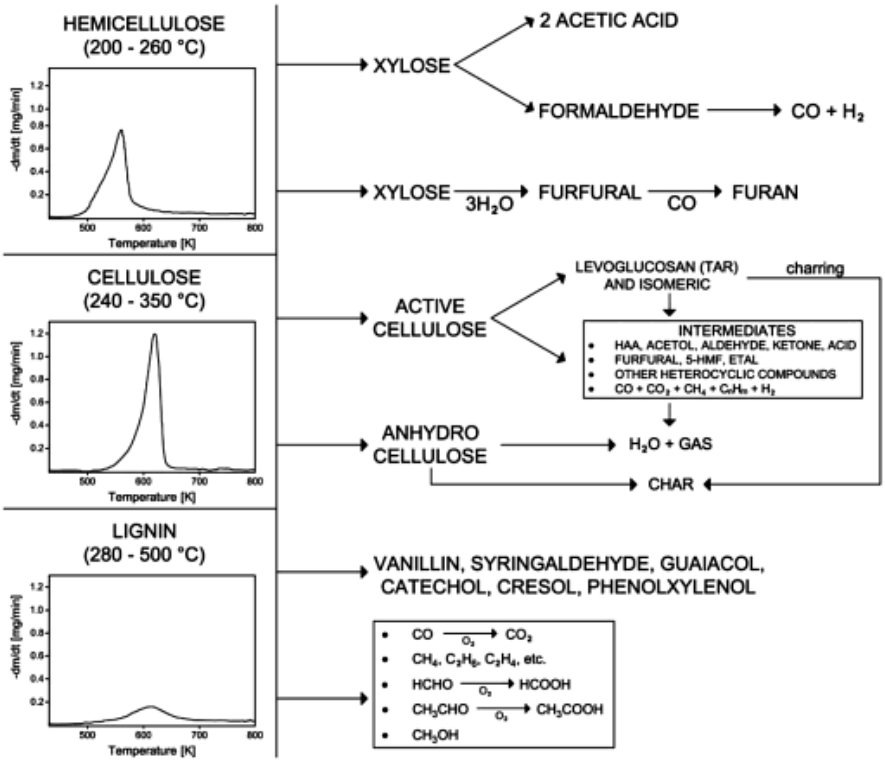

Figure 3.7: Devolatilisation pathway of ligno-cellulosic biomass (126)

The hemicellulose and then the cellulose and lignin start to decompose with long polymeric chains cracking to produce vapours which leave the particle via the pores formed during the drying stage. The volatiles are comprised of these vaporised chains which ignite when reacted with oxygen producing flaming combustion. During this stage a wide range of gases are produced dependent on the temperature and part of the plant undergoing

devolatilisation. Hemicellulose is the first to decompose (240-260^{o}C) forming acetic acid, formaldehyde, carbon monoxide, hydrogen, furfural and furan. The first stage in the decomposition of cellulose is the production of active cellulose which will then produce charcoal by dehydration or levoglucosan depending on the temperature. The levoglucosan will then decompose further to form hydroxyl-acetaldehyde, acetol, furfural, CO and a range of other compounds. The final fraction of the plant that starts to decompose is the lignin which produces aromatic compounds and the largest fraction of the char. The aromatics are produced as the straight chain links of the lignin decompose with phenols, carbon dioxide, hydrocarbons, formic acid, acetic acids, methanol and higher fatty acids also being produced (126). Lignin also plays an important role in the pellet production process. In woods containing around 10% moisture the lignin begins to soften at ~130^{o}C leading to a higher abrasive resistance pellet decreasing the amount of fines produced (111).

The exact quantity of the cellulose, hemicellulose and lignin content differs between biomass types and so effect both the physical and chemical processes during combustion (123).

3.5.2.3 Ignition and combustion of volatiles in both coals and biomass fuels

The ignition and combustion of the volatiles released during pyrolysis of the fuel particle results in the flaming combustion stage seen in Figure 3.3. The ignition of a particle can occur due to two scenarios depending on particle composition, size and temperatures. The first scenario is homogeneous ignition which is the ignition of the volatiles released during pyrolysis of the raw fuel when oxidised by the furnace atmosphere (gas-gas combustion). The second heterogeneous ignition relates to the direct attack of the oxidiser on the char matrix (gas-solid combustion). Heterogeneous ignition is associated with higher rank low volatile containing coals (138) homogeneous with high volatile content coal and biomass.

The homogeneous ignition begins with the ignition of the volatiles and oxygen mixture, present from either the combustion atmosphere or derived from the fuel, close to the particle surface. Once ignited a gas flame surrounds the particle and prevents the external oxidiser from reaching and attacking the surface of the particle and causing heterogeneous ignition of the char (138). The low carbon content, low heating value and high moisture content of biomass fuels relative to coals makes biomass more difficult to ignite and can cause problems with flame stability in pf fired systems. However once ignited the burning rate of biomass fuels is significantly higher than coals due to the higher volatile content, the rapid release of the volatiles and the remaining high porosity particle increasing surface area

and availability of active sites for oxygen to penetrate (123). In practice the devolatilisation, ignition and combustion of the volatiles does not occur in isolation and a small fraction of char oxidation (heterogeneous reaction) occurs alongside (123), the mechanisms of which are outlined in the next section.

3.5.3 Char combustion

The heterogeneous char oxidation reaction is the final step of solid fuel combustion (Figure 3.3). The char oxidation step can be several orders of magnitude slower than the devolatilisation step and is often the rate determining step in the overall combustion process (91). The same combustion mechanisms and main chemical reactions outlined below can be used to describe the combustion of both coal and biomass chars.

The char combustion mechanisms can be described by the following five steps (122):

1- Diffusion of reactant gases (O_2, CO_2, H_2O) through a boundary layer surrounding the particle to the solid surface of the particle and into the pore structure.

2- Adsorption of reactants on the solid

3- Chemical reaction with the particle surface

4- Desorption of the surface reaction products

5- Diffusion of the gaseous reaction products into the bulk gas phase

The overall char combustion reactions are described in R 3.1 – R 3.3 (122):

$$1 - \text{Char} + \frac{1}{\varphi}O_2 \rightarrow \left(2 - \frac{2}{\varphi}\right)CO + \left(\frac{2}{\varphi} - 1\right)CO_2 \qquad \text{R 3.1}$$

$$2 - \text{Char} + CO_2 \leftrightarrow CO + CO \qquad \text{R 3.2}$$

$$3 - \text{Char} + H_2O \rightarrow H_2 + CO \qquad \text{R 3.3}$$

Reaction R 3.2 is known as the Boudouard reaction and is favoured at higher temperatures (>700^{o}C) (139).

The reaction pathway of the char is not solely dependent on the chemical composition to the same extent as in the devolatilisation step. Instead the physical structure of the char, surface area, particle size, pore structure and inorganic content (ash) and active site concentration play a significant role (122). Active site theory proposes that reactions occur at favoured sites on the surface of the char which are attributed to i) carbon edges or defects

throughout the carbon structure (the higher the degree of coalification the fewer carbon defects (140)), ii) inorganic impurities (ash content) and iii) heteroatoms e.g. hydrogen, oxygen, nitrogen and sulphur (141).

At each of the active sites the following may occur i) reactant adsorption onto the particle surface (chemisorption), ii) migration of intermediates, and iii) desorption of the gaseous products resulting in a free carbon site (141-143). Both the adsorption of oxygen to the char surface and desorption of the gaseous products can occur to a single site or dual site mechanisms. The single site mechanism requires one available carbon site which can lead to the simultaneous production of gaseous species e.g.:

$$O + C_f \rightarrow C(O) \qquad \text{R 3.4}$$

$$CO_2 + C_f \rightarrow C(O) + CO \qquad \text{R 3.5}$$

C(O) denotes a carbon site filled with atomic oxygen and C_f denotes a free carbon site.

The dual site mechanism requires two free active sites to produce an intermediate which may migrate to a new site to form a more stable surface intermediate C(O) or vice versa.

$$O_2 + 2C_f \rightarrow 2C'(O) \qquad \text{R 3.6}$$

$$C'(O) \leftrightarrow C(O) \qquad \text{R 3.7}$$

C'(O) denotes a mobile site and C(O) an immobile (or less mobile) site.

The surface intermediates may then undergo desorption by the single site mechanism or the dual site mechanism:

$$C(O) \rightarrow CO + C_f \qquad \text{R 3.8}$$

$$C'(O) + C'(O) \rightarrow CO_2 + C_f \qquad \text{R 3.9}$$

The active site theory assumes the following:

1 – Localised adsorption via collisions with active sites

2 – One adsorbed molecule or atom per site due to strong valence bond

3 – A constant surface mechanism (chemisorption/migration/desorption)

4 – The surface coverage is less than a complete monolayer

The reactions R 3.1 - R 3.9 occur due to both the chemical steps (active site theory), and the diffusion of volatiles out and reactant gases in throughout the porous structure of the char.

During the combustion of char, the reactant, usually oxygen, diffuses from the combustion atmosphere through the boundary layer to the surface of the char and penetrates the porous particle. The oxygen reacts with the carbon on the surface and at the pore walls producing CO, which can react in the gas phase in the area surrounding the particle to form CO_2. As the char is depleted the pore structure evolves affecting the overall surface area, active site concentrations and gas diffusion (of both the evolution of the remaining volatiles and penetration of the reactant gases present in the combustion atmosphere) within the pore structure which further inhibits the combustion process (91).

The rate limiting step in the oxidation of the char can be controlled by the rate of chemical reaction (the adsorption of the reactant, the surface reaction or the desorption of the products) or by the gaseous diffusion (bulk or pore diffusion) of reactants or the combustion products (CO, CO_2) (136). A three zone theory (Figure 3.8) of char oxidation based on reaction rates has been developed to identify which of the above limiting steps (chemical or physical) control the rate char combustion (91, 136, 142).

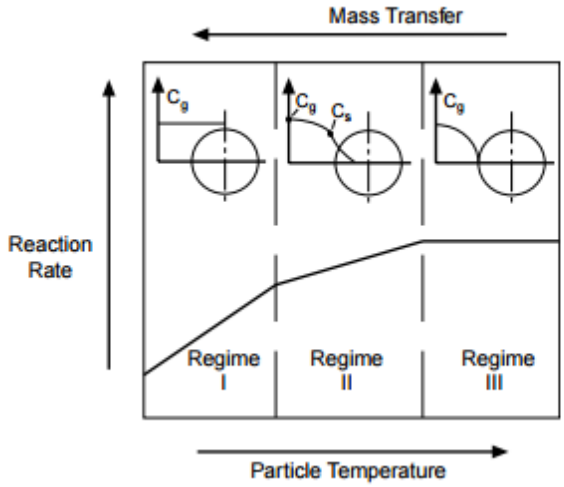

Figure 3.8: Three zone char oxidation rate controlling regime (144)

In regime I the combustion rate is fully controlled by the chemical reaction (kinetically controlled). Under these conditions the diffusion rates are much faster than the chemical reaction rates ensuring kinetic control (127). In regime I the reactant concentration (C_g) throughout the particle is equal to the concentration in the bulk gas phase in the combustion atmosphere (91, 107, 136) which can be determined by the Thiele modulus and the effectiveness factor. The Thiele modulus is defined as the ratio of overall reaction rate to internal diffusion rate, and the effectiveness factor is defined as the ratio of the actual

reaction rate to that which would occur if all the surface throughout the internal pores were exposed to oxygen at the same condition as that existing at the external surface of the char particle (145). The Thiele modulus (φ) and the effectiveness factor (η) are expressed by:

$$\varphi = \left(\frac{d_p}{2}\right)\left(\frac{A_G.\rho_P.k_s.C_o^{m-1}}{D_e}\right)^{0.5} \qquad \text{Eq 3.2}$$

$$\eta = \frac{d_\rho.R_c}{4\varphi^2.D_e.C_o} \qquad \text{Eq 3.3}$$

Where, d_p is the surface mean diameter (m), A_g the BET surface area ($m^2\ kg^{-1}$), ρ_P the particle apparent density ($kg\ m^{-3}$), k_s the intrinsic reactivity coefficient ($kg\ m^{-2}kPa^{-n}\ s^{-1}$), C_O the oxygen concentration at the particle surface ($kg\ m^{-3}$), m the true reaction order, D_e the effective pore diffusion coefficient ($m_2\ s^{-1}$) and R_C the observed reaction rate ($kg\ m^{-2}\ s^{-1}$) (145). In regime 1 the Thiele modulus should be small and the effectiveness factor should ideally be unity (127). This regime occurs at low temperatures, below 873K in coal chars (144) and with char particles small enough so that the diffusion rate is much faster than the chemical reaction rate (127) .

Regime II is characterised by control due to both chemical reaction and pore diffusion causing the particle to burn at both the surface and internally in the porous structure. Reactants can partially penetrate the particle but uniform oxygen levels within the particle cannot be reached due to diffusion limitations (91, 107, 136). In regime II the Thiele modulus is greater than unity and the effectiveness factor less than unity (127). This regime occurs at temperatures between 873-1073K in coal chars (144).

In Regime III the reaction only occurs at the surface of the char particle, as the reactant gas cannot penetrate the particle and the rate is controlled by diffusion through the boundary layer (91, 107, 136). This regime occurs at temperatures above 1073K in coal chars (144). Regime I is the focus of char reactivity study which can be found in section 7.

3.6 Combustion in oxy-fuel environments

As outlined in the introduction, oxy-fuel combustion occurs in an O_2/CO_2 atmosphere rather than an air atmosphere. The switch to an oxy-fuel combustion environment effects both the operation of the boiler, e.g. flame temperatures, flame ignition and stability, changes to heat transfer properties and reduction of SOx and NO_x emissions (122) as well as the combustion behaviour of the fuel. In this work the effect of the combustion environment on the fuel combustion behaviour is investigated. The thermo-physical properties of CO_2 and N_2 are

outlined in Table 3.4 and their influence on devolatilisation and char combustion are explained in the following sections.

Table 3.4: Properties of gases at 1123^{o}C and atmospheric pressures (51)

Property	**N_2**	**CO_2**	**Ratio CO_2/N_2**
Density, ρ (kg/m^3)	0.244	0.383	1.6
Molecular weight (kg/kmol)	28	44	1.6
Thermal conductivity, k (W/mK)	0.082	0.097	1.2
Specific heat capacity, Cp (kJ/kmol k)	34.18	57.83	1.7
Specific heat capacity, Cp (kJ/kg K)	1.22	1.31	1.1
Heat sink, ρ.Cp (kJ/m^3 K)	0.298	0.502	1.7
Dynamic viscosity, μ (kg/m s)	4.88e-05	5.02e-05	1.0
Kinematic viscosity, v (m^2/s)	2.00e-04	1.31e-04	0.7
Mass diffusivity of O_2 in X (m^2/s)	1.7e-04	1.3e-04	0.8

The increased density of CO_2 results in lower gas velocities in the boiler which increases the particle residence times. The heat capacity of CO_2 is higher than N_2 and as a result the flame temperatures are reduced at the same oxygen levels. If the adiabatic flame temperatures seen in air combustion are to be achieved then the oxygen levels in an oxy-fuel boiler need to be increased. The combination of the increased density and the increased heat capacity (Cp.ρ) results in a reduction in the combustion gas temperature which may affect char burnout (122). The reduction in the diffusivity of oxygen in CO_2 relative to N_2 limits the reaction rate of the solid fuels which in turn reduces the heat release and particle temperature. This in addition to the decrease in gas temperatures due to the higher heat capacity of CO_2 will further reduce the combustion rate at the same oxygen concentrations (51). Existing boilers have been carefully designed to operate efficiently based on the radiative and convective heat transfer properties seen in air combustion. The radiative heat transfer, the main contributor to heat transfer from a flame (51), is controlled by flame temperatures and the radiative properties of gas. The CO_2 and H_2O that would be present in an operational boiler as part of the recycle stream, have higher emissivity's compared to N_2 leading to the increased radiative heat transfer compared to conventional air fired combustion (61, 62, 146, 147). The increase in radiative heat transfer in the flame zone (furnace) results in a lower temperature gases entering the convective sections (superheater, economiser and primary air heater) lowering the heat transfer in these sections (61). In addition to the gas temperature the convective heat is a function of the Reynolds number (velocity, viscosity), the Prandtl number and the thermal conductivity of the flue gas. The changes in gas volumes in addition to the above make determining the

changes to radiative and convective transfer difficult to determine and CfD modelling is required to understand the full impact (51).

3.6.1 Devolatilisation and ignition in oxy-fuel environments

The devolatilisation process in oxy-fuel follows the same principals as in air, that is, heating up of the particle, pyrolysis and the consumption of the evolved volatile species. The replacement of N_2 with CO_2 in a boiler leads to lower flame temperatures due to the higher heat capacity of CO_2 as shown in Table 3.4. In order to increase flame temperatures similar to those seen in air combustion and to improve flame stability in pulverised fuel boilers an increase in O_2 concentration (>21%) is required (51, 148). If the flame temperature is reduced relative to that seen in air combustion then the heating up of the particle (Eq 3.1) as it enters a flame and resulting devolatilisation will differ and the extent of this is an important factor in the combustion efficiency of a pf boiler. The lack of any commercial scale oxy-fuel plant, and as a result lack of operating experience at that scale, means that the knowledge surrounding oxy-fuel combustion is derived from pilot and laboratory scale experiments.

Work carried out by Molina et al (148) investigated ignition and devolatilisation properties by entraining bituminous coal into gas mixtures with either N_2 or CO_2 with oxygen concentrations of 21 and 30%. The work was carried out using a laminar optical entrained flow reactor at constant temperature. They identified the different phenomena that occur during particle combustion and the difference between the combustion environments. Molina et al described the first stage, i.e. the heating up process of a non-reactive particle to determine how the effect of the combustion environment according to Eq 3.4.

$$\frac{dT_p}{dt} = \frac{-3}{C_p \rho_p r_p}\left[\varepsilon\sigma\left(T_{part}^4 - T_w^4\right) + h\left(T_{part} - T_g\right)\right] \quad \text{Eq 3.4}$$

Where T_p, T_w and T_g are the particle, wall and gas temperatures, C_p, ρ_p, r_p and ε are the particle heat capacity, density, radius and emissivity respectively; σ is the Stephen Boltzmann constant and h is the coefficient for convective heat transfer. In the above equation the only properties that are functions of gas properties are T_g and h. The temperature of the gas T_g was kept constant in all environments so the only possible effect on the heating rate as a function of atmosphere is the heat transfer properties of CO_2 and N_2. The heat transfer coefficient h was calculated from the assumption that the Nusselt number is equal to two. This suggests that the Reynolds number is expected to be low (149) and that the particle is small enough to move at the same speed as the entrained gas

atmosphere. This assumption is equipment and operation condition specific and care should be taken when determining the true value of Nu.

$$\mathrm{Nu} = \mathrm{hD}\lambda^{-1} \quad \text{Eq 3.5}$$

Where D is the particle diameter and λ the thermal conductivity. The only gas property that effects the initial particle heating is the thermal conductivity and as the ratio of the thermal conductivity of N_2/CO_2 is close to one at the temperatures used in their work. The result is that the difference in the heating rates of an inert particle is negligible between N_2 and CO_2 atmospheres. Toftegaard noted that this is only true in the case of equal gas phase temperatures T_g and noted that this is not necessarily true in the case of boilers (51). In relation to work carried out in this thesis the same phenomena as outlined by Molina is expected as the fuels are heated using a temperature programmed thermogravimetric analyser at the same heating rate in all environments. That is T_g would be identical in both cases.

The ignition behaviour was also determined by Molina et al. (148) and it was found that a minor delay in ignition behaviour was seen when coal was combusted in oxy-fuel environments (at the same oxygen levels). The delay was attributed to the increase in heat sink (ρ.Cp) in CO_2 based atmospheres absorbing more of the heat that is chemically released than is absorbed in air combustion. Although a slight delay in ignition was seen no measurable difference in the duration of the volatile combustion after ignition was seen. The authors increased the levels of oxygen present in both the N_2 and CO_2 based atmospheres and found that ignition was accelerated due to an increase in the localised mixture reactivity. It was also found that when the particle of coal was combusted in 30% O_2 in CO_2 (at which point the flame temperatures are similar to air) that the ignition time and devolatilisation time were similar to those seen when the particle was combusted in air (148).

Murphy et al (150) used the same reactor as above to investigate the effect of increased O_2 levels in N_2 and proposed that the increased devolatilisation rate with increasing O_2 is the result of [1] the closer proximity of the volatiles flame to the coal particle, and [2] a higher temperature volatile flame. The volatile flame temperature increased from 2190K at 6% O_2 to 2860K at 36% O_2 (150).

Riaza et al (151) investigated the ignition behaviour of coal and biomass blends in air and O_2/CO_2 environments with oxygen levels of 21-35% in an entrained flow reactor. Again it

was found that the ignition temperature was increased when N_2 is replaced by CO_2 at the same O_2 concentrations. This was attributed to the higher specific heat of CO_2 causing a decrease in the gas temperature and therefore a reduction in the particle temperature. When the oxygen concentration was increased up to 35% the ignition temperature decreased in both the coal and coal/biomass blends. This was attributed to the increase in the mass flux of O_2 to the surface of the particle, the rate of devolatilisation and the oxidation rate of volatiles (151).

Work has been performed by several research groups to determine the char combustion behaviour and the effect of char production atmosphere on volatile release. Rathnam et al (152) produced chars from coals using a drop tube reactor in N_2 and CO_2 atmospheres and as a result investigated the devolatilisation behaviour through the change to char properties. When the chars were produced in a CO_2 environment, enhanced devolatilisation in CO_2 atmospheres was seen compared to N_2. This was also seen in work by Irfan et al (153), who used a TGA to determine devolatilisation behaviour of coal and a biomass sample. In both cases the effect of CO_2 was attributed to the char gasification reaction (R 3.2) occurring alongside devolatilisation at increased temperatures (152, 153). Rathnam et al (152) also measured the surface area of the chars produced in N_2 and CO_2 atmospheres and found that, due to the char gasification reaction in CO_2 atmospheres (R 3.2), the surface area had increased by as much as 40%. As mentioned earlier the availability of active sites is of great importance in the char combustion stage.

The review of devolatilisation in oxy-fuel environments has shown that the change in combustion atmosphere will affect the ignition time but is not expected to affect the devolatilisation rate after ignition. The heat transfer to the particle is affected by the gas temperatures that would be reduced in a CO_2 atmosphere in a pf boiler at the same oxygen levels relative to air. Increased oxygen levels will increase flame temperatures, devolatilisation rates, diffusion rates of O_2 and consumption of the volatiles, due to localised mixture reactivity. Enhanced devolatilisation is also seen in CO_2 atmospheres due to the char gasification reaction, and its effects on char combustion in oxy-fuel environments is reviewed in the next section.

3.6.2 Char combustion in oxy-fuel environments

Char combustion is the rate limiting step in the overall combustion process. The change in combustion environment and its effect on this step must be understood in order to develop

efficient combustion systems. The reaction steps associated with the combustion of chars is outlined in section 3.5.3.

There are several ways in which the change in combustion atmosphere can influence the combustion of char (122, 154):

- The lower diffusivity of O_2 in CO_2 (Table 3.4) reduces the availability of O_2 at the particle surface reducing the char burning rate
- The CO_2 in the bulk gas stream could reduce the particle peak temperature due to the higher heat capacity of CO_2, reducing the burning rate
- The adsorption of CO_2 on to the particle surface could inhibit the adsorption of O_2 through competition for available active sites, reducing the burning rate
- Direct gasification of the char by CO_2 could contribute to the overall process increasing the combustion rate

The majority of the experimental work on char combustion is reported in terms of char reactivity (127, 150, 152, 155-161) and the approach to this is outlined in the next section.

3.7 Reaction rates and chemical kinetics

All chemical reactions take place at a definite rate and are dependent on the conditions of the system, such as temperature, radiation effects, concentration of reactants, and the presence of a catalyst or inhibitor (107). A change in the above conditions would result in a change in reaction rates which will effect process performance. In this work the effect of the reactants, fuel, O_2 and CO_2 and the temperatures of the reactions are investigated to determine chemical kinetics and model the devolatilisation and char combustion processes.

In the combustion process an understanding of the chemical kinetics of both the devolatilisation stage and char combustion stage (the rate limiting step) are important in the design and modelling of the complete boiler system and process performance. The reactivity and the determination of the kinetic parameters, such as the activation energy and pre-exponential factor, can be used to compare the behaviour of a range of fuels and the different conditions of a system, in this case the change in combustion environment (162).

3.7.1 Devolatilisation reaction rates

The reaction rate is dependent on the energy and frequency of collisions between reacting molecules and the temperature at which the reaction is taking place. The reaction rate constant can be summarised by the Arrhenius equation given in Eq 3.6:

$$k = Ae^{-E_a/RT} \quad \text{Eq 3.6}$$

k - the reaction rate constant (s^{-1})

A - the pre-exponential factor (s^{-1})

E_a - activation energy (kJ mol^{-1})

R - gas constant (8314 kJ $mol^{-1}.K^{-1}$)

T - temperature (K)

In the Arrhenius equation k is the rate constant, A is the frequency factor and is related to the number of collisions in the reaction is specific to each reaction and is temperature dependent. E_a is the activation energy and is the minimum energy needed for the reaction to occur. R is the gas constant and T is the temperature at which the reaction is occurring (163).

The reaction schemes associated with the multiple reactions seen in coal and biomass combustion make extracting kinetic data difficult (164). As a result the mass loss of a sample as it undergoes heating (performed using thermogravimetric analysis) can be used to represent these reactions globally and allow for the determination of apparent first order kinetic parameters. This popular method (165) of extracting kinetic data is known as the one step global model (166) or the reaction rate constant method (164) and is utilised throughout this work.

At any given temperature, if the mass loss with time is assumed to be the result of one or more first order reactions, dependent on the concentration of only one reactant, then the rate constant k as a function of temperature can be described by the following relationship (164):

$$k = -\frac{1}{m-m_\infty} . \frac{dm}{dt} \quad \text{Eq 3.7}$$

Where m is the initial mass of the sample, m∞ is the terminal mass and dm/dt is the derivative mass loss taken from experimental data. The experimental data can be used to obtain the rate constant k and can be used to identify the kinetic parameters A and E_a through the following equation:

$$\ln k = \ln A - \frac{E_a}{RT} \quad \text{Eq 3.8}$$

These kinetic parameters and rate constants can then be used to compare fuels and the change in experimental conditions. In this work the difference between coals, biomass and

a torrefied biomass in terms of devolatilisation in nitrogen, carbon dioxide and increased oxygen environments is investigated.

3.7.2 Char reaction rates

As mentioned earlier the char combustion stage is the rate limiting step for the overall combustion of solid fuels. The heterogeneous reactions and mechanisms that occur are outlined in section 3.5.3. The heterogeneous conversion and char reactivity are determined by both the chemical composition and the physical characteristics (surface area etc.) (167). It is difficult to measure each of the physical and chemical characteristics as they vary as the char undergoes conversion, i.e. the development of the porous network changes as combustion proceeds. As a result a global kinetic model incorporating all of the reactions based on mass loss is usually employed to determine the overall rate of the char combustion process (127).

The description of the char reaction rate can be based on different definitions dependent on the Regime in which the combustion is taking place (See Figure 3.8). The simplest form of the reaction rate can be taken directly from experimental conversion data under low temperature, isothermal conditions and is known as the apparent rate (141). Several kinetic models have been developed to express the conversion of char based on fundamental assumptions regarding structural parameters which are outlined below (142, 168, 169).

The simplest kinetic model is the volumetric model which assumes the reaction surface area decreases linearly as conversion proceeds resulting in a homogenous reaction throughout the particle (170) and the overall kinetically controlled reaction rate can be described by:

$$\frac{dx}{dt} = R_{app}\,(1 - x)$$

Eq 3.9

R_{app} – The apparent reaction rate constant (s^{-1})

x – Conversion

dx/dt – Rate of conversion

The shrinking core model (171) assumes that a char is composed of an assembly of uniform particles and that the reactions take place on the surface of these particles. The space between the spherical particles represents the porous network of the char. As conversion

proceeds the initial structure is maintained but the individual particles shrink. The overall kinetically controlled reaction rate is described as:

$$\frac{dx}{dt} = R_{app}.(1-x)^{2/3} \quad \text{Eq 3.10}$$

The random pore model (172) assumes the char comprises of overlapping cylindrical surfaces reducing the overall surface area available for the reaction to proceed relative to the assumptions made in the shrinking core model. The available surface area changes as the reaction proceeds due to pore growth and the destruction and coalescence of the porous network (represented by the cylindrical surfaces) which is more representative than the assumption made in the volumetric model.

$$\frac{dx}{dt} = k\,(1-x)[1-\Psi \ln(1-x)]^{1/2} \qquad \text{Eq 3.11}$$

Where Ψ relates to the pore structure of the unreacted char.

The apparent rate constant (R_{app}) can again be related to the Arrhenius equation (Eq 3.6) and apparent kinetic parameters derived using Eq 3.8. However this does not take into account the influences of mass transport limitations and the nature of the char porosity (169). In the case of heterogeneous reactions the pre-exponential factor, A, condenses the influences of reactant pressures and availability of reactants at the active sites into one term when the apparent reactivity is determined.

The reaction rate of char is determined by the number of active sites, that is the concentration of carbon edges and defects, mineral matter and trace elements, and the availability of reactants at these active sites (142). The reaction of char occurs at the char surface, and by measuring the char surface area the reaction rates can be determined per unit area (intrinsic reactivity) giving a greater understanding of both char structure as a result of the devolatilisation conditions and the char combustion processes.

The intrinsic reactivity can be determined from the char surface area and the apparent reaction rate as follows (169):

$$R_i = \frac{R_{app}}{S} \qquad \text{Eq 3.12}$$

R_i – The intrinsic reaction rate constant (g m^{-2} s^{-1})

R_{app} – The apparent reaction rate (s^{-1})

S – Surface area (m^2 g^{-1})

Under Regime I conditions, that is that the reactant gas concentration is uniform throughout the particle and the reaction rate is chemically controlled, an n^{th} order rate equation can be applied to incorporate the effect of O_2 partial pressure on the reaction rate. This method does not take into account the mass transfer limitations associated with Regime II or III (142, 169). The n^{th} order rate equation can be seen in Eq 3.11, the temperature is modelled by an Arrhenius approach and the influence of the partial pressure of the reactant (in this case O_2) is incorporated by an n^{th} order term:

$$R_i = A_i \exp\frac{-E_a}{RT} \cdot P_{O_2}^n / S \qquad \text{Eq 3.13}$$

R_i – Intrinsic reactivity derived from R_{app} and S (g m^{-2} s^{-1})

A_i – Pre-exponential factor in relation to partial pressure (s^{-1} Pa^{-n})

E_a – Activation energy (kJ mol^{-1})

R - Gas constant (8314 kJ $mol^{-1}.K^{-1}$)

T - Temperature (K)

P_{O2} – Partial pressure of oxygen (Pa)

n –Reaction order

S – Char surface area (m^2 g^{-1})

The n^{th} order term relates to the reaction order with respect to oxygen and is expected to fall between 0 and 1 and roughly between 0.5 and 1 (127). The true reaction order and true kinetic parameters can be extracted from the experimental data.

Several more complicated models have been developed to express the adsorption and desorption processes seen in Regimes II and III (142, 168, 169).

Work by Chen et al (60) performed a review of experimental studies investigating the combustion rates of coal chars to determine which of the reactions and mechanisms (section 3.5.3) are at play at a variety of experimental temperatures (with reference to the three zone theory mentioned in section 3.5.3) and oxygen conditions. As reviewed by Chen et al. Figure 3.9 shows three regions were the experimental data were obtained: Region A at low temperatures and oxygen concentrations from 0-100%; Region B high temperatures and high oxygen concentrations; Region C high temperatures and low oxygen concentrations. In Region A the char oxidation reaction, R 3.1, is the dominant reaction. In this temperature range (typical TGA experimental temperatures) the rate is kinetically controlled and falls into regime I according to the three zone theory (60).

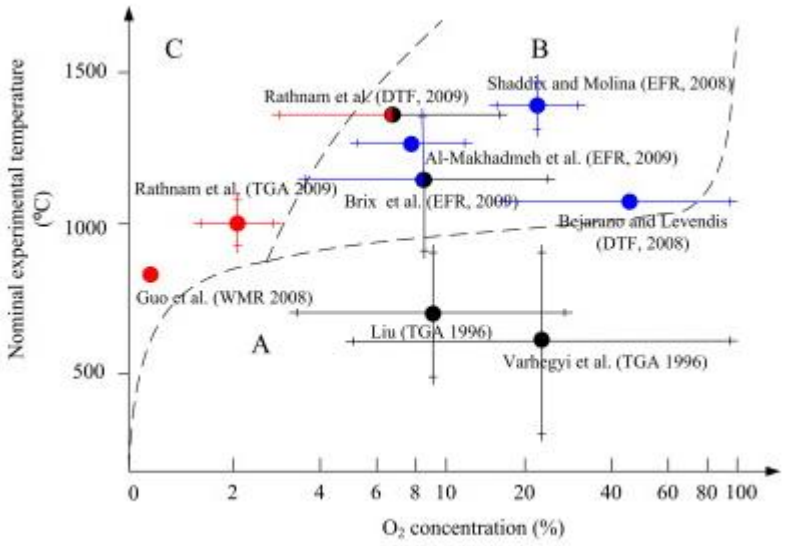

Figure 3.9: Char oxidation and gasification experiments in oxy-fuel conditions (60)

In Region B the char oxidation is again deemed dominant but the char consumption is defined as regime II or III as char combustion is dominated by internal or external diffusion. The temperatures at which the experiments were performed in this region are typically seen in drop tube reactors and entrained flow reactors. The slower diffusion rates of O_2 in CO_2 is shown to slow char combustion at a given oxygen concentration (60). In Region C, defined as low O_2 and high temperatures, the char gasification reaction, R 3.2, is dominant. The work in this thesis investigates the combustion behaviour of high temperature, high heating rate chars combusted at temperatures associated with Region I of the three step model. As the experiments fall into Regime I the intrinsic reactivity model described above is deemed sufficient for the modelling of the char reaction kinetics.

3.8 NO_x formation in solid fuel combustion

Emissions of NO_x from combustion processes continue to be an environmental concern (173) and are regulated under the Industrial Emissions Directive. The NO_x emissions from large combustion plant are primarily nitric oxide (NO) with smaller amounts of nitrogen dioxide (NO_2) which is harmful to human health (173). The NO is converted to NO_2 in the atmosphere through the reaction with O_2 to form ozone (O_3) a secondary pollutant (119). Nitrous oxide (N_2O) can also be formed from the reaction of NO with a char (119) but the formation of N_2O is significant in fluidised bed combustion and is negligible in most combustion systems (173).

There are three main routes for the formation of NO_x ($NO + NO_2$) during combustion:

- Thermal NO_x formed by the reaction of oxygen and nitrogen in the air at elevated temperatures of about 1800K (119).
- Prompt NO_x formed from the reaction of partial combustion products with atmospheric N_2 at temperatures cooler than those for thermal NO_x (174) and
- Fuel NO_x from the oxidation of the nitrogen chemically bound within the fuel (119) at temperatures as low as 973K in coal combustion (174)

In solid fuel combustion systems the fuel NO_x is the major source of NO with a small contribution from thermal NO_x (173). When 100% biomass is combusted the flame temperatures are lower than in coal combustion so the contribution from thermal NO_x to the total NO_x is lower than that seen in coal combustion (119, 175).

The fuel bound nitrogen, the main source of NO_x emissions, is released in the volatile or char combustion stage and the split is dependent on the fuel structure, the temperature and particle residence time. The partitioning of the nitrogen species is important as the N released in the volatile stages is controlled more easily using staged burners (176) or low NO_x burners, where up to 90% of the fuel nitrogen is converted to N_2 under fuel rich conditions. The N present in the remianing char burned under lean conditions in the secondary burner stage is largely converted to NO (119).

The nitrogen compounds released during the devolatilisation stage are primarily released as NH_3 and HCN which undergoes the following reaction during combustion:

$HCN + 5/4O_2 \rightarrow NO + CO + 1/2H_2O$ R 3.10

$HCN + 3/2O_2 + NO \rightarrow N_2O + CO_2 + 1/2H_2O$ R 3.11

$HCN + 3/4O_2 \rightarrow 1/2N_2 + CO_2 + 1/2H_2O$ R 3.12

$NH_3 + 5/4O_2 \rightarrow NO + 3/2H_2O$ R 3.13

$NH_3 + 3/4O_2 \rightarrow 1/2N_2 + 3/2H_2O$ R 3.14 (121)

In the char combustion stage the nitrogen is mainly oxidised to NO and N_2O which are then partially reduced to N_2. The NO is reduced through reactions with carbon in the char, CO and NH_3. The N_2O is again reduced through reaction with char and CO but may also be reduced through the effects of temperature. The reduction pathways of the NO and N_2O released in the char combustion stage are outlined below (121):

$NO + NH_3 + 1/4O_2 \rightarrow N_2 + 3/2H_2O$ R 3.15

$NO + 2/3NH_3 \rightarrow 5/6N_2 + H_2O$ R 3.16

$NO + C(Char) \rightarrow 1/2N_2 + CO$ R 3.17

$N_2O \rightarrow N_2 + 1/2O_2$ R 3.18

$N_2O + C(Char) \rightarrow N_2 + CO$ R 3.19

$N_2O + CO \rightarrow N_2 + CO_2$ R 3.20

In general the NO and N_2O emissions are increased as the nitrogen in the fuel is increased and the higher the volatile content of the fuel the higher the NO emissions and lower the N_2O emissions. This is due to the higher NH_3 released in the devolatilisation process which results in NO formation rather than HCN which produces both NO and N_2O. Biomass is a lower rank fuel than coal with a higher volatile content that would tend to produce higher levels of NH_3 leading to formation of NO rather than N_2O (121).

Di Nola et al. (177) investigated the partitioning of nitrogen in terms of NH_3, HCN and HCNO during pyrolysis in a nitrogen atmosphere of a bituminous coal and biomass samples using a TGA. They found that a higher percentage of fuel bound nitrogen is converted into volatiles for biomass than for coal during pyrolysis and that NH_3 is the main N-product released in the evolved volatile species.

Tsubouchi et al (178) investigated the nitrogen release from two low rank coals using a drop tube reactor (10^4-10^5 ^oC min^{-1}) and compared it to previous work that utilised a fixed bed reactor (400^oC min^{-1}). They reported that when the coals were pyrolysed using the DTR, more of the coal bound nitrogen was retained in the char and that the remainder was released as tar N, HCN and NH_3. During the slower pyrolysis the main N emission was found to be N_2. The effect of the residence time (0-120 s) of the fuel within the DTR at 1300^{o}C was also investigated and it was found that as the residence time increased the N_2 and NH_3 yield increased and the char bound N was decreased. This may be the result of the enhanced devolatilsation that would be expected with an increase in residence time at these temperatures as discussed earlier. The increase in NH_3 could also be an indicator of the enhanced devolatilisation as this was found to be the main component of the volatile yield in the work performed by Di Nola et al (177).

Tsubuchi also investigated the effect of temperature on nitrogen release during pyrolysis of coals. A fixed bed reactor heated at 400^{o}C min^{-1} to 1000-1350^{o}C was used to investigate the

pyrolysis behaviour of ten coals. It was shown that as the reactor temperature was increased N_2 increased significantly and that HCN and NH_3 also increased but not significantly. The amount of char N was significantly decreased and nitrogen in the tar also decreased but not to the same extent. The increase in N_2, HCN and NH_3 with temperature originates from the volatile N, tar N and char N (179). This suggests that as the pyrolysis temperature increased an increase in volatile N is seen due to the enhanced devolatilisation.

3.8.1 NO_x emissions in oxy-fuel combustion

Oxy-fuel combustion has the potential to reduce NO_x emissions to about 1/3 of those seen in conventional air combustion (50) as the result of several mechanisms outlined below:

- Decrease in thermal NO_x due to the low concentration of N_2 from air in the combustor
- The reduction in recycled NO_x
- The interaction between the recycled NO_x and fuel bound nitrogen

(180).

Okazaki et al investigated NO_x emissions in a combustion environment containing 21% O_2 in CO_2 at 1450K. At these conditions ~80% of the flue gas is recycled back into the combustor to give the high levels of CO_2 and it was found that 50% of the recycled NO is reduced to N_2 and that the recycling of the NO in the flue gas was the dominant mechanism for the reduction of NO_x under these conditions (180).

Buhre et al (50) suggested that the emission of NO_2 (ppm) may be higher than in air combustion due to the recycling of the flue gas, the lower gas volumes seen in oxy-fuel combustion and the decrease in efficiency due to the required oxygen production plant and CO_2 compression units required.

Shaddix and Molina et al. (181) investigated NO_x formation during combustion of pulverised coals and their chars in N_2 and CO_2 based environments with 12, 24 and 36% oxygen concentration using a down fired entrained flow reactor. They noted that when the coal was fed into the reactor the NO_x emissions increased with increasing oxygen and that at oxygen concentrations of 24 and 36% the NO_x formed in CO_2 environments is decreased. As the oxygen concentration was increased the degree of fuel N conversion also increased. In a Pittsburgh coal sample the degree of conversion increased from 20-55% when the O_2 concentration was increased from 12-36% in N_2. When a CO_2 based atmosphere was used at the same oxygen concentrations the fuel N conversion was ~10% lower at O_2

concentrations greater than 12%. The decrease in fuel N conversion in a second coal also showed the same trends in terms of change from N_2 to CO_2 and change in O_2 concentrations. A char was made from the Pittsburgh coal and combusted under the same conditions as above to determine the split between volatile NO_x and char NO_x. It was found that at high O_2 concentration that the volatile generated NO_x is a larger fraction of the total NO_x. This was associated with the effect of the increased O_2 concentration on the volatile combustion temperatures. The change to CO_2 based environments was shown to have a small influence on char N conversion at the higher O_2 levels and a negligible influence at 12% O_2. For the two coals it was found that the CO_2 diluent has a much larger effect on the fuel N conversion during devolatilisation at increased O_2 concentrations.

Farrow et al (182) investigated the pyrolysis behaviour of biomass in N_2 and CO_2 atmospheres using a DTR at 900, 1100 and 1300^{O}C and a residence time of 50-600 ms. In both pyrolysis atmospheres the fuel N released into the volatile phase increased with temperature as a result of the increase in volatile yield. The char N yields were determined and it was found that when a fuel was pyrolysed in CO_2 the higher volatile yields result in higher proportions of nitrogen being transformed into the gaseous volatile phase. They stated that as the reduction in char N is observed that the NO_x formation during combustion of biomass in oxy-fuel may also be reduced.

3.9 Conclusions

Coal and biomass, although different fuels, in terms of their chemical composition, undergo the same physical processes during combustion, that is drying, devolatilisation and finally char combustion. The switch to an oxy-fuel combustion atmosphere is not expected to effect the initial drying stage as this is a heat transfer process. The change in combustion environment has been shown to effect the devolatilisation behaviour, with delays in ignition times and an increase in the ignition temperatures which is attributed to the decrease in local particle temperature due to the higher heat capacity and increase in thermal sink of the CO_2 based atmosphere. The change to oxy-fuel combustion can affect the char combustion stage in several ways. The addition of high levels of CO_2 in the oxy-fuel environment can enhance the Boudouard reaction increasing the rate of combustion, this is particularly important under Regime I conditions (kinetic control). The rate of char combustion may be reduced due a number of mechanisms: the first , the lower diffusivity of O_2 in CO_2 reducing the availability of O_2 at the particle surface which is important under

Regime II and III (diffusion control); secondly, CO_2 in the bulk gas phase could again reduce particle temperature as seen in the devolatilisation stage; and finally the competition between the O_2 and CO_2 for the active sites present throughout the chars porous network. Oxy-fuel combustion atmospheres have also been shown to potentially improve NO_x emissions through the reduction of thermal NO_x and enhanced N release during devolatilisation. The work in this thesis investigates the combustion behaviour in air and oxy-fuel environments through combustion experiments and the use of devolatilisation and char combustion kinetic models.

4 Experimental methodology

4.1 Introduction

This chapter describes the experimental methodologies and the instrumentation utilised to understand the fundamental combustion behaviour of fuels in air and oxy-fuel environments. The chapter starts with a description and justification for the fuels selected and allocates fuel and char IDs used throughout this work. The chapter then introduces the methodology for the fundamental fuel characterisation before explaining the experimental procedures for overall fuel combustion, char production and its combustion and the derivation of the devolatilisation and char combustion kinetic parameters and their use in predicting the mass loss behaviour. Finally an experimental overview is given for each of the fuels.

4.2 Fuel selection and identification

The fuels seen Table 4.1 were selected after lengthy discussions with the entire BIO-CAP UK research team. It was decided that the fuels had to be commercially available and that enough material could be sourced for the pilot scale project at the PACT facilities (~1.5 tonnes required for pilot scale tests). Four of the fuels used can be seen in Figure 4.1 and Figure 4.2 and the suppliers of the fuel, the fuel ID and the char ID defined by production method and atmosphere can be seen in Table 4.1 and Table 4.2.

Figure 4.1: Biomass samples used in this work, North American white wood pellet (left) and torrefied spruce (right)

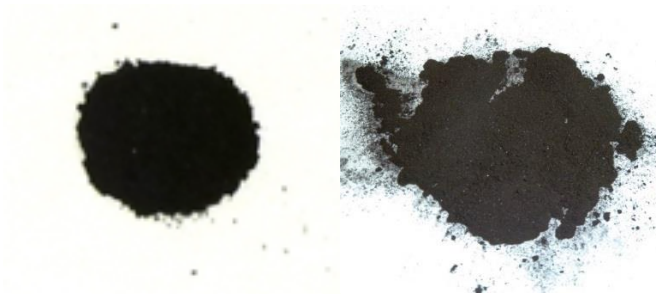

Figure 4.2: Coal samples used in this work, El Cerrejon (left) Pittsburgh #8 (right) (183)

Table 4.1: Fuels selected, reasoning, description and source

Fuel	Form	Fuel ID	Description	Provided to Leeds by
El Cerrejon (1) coal	Pre - Milled	ELC	The El Cerrejon sample was provided by J Szuhanski and was originally intended for use at the PACT facilities.	J. Szuhanski
El Cerrejon (2) coal	Pre-Milled	PEL	Supplied to PACT by an industrial partner to be used in the 250kW trials.	J. Szuhanski
Pittsburgh #8 coal	Lumps	PIT	A reference coal, since it is a fuel that has been extensively characterised	Shipped to L. Darvell directly from the colliery
North American White Wood Pellet (1)	Pellet	WWP	Originally sourced directly from an industrial partner. Note that it was a small sample- enough for analysis only	B. Dooley
North American White Wood Pellet (2)	Pellet	PWWP	Supplied to PACT by an industrial partner to be used in the 250kW tests	J. Szuhanski
Torrefied Spruce pellet	Pellet	TSP	Supplied by E.ON as part of the project brief to investigate a torrefied biomass. Note that the torrefaction conditions are unknown	R. Irons (E.ON)

Table 4.2: Char identification and ID to be used throughout the thesis

Fuel	Char production method	Char production environment	Char ID
El Cerrejon (1) coal	TGA	N_2	PEL N_2
		CO_2	PEL CO_2
	DTR	N_2	PEL DTR
El Cerrejon (2) coal	TGA	N_2	ELC N_2
		CO_2	ELC CO_2
Pittsburgh #8 coal	TGA	N_2	PIT N_2
		CO_2	PIT CO_2
North American White Wood Pellet (1)	TGA	N_2	WWP N_2
		CO_2	WWP CO_2
North American White Wood Pellet (2)	TGA	N_2	PWWP N_2
		CO_2	PWWP CO_2
	DTR	N_2	PWWP DTR
Torrefied Spruce pellet	TGA	N_2	TSP N_2
		CO_2	TSP CO_2

4.3 Fundamental fuel characterisation

The fundamental characterisation of the fuels allows for comparison of both the fuels and their chars in terms of their chemical properties. Chars were produced in an N_2 and CO_2 atmosphere using a thermogravimetric analyser (TGA) at ballistic heating rates and in N_2 using a drop tube reactor (DTR). This analysis helps to provide some understanding of the fundamental chemical processes occurring in each of the experiments.

4.3.1 Sample preparation

In order to characterise the fuels the samples first needed to be prepared. The biomass and torrefied biomass samples were supplied in pellet form, the PEL and ELC coals in powder form and the PIT in lump form.

4.3.1.1 Retsch SM300 cutting mill

The Retsch cutting mill (Figure 4.3) was used to break up the biomass and torrefied pellets and reduce the particle size to <5 mm. The samples were loaded via the top of the cutter and fed by gravity to a rotor with three stainless steel blades spinning at 1300 rpm. The reduced biomass particles fall through a 5mm mesh sieve into the collection pot and the size is further reduced in a ball mill.

Figure 4.3: Retsch SM300 Cutting Mill

4.3.1.2 Retsch PM100 ball mill

The three coals and "post cutting mill biomass" samples were reduced further using the Retsch PM100 ball mill (Figure 4.4). The samples were added to a 250 mL stainless steel grinding jar with 15 x 20mm stainless steel balls and locked securely into the mill housing. The mill was then programmed to spin at 400 rpm for 3 minutes then stopped for 5 minutes and then the process repeated. This allowed the mill to run continuously without the samples over-heating. The ball mill was able to provide sample at the required size for the DTR work, proximate and ultimate analysis. Fuels for use in the TGA were reduced further using the cryomill.

Figure 4.4: Retsch PM100 Ball Mill

4.3.1.3 SPEX 6770 Freezer mill

The cryomill (Figure 4.5) was used to provide particles <90µm for use in the TGA. In order to acquire a homogenous and representative sample, 3- 4g of ball milled sample were placed into the cryomill. Once milled the samples were passed through a 90µm sieve and any parts too large were re-milled in the cryomill.

Figure 4.5: SPEX 6770 freezer mill

4.3.1.4 Retsch AS 200 vibratory sieve shaker

The sieve shakers (Figure 4.6) were utilised in order to separate the samples to the required size fractions. The size fractions required are as follows, the TGA work <90 µm, the drop tube reactor coals 75-180 µm and biomass 212-355 µm and the proximate and ultimate analysis <1 mm.

Figure 4.6: Retsch AS200 vibratory sieve shaker

4.3.2 Proximate analysis

4.3.2.1 Standard proximate analysis of raw fuels

The proximate analysis gives an understanding of the fuel composition in terms of the moisture, volatile, fixed carbon and ash content and can be used to help determine the coal type as defined in Table 3.2. All fuels were analysed in duplicate for their moisture, volatiles and ash contents according to the following European Standards, the raw biomass samples including the torrefied sample were analysed according to - BS EN 14774-3:2009 (moisture) (184), BS EN 15148:2009 (volatiles) (185) and BS EN 14775:2009 (ash) (186). The coal samples were analysed according to - BS ISO 11722:2013 (moisture) (187), BS ISO 562:2010 (volatiles) (188) and BS ISO 1171:2010 (ash) (189). The determination of content based on the dry and dry ash free yields and the fixed carbon, on an as analysed basis (ad) were determined using the results of the above experiments and Eq 4.1-4.3. The average moisture and ash content was used to calculate the dry and dry ash free basis.

$$\mathrm{V, FC, A_{dry}} = \mathrm{V, FC, A_{ad}} \cdot \frac{100}{100 - \mathrm{M_{ad}}} \qquad \text{Eq 4.1 (190)}$$

$$\mathrm{V, FC, A_{daf}} = \mathrm{V, FC, A_{dry}} \cdot \frac{100}{100 - \mathrm{A_{dry}}} \qquad \text{Eq 4.2 (190)}$$

$$\mathrm{FC_{ad}} = 100 - \mathrm{V_{ad}} - \mathrm{A_{ad}} - \mathrm{M_{ad}} \qquad \text{Eq 4.3 (191)}$$

Proximate analysis were performed on each sample in duplicate and in order to determine the absolute error between the results of the moisture, volatile and ash content, standard error tests were performed using the following equations:

$$\mathrm{SE_x} = \frac{\mathrm{s}}{\sqrt{\mathrm{n}}} \qquad \text{Eq 4.4}$$

E_x – Absolute error in the moisture, volatiles, fixed carbon and ash

s – Standard deviation (Eq 4.5)

n – Number of samples

$$\mathrm{s} = \sqrt{\frac{\Sigma(\chi - \mu)^2}{\mathrm{n} - 1}} \qquad \text{Eq 4.5}$$

χ– Measured values

μ - Mean

The absolute error in the fixed carbon was then determined using the absolute errors of the moisture, volatiles and ash analysis (ad basis) as calculated above and the following equation:

$$FC_E = \sqrt{M_E^2 + V_E^2 + A_E^2} \qquad \text{Eq 4.6}$$

M_E – Absolute error in the moisture

V_E – Absolute error in the volatiles

A_E – Absolute error in the ash

FC_E – Absolute error in the fixed carbon

4.3.2.2 Proximate analysis using the TGA of raw fuel and chars

The low char yields found in this work, particularly those from the biomass samples, make proximate analysis of the chars by the conventional British standard methods difficult. As a result it was decided that the proximate analysis of the fuels would be repeated using a TGA for direct comparison with the char proximate analysis, also performed using the TGA. It is recognised that volatile matter measured via TGA may differ to that measured by the British standard method, and so the results are only applied in a comparative way.

In order to perform the TGA proximate analysis chars were first produced using the method outlined in Section 4.6. The samples (raw fuel and chars) were heated in the TGA in a nitrogen atmosphere at 10^{o}C min^{-1} to 105^{o}C and held there for 5 minutes, then heated to 900^{o}C at 20^{o}C min^{-1} and held for 15 minutes before being cooled to 40^{o}C. At this point the nitrogen atmosphere was replaced by air and samples heated to 550^{o}C for the raw biomass and their chars and 815^{o}C for the coal and their chars at 20^{o}C min^{-1} and held for 10 minutes. The moisture, volatile, fixed carbon and ash content were determined from the mass loss plot produced, as can be seen in Figure 4.7.

As the moisture, volatiles, fixed carbon and ash were determined directly from Figure 4.7 the absolute errors between two TGA proximate analysis experiments per sample were determined using Eq 4.4 and Eq 4.5 and the variation in the measurements.

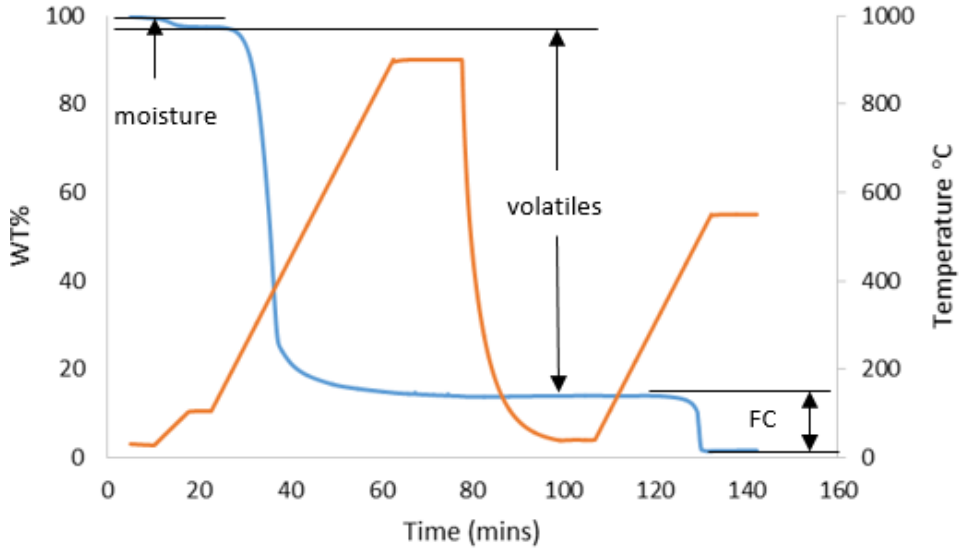

Figure 4.7: Proximate analysis of PWWP, example of data extracted from TGA curves

4.3.2.3 Determination of relative volatile and fixed carbon yield

In order to determine the effect of the char production environment and technique (N_2 vs CO_2 and TGA vs DTR) the volatile and fixed carbon contents of the raw fuels and chars were analysed. The volatile and fixed carbon contents of the chars are reported in terms of percent relative to the content in the raw fuel as determined using the following equation:

$$Y_x = \frac{100}{Y_f} \text{ x } (Y_{char} \text{ x } \frac{Y_c}{100}) \qquad \text{Eq 4.7}$$

Y_x – Component x relative to content in the raw fuel (db) (wt%)

Y_f – Component x in the fuel (db) (wt%)

Y_{char} – The char yield determined (db) (wt%)

Y_c - Component x yield in the char (db) (wt%)

NOTE: The volatile and fixed carbon content of the fuels and chars used in the above equation were determined using the TGA method.

The absolute error associated with the relative yield was determined from the errors associated with Y_f, Y_c determined from the proximate analysis done in duplicate and Y_{char} determined from the variation in char yield as described in section 4.5.3.2. The absolute errors were converted to % relative errors to allow for the determination of the absolute error in the relative volatile or fixed carbon yield.

$$\%RE = \frac{E_x}{x} . 100 \qquad \text{Eq 4.8}$$

%RE - % Relative error in the Y_f, Y_c or Y_{char}

E_x – Absolute error in Y_f, Y_c or Y_{char}

X – Average measurement of Y_f, Y_c or Y_{char}

$$E_x = \frac{\sqrt{\%Y_f^2 + \%Y_c^2 + \%Y_{char}^2}}{100} . Y_x \qquad \text{Eq 4.9}$$

E_x - Absolute error in the determination of relative component x yield

$\%Y_{f,c,char}$ - % Relative error in the Y_f, Y_c or Y_{char} as determined by Eq 4.8

Y_x – Component x yield relative to content in the raw fuel (db) (wt%)

An example calculation of the relative volatile yield and the associated errors can be found in the Appendix section 12.1.1.

4.3.3 Ultimate analysis

The ultimate analysis was performed using a CE Instruments Flash EA 1112 Series elemental analyser, Figure 4.8, for the coal, biomass and char samples following the methodology laid out in the European Standard BS EN 16948:2015 (192). A second instrument, Analytik Jena Multi 5000 elemental analyser, Figure 4.9, capable of measuring nitrogen at levels between 0.01 and 0.5 wt%, was used to determine the low levels of nitrogen typically found in the biomass, torrefied fuels and their chars.

4.3.3.1 CE Instruments Flash EA 1112 Series elemental analyser

Calibration standards and 2-4mg of each sample (in duplicate) were added to small tin capsules that were then weighed and folded to remove any air. The calibration standards selected for the raw fuel were: atropine, methionine, cystine, sulphanilamide and BBOT (2, 5 Bis – (5–Tert-Butyl-Benzoxazol-2-yl)-thiopene). The char samples contain a higher wt% of carbon and lower nitrogen and so it was decided to use a polystyrene (92% C) and soil (0.21% N) in addition to BBOT and oatmeal.

The standards were placed into the auto sampler followed by the samples with a quality control of either oatmeal or BBOT after no more than every ten samples to validate the unknown results. The folded tin capsules containing the samples fall into a combustion reactor at 900°C to produce elemental gases CO_2, H_2O, N_2 and SO_2 which are then transferred to a reduction tube at 650°C via a helium carrier gas which reduces NO_x to N_2 and oxidises CO to CO_2. These gases then enter a gas chromatography column where they are separated

before being detected by a thermal conductivity detector (TCD). The TCD is among the most commonly used measuring devices for monitoring substances separated in a column. The detector measures a change in the thermal conductivity of the helium carrier gas caused by the presence of the eluted CO_2, H_2O, N_2 or SO_2 (193).

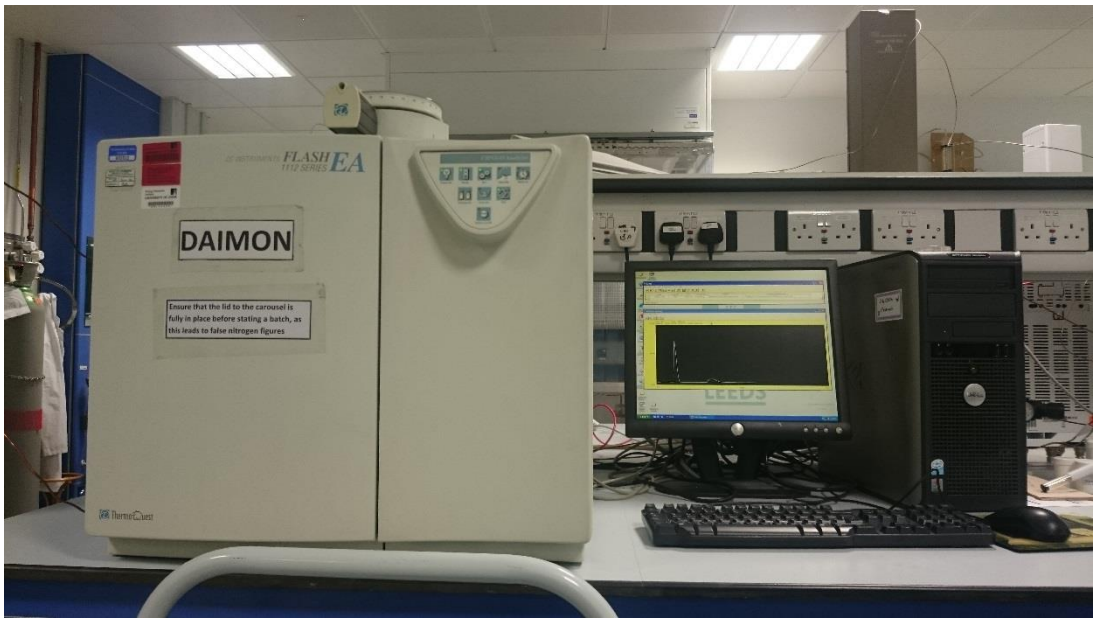

Figure 4.8: CE Instrument Flash EA 112 Series elemental analyser

The results of the CHNS analysis are on an as received basis, these were converted to a dry and dry ash free basis using the following equations:

$$\mathrm{C,N,S_{\,dry}} = \mathrm{C,N,S_{ad}} \times \frac{100}{100-\mathrm{M_{ad}}} \qquad \text{Eq 4.10 (194)}$$

$$\mathrm{H_{dry}} = \left(\mathrm{H_{ad}} - \frac{\mathrm{M_{ad}}}{8.397}\right) \times \frac{100}{100-\mathrm{M_{ad}}} \qquad \text{Eq 4.11 (194)}$$

$$\mathrm{C,N,S_{\,daf}} = \mathrm{C,N,S_{ad}} \times \frac{100}{100-\mathrm{M_{ad}}-\mathrm{A_{ad}}} \qquad \text{Eq 4.12 (190)}$$

M_{ad} - Moisture as analysed

A_{ad} - Ash as analysed

The oxygen content was determined by difference using the following equation:

$$\mathrm{O_{dry}} = 100 - \mathrm{C_{dry}} - \mathrm{H_{dry}} - \mathrm{N_{dry}} - \mathrm{S_{dry}} - \mathrm{A_{dry}} \qquad \text{Eq 4.13}$$

The absolute error in the C,H,N,S analysis on an as received basis was determined using Eq 4.4 and Eq 4.5. The absolute error in the C,H,N, S were then used with the average moisture and ash contents determined using the British standard proximate analysis method to determine the error in the ultimate analysis on a dry and dry ash free basis. The British standard moisture and ash content were used as the size fraction of the fuels used in the ultimate analysis were the same as that used in the British Standard proximate analysis (<1mm). The standard error on a daf basis can be expressed in terms of the absolute errors associated with the elemental, moisture and ash content as follows:

$$\mathrm{C,H,N,S_{AE}} = \mathrm{C,H,N,S_{E1}}\ \mathrm{x}\ \frac{100}{100-\mathrm{M_E}-\mathrm{A_E}} \quad \text{Eq 4.14}$$

C,H,N,S_{AE} – Absolute error on a daf basis

C,H,N,S_{E1} – Absolute error on a as analysed basis

M_E – Absolute error of the moisture content determined by British standard method

A_E – Absolute error of the ash content determined by British standard method.

In order to determine the absolute error on a daf basis, the percent relative error of the C,H,N,S, the moisture and ash was determined using Eq 4.8 and then applied to Eq 4.9.

The absolute error in the oxygen was determined from the absolute errors of the C,H,N,S on a dry basis:

$$\mathrm{O_{AE}} = \sqrt{\mathrm{A_{eC}}^2 + \mathrm{A_{eH}}^2 + \mathrm{A_{eN}}^2 + \mathrm{A_{eS}}^2} \quad \text{Eq 4.15}$$

$A_{e\ C,H,N,S}$– Absolute errors in C,H,N,S on a daf basis

The carbon and nitrogen content of the chars relative to the raw fuel were determined to give a better understanding of the devolatilisation process and to understand the effect on char preparation environment on nitrogen partitioning. The relative yield and the associated errors were determined using the same methodology as the volatile and fixed carbon yield outlined in section 4.3.2.3 using Eq 4.7-4.9.

4.3.3.2 Analytik Jena Multi 5000 elemental analyser

The Analytik Jena Multi 5000 elemental analyser was used to detect low nitrogen contents of the biomass, torrefied biomass and their chars. The unit utilises chemoluminesence (CLD) to detect the elemental N in each sample. The samples were weighed (2.5 mg) added to sample boats and placed on the auto sampler.

Figure 4.9: Analytik Jena Multi 5000 elemental analyser

The boat containing the sample is fed into the furnace at 1050°C and pyrolysed in an argon atmosphere before being combusted in oxygen atmosphere producing the elemental gas which is then fed to the CLD. The principle of the CLD is outlined below:

$$N + O_2 \rightarrow NO_x(NO, NO_2 \ldots) + CO_2 + H_2O \qquad \text{R 4.1}$$

$$NO + O_3 \rightarrow NO_2^* + O_2 \qquad \text{R 4.2}$$

$$NO_2^* \rightarrow NO_2 + hv \qquad \text{R 4.3}$$

The nitrogen bound in the fuel is released as oxides during pyrolysis and combustion. The NO_2 produced during combustion is led through a converter and reduced to NO through exposure to O_3 produced within the reactor. During this reaction NO_2^* in an excited state is generated temporarily and emits visible light on return to ground state. The emitted light is proportional to the NO_2^* thus giving a measure of the concentration (195).

The instrument is calibrated to 0.5 wt% nitrogen and a quality control of olive stone (0.2% N) was used after at most every 6 standards. The resulting N determinations were then used

in the calculation of the CHNS data above for the biomass, torrefied biomass and their chars. The coals and their chars are outside of the detection limits of the Analytik and CE Flash was deemed acceptable for the higher N detections.

4.3.4 Determination of HHV

The higher heating values of the biomass, torrefied and their chars were determined using the Friedl correlation (196, 197) and coals and their chars determined using the Milne correlation (198). The composition of the samples determined from the proximate and ultimate analysis is used to predict the HHV as follows:

Friedl correlation

$$\mathrm{HHV_{dry}} = 3.55\mathrm{C}^2 - 232\mathrm{C} - 2230\mathrm{H} + 51.2\mathrm{C\ x\ H} + 131\mathrm{N} + 20600 \quad \text{Eq 4.16}$$

C,H,N wt% on a dry basis

HHV_{dry} (kJ/kg)

Milne correlation

$$\mathrm{HHV_{Milne}} = 0.341\mathrm{C} + 1.322\mathrm{H} - 0.12\mathrm{O} - 0.12\mathrm{N} + 0.0686\mathrm{S} - 0.0153\mathrm{Ash} \quad \text{Eq 4.17}$$

C, H, N, O and S and ash are the mass fractions on a dry basis.

The error in the HHV calculation was determined by the absolute error as seen in Eq 4.4 and 4.5.

4.3.5 Grindability test of the torrefied spruce

The milling behaviour of fuels and the resulting particle size distribution is important for combustion stability and efficiency, emissions control such as NO_x and for minimising the amount of unburnt carbon in ash (197). In general biomass cannot be milled in bituminous coal mills due to the fibrous nature of biomass (199). The torrefaction process reduces the fibrous nature of the biomass fuel potentially improving the milling behaviour (197).

The Hardgrove grindability Index (HGI) is the most common grindability test for coals (200), however this method is not suitable for the lower density biomass which would be too voluminous to use in the Hardgrove grindability equipment. A modified HGI has been developed by Bridgeman et al (197) that requires a fixed volume of sample rather than a fixed mass seen in the original HGI. The degree of torrefaction of the TSP sample is unknown

to the author and the modified HGI was performed to better understand the possible torrefaction conditions.

The modified Hardgrove index test was performed in order to determine the grindability behaviour of the torrefied spruce. The TSP fuel was delivered in pellet form and ~ 1 kg was milled in the Retsch SM300 Cutting Mill outlined in section 4.3.1.1. The milled sample was then sieved using 600 µm – 1.18 mm which is the size fraction required for the modified HGI test.

4.3.5.1 Modified HGI methodology

- 50 cm^3 of the milled TSP (600 µm – 1.18 mm) sample is measured out and weighed
- The 50 cm^3 sample is then placed into a 250 ml capacity stainless steel milling cup with 15 x 20 mm stainless steel balls and ground for 2 min at 165 rpm using the Retsch PM100 ball mill described in section 4.3.1.2.
- The milled sample was then removed and separated using a 75 µm sieve and size fractions weighed. If a loss of sample greater than 0.5 g was seen the test was aborted and repeated.
- The mass of the sample (g) passing through the 75 µm sieve (m_1) is calculated using the following equation:

$$m_1 = \mathrm{m_v} - \mathrm{m_2} \quad \text{Eq 4.18}$$

  Where m_V = mass of the 50 cm^3 of sample, m_2 = mass of the sample collected on the 75 µm sieve

- The process is repeated three times and the average results taken

The modified HGI method that was developed by Bridgeman et al used the exact mill that the above experiments were performed in and the calibration of the mill using known HGI coals presented in (197) were used to determine the HGI equivalent for the TSP fuel.

Using the calibration curve (Figure 4.10) the HGI equivalent was determined using the following formula:

$$\mathrm{HGI_{Eq}} = \frac{(\mathrm{m}-0.9856)}{0.1575} \quad \text{Eq 4.19}$$

In addition to the determination of the HGI_{Eq} the particle size distribution of the milled fuels was determined by sieving the fuels using sieves with mesh sizes of 600, 355, 212, 150, 75 and 53 µm (197).

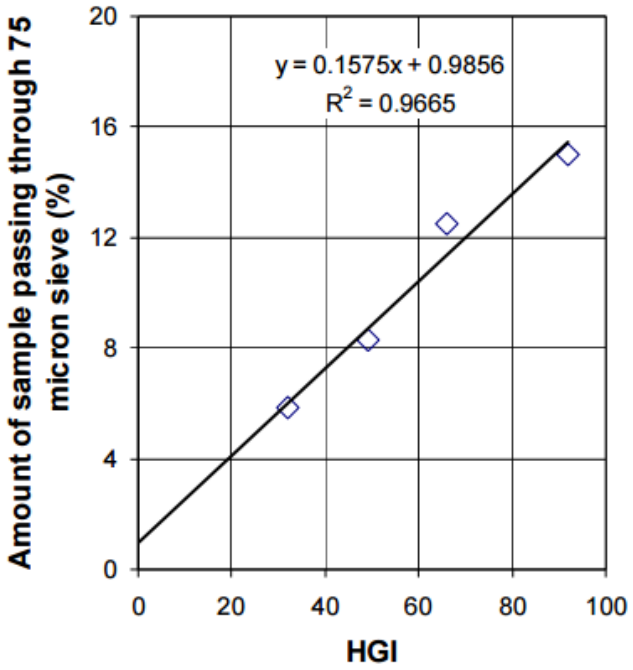

Figure 4.10: Calibration curve from four standard reference coals of HGI 32, 49, 66 and 92 for a Retsch PM100 ball mill (197)

4.3.6 Surface area analysis

Surface area measurements were performed in order to determine the intrinsic reactivity of the chars produced in N_2 and CO_2 atmospheres and using the DTR in N_2.

4.3.6.1 Physisorption isotherms

The determination of surface area by physical adsorption or physisorption is a widely used technique. In general adsorption occurs whenever an adsorbate accumulates at an interface through weak intermolecular forces resulting from van der Waals interactions (201). This phenomenon is used to determine the surface area of a sample through the relationship between the quantity of adsorbate adsorbed (in this case nitrogen) and the pressure at which the adsorbate was introduced to the sample at constant temperature. The sample is usually cryogenically cooled to ensure a constant temperature and the adsorbate (in this case nitrogen) introduced at a range of increasing pressures. At low pressure the adsorbate begins to adsorb on to the isolated sites of the surface and as the pressure is increased the number of adsorbed molecules increase to form a monolayer on the sample surface. As the pressure is increased further the adsorbate will start to form a multilayer until the pressure is high enough to cause complete coverage of the sample and fill all of the pores. The adsorptive gas pressure is then reduced evaporating the condensed gas from the system.

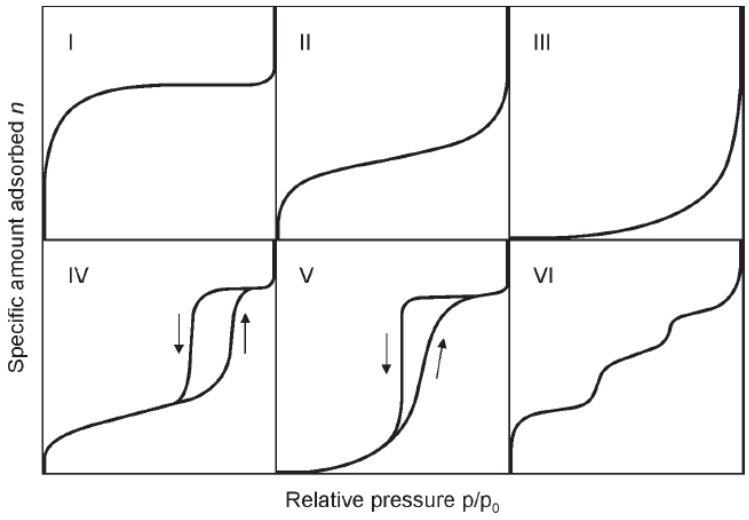

Figure 4.11: Classification of physisorption isotherm types

The result of the above measurements is a physisorption isotherm (Figure 4.11) from which the surface area can be derived using the Brunauer-Emmett-Teller (BET) method and the density function theory method (DFT) (201). The majority of physisorption isotherms fall into the six categories as shown in Figure 4.11.

Type I are seen in microporous (pores of internal width less than 2nm) solids having relatively small external surfaces e.g. activated carbons.

Type II are seen in non-porous or macroporous (pores of internal width greater than 50nm). The isotherm represents unrestricted monolayer-multilayer adsorption.

Type III are not common isotherms. In this case adsorbate-adsorbate interactions play an important role.

Type IV contain a characteristic hysteresis loop associated with condensation taking place in mesopores (pore of internal width between 2-50 nm). The initial part of this type of isotherm is attributed to monolayer-multilayer adsorption. The presence of a hysteresis loop is an indication of capillary condensation

Type V isotherms are uncommon and are related to Type III isotherms in that the adsorbent-adsorbate interaction is weak and that they exhibit hysteresis as seen in type IV

Type VI represent multilayer adsorption on a uniform non-porous surface. The step height represents the monolayer capacity for each adsorbed layer. An isotherm of this type could be obtained with graphitized carbon (201, 202).

4.3.6.2 Determination of surface area using BET

The BET equation used to determine the surface area from the physisorption isotherm can be seen below (201).

$$\frac{1}{n_a(\frac{P_o}{P}-1)} = \frac{C-1}{n_m C}\ x\ \frac{P}{P_o} + \frac{1}{n_m C} \qquad \text{Eq 4.20}$$

P – Partial vapour pressure of the adsorbate gas

P_o – Saturation pressure of the adsorbate gas

n_a – The amount adsorbed at the relative pressure p/p_o

n_m - Monolayer capacity of the adsorbent

C – A constant that is dependent on the isotherm shape

If $(1/(n_a(P_o/P-1)$ is plotted against (P/P_o) a linear relationship is given allowing for the determination of n_m at relative pressures below 0.3. The surface area can then be determined from the monolayer capacity n_m determined above.

$$A_{BET} = n_m\ x\ L\ x\ a_m \qquad \text{Eq 4.21}$$

A_{BET} – Surface area ($m^2\ g^{-1}$)

L – Avogadro constant

a_m – Molecular cross sectional area of a nitrogen molecule = 0.162 nm^2 at 77K

4.3.6.3 Surface area methodology

A Quantachrome Nova 2200 E (Figure 4.12) was utilised to degas and measure the surface area of chars. The chars produced using the TGA and DTR as described in section 4.5 were weighed and added to a 9mm sample tube and placed into the vacuum degas station. The samples were degassed under vacuum for 1 hour at 90°C to remove any moisture then the temperature raised to 300°C and held for a minimum of 6 hours. The samples were then removed and weighed to ensure that absorbed moisture and gas is removed. The sample tube was then placed into the measurement side of the NOVA where full isotherms were generated. Measurements were determined at liquid nitrogen temperatures (77°K) using nitrogen as the adsorbate at relative pressures between 0.05 and 1. BET surface areas were determined from the adsorption plot generated at relative pressures between 0.05 and 0.3. The resulting surface areas were then used to determine the intrinsic reactivity of the chars as described in section 4.7.2.3.

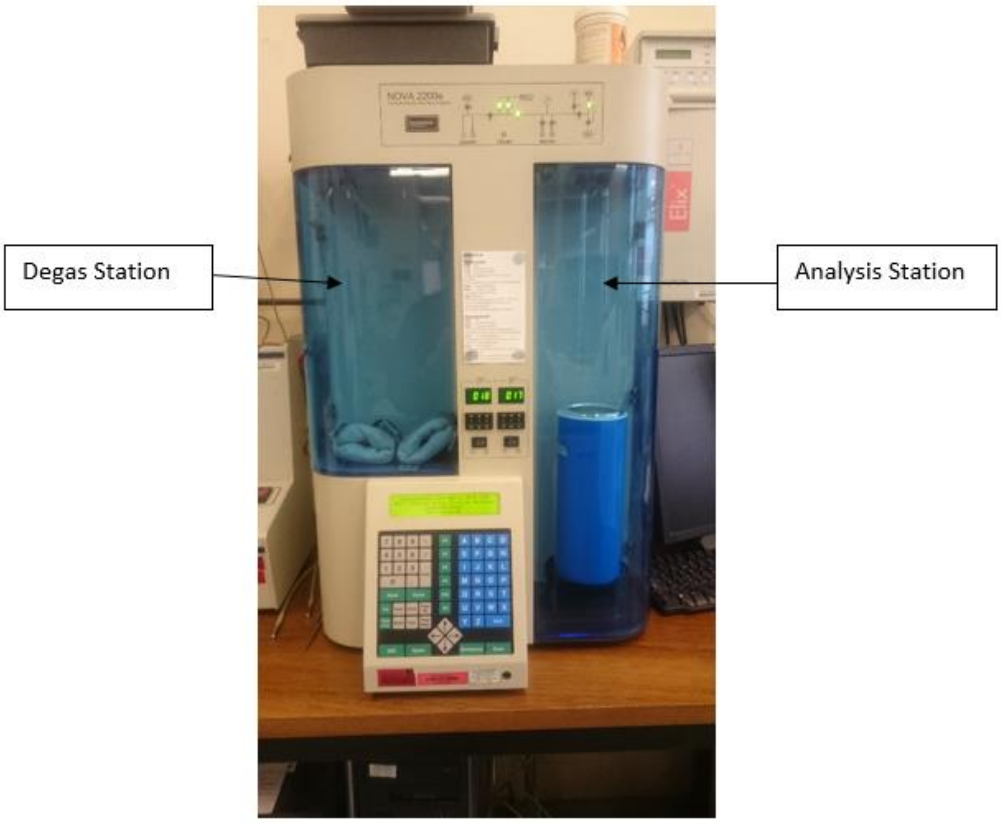

Figure 4.12: Quantachrome NOVA 2200E

4.3.7 Scanning electron microscopy

Scanning electron microscopy (SEM) provides an in depth image of a particle surface aiding in the characterisation of the raw fuels and chars. In SEM imaging a beam of electrons are emitted from an electron gun (cathode) which is focused on the sample. The electrons beam is accelerated through a high voltage (in this case 5 or 15 kV) and pass through a system of electromagnetic lenses to produce a thin beam of electrons. The beam then reaches the surface of the sample and either secondary electrons (SE) or backscattered electrons (BSE) are released dependent on the analysis type selected. When SE is selected the beam hits the sample the electrons are absorbed and its own electrons are released which are then detected by a detector which uses the information to produce an image. In BSE mode the electrons focused onto the surface are reflected back from the sample surface and then detected allowing for the generation of the image.

SEM imaging of the raw fuels and chars were taken using the Hitachi Table top TM3030 Plus scanning electron microscope shown in Figure 4.13. The chars produced using the TGA and DTR as described in sections 4.5 were placed onto an adhesive pad which was placed onto a

small sample holder. The holder was then placed onto the sample holder stand and installed in the SEM. Once installed the system was placed under vacuum and images taken at a range at 5 kV and over a range of magnifications. In most high vacuum SEM systems the sample is usually coated in a thin layer of metal to prevent accumulation of electrons on the surface generating charge up. The Hitachi uses a low vacuum functionality to reduce the amount of charge up meaning that the thin metal layer is not required.

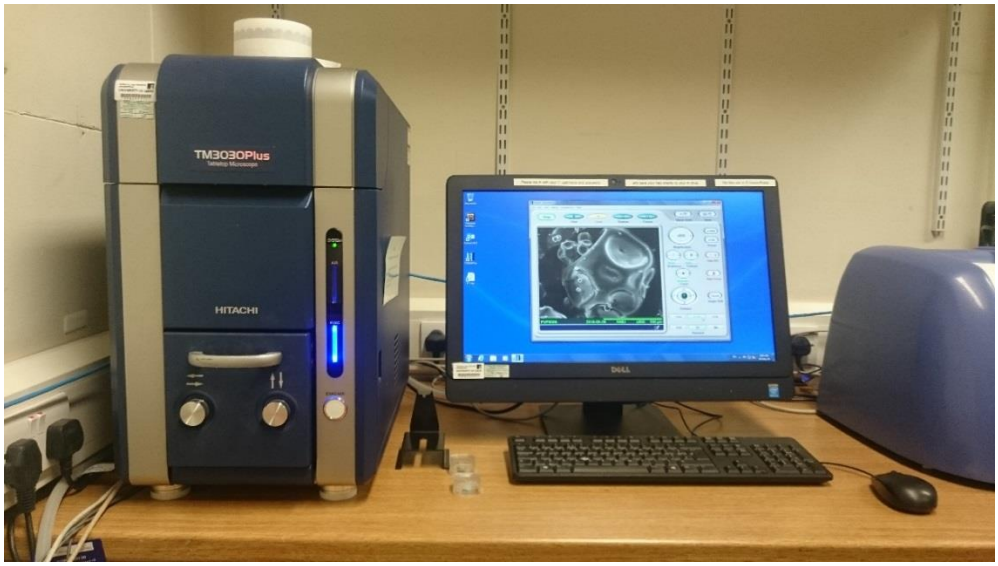

Figure 4.13: Hitachi Table top TM3030 Plus SEM

4.4 Combustion and pyrolysis behaviour of the raw fuels determined by thermogravimetric analysis (TGA)

4.4.1 Introduction

This section outlines the methodology for the determination of combustion behaviour of the raw fuels in air and the full range of oxy-fuel environments (5-30% O_2/CO_2). It includes a description of the equipment, the combustion atmospheres selected and how they were achieved, the heating profiles and how the resulting data is analysed.

4.4.2 Thermogravimetric analysis

The combustion and pyrolysis characteristics were determined using a TA Q5000 thermogravimetric analyser as seen in Figure 4.14. The TGA comprises of a hang down balance located inside a furnace, built in mass flow controllers that are able to control the

flow rate of air and nitrogen to the furnace and an auto-sampler. The TGA is fully programmable and is capable of ballistic heating rates of up to 1000°C min^{-1}, which was utilised in the production of char.

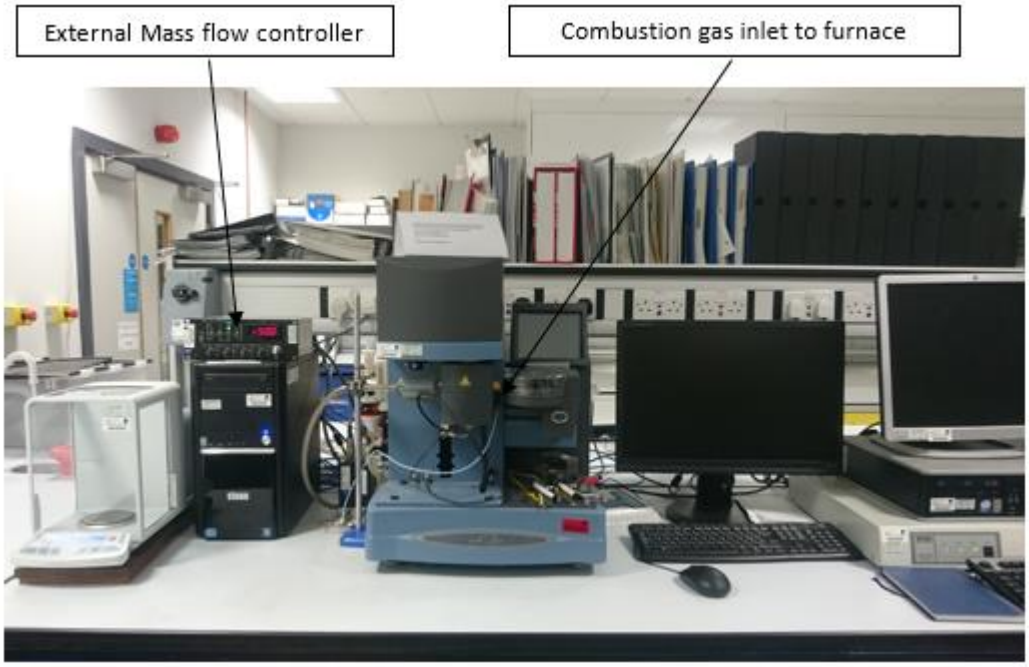

Figure 4.14 TA Q5000 TGA used for the combustion of raw fuel and chars

Platinum crucibles used for sample containment were cleaned using a Bunsen burner to remove any residues and then tared using the instrument's automatic calibration functions. During the combustion runs ~5mg of sample cryomilled to <90 µm was placed on to the pans and pans loaded on to the auto sampler. The sample size used (<90 µm) was used in order to reduce the effects of heat transfer through the particle and to ensure that combustion was controlled kinetically (203). In both the air and the oxy-fuel combustion tests the same programme was used, firstly the furnace temperature was set to 0°C (in order to make sure that the TGA did not start to heat up) with a N_2 purge gas with a flow rate 100 ml min^{-1} for five minutes to purge the furnace. At the same time a flow of N_2 is fed to the balance housing situated above the furnace to protect the balance from any contamination from the furnace atmosphere. This flow of N_2 to the balance housing is constant throughout the heating profile. Once the furnace was purged, the gas to the furnace was switched to air at a flow rate of 50 ml min^{-1} and held at 0°C for 5 minutes to allow the balance to equilibrate. The furnace was then heated at 10°C min^{-1} to 105°C and held for 10 minutes to dry the sample before being heated to 900°C at the same heating rate and held for 10 minutes. Pyrolysis tests were performed using the same conditions described above in N_2 and CO_2 atmospheres

(CO_2 provided by external mass flow controller). Gasification experiments of the chars produced in CO_2 were performed using the same methodology as above in 100% CO_2 atmospheres at temperatures up to 1000°C.

4.4.2.1 Combustion in oxy-fuel environments using the TGA

In order to determine the effect of the combustion environment the fuels were combusted in air and a range of O_2/CO_2 atmospheres ranging from 5-30%O_2 in CO_2 by volume. The TA Q5000 has internal mass flow controllers for the delivery of air or N_2 to the furnace but are not able to deliver the oxy-fuel gases. However, the gas inlet to the furnace is accessible on the front of the unit and MKS Mass Flow Controllers and a MKS 4 channel readout module were utilised to provide the desired atmosphere to the furnace via the furnace gas inlet as seen in Figure 4.14.

Two gas cylinders, the first containing 99.99% research grade CO_2 and the second containing 30%O_2/70% CO_2 volume basis were connected to the mass flow controllers. The 30%O_2/70% CO_2 cylinder was selected rather than a 100% O_2 cylinder as the combustion atmosphere of real world CCS plants is not expected to exceed this, and as a matter of health and safety within our laboratory. The mass flow controllers allowed the individual gases to be controlled before being mixed in the inlet pipe before entering the furnace. The flow rates of the gases and desired combustion atmospheres is shown in Table 4.3.

Table 4.3 Flow rates of gases used to provide the oxy-fuel combustion atmosphere

Combustion atmosphere % O_2 in CO_2 volume basis	**Flow Rate (ml min^{-1})**		**Total flow rate ml min^{-1}**
	30%O_2 /70% CO_2	**99.99% CO_2**	
0	0	50	50
5	8.3	41.7	50
10	16.7	33.3	50
21	35.0	15.0	50
25	41.7	8.3	50
30	50.0	0.0	50

Example – Determination of desired flow rate if the required O_2 level is 21%

Flow rate of O_2/CO_2 mix = 35 ml min^{-1}

Flow rate of CO_2 in O_2/CO_2 mix = 0.7 x 35 = 24.5 ml min^{-1}

Flow rate of 99.9% CO_2 = 15 ml min^{-1}

Total flow rate of CO_2 = 15 + 24.5 = 39.5 ml min^{-1}

Total flow = 50 ml min^{-1} of which the O_2 = 10.5 ml min^{-1} = 21% by volume

The procedure followed that of the air combustion experiments except for the change to external mass flow controllers.

4.4.2.2 Analysis of the thermogravimetric data for the comparison of combustion behaviour

The TGA produces a mass loss curve plotted against time and a derivative mass loss curve (wt% s^{-1}). The peaks seen in the derivative mass loss curve can be associated with the devolatilisation and char combustion stages easily in the biomass samples, while the devolatilisation stage of coal combustion is harder to detect due to the low volatile content. In order to compare the fuels key temperatures and mass loss rates identified:

a- Temperature at which the rate of mass loss achieved 0.016 Wt% s^{-1} (1 wt% min^{-1})
b- Temperature at which the maximum rate of devolatilisation is seen
c- Temperature at which the maximum rate of char combustion is seen
d- Temperature at which the maximum rate of weight loss (in the case of one unresolved peak) is seen
e- Burn out temperature, the temperature at which the rate of mass loss is equal to 0.016 Wt% s^{-1} (117, 204)
f- The temperature at which maximum mass gain is seen as a result of oxygen chemisorption in the coal samples
g- The mass gain in the coal samples due to chemisorption

a and b were resolved for the biomass and torrefied biomass samples, but not for the coal, hence c is reported in the latter case.

4.4.2.2.1 Determination of active surface area using thermogravimetric analysis

In the thermogravimetric analysis of the three coals a mass gain is seen at temperatures above 105^{o}C due to the chemisorption of oxygen onto the fuel surface. The active surface area (ASA) of the raw coals was estimated from the non-isothermal TGA combustion experiments performed in air and oxy-fuel environments outlined in the previous section. According to active site theory reactions only occur at active or favoured sites as described in section 3.5.3 in relation to chars. The same mechanisms are at play during low temperature oxygen chemisorption of raw coals as those described for oxygen-char chemisorption (205, 206). In each of the TGA experiments the wt% mass gain was determined, from at the point that the drying stage had stopped to the maximum mass seen.

The wt% was then used to determine the mass of oxygen chemisorbed by normalising the initial mass to 100g and ASA determined using the following equation.

$$ASA = \left\{ \frac{\left[\left(\frac{m_O}{Mw_{O2}} \quad L \right) . \; A_O \right]}{100} \right\} / 10^{18} \quad \text{Eq 4.22}$$

ASA – Active surface area ($m^2 g^{-1}$)

m_O – the mass gain taken from the combustion TGA experiments (g)

Mw_O – molecular weight of oxygen (16 g mol^{-1})

L– Avogadro's constant (6.02214 x 10^{23} mol^{-1})

A_O – Area of a single oxygen atom (0.83 nm^2)

100 – normalised mass (g)

(205)

4.5 Char production techniques

4.5.1 Introduction

The chars were produced via two methods: the first, at ballistic heating rates, in the TGA; the second, chars derived from the PEL and PWWP fuels using the drop tube reactor (DTR). This section outlines the two different methods of char production and the determination of the char yield.

4.5.2 Char production using TGA

The TGA was used to produce chars in both N_2 and CO_2 atmospheres from all of the raw fuels heated at ballistic heating rates (1000°C min^{-1}) to produce devolatilisation characteristics more similar to those seen in a DTR (207) compared to slow heating rate char production. The platinum pans were first cleaned and tared, in the gas atmosphere that the char was to be produced in (N_2 or CO_2) , and then 15mg of sample (<90um) added. The required atmospheres were supplied directly by the TGA mass flow controllers in chars made in N_2 and by the external mass flow controllers in chars made in CO_2 atmospheres, as described in section 4.4.2.1. The initial section of the heating profile was the same as in the combustion case as the furnace is purged to ensure the required atmosphere. The furnace was held at 20°C for 5 minutes with the flow rate of gas set to 50 ml min^{-1}, to allow the system to stabilise. Once stable, the furnace is heated to 1000°C ± 5°C in one minute then returned to room temperature without the aid of any cooling systems. The mass loss curves and

temperature profile were then reviewed to determine that the correct temperatures were reached and the char remaining on the sample pan removed and placed into a glass vile and stored in a desiccator.

The char yield is easily available from the mass loss plot and recorded from the point at which the sample returned to room temperature. The mean value of the char yields was determined from the repeated TGA runs. In order to produce enough char for proximate and ultimate analysis, the kinetic determination and surface area measurements several char production runs using the TGA were performed and average char yields determined. In the case of the coal samples the char yield was significantly higher than the biomass samples requiring less TGA char production runs to produce enough char for further analysis. In the determination of the char yield the number of repeats for the coals was 10, the TSP sample required 30 repeats and the biomass samples 50 repeats. An example of the mass loss plots produced from char production using the TGA can be seen in the appendix (Section 12.2).

4.5.3 Char production using Drop Tube Reactor (DTR)

The DTR provides a way to closely resemble what happens to a particle in a pulverised fuel boiler in terms of temperatures and heating rates (207). Chars were produced from the PWWP and PEL fuels and compared to the TGA ballistic chars of the same fuels, in terms of char reactivity.

4.5.3.1 Drop tube reactor

The drop tube reactor (DTR) is shown in Figure 4.15 and comprises of a vertically mounted furnace, PID controllers, cooled sample inlet and char collection pots, a heat exchanger, a pump and an O_2 analyser as shown Figure 4.17. The DTR consists of an alumina tube of 1400 mm in length and an internal diameter of 65 mm inside an electrically heated vertical furnace. The furnace comprises of three independently controlled heating zones that produce an isothermal reaction zone of 455 mm (Figure 4.16). The average temperature of the heated reaction zone was measured at seven points using a K type thermocouple and resulted in an average temperature of 1062 ±5^{o}C (208).

The DTR was heated to 1100^{o}C at 10^{o}C min^{-1} and held at that temperature for the remainder of the experiment, at the same time the cooling system was turned on to prevent the inlet and catch-pots reaching elevated temperatures. Once at 100^{o}C the O_2 analyser was calibrated using 99.9% nitrogen and a 5% O_2 in nitrogen mix.

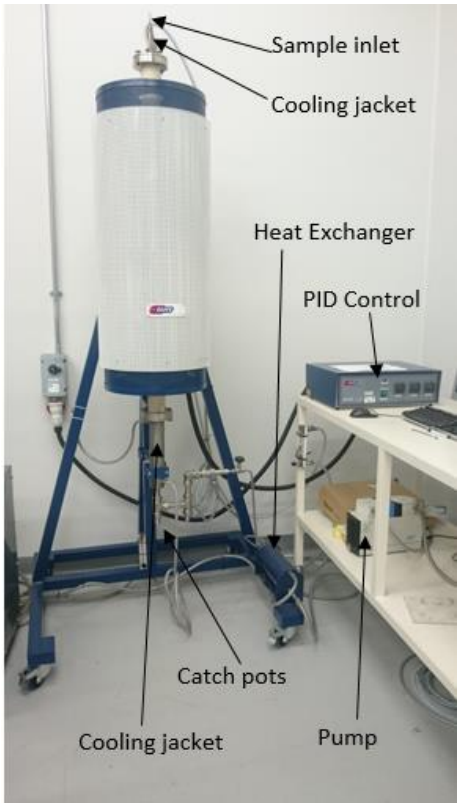

Figure 4.15: Drop tube reactor

After calibration the nitrogen flow into the system was set to 16L min^{-1} to provide the required particle residence time of ~0.5 s in the isothermal reaction zone (assuming the particle travels along the centreline of the furnace) and oxygen concentration of 1%. The O_2 concentration was set to 1% to help prevent the fuels sticking to the sample inlet or the chars sticking to the inside of the reactor and making it almost impossible to capture the chars (208). The milled samples PEL (75-180 µm) and PWWP (212-355 µm) (sizes chosen to minimise char burnout) were loaded manually into the top of the DTR where they fall into the reaction zone. The char produced falls directly into the catch-pots and the volatiles released along, with the nitrogen atmosphere, are drawn via the heat exchanger and pump to the oxygen analyser and then to the laboratory extraction system.

The oxygen content within the reactor is constantly monitored to ensure the correct O_2 levels inside the reactor. The chars were then collected and used to determine proximate and ultimate analysis (for comparison to the raw fuels and the determination of the char yield), surface areas and for char combustion tests.

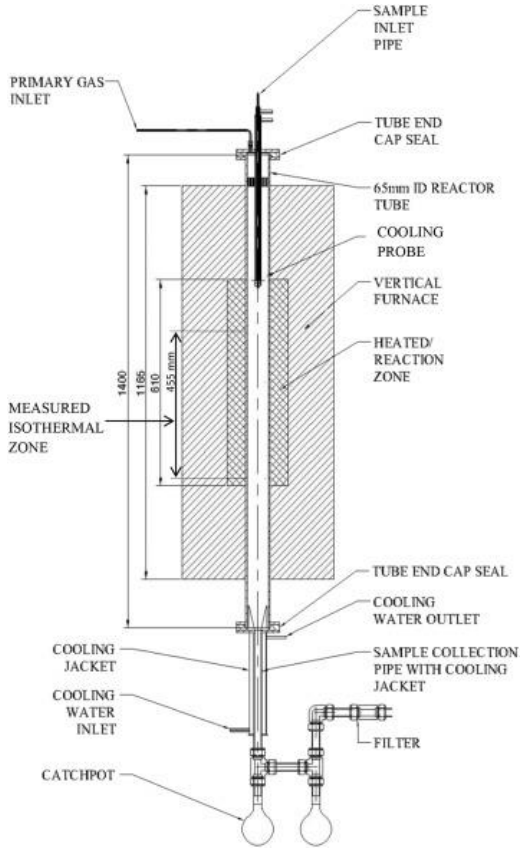

Figure 4.16: Schematic of the drop tube reactor (208)

Figure 4.17: Mitchell O_2 analyser

4.5.3.2 Char yield determination

The yield of the char produced in the TGA was taken directly from the mass loss profile produced and assumed to be dry. In order to produce enough char for the proximate, ultimate, surface area and kinetic analysis many TGA runs were needed. The average char yield was determined from these runs and the absolute error (with a 95% confidence level) using the following equations:

$$E_x = \frac{s \text{ x } 1.96}{\sqrt{n}} \qquad \text{Eq 4.23}$$

s – standard deviation (Eq 4.5)

n – number of samples

The char yield was determined on a dry basis using the following equation:

$$\text{Char yield}_{dry} = \text{Char yield}_{ad} \text{ x } \frac{100}{100-M} \qquad \text{Eq 4.24}$$

ad – as determined by TGA

M – moisture content in the raw fuel as determined by TGA method

The error in the char yield on a dry basis was determined using the percent relative errors (Eq 4.8 and 4.9) associated with the char yield at a 95% confidence level and the relative error associated with the char as follows:

$$\text{Absolute error char yield dry basis} = \frac{\sqrt{\%E1^2+\%E2^2}}{100 \text{ x Char yield}_{dry}} \quad \text{Eq 4.25}$$

E_1 – Percent relative error in the char yield as measured by the TGA

E_2 – Percent relative error in the moisture as measured by the TGA

The char yield from the DTR is difficult to determine directly by weighing the feedstock and chars produced, due to losses in the system e.g. the char particles sticking to the inside of the reactor and catch pot system. In order to determine the theoretical char yield the weight loss has been calculated indirectly using the ash tracer method (209).

$$\text{Char Yield } = 100 - \Delta W = 100 - (1 - \frac{P_1}{P_2}) \text{ x } 100 \quad \text{Eq 4.26}$$

P_1 = Ash wt% in the fuel dry basis

P_2 = Ash wt% in the char dry basis

This can be considered a % conversion.

The absolute error of the char yield using the DTR was determined from the relative errors of the ash component in the raw fuel (P_1) and DTR chars (P_2) as measured in section 4.3.2.2.

4.6 Char Combustion

The chars produced in the TGA and DTR were combusted using the TGA in the same gas atmospheres as laid out in Table 4.3. The chars produced in CO_2 using the TGA were combusted in O_2/CO_2 atmospheres ranging from 5-30% O_2 and the chars produced in N_2 using the TGA and the chars prepared using the DTR were combusted in air. All of the chars were combusted non-isothermally in order to determine kinetic parameters. Table 4.4 outlines the heating rates used in the non-isothermal combustion runs.

4.6.1 Non-isothermal combustion

Non-isothermal combustion experiments were performed in order to reduce the total number of experiments required to analyse the char combustion behaviour in the full range of O_2/CO_2 atmospheres. If the isothermal method was used it is estimated that ~60 experiments would be required to determine the kinetic behaviour of each of the chars over the full range of combustion atmospheres. The oxy-fuel combustion environment was as supplied to the TGA using the mass flow controllers and bottled gases as outlined in section 4.4.2.1.

4.6.1.1 Non-isothermal coal char combustion

The coals produced relatively high char yield (~57 wt%) compared to the biomass (6wt% in CO_2) so the methodology for char combustion differs. In the coal samples ~10 mg of raw fuel was added to the TGA pans and loaded into the TGA. The desired char production atmospheres were selected (N_2 or CO_2) and the fuels heated to 1000^oC at 1000^oC min^{-1} to produce the char. The TGA was then cooled to 30^oC in the char production atmosphere (N_2 or CO_2) at which point the combustion atmosphere (air or 5-30% O_2/CO_2) selected and sample heated to 900^oC at 10^oC min^{-1}.

4.6.1.2 Non-isothermal combustion of biomass, torrefied biomass and drop tube reactor chars

The char yield of the biomass and TSP samples were much smaller than the coal chars and too small to carry out char production and direct char combustion as seen in the coals. As a

result multiple char production runs were performed using the TGA as described in 4.5.2 and chars collected and stored in a desiccator to minimise uptake of moisture. The chars (~5mg) were then added to the TGA pans and combusted using the TGA, in the combustion atmospheres described in Table 4.3 and at the heating rates listed in Table 4.4. The DTR chars were also collected and stored in the desiccator before being combusted in air in the TGA. The TSP and PEL DTR chars were combusted at the same heating profile as the same chars produced using the TGA (Table 4.4). In the case of the biomass samples it was found that at high oxygen concentrations (>21%O_2) that the chars were very reactive and unreliable mass loss data was recorded. In order to produce reliable data and extract reliable kinetics the heating rate in both air and oxy-fuel environments was reduced to 5$^oC\ min^{-1}$.

Table 4.4: Char combustion methods, and heating rates used during char combustion

Char production atmosphere		Non-isothermal Combustion	Heating Rate ($^oC\ min^{-1}$)
PEL	N_2	✓	10
	CO_2	✓	10
	DTR	✓	10
ELC	N_2	✓	10
	CO_2	✓	10
PIT	N_2	✓	10
	CO_2	✓	10
PWWP	N_2	✓	5
	CO_2	✓	5
	DTR	✓	5
WWP	N_2	✓	5
	CO_2	✓	5
TSP	N_2	✓	10
	CO_2	✓	10

NOTE: Chars prepared in CO_2 environments combusted in 5, 10, 21, 25 and 30% O_2 in CO_2

The mass loss profiles generated during the non-isothermal combustion experiments were then analysed to determine the maximum rate of weight loss and the temperature at which it occurred and to derive kinetic data as explained in the following sections.

4.7 Determination of kinetic parameters

Kinetic parameters were determined for both the devolatilisation and char combustion stages in order to determine the effect of combustion environment on each stage to allow for the comparison of the fuels.

4.7.1 Determination of the devolatilisation kinetics and associated parameters from non-isothermal combustion of the fuels (TGA)

The fuels were combusted non-isothermally as outlined in section 4.4.2 and mass loss profiles used to extract the devolatilisation kinetic parameters assuming a simple first order single step Arrhenius reaction. The reaction rate constant method is described in the literature review in section 2.7.1.

The mass loss profile was assumed to be the result of one or more first order reactions and the rate constant was determined from the mass loss profile using the following formula:

$$k = -\frac{1}{m-m_\infty} \cdot \frac{dm}{dt} \qquad \text{Eq 4.27}$$

Where,

k – the apparent, first order reaction rate constant (s^{-1})

m – the initial mass (wt%)

m_∞ - the terminal mass (wt%)

dm/dt – rate of mass loss (wt%. s^{-1})

The calculated value of k is reliant on the chosen terminal mass and can deviate greatly as a result of the chosen value of m_∞ (164). In order to determine the reactivity during devolatilisation the terminal mass was taken at the end of the devolatilisation stage as suggested by the DTG profiles. In the case of the coal fuels where one unresolved peak is seen the determination of m_∞ is more difficult and the volatile content determined by proximate analysis used to help identify the correct value of m_∞.

The reaction rate constants were then used to determine the kinetic parameters A and E_a using the Arrhenius equation:

$$k = A.\, e^{-E_a/RT} \qquad \text{Eq 4.28}$$

A - the pre-exponential factor (s^{-1})

E_a - activation energy (kJ mol^{-1})

R - gas constant (8.314 kJ $mol^{-1}.K^{-1}$)

T - temperature (K)

The kinetic parameters E_a and A were then determined by performing a logarithm of each side of the Arrhenius equation and plotting ln(k) vs 1/T. A least squares regression line of the form y = mx + c can be fitted to the plot and coefficients extracted.

$$E_a = -8.314.\ m\ (kJ\ mol^{-1}) \quad \text{Eq 4.29}$$

$$A = e^c \quad (s^{-1}) \qquad \text{Eq 4.30}$$

In order to determine that the correct kinetic parameters were determined the mass loss profiles were predicted using the calculated values of E_a, A and k.

$$\mathrm{k} = -\frac{1}{\mathrm{m}-\mathrm{m}_\infty}.\frac{\mathrm{dm}}{\mathrm{dt}} = \frac{1}{1-x}.\frac{\mathrm{d}x}{\mathrm{dt}} \qquad \text{Eq 4.31 (210)}$$

$$\mathrm{k}(1-x) = \frac{dx}{\mathrm{dt}} \qquad \text{Eq 4.32 (162)}$$

Where,

x – is the fractional conversion = $(1-W/W_o)$

m – is the sample weight

m_∞ – is the original sample weight

At initial conditions x = 0 and t = 0 and after the integration of $\mathrm{k}(1-x) = \frac{dx}{\mathrm{dt}}$ Eq 4.32 yields:

$$\mathrm{kt} = -\ln(1-x) \qquad \text{Eq 4.33 (162)}$$

The mass loss profile taken from the experimental data were plotted against the predicted mass loss determined using Eq 4.31 – Eq 4.33 in the temperature region at which the devolatilisation stage is seen and R^2 correlation determined to ensure the correct kinetic parameters were chosen. The high R^2 correlation coefficient values indicate that the reaction model fits the experimental data.

4.7.2 Determination of the char kinetics and associated parameters from non-isothermal combustion (TGA)

The chars produced using the TGA and DTR outlined in Table 4.4 were combusted non-isothermally and the apparent kinetics obtained using an m^{th} order model, an n^{th} order reaction model developed and the intrinsic reactivities of the coals determined.

4.7.2.1 Determination of an m^{th} order apparent char kinetic model from non-isothermal experiments

The rate of char oxidation can also be modelled as a single step type Arrhenius reaction described by the following equation:

$$R_{app} = \frac{dx}{dt}\frac{1}{(1-x)^m} = A_{app}\exp^{-Ea_{app}/RT} \qquad \text{Eq 4.34}$$

Where,

R_{app} – the reaction rate constant (s^{-1})

A_{app} - the pre-exponential factor (s^{-1})

Ea_{app} - activation energy (kJ mol^{-1})

R - gas constant (8.314 kJ mol^{-1} K^{-1})

T - temperature (K)

^{m} - is the reaction order with respect to char conversion.

x –the conversion of the char defined as:

$$x = \frac{M_o - M}{M_o - M_f} \qquad \text{Eq 4.35}$$

Where

M_o – the initial mass of the sample

M – is the mass of the sample at time t (wt%)

M_f – is the mass of the ash fraction present in the char (wt%)

In order to determine comparable reaction rates, R_{app}, was determined for char conversions of 0.05 – 0.85. This allowed the global comparison of the char reaction rates without any influence of the phenomena seen at the start and end of mass loss (211). Firstly R_{app} was determined over the full range of mass loss and a plot of Ln R_{app} vs 1/T over the range of x = 0.05 to x =0.85 were plotted. In order to produce a global reaction rate the line of Ln R_{app} vs 1/T must be straight and the reaction order term ^{m} is used in order to provide the largest value of R^2 over the full range of oxygen concentrations of oxy-fuel environments for each

fuel. The ^{m} term gives an understanding of the change porosity and surface area developments as the char undergoes combustion. If m = 1 as seen in the volumetric model outlined in (212) this indicates that the surface area decrease linearly with char conversion. The kinetic parameters A_{app} and Ea_{app} were then determined from the straight line as described in section 4.7.1.

The values of A_{app} and Ea_{app} were then used to determine the reaction rate constant R_{app} and from this, the conversion determined using Eq 4.34. In order to determine the quality of fit between the predicted conversion and the experimental conversion the deviation between the experimental and predicted curves was obtained using the following expression over the conversion range of (1-x) = 0 – 1:

$$\mathrm{DEV}\ (1-\mathrm{X})(\%) = 100\ \mathrm{x}\ \frac{\sqrt{\frac{\mathrm{S}}{\mathrm{N}}}}{(1-\mathrm{X})\mathrm{max}} \quad \text{Eq 4.36}$$

$$\mathrm{S} = \sum_{\mathrm{i=1,N}}[(\mathrm{Y})_{\mathrm{exp}} - (\mathrm{Y})_{\mathrm{pre}}\}^2 \quad \text{Eq 4.37}$$

Where,

$_{exp}$ - experimental

$_{pre}$ - predicted

N - number of data points

Y – (1-x) or (dx/dt) (213)

4.7.2.2 Determination of reaction order and development of a nth order global char combustion model

The nth order reaction model is used to provide a simple model that predicts the reactivity of a fuel in all of the oxy-fuel combustion environments with a single value of A and Ea. The nth order model incorporates a term taking into account the partial pressure of oxygen and the reaction order with respect to oxygen concentration as outlined below.

$$\mathrm{R_n} = \frac{\mathrm{dx}}{\mathrm{dt}}\frac{1}{(1-\mathrm{x})^{\mathrm{m}}} = A_n\ \exp^{-Ea_n/\mathrm{RT}}\ \mathrm{P_{o2}^n} \quad \text{Eq 4.38}$$

In this case a new term A’ can be introduced (214) which incorporates both the pre-exponential factor A and the partial pressure and reaction order n.

$$\mathrm{R_n} = \frac{\mathrm{dx}}{\mathrm{dt}}\frac{1}{(1-\mathrm{x})^{\mathrm{m}}} = \mathrm{A'}\ \exp^{-\mathrm{Ea/RT}} \qquad \text{Eq 4.39}$$

Where, R_n – (s^{-1}) and A’ – (s^{-1})

In this model a single value of the activation energy and the pre-exponential factor is required and the activation energy was taken as the average of Ea_{app} determined from the apparent char kinetics. The determination of the pre-exponential factor is outlined later in this section. As a single value is used for the activation energy the value of A' was recalculated at each oxygen concentration by minimising the value of DEV (1-x) determined using Eq 4.36. The values of A' were determined at each oxygen concentration and from this, the reaction order with respect to oxygen determined using the following equation:

$$n = \frac{\text{Ln } A'_i - \text{Ln } A'_j}{\text{Ln } P_{O2\,i} - \text{Ln } P_{O2j}} \qquad \text{Eq 4.40}$$

Where,

A'_i – determined at 5% O_2

A'_j –determined at 30% O_2

(214)

The reaction order n was determined over the full range of oxygen environments to determine an average value. The value of the pre-exponential factor could then be determined from the knowledge of A' and P_{O2}^n at each oxygen concentration and average taken for use in the model using:

$$A_n = \frac{A'}{P_{O2}^n} \qquad \text{Eq 4.41}$$

Where,

A_n – pre-exponential constant (s^{-1}. Pa^{-1})

Once all of the parameters in Eq 4.38 were known, the reactivity R_n was determined, the conversion predicted and the deviation from the experimental data determined using Eq 4.36 and Eq 4.37.

4.7.2.3 Determination of the intrinsic reactivity of coal chars from non-isothermal experiments

The intrinsic reactivity was determined using the n^{th} order reaction model and knowledge of the coal char surface areas reported in section 5.5 using the following equation:

$$R_i = \frac{R_x}{S} = \frac{A_n \exp^{-Ea_n/RT} P_{o2}^n}{S} \qquad \text{Eq 4.42}$$

Where,

R_i – the intrinsic reactivity (kg. m^{-2}. s^{-1})

R_x – is the either the R_{app} in the case if chars produced in nitrogen and combusted in air or R_n when the chars are produced in CO2 and combusted in oxy-fuel environments.

s – the surface area (m^2 kg^{-1}) as determined by BET method outlined in section 4.3.6.

The intrinsic reactivity was determined over the conversion range of 0.05 – 0.85. In the case of the N_2 chars where only one oxygen concentration was used for the combustion experiments the apparent reactivity was used to determine the intrinsic reactivity.

4.8 Overview of experiments performed on each fuel

The experimental procedure outlined throughout this chapter were performed on a variety of the parent fuels and their chars. The experimental matrix can be seen in Table 4.5 and Table 4.6.

Table 4.5: Overview of which experiments performed on the coals and their chars

		PEL				ELC			PIT		
Experiment		**Fuel**	**PEL N_2**	**PEL CO_2**	**PEL DTR**	**Fuel**	**ELC N_2**	**ELC CO_2**	**Fuel**	**PIT N_2**	**PIT CO_2**
Proximate Analysis	British Standard	✓	-	-	-	✓	-	-	✓	-	-
	TGA	✓	✓	✓	✓	✓	✓	✓	✓	✓	✓
Ultimate Analysis		✓	✓	✓	✓	✓	✓	✓	✓	✓	✓
Low Nitrogen Analysis		-	-	-	-	-	-	-	-	-	-
Grindability Test		-	-	-	-	-	-	-	-	-	-
SEM		✓	✓	✓	✓	-	-	-	-	-	-
Surface Area		✓	✓	✓	✓	✓	✓	✓	✓	✓	✓
Pyrolysis	N_2	✓	✓	-	✓	✓	✓	-	✓	✓	-
	CO_2	✓	-	✓	-	✓	-	✓	✓	-	✓
Overall Combustion Behaviour	Air	✓	✓	-	✓	✓	✓	-	✓	✓	-
	Oxy-fuel (5-30% O_2/CO_2)	✓	-	✓	-	✓	-	✓	✓	-	✓
Devolatilisation kinetics		✓	-	-	-	✓	-	-	✓	-	-
Char production	DTR	✓	-	-	-	-	-	-	-	-	-
	TGA N_2	✓	-	-	-	✓	-	-	✓	-	-
	TGA CO_2	✓	-	-	-	✓	-	-	✓	-	-
Char combustion behaviour	Air	-	✓	-	✓	-	✓	-	-	✓	-
	Oxy-fuel (5-30% O_2/CO_2)	-	-	✓	-	-	-	✓	-		✓
Char kinetics	Apparent m^{th} order	-	✓	✓	✓	-	✓	✓	-	✓	✓
	n^{th} order	-	-	✓	✓	-	-	✓	-	-	✓
	Intrinsic	-	✓	✓	✓	-	✓	✓	-	✓	✓

Table 4.6: Overview of which experiments performed on the biomass fuels and their chars

		PWWP				WWP			TSP		
Experiment		**Fuel**	**PWWP N_2**	**PWWP CO_2**	**PWWP DTR**	**Fuel**	**WWP N_2**	**WWP CO_2**	**Fuel**	**TSP N_2**	**TSP CO_2**
Proximate Analysis	British Standard	✓	-	-	-	✓	-	-	✓	-	-
	TGA	✓	✓	✓	✓	✓	✓	✓	✓	✓	✓
Ultimate Analysis		✓	✓	✓	✓	✓	✓	✓	✓	✓	✓
Low Nitrogen Analysis		✓	✓	✓	✓	✓	✓	✓	✓	✓	✓
Grindability Test		-	-	-	-	-	-	-	✓	-	-
SEM		✓	✓	✓	✓	-	-	-	-	-	-
Surface Area		-	-	-	-	-	-	-	-	-	-
Pyrolysis	N_2	✓	✓	-	✓	✓	✓	-	✓	✓	-
	CO_2	✓	-	✓	-	✓	-	✓	✓	-	✓
Overall Combustion Behaviour	Air	✓	✓	-	✓	✓	✓	-	✓	✓	-
	Oxy-fuel (5-30% O_2/CO_2)	✓	-	✓	-	✓	-	✓	✓	-	✓
Devolatilisation kinetics		✓	-	-	-	✓	-	-	✓	-	-
Char production	DTR	✓	-	-	-	-	-	-	-	-	-
	TGA N_2	✓	-	-	-	✓	-	-	✓	-	-
	TGA CO_2	✓	-	-	-	✓	-	-	✓	-	-
Char combustion behaviour	Air	-	✓	-	✓	-	✓	-	-	✓	-
	Oxy-fuel (5-30% O_2/CO_2)	-	-	✓	-	-	-	✓	-		✓
Char kinetics	Apparent m^{th} order	-	✓	✓	✓	-	✓	✓	-	✓	✓
	n^{th} order	-	-	✓	✓	-	-	✓	-	-	✓
	Intrinsic	-	-	-	-	-	-	-	-	-	-

5 Fundamental characterisation of the fuels and their chars

5.1 Introduction

This chapter provides the proximate and ultimate analysis of the fuels and their chars produced using ballistic heating rate TGA in N_2 and CO_2 atmospheres and the chars produced using the DTR in a N_2 atmosphere. The effect of the char production method and atmosphere on char yield, composition, the nitrogen partitioning and physical properties such as surface area are discussed. The rate of oxygen consumed in the TGA is compared to the oxygen requirements for complete combustion of the fuels using the ultimate analysis data to ensure that sufficient oxygen is present in the TGA during combustion experiments. The heating rates of the fuel particles in the TGA and DTR is also determined to help understand the char production process. The results of the modified HGI index is included to estimate the degree of torrefaction experienced by the TSP sample. Finally the SEM images taken of the PEL and PWWP chars in all preparation atmospheres and by the two methods are shown and the differences discussed.

5.2 Raw fuel characterisation

The proximate, ultimate analysis and determination of the HHV were performed as outlined in section 4.3 and the analysis can be found in Table 5.1 and Table 5.3.

5.2.1 Raw fuel proximate analysis

The coal samples contain similar levels of volatiles and fixed carbon while the PIT sample contains less moisture and higher ash content. The three coals can be classified according to Table 3.2, the PEL is classed as High Vol A bituminous coal with ELC and PIT classified as High Vol C bituminous coal.

Table 5.1: Proximate analysis of the raw fuels using the British Standard methodology

Fuel	M (% ad)	±	Vol (% daf)	±	FC (% daf)	±	Ash (% db)	±
PEL	5.07	0.07	39.05	0.02	60.95	0.02	4.35	0.05
ELC	6.95	0.03	41.13	0.46	58.78	0.46	3.13	0.04
PIT	1.80	0.03	40.26	0.21	59.74	0.21	7.09	0.06
PWWP	6.69	0.02	84.25	0.40	15.75	0.40	0.70	0.01
WWP	7.81	0.04	84.54	0.03	15.46	0.03	0.91	0.07
TSP	5.09	0.01	76.23	0.21	23.77	0.21	0.44	0.16

ad - As determined basis, db - dry basis, daf - dry ash free basis
± - Absolute error (Section 4.3.2.1)
Note : The fuel identifications can be found in Table 4.2.

The biomass and TSP samples contain twice the amount of volatiles present in the coals and have lower fixed carbon and ash content. The two white wood pellets are very similar with all values within ~1wt% of each other. The torrefaction conditions of the TSP are not known by the author or by the supplier, but the level of volatiles and fixed carbon are in between the biomass and coal samples. This would be the expected outcome of the process as the amount of volatiles present in a fuel is reduced during the torrefaction process (208).

The fuels were used to produce chars in N_2 and CO_2 atmospheres (TGA) and at different heating rates (TGA and DTR). Proximate analysis of the chars were performed using a TGA as the total mass yield is not large enough for the standard proximate analysis. The difference in the method of determination of the proximate analysis may lead to errors in the comparison of raw fuels to their chars in terms proximate and ultimate analysis. In order to perform a direct comparison between the fuels and chars, proximate analysis of the fuels were performed using the TGA (See section 4.3.2.2) and can be seen in Table 5.2.

Table 5.2: Proximate analysis of the raw fuels using thermogravimetric analysis

Fuel	M (% ad)	±	Vol (% daf)	±	FC (% daf)	±	Ash (% db)	±
PEL	1.83	0.08	41.35	0.45	58.65	0.45	3.83	0.08
ELC	0.81	0.04	43.61	0.06	56.39	0.06	1.58	0.41
PIT	0.65	0.02	44.70	0.46	55.30	0.46	8.45	0.22
PWWP	1.61	0.03	89.17	0.27	10.83	0.27	0.83	0.03
WWP	1.93	0.05	89.25	0.02	10.75	0.01	1.56	0.24
TSP	1.20	0.03	80.73	0.32	19.26	0.32	0.61	0.01

ad - As determined basis, db - dry basis, daf - dry ash free basis
± - Absolute error (Section 4.3.2.1)
Note : The fuel identifications can be found in Table 4.2.

The difference between the determination of proximate analysis by British Standard and thermogravimetric method can be seen in Table 5.1 and Table 5.2. The fuels used in TGA proximate analysis were milled to <90µm as this is the size used to produce chars, while the British Standard proximate analysis requires a sample size of less than 1mm. The moisture content of all of the fuels is lower in the TGA proximate analysis due to the loss of additional moisture in the milling process. The volatile content is higher in all fuels when determined by TGA due to the slower heating rates and therefore increased residence time. In the standard proximate analysis the fuel is added to a furnace at 900°C and held for 7 minutes while in the TGA method the fuel is heated from 105°C to 900°C increasing the residence time to ~1hr. The increase in volatile content results in a decrease in fixed carbon. The ash content is similar to that determined using the British standard method (Table 5.1).

5.2.2 Raw fuel ultimate analysis

The ultimate analysis provides a chemical composition analysis of the fuels and can be seen in Table 5.3 and the determination of the HHV in Table 5.4. The PEL has the highest carbon content and thus HHV, with the remaining coal samples ELC and PIT having similar levels of carbon and HHV values. The remaining three biomass samples have levels of carbon at just over 50 wt% and similar HHV values, however both significantly lower than the coals.

Table 5.3: Ultimate analysis (daf) of raw fuels

	C	±	H	±	N	±	S	±	$O_{(b)}$	±
PEL	83.43	1.12	5.45	0.05	1.70	-	0.70	0.01	8.82	1.12
ELC	78.04	0.23	4.95	0.14	2.38	0.12	0.72	0.02	13.92	0.30
PIT	75.66	0.36	5.51	0.14	2.78	0.07	2.96	0.02	13.08	0.39
PWWP	52.27	0.21	6.04	0.07	0.23[(a)]	-	ND	-	41.46	0.22
WWP	51.45	0.79	2.19	0.02	0.14[(a)]	0.01	0.01	-	46.21	0.41
TSP	53.74	0.56	5.20	0.16	0.16[(a)]	-	0.07	-	40.83	0.59

[(a)]Determined by low nitrogen analyser
[(b)] Determined by difference
daf - dry ash free basis, ND - not detected
± Absolute error (Section 4.3.3.1)
Note : The fuel identifications can be found in Table 4.2.

The coals contain higher levels of nitrogen and sulphur relative to the biomass samples, while biomass contains higher oxygen content. The PIT coal has a much higher sulphur content than the PEL and ELC coals while very little if any was detected in the biomass samples.

Table 5.4: HHV of the raw fuels

	HHV(MJ/kg) (db)	±
PEL	32.87 [(a)]	0.59
ELC	30.22 [(a)]	0.13
PIT	29.19 [(a)]	0.04
PWWP	20.72 [(b)]	0..12
WWP	18.84 [(b)]	0.11
TSP	21.01 [(b)]	0.32

db – Dry basis
[(a)] Determined using the Milne equation
[(b)] Determined using the Friedl equation

The HHV values determined for the fuels in Table 5.4 are within the expected range. The PIT coal is a well-researched fuel and the HHV determined is in good agreement with that measured by bomb calorimetry by Mason (215) and that reported in the ECN Phyllis2 database (216).

5.3 Char characterisation

The TGA and DTR char yields, char proximate and char ultimate analysis are outlined in the following sections and the effect of the environment and char production method discussed.

5.3.1 Char yield

The theoretical char yield, actual yields of the chars produced in N_2 and CO_2 determined by TGA, and yields of chars produced using the DTR in N_2 on a dry basis can be seen in Figure 5.1 and numerical values in Table 5.5. The levels of uncertainty in the char yields takes into account the variation in moisture content in the raw fuel, as determined by TGA, and the variation in char yields as measured in each atmosphere and production method. The larger error bars seen in the coals is due to the low moisture content and associated errors. For a more detailed explanation of the propagation of errors please see section 4.5.3.2.

The coal char yields are similar to the theoretical yield (fixed carbon + ash) when chars are produced using the TGA regardless of the char production atmosphere. The char yields in N_2 and CO_2 atmospheres are almost identical with the PEL having the largest difference, 1 wt% increase in the PEL CO_2 char, whilst the ELC and PIT chars have a difference of just ~0.03 wt%. This suggests that at the heating rates and temperatures used in this work the char production atmosphere has little effect on the char yields of coals.

The biomass and TSP samples yielded much less char than the coal samples due to the higher volatile content in the parent fuel (Table 5.1) and the higher organically bound oxygen levels in the biomass samples (Table 5.3). This provides readily available oxygen that oxidises the volatiles released enhancing the amount of decomposition seen in the PWWP, WWP and TSP samples (102). When the biomass and torrefied biomass chars are produced in an N_2 atmosphere the char yield is slightly higher that the theoretical yield but the chars produced in the CO_2 environment have a significantly lower char yield. The PWWP and WWP yields in CO_2 are ~ 50% and the TSP is ~75% of those seen in N_2 atmosphere. This phenomena is not seen in the coal samples and is thought to be due to the increased reactivity of the biomass fuels. The enhanced devolatilisation seen in the biomass and TSP fuels is due to the CO_2 char reaction:

$$\mathrm{Char} + \mathrm{CO_2} \leftrightarrow \mathrm{CO} + \mathrm{CO}$$

Comparison of the theoretical yield to the actual yield verifies the reaction of carbon with CO_2,as the theoretical yield is the mass of ash and fixed carbon in the raw fuel as determined by TGA proximate analysis.

Chars produced using the DTR results in a lower yield than seen in TGA in N_2 for both the PEL and PWWP fuels. This is believed to be the result of the 1% oxygen levels present in the DTR (to prevent the char from sticking) and the increased reactivity of both fuels at the temperatures and heating rates used in the DTR (156, 217) (1273 K at 1000 K min^{-1} in the TGA and 1373K at 10^4 – 10^5 K min^{-1} in the DTR).

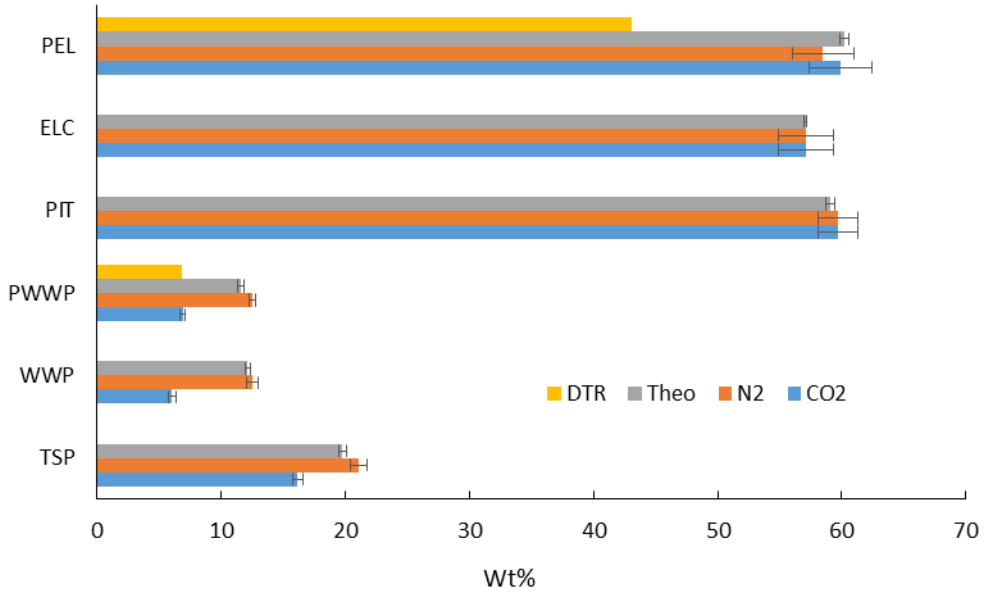

Figure 5.1: Char yields (dry basis) for chars produced using the TGA (N_2 and CO_2), in the DTR and theoretical yields (FC + Ash in raw fuel as determined by TGA proximate analysis)

Work by Molina et al. (148) suggested that when a non-reactive particle is heated in N_2 or CO_2 at the same heating rate and final temperature the only effect of the change in environment is the thermal conductivity of the atmosphere. In the case of N_2 and CO_2 the ratio of thermal conductivity is ~1.1 at the temperatures seen in the TGA. In this case the particle is reactive but the devolatilisation behaviour of the coals (in terms of char remaining after pyrolysis) is very similar in both N_2 and CO_2 atmospheres.

The majority of the work in literature investigating pyrolysis behaviour in relation to oxy-fuel has been performed on coals. Rathnam et al (218) investigated the pyrolysis behaviour of four coals in N_2 and CO_2 using a TGA. They noted that when heated at a slow heating rate

(25K min^{-1}) the mass loss rate of the coals in both the CO_2 and N_2 atmosphere are similar up to 1030 K at which point the rate of mass loss in the CO_2 atmosphere starts to increase compared to N_2. The additional mass loss seen in the CO_2 atmosphere was attributed to the char – CO_2 gasification reaction.

Li et al (219) also investigated pyrolysis behaviour of a bituminous coal using a TGA at heating rates of 30 K min^{-1} in N_2 and in 21%N_2/79%CO_2. The char yield in the 100% N_2 atmosphere was found to be slightly higher (3 wt%) than in the N_2/CO_2 atmosphere. The enhanced devolatilisation in the CO_2 based atmosphere was attributed to the char – CO_2 reaction at elevated temperatures.

Zhou et al. (220) used a TGA to investigate the pyrolysis behaviour of four coals in 100% N_2 and CO_2 atmospheres (1273 K 20 K min^{-1}). Enhanced devolatilisation was seen in all coals in the CO_2 atmosphere but the degree of increased mass loss was found to be coal rank dependent.

Although the work carried out by Rathnam, Li and Zhou use a TGA and similar maximum temperatures (1000^oC) the heating rate is much slower than the ballistic heating rates used in this work (25-30K min^{-1} compared to 1000K min^{-1}). The increase in heating rate, and therefore decreased residence time at elevated temperatures, in the work in this thesis is believed to be the reason for the similarity in char yields of the coals in both N_2 and CO_2 atmospheres. Further evidence of this is seen in Figure 6.14 and Figure 6.15, where the pyrolysis behaviour of the fuels in N_2 and CO_2 at slow heating rates (10 K min^{-1} to 1173 K) can be seen. At the slower heating rates the char – CO_2 reaction is evident and char yields in CO_2 atmospheres are similar to the levels of ash determined in Table 5.1.

Drop tube reactors have widely been used to investigate devolatilisation behaviour of fuels at higher heating rates and temperatures than those seen in analysis by TGA. Borrego and Alvarez (156) used a DTR to investigate char characteristics of coals in N_2 and CO_2 atmospheres with oxygen levels of 0-21%. The temperature of the DTR was 1573 K and heating rate not specified, but as this is a DTR it is expected to be 10^4-10^5 K min^{-1}. They reported that enhanced devolatilisation was seen in N_2 and CO_2 environments compared to the expected volatile yield as determined by proximate analysis (theoretical yield). Although Borrego reports in terms of devolatilisation the char yield can be inferred from the experimental results. Borrego also found that the chars produced in N_2 had higher volatile yields than those produced in CO_2 and suggested that CO_2 is participating in the crosslinking reactions at the char surface, reducing the plasticity and preventing the coalescence of

aromatic structures. Again the char yields can be inferred from the volatile yields and in contrast to the work done by Rathnam et al., Li et al. and Zhou et al. the char yield in the CO_2 environment is higher than that in the N_2 atmosphere.

Brix et al. (221) investigated the devolatilisation behaviour of coals in N_2 and CO_2 atmospheres in an entrained flow reactor at 1673 K. The heating rates of the entrained flow reactor are reported as similar to those seen in a DTR and in this case it was found that no noticeable difference in char yield could be found between N_2 and CO_2 atmospheres. They also attributed the differences seen in char yields when using a TGA at slow heating rates can be attributed to the particle temperature histories and long residence times which can induce the CO_2 gasification reaction in reactive coals.

Less work has been done to investigate biomass devolatilisation behaviour in N_2 and CO_2 atmospheres. Farrow (222) used a DTR to investigate the devolatilisation behaviour of a sawdust at 1173 K – 1573 K and found that for a biomass sample the char yield in a CO_2 environment is significantly lower than the N_2 produced char. The author varied both the temperature and residence time in the DTR and found that as either one was increased the difference between char yields decreased. This was attributed to the decrease in char yield at both increased temperatures and residence time and hence the lower significance of char – CO_2 gasification reactions.

It can be seen from the discussion that the expected difference in char yields in N_2 and CO_2 environments is both fuel and temperature history dependent. At slower heating rates the CO_2 produced chars are expected to be significantly lower in quantity than the N_2 chars. At higher heating rates and maximum temperatures the effect of the char – CO_2 gasification reaction is unclear. Char yields from coals may be higher, lower or similar, although the difference between the two atmospheres is smaller than that seen in low heating rate work. The difference in char yield trends has been attributed to the coal type and in particular the propensity for crosslinking reactions resulting in higher char yields in CO_2 atmospheres. The increased reactivity of biomass, due to the higher volatile content and more reactive char results in a lower char yield in CO_2 atmospheres relative to N_2 atmospheres.

5.3.2 Char proximate analysis

The proximate analysis of the chars was performed using the TGA due to the low char yield from both the DTR and TGA char production methods and the ultimate analysis were performed using the same method as the raw fuels.

The chars produced using the TGA in N_2 and CO_2 atmospheres are very similar for the three coal samples with the volatiles, fixed carbon and ash (dry basis) within 1 wt% between the two environments. This would be expected from the char yields determined in the previous section.

Table 5.5: Proximate analysis (db) of chars produced using the TGA in N_2 and CO_2 and chars produced using the DTR in N_2 and char yield (db)

		Vol	±	FC	±	Ash	±	Yield	±
PEL	N_2	4.10	0.02	87.83	0.44	8.07	0.42	58.50	2.47
	CO_2	5.09	0.34	86.44	0.72	8.47	0.39	59.92	2.55
	DTR	8.22	0.19	82.87	0.87	8.91	0.68	43.03	0.03
ELC	N_2	4.29	0.33	91.28	0.47	4.43	0.14	57.13	2.20
	CO_2	4.85	0.39	91.12	1.06	4.03	0.67	57.10	2.25
PIT	N_2	2.91	0.02	82.23	0.21	14.86	0.22	59.68	1.57
	CO_2	3.83	0.02	81.73	0.36	14.44	0.37	59.71	1.60
PWWP	N_2	7.75	0.02	83.45	0.10	8.80	0.08	12.51	0.29
	CO_2	12.07	0.38	73.92	0.58	14.01	0.20	6.89	0.23
	DTR	31.84	0.48	55.98	0.27	12.18	0.21	6.80	0.01
WWP	N_2	8.00	0.16	83.81	0.05	8.19	0.11	12.54	0.48
	CO_2	15.14	0.5	67.11	0.02	17.75	0.33	6.03	0.32
TSP	N_2	5.53	0.5	91.27	0.69	3.20	0.01	21.05	0.69
	CO_2	7.01	1.03	88.84	0.89	4.14	0.34	16.16	0.43

db - dry basis
± - Absolute error (Section 4.3.2.2)
Note : The fuel identifications can be found in Table 4.2.

The change in char production atmosphere has a greater effect on the biomass and TSP fuels as would be expected from the char yields. The volatile content of the biomass and TSP chars produced in CO_2 is higher and fixed carbon content lower compared to their analogue produced in N_2. The difference in properties between the two atmospheres is greatest in the raw biomass fuels (PWWP and WWP) with an increase in volatile content of 5-7 wt% and decrease in fixed carbon 10-16 wt%. The TSP sample falls in between the coal and biomass samples in terms of changes to volatile and fixed carbon content resulting from the change in char preparation environment.

These figures are slightly deceiving when taken in isolation; in order to fully understand the effect of the reaction atmosphere and the production method (TGA vs DTR) on

devolatilisation during char production it is important to also consider the char yield. Using the char yields and both the volatile contents of the fuels and their chars, a mass balance can be performed to determine the percentage of the volatile content present in the fuel remaining in the chars (Figure 5.2). For an example calculation of the relative volatile yield and the propagation of absolute errors please see section 4.3.2.3 in the methodology section and section 12.1 in the appendix.

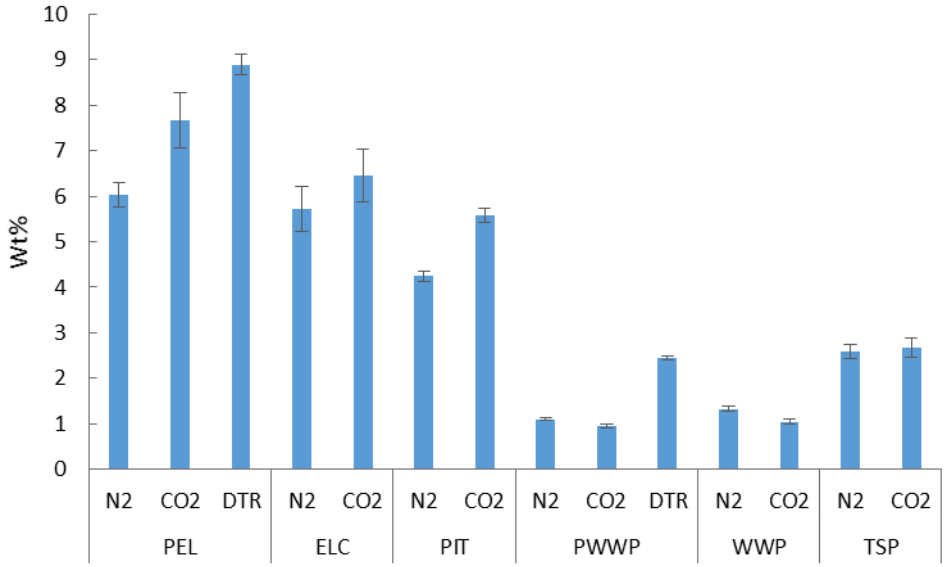

Figure 5.2: Wt% of volatiles remaining in the char (db) relative to the volatile content (db) of the raw fuel

The relative volatile yield can be seen in Figure 5.2. It can be seen that a greater amount of the volatiles present in the coals are retained when compared to the biomass and TSP fuels. The coal chars show enhanced devolatilisation in the chars produced in N_2 environments with ~1.5 wt% increase in the volatiles retained. The decrease in volatile release in CO_2 atmospheres has been associated with the crosslinking of CO_2 at the char surface preventing devolatilisation (135, 156, 223). The change in atmosphere has the reverse effect on the biomass samples with enhanced devolatilisation seen in the CO_2 chars, although the difference is only ~0.3 wt%. The volatile yields in the TSP sample are almost identical with the volatile yield in the char produced in CO_2 only 0.07 wt% higher. The chars produced in the DTR retain a higher percentage of the original volatiles compared to the N_2 TGA chars due to the lower residence time seen in the DTR.

In all of the fuels a small percentage of the original volatile content is still present in all of the chars meaning that complete devolatilisation is not seen during the char production

process. In order for the char yield to be less than the theoretical there must be a loss in fixed carbon during the char production process.

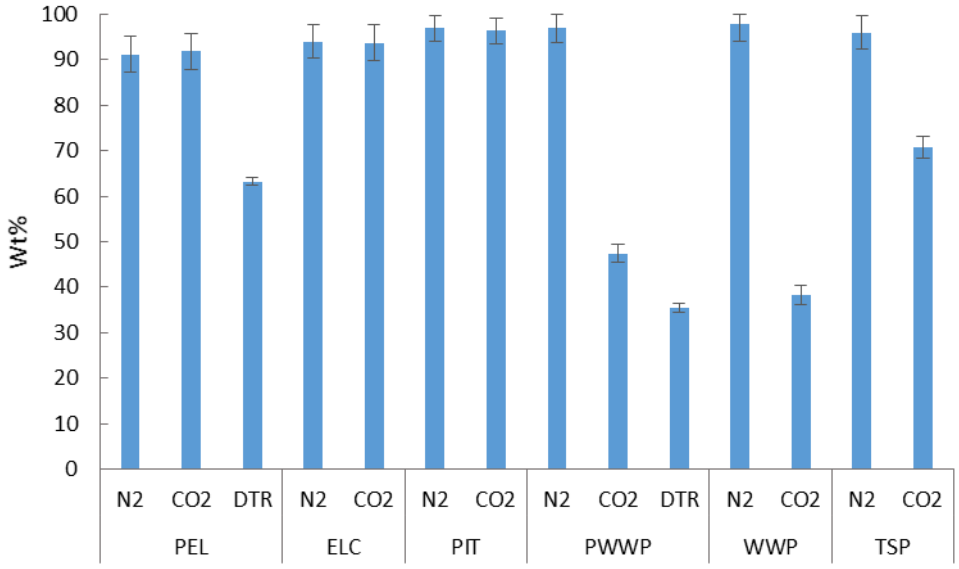

Figure 5.3: Wt% of fixed carbon (db) remaining in the char relative to the fixed carbon content (db) of raw fuel

The fixed carbon content in the char as a percentage of the fixed carbon present in the raw fuels can be seen in Figure 5.3. In all cases part of the fixed carbon present in the raw fuel is consumed during the char production process. The coal samples retain the majority of the fixed carbon in their chars with negligible difference between the char production environments, again highlighting the similarities in char production in the N_2 and CO_2 atmospheres.

The biomass and TSP chars produced in the CO_2 atmosphere retain less of the fixed carbon present in the fuel than in the N_2 atmosphere, evidence of the char – CO_2 gasification reaction. The biomass chars produced in CO_2 retain 50-60% less of the fixed carbon present in the fuels in the biomass and 30% less in the TSP sample. The loss of fixed carbon results in the lower char yields seen for the biomass and TSP chars.

The change in char production technique (ballistic heating in the TGA vs DTR) also produced chars with different characteristics. In both the PEL DTR and PWWP DTR chars, the fixed carbon content decreased while the volatile content increased compared to chars produced in N_2 using the TGA. It is difficult to determine the exact reasoning for the difference in DTR chars as several parameters were changed during the experiments. Firstly the particle sizes used in the DTR are larger, the coals were 75-180 µm and the biomass samples 212-355 µm,

compared to <90 µm used in the TGA. Work by Mani et al (130) using a TGA to perform pyrolysis of in N_2 and found that the volatile content and fixed carbon content of a biomass char is increased with the increase in particle size of the raw fuel. The authors also investigated the effect of heating rates and found that when heating rates were increased (5 K min^{-1} – 20 K min^{-1}) the char yield also increased. This was attributed to more effective heat transfer to the centre of the particle, and as a result increased devolatilisation, at lower heating rates.

Yan et al (217) investigated the effect of increasing temperatures (1173 K – 1573 K) and heating rates (slow 10^{-1} – 10^{1} K min^{-1} and fast 10^{2} – 10^{4} K min^{-1}) on the devolatilisation of coal using a DTR. It was reported that in, contrast to the work by Mani et al. as heating rates and temperatures are increased the conversion of carbon to light gases is increased and hence char yield decreases.

With respect to the DTR chars and TGA chars seen in this work, the increase in volatile content remaining in the DTR chars relative to the TGA N_2 chars is thought to be due to the increased particle size and decreased residence time in the DTR. The decrease in fixed carbon seen in the DTR is linked to the higher heating rates and increased maximum temperatures which is expected to result in carbon to light gas conversion (125).

5.3.3 Char ultimate analysis

The ultimate analysis of the chars produced can be seen in Table 5.6 and Table 5.7. The chars produced from the coals in N_2 have a slightly higher carbon content (wt% basis) than those produced in CO_2, whilst in the biomass samples the trend is reversed, with the chars produced in N_2 having a lower carbon content than those produced in CO_2. The TSP sample has carbon contents on a wt% basis that is almost identical in both char production atmospheres. Hydrogen content in all chars is low with no real difference between the two char production atmospheres. No sulphur was detected in the biomass and TSP chars but small traces were detected in the coal chars but again no trends could be determined between char production atmospheres. The oxygen contents of the biomass chars is significantly higher than the coal chars. The oxygen concentration of the coal chars produced in N_2 is lower than that of the CO_2 char, which is reversed in the biomass chars with CO_2 produced chars containing the amount of oxygen. The increased oxygen content of the biomass chars is one reason for their increased reactivity compared to coal chars which is discussed in section 7.

The chars produced using the DTR have significantly lower carbon contents due to the larger higher degree of carbon burnout and the increase in the amount of volatiles present, as shown in Table 5.5 and suggested by the higher levels of hydrogen and oxygen (associated with volatiles) present in the chars.

Table 5.6: Ultimate analysis of chars (DAF) produced using the TGA in N_2 and CO_2 and chars produced using the DTR in N_2

Daf Basis (wt%)		C	±	H	±	N	±	S	±	O	±
PEL	N_2	95.49	0.65	0.62	0.03	1.80	0.09	0.09	0.01	2.01	0.49
	CO_2	92.45	0.65	0.73	0.12	1.69	0.04	0.41	0.03	4.73	0.53
	DTR	87.32	1.45	0.93	0.03	1.59	0.03	ND	-	10.16	1.40
ELC	N_2	91.66	0.24	0.51	0.06	1.26	0.46	0.07	0.07	6.50	0.50
	CO_2	91.16	1.60	0.58	0.02	1.33	0.40	ND	-	6.94	1.53
PIT	N_2	96.81	0.66	0.49	0.01	1.18	0.28	1.78	0.08	0.69	0.68
	CO_2	92.02	1.03	0.56	0.01	1.75	0.02	2.22	0.03	3.45	0.96
PWWP	N_2	84.53	0.77	0.63	0.02	0.13[(a)]	-	ND	-	14.71	0.77
	CO_2	88.75	0.65	0.66	0.03	0.17[(a)]	-	ND	-	10.43	0.62
	DTR	77.11	1.36	1.75	0.19	0.21[(a)]	-	ND	-	20.69	1.36
WWP	N_2	87.87	0.93	0.41	0.07	0.13[(a)]	-	ND	-	12.22	0.93
	CO_2	95.52	0.48	0.51	0.01	0.17[(a)]	-	ND	-	3.81	0.30
TSP	N_2	93.40	0.56	0.48	0.01	0.08[(a)]	-	ND	-	6.04	0.56
	CO_2	93.22	0.36	0.43	0.01	0.09[(a)]	-	ND	-	6.25	0.29

[(a)]Determined by low nitrogen analyser
[(b)] Determined by difference
daf - dry ash free basis, ND - not determined
NOTE: The fuel char identifications can be found in Table 4.2.

Table 5.7: HHV of the chars produced in the TGA and DTR

		HHV (MJ/kg) (db)	±
PEL	N_2	30.14[(a)]	0.26
	CO_2	28.92[(a)]	0.04
	DTR	27.04[(a)]	0.64
ELC	N_2	29.56[(a)]	0.03
	CO_2	29.24[(a)]	0.93
PIT	N_2	26.25[(a)]	0.21
	CO_2	25.40[(a)]	0.39
PWWP	N_2	24.81[(b)]	0.30
	CO_2	24.54[(b)]	0.23
	DTR	23.35[(b)]	0.18
WWP	N_2	25.51[(b)]	0.48
	CO_2	24.71[(b)]	0.11
TSP	N_2	29.78[(b)]	0.27
	CO_2	29.20[(b)]	0.15

[(a)] Determined using the Milne equation
[(b)] Determined using the Friedl equation

It is again useful to determine the relative carbon contents of the chars in relation to the carbon content present in the raw fuel taking into account the char yields (Figure 5.4). The coals show a small reduction in carbon in chars produced in CO_2 atmospheres. The biomass samples show a larger reduction in carbon content in those chars made in CO_2 with levels in those chars roughly half that found in chars produced in N_2 for the WWP and PWWP samples. The TSP CO_2 char retains ~2/3 of the carbon that is retained in the char produced in N_2. This is further evidence of the CO_2 char gasification reaction described in section 3.5.3.

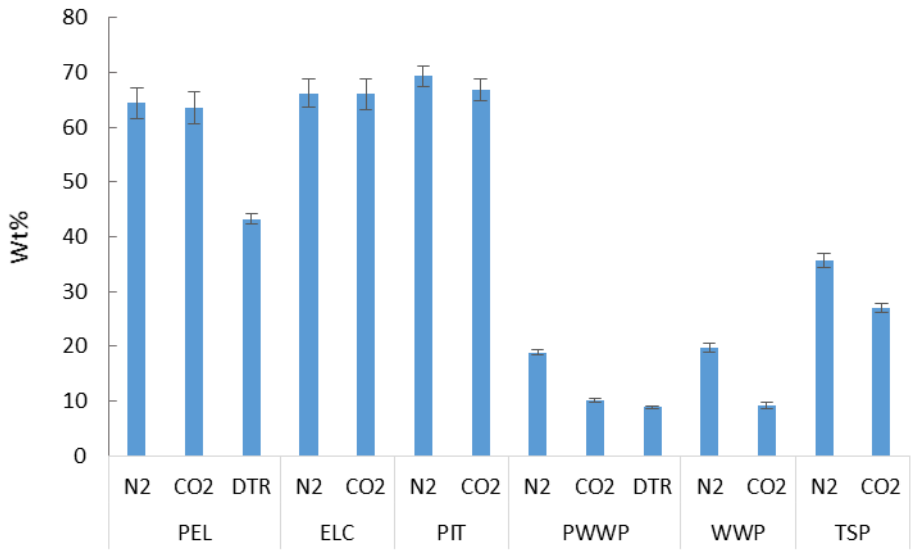

Figure 5.4: Wt% of carbon (db) remaining in the char relative to the carbon content (db) of raw fuel

5.3.4 Nitrogen partitioning

The relative nitrogen content was also determined using the char yields (Table 5.5) and nitrogen content of the chars (Table 5.6) shown in Figure 5.5. The error bars associated with the coal char nitrogen content are large relative to the biomass samples due to the different equipment used in the analysis. The biomass raw fuel and char nitrogen analysis was performed using an Analytik Jena Multi 5000 with a much lower detection level, however the coals contain nitrogen levels beyond the calibration limits of this analysis.

In all samples the nitrogen present in the raw fuel is low with the coals containing ~2 wt% and the biomass ~0.2 wt% (Table 5.3). The coal samples retained much more of the nitrogen than the biomass and TSP samples in their chars, which is the result of the decreased volatile content present in the coals relative to the biomass samples (Table 5.1). The decrease in

char bound N is the result of the increase in fuel bound N released during the devolatilisation stage. This agrees with earlier work performed by Di Nola et al. (177).

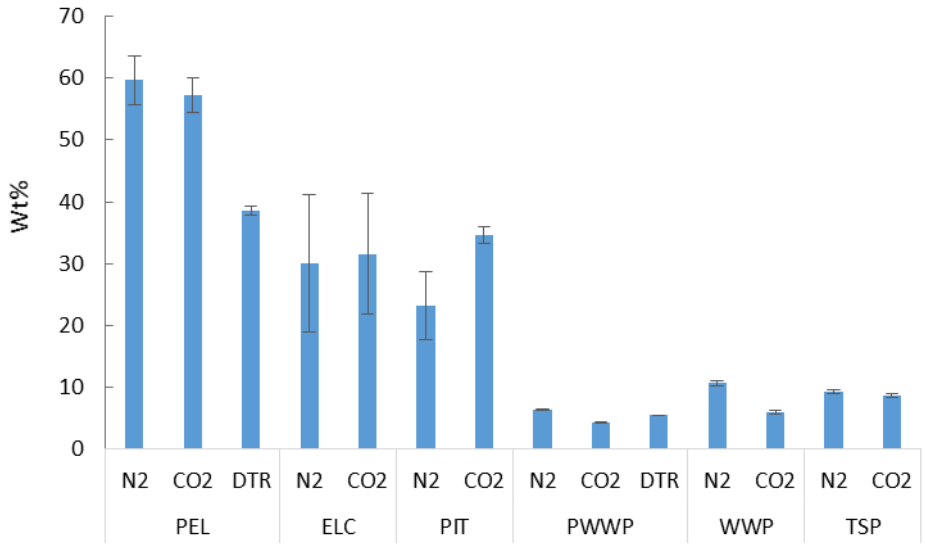

Figure 5.5: Wt% of nitrogen (db) remaining in the char relative to the nitrogen content (db) of raw fuel

The effect of the change in char production atmosphere is shown to have only a small effect on nitrogen partitioning. The N retained in the PEL N_2 char is greater than in the PEL CO_2 char. The remaining coals show the reverse trend with the ELC and PIT CO_2 chars retaining high levels of the fuel bound N. It should be noted that the error bars associated with the ELC and PIT N_2 char N content are quite large relative to the calculated values. This is the result of the absolute error measured in the char N and low nitrogen content in the chars as can be seen in Table 5.6. The increase in char bound N in the ELC CO_2 and PIT CO_2 chars is believed to be due to the lower volatile release seen during char production Figure 5.2 thought to be the result of cross-linking and recombination of the char fragments to the char surface.

The biomass and TSP chars prepared in CO_2 atmospheres have a slightly lower (2-5%) nitrogen retention than those produced in N_2. The decrease in Nitrogen content in the CO_2 chars can be related to the decrease in char yield (Figure 5.1) and enhanced devolatilisation seen in CO_2 atmospheres. The same trend is seen in work by Farrow et al. (182) who investigated the effect of pyrolysis atmosphere on nitrogen partitioning using several biomass samples and noted that the increase in volatile yield resulted in lower char N.

As mentioned in the literature review (section 3.8), the fuel bound nitrogen in the principal contributor to the total NO_x produced in a pulverised fuel boiler. The formation of fuel bound NO_x is limited through the use of low-NO_x burners or furnace air staging where the easily managed N released during devolatilisation is converted to N_2. It can be clearly seen from Figure 5.5 that the biomass and TSP fuels release the majority of their fuel bound N in the devolatilisation stage of combustion (regardless of char production atmosphere) making control of NO_x formation easier relative to coal. The coals show a different trend with the PEL coal retaining the majority of the N in its char and the remaining coals retaining relatively high proportions in their char when compared to the biomass chars.

Comparison of char N retention as a result of char production atmosphere suggests that more N is released in biomass, and TSP CO_2 chars during devolatilisation which is favourable for control of NO_x emissions. The coals however show a variation in N partitioning when comparing char production atmosphere which suggests that in some fuels the release of fuel bound N in the devolatilisation stage maybe inhibited in oxy-fuel environments and therefore additional NO_x control measures may be required. This is of particular importance in new build oxy-fuel where flame temperatures may be higher than those seen in air combustion (retro fitted CCS plants suggest oxygen concentrations should be selected to give flame temperatures similar to those seen under air combustion in the same unit) enhancing NO formation which is not as easily reduced as N released in the devolatilisation stage.

5.4 Oxygen consumption in TGA experiments

Knowledge of the composition of the fuels allows the author to compare the oxygen requirements of the system compared to the rate at which oxygen is entering the TGA ensuring that the combustion of the fuel is not limited due to oxygen deficiency. The molar flow rates of oxygen entering the TGA were determined from the volumetric flow rates of the O_2/CO_2 gas mixtures reported in Table 4.3.

Table 5.8: Oxygen molar flow rate into the TGA at 5- 30% oxygen concentrations

O_2 Concentration	**30% O_2/ 70 % CO_2 (ml min^{-1})**	**O_2 flow rate (ml min^{-1})**	**O_2 flow rate (mol min^{-1})**
5	8.3	2.5	9.75×10^{-5}
10	16.7	5.0	1.95×10^{-4}
21	35.0	10.5	4.01×10^{-4}
25	41.7	12.5	4.87×10^{-4}
30	50.0	15.0	5.85×10^{-4}

Note: Density of O_2 @ 300 K (1.25×10^{-3} g ml^{-1}) (224)

The composition of the fuel is known and the total oxygen requirement for complete combustion can be easily determined for each using the C, H, N, S results reported in Table 5.3 and Table 5.6 and the assumption that 5 mg of each was added to the TGA in each of the experiments. The analysis of the PEL fuel combusted in 5% O_2 (the lowest oxygen concentration) can be seen below. This assumes a mass of 5 mg and that the combustion products are CO_2, H_2O, NO_2 and SO_2.

Table 5.9: Total oxygen demand in PEL fuel

(daf)	Wt%	Mass (mg)	mol C,H,N,S	mol of O_2 required
C	83.46	3.94	3.28×10^{-4}	3.28×10^{-4}
H	5.45	0.26	2.55×10^{-4}	6.37×10^{-5}
N	1.70	0.08	5.73×10^{-6}	5.73×10^{-6}
S	0.70	0.03	1.03×10^{-6}	1.03×10^{-6}
Total		4.31	5.89×10^{-4}	3.98×10^{-4}

The total oxygen demand to ensure complete combustion for the PEL fuel is 3.98×10^{-4} mol of O_2. This does not take into account the oxygen present in the fuel and so the oxygen demand is over estimated. The excess oxygen percentage supplied to the TGA was determined using Eq 5.1:

$$\frac{mol\ O_{2\ in} - mol\ O_{2\ req}}{mol\ O_{2\ req}}\ x100 \qquad \text{Eq 5.1}$$

mol $O_{2\ in}$ = 9.75×10^{-5} mol min^{-1} x 120 min = 1.17×10^{-2} mol (in the 5% O_2/CO_2 atmosphere)

mol $O_{2\ req}$ = 3.98×10^{-4} mol

Note the duration of the combustion experiments is 120 minutes.

The excess oxygen percentage is 2837 %, well in excess of that required for complete combustion. However as the combustion experiments were temperature programmed the total excess oxygen percentage is not reflective of the true oxygen demands at elevated temperatures. Instead it was decided to determine the oxygen demand at the maximum rates of mass loss observed in the combustion experiments which are reported in Table 6.1 and Table 6.3. However, the composition of the fuels are unknown at these points in the combustion profiles and need to be estimated. In the case of the biomass and TSP fuel the maximum rate of mass loss is seen in the devolatilisation stage (dm/dt_v) and it was assumed that the composition of the fuel is the same as the raw fuel. The coal maximum rate of mass loss (dm/dt_c) is seen at higher temperatures and it was assumed that the composition purely carbon. It is know that these assumptions may greatly differ from the actual composition of

the fuels at the time when the maximum rates of mass loss is observed but deemed sufficient in order to estimate oxygen demand. The PEL fuel was again used to determine the oxygen demand at the maximum rate of mass loss assuming a starting mass of 5 mg (ar basis).

The maximum rate of mass loss (dm/dt_c) in the 5% O_2/CO_2 atmosphere is 6.54 wt% min^{-1} (Table 6.6). Based on 5 mg of fuel, the rate of mass loss is 0.327 mg min^{-1}.

Assuming that this is carbon conversion, 2.72 x 10^{-5} mol of O_2 are required and the molar flow rate of O_2 in the 5% O_2/CO_2 atmosphere is 9.75 x 10^{-5}. The excess oxygen percentage determined using Eq 5.1 is 258 %, significantly higher than is required. Again this does not take in account the oxygen present in the fuel which is available for combustion.

In the case of the biomass fuels where the composition of the fuel at the point of maximum rate of mass loss is assumed to be the same as the original fuel, the oxygen demand was determined as follows.

PWWP maximum rate of mass loss (dm/dt_v) in 5% O_2/CO_2 is 10.62 wt% min^{-1} (Table 6.9).

Based on 5 mg of fuel, the rate of mass loss is 0.531 mg min^{-1}

C content = 52.27 (wt%) / 100 x 0.531 mg min^{-1} = 0.276 mg min^{-1} = 2.31 x 10^{-5} mol min^{-1}

H Content = 6.04 (wt%) / 100 x 0.531 mg min^{-1} = 0.032 mg min^{-1} = 3.18 x 10^{-5} mol min^{-1}

N Content = 0.23 (wt%) / 100 x 0.531 mg min^{-1} = 1.22 mg min^{-1} = 8.72 x 10^{-8} mol min^{-1}

Note the C, H and N data taken from Table 5.3.

The total number of mols of O_2 required is 3.11 x 10^{-5}. Using equation 5.1 the excess oxygen concentration was determined as 213 %, again this does not take in to account the oxygen in the fuel and is still significantly higher than is required for complete combustion.

The excess oxygen percentage for all of the fuels combusted in 5% and 30% O_2/CO_2 can be seen in Table 5.10.

Table 5.10: Excess oxygen percentage in the TGA

	O_2 concentration	Excess oxygen (%)
PEL	5	258
	30	1410
ELC	5	212
	30	1088
PIT	5	279
	30	1432
PWWP	5	213
	30	675
WWP	5	217
	30	1025
TSP	5	155
	30	628

In all cases the oxygen fed into the TGA is in excess of that required for complete combustion at the maximum rate of mass loss and the degree of excess oxygen increases as the oxygen concentration in the combustion atmosphere increases. Again as the oxygen present in the fuels is not accounted for in the determination of oxygen demand, it is expected that the values reported in Table 5.10 are underestimated. It is suggested that the combustion of fuels in the TGA with a total flow rate of 50 ml min^{-1} is sufficient to ensure complete combustion. The variation of the sample mass in the TGA at the same oxygen flow rates would have been a useful experiment to perform in order to determine if the oxygen concentration was sufficient, through the identification of the maximum rates of mass loss, and is suggested for future work.

5.5 Particle heating rates during devolatilisation

5.5.1 Determination of biot number

The particles used in the DTR and TGA experience different heating profiles due to the different temperatures, heating rates and particle sizes used in each piece of equipment. It is useful to determine the difference between the gas atmosphere temperature present in the TGA and the DTR and the particle temperatures to help understand the devolatilisation process using Eq 3.4 (148). The rate of devolatilisation is controlled by either external heat transfer, internal heat transfer, as described in section 3.5.2, or chemically controlled when the particle size is small (203). In order to determine if devolatilisation is heat transfer or chemically controlled it is useful to determine the Biot number which is the ratio of internal to external heat transfer. In the case of the heating of a fuel particle, if the Biot number is

<0.1 then the it is suggested that the particle is heated due to external heat transfer and that the internal temperature of the particle is uniformed (203). The Biot number is described below by Eq 5.1 (203).

$$\mathrm{Bi} = \frac{\tau_{\mathrm{heatint}}}{\tau_{\mathrm{heatext}}} \qquad \text{Eq 5.2}$$

Assuming that the particle does not undergo a chemical reaction and that the heating rate is controlled by internal thermal conduction then $\tau_{heatint}$ can be described by Eq 5.3 and 5.4.

$$\tau_{\mathrm{heatint}} = 0.2\, a^2/\kappa \qquad \text{Eq 5.3}$$

a – particle radius (m)

κ – thermal diffusivity ($m^2\ s^{-1}$)

$$\kappa = \lambda_s/(\rho.\mathrm{Cp}) \quad \text{Eq 5.4}$$

λ_s – thermal conductivity of the fuel particle ($W\ m^{-1}\ K^{-1}$)

ρ – particle density ($kg\ m^{-3}$)

C_P – specific heat capacity of the particle ($W\ m^{-1}\ K^{-1}$)

The external heating of the particle from its hotter surroundings can be described by Eq 5.5-5.6)

$$\tau_{\mathrm{heatext}} = a\rho\mathrm{Cp}/3h \qquad \text{Eq 5.5}$$

h –surface heat transfer coefficient ($W\ m^{-2}\ K^{-1}$)

$$h = \mathrm{Nu}\,\lambda_{\mathrm{ext}}/2a \qquad \text{Eq 5.6}$$

λ_{ext} – thermal conductivity of the gas ($W\ m^{-1}\ K^{-1}$)

Nu – Nusselt number

The Nusselt number can be estimated from the Reynolds number as seen in Eq 5.7.

$$\mathrm{Nu} = 2 + 0.6\,\mathrm{Re}^{1/2}\mathrm{Pr}^{1/3} \qquad \text{Eq 5.7}$$

Pr – Prandtl number (0.71)

The Reynolds number for a gas passing of a sphere is described by Eq 5.8.

$$\mathrm{Re} = \mathrm{ud}/\nu \qquad \text{Eq 5.8}$$

u – gas velocity (m s^{-1})

d - diameter of the particle (m)

v – kinematic viscosity of the gas (m^2 s^{-1})

Combination of Eq 5.2 – 5.8 leads to the definition of the Biot number as

$$\mathrm{Biot} = 0.6 \text{ x } \left(\frac{\mathrm{Nu}}{2}\right) \text{x } \left(\frac{\lambda_s}{\lambda_{ext}}\right) \qquad \text{Eq 5.9}$$

The parameters for the fuels, gas and equipment used to determine the biot numbers can be seen in Table 5.11.

Table 5.11: Parameters used in the determination of Biot numbers

Particle Properties	**Biomass**	**Coal**
d (TGA) (µm)[(1)]	90	90
d (DTR) (µm)[(1)]	350	180
λ_s (W m^{-1} K^{-1}) (203)	0.12	0.26
Cp (J kg^{-1} K^{-1}) (215)	1600	1088
ρ (kg m^{-3}) (215)	500	1080
Gas Properties	**N_2**	**CO_2**
λ_{ext} (TGA @ 1273 K) (W m^{-1} K^{-1}) (225)	8.19 x 10^{-2}	8.20 x 10^{-2}
λ_{ext} (DTR @ 1335 K) (W m^{-1} K^{-1}) (225)	8.66 x 10^{-2}	-
v kinematic viscosity (m^2 s^{-1}) (TGA)	1.70	1.05
v kinematic viscosity (m^2 s^{-1}) (DTR)	1.96	-
Equipment properties	**TGA**	**DTR**
Nu	2	2 (203)

[(1)] The particle diameter used in the determination of the Reynolds number was taken as the maximum particle size used in each experiment

In the case of the DTR the Nu is equal to two as the particle is assumed to be falling at the same velocity as the gas through the reactor (203). The Nu determined for the TGA was also found to be close to two (2.0011) as the velocity of the gas (7.34 x 10^{-3} m s^{-1}) and resulting Reynolds numbers are low (7.43 x 10^{-3}). The calculated Biot numbers for the biomass and coal particles heated in the TGA in N_2 and CO_2 atmospheres and DTR in N_2 can be seen in Table 5.12.

Table 5.12: Biot numbers of fuels heated using a TGA and DTR

Fuel and Atmosphere	Biot TGA	Biot DTR
Biomass N_2	0.41	0.43
Biomass Co_2	0.41	-
Coal N_2	0.19	0.20
Coal CO_2	0.19	-

The low velocity of the gases in the TGA (Table 5.11) lead to a low Reynolds number (4.3 x 10^{-6} in the case of the biomass particle in a N_2 atmosphere) which in turn reduces the effect of the particle size on the Biot number. As the Biot numbers are small it is decided that a lumped model of heat transfer is acceptable in estimating the particle temperature in both the TGA and DTR.

5.5.2 Determination of the particle temperature in the TGA and DTR

The determination of the particle temperatures in the TGA and DTR were determined using Eq 3.4 reported in the literature review and repeated here (Eq 5.10). The equation assumes that the particle is non-reactive, which is not the case here, but gives some insight into the heating profile of the particle in both the TGA and DTR.

$$\frac{dT_p}{dt} = \frac{-3}{C_p \rho_p a}\left[\varepsilon\sigma\left(T_{part}^4 - T_w^4\right) + h\left(T_{part} - T_g\right)\right] \qquad \text{Eq 5.10}$$

Cp – specific heat capacity of fuel (J kg^{-1} K^{-1})

a – radius of particle (µm)

ρ – density of fuel (kg m^{-3})

ε – emissivity of particle surface (0.85)

σ – Stefan-Boltzmann constant (5.67 x 10^{-8} W m^{-2} K^{-4})

T_{part} – particle temperature (K)

T_w – temperature of the furnace (K)

T_g – gas temperature (K) (in this case assumed the same as T_w)

h – coefficient for convective heat transfer (W m^{-2} K^{-1}), determined using Eq 5.4 – 5.7 over the heating profile of the TGA.

Assuming that the particle is non-reactive, the Cp and mass of the fuel on the TGA pan is constant throughout the heating profile seen in the TGA. The approximate particle temperature of the biomass and coal fuels in the TGA can be seen in Figure 5.6.

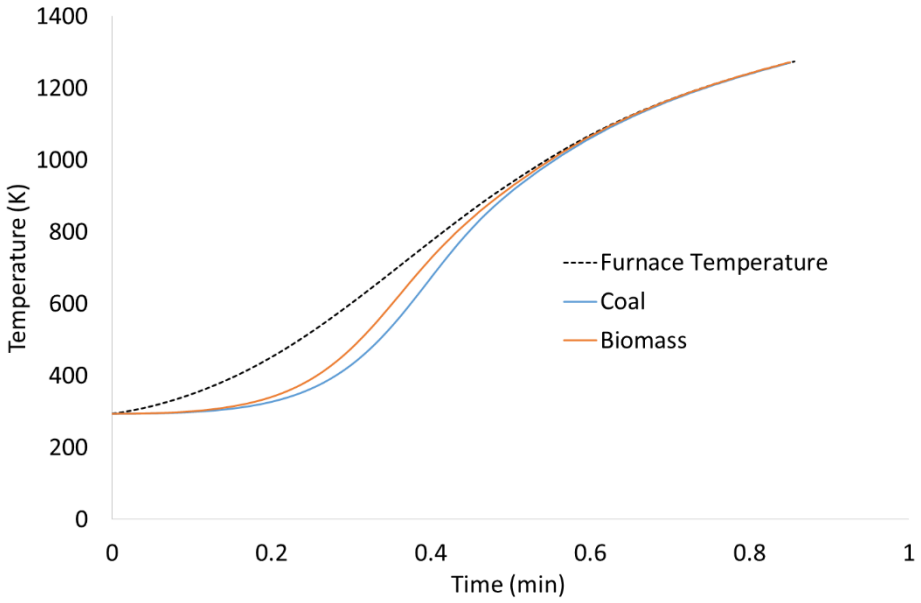

Figure 5.6: Predicted biomass and coal particle temperature heated in the TGA at ballistic heating rates (1000 K min^{-1}) in an N_2 atmosphere

Figure 5.6 estimates the temperature profile of a single particle of biomass and coal which is not the case in the TGA. Many particles are placed onto a sample pan but are assumed to be independent, well dispersed and not exchanging heat and that the estimation of the particle temperature is sufficient.

The temperature profile of a biomass or coal particle heated in a CO_2 atmosphere is identical to the N_2 atmosphere as the only change is in the thermal conductivity, density of gas which leads to a difference in the kinematic viscosity. These small differences result in a small change in the coefficient for heat transfer but no noticeable difference in the overall particle heating rates.

In the case of the DTR, the temperature profile of the particle is unknown and instead the time taken for the particle to reach the DTR temperature (1062 K) was determined using Eq 5.10 and can be seen in Table 5.13.

Table 5.13: Time for particle to reach DTR temperature

	Biomass (350 µm)	Coal (180 µm)
Time (s)	0.021	0.009

The biomass takes longer to reach the furnace temperature due to both the larger particle size used (maximum 350 µm) and the increase in specific heat capacity (1600 compared to 1088 J kg^{-1} K^{-1} for the coal). The residence time of the particle in the DTR is 0.5 seconds allowing sufficient time for the particle to reach the furnace temperature and the devolatilisation process to occur.

It is clear that the particle heating rates are faster in the DTR than is seen in the TGA which result in an increased rate of devolatilisation in the DTR which in turn is shown to effect both the surface area (section 5.6) and the char combustion kinetics (section 8).

5.6 Surface area

Surface area is an important physical characteristic in determining the combustion behaviour and reactivity of a char as discussed in the literature review (section 3.5.3). Surface area measurements were performed on all chars produced, however the biomass and torrefied biomass char surface areas were unreliable due to the low char yields obtained (6-20 wt%) and the low density of the biomass chars. The Quantachrome NOVA 2200E used for the analysis requires only a small amount of sample but due to the low density of the biomass char the sample is not fully submerged into the liquid N_2. After many experiments varying the degas conditions (time and temperature) and the analysis conditions (sample size and equilibrium time) over a period of eight months, that required many ballistic TGA runs to produce the char, it was decided that the surface areas of the biomass chars could not be determined by this method. It is suggested that longer length sample tubes could be used to allow for a larger mass of biomass char to be placed into the NOVA 2200E which may improve the measurement of surface areas. Due to time constraints it was decided to perform a literature review to try and determine relevant surface areas of biomass chars produced in N_2 and CO_2 environments at comparable heating rates.

The surface areas of the coal chars produced using the TGA and DTR (PEL DTR) can be seen in Table 5.14. The ELC chars have the highest surface areas followed by the PEL then the PIT chars which are significantly lower. Suuberg et al (226) investigated the development of porosity in coal chars using a Pittsburgh# 8 and Beluah-Zap lignite by producing chars in a

tube furnace in a nitrogen atmosphere at 1273 K with a residence time of 2 hours. It was found that the surface area of the chars differed greatly with the surface area of the Beluah-Zap lignite at just over 100m^2 g^{-1} and the Pittsburgh#8 surface area at practically 0 m^2 g^{-1}. They determined that the Pittsburgh# 8 coal softened during pyrolysis and the material was able to reorder itself, reducing the free volume, and thus reducing the surface area. Although the residence time in the work by Suuberg et al is much longer than that utilised in this work, Pittsburgh#8 is known to be a highly softening coal at comparable heating rates and particle sizes (227, 228).

Table 5.14: Surface area of the chars produced using the TGA and DTR

Char preparation atmosphere		BET (m^2 g^{-1})
PEL	N_2	14.91
	CO_2	115.22
	DTR	80.82
ELC	N_2	52.90
	CO_2	129.24
PIT	N_2	1.68
	CO_2	6.22

When the PEL, ELC and PIT fuels are pyrolysed in CO_2 the surface area is increased due to the char-gasification reaction (218). The PEL DTR char also has an increased surface area relative to the PEL N_2 char due to the higher devolatilisation rates, evidence of which can be seen in the SEM analysis in Figure 5.7.

The measurement of coal chars produced in N_2 environments is well developed but there is a large range in reported BET surface measurements. Values of char surface areas of chars produced at a variety of temperatures and in both N_2 and CO_2 can be seen in Table 5.15. The surface area measurements of the PEL, ELC and PIT chars fall in the wide range of surface area values reported in Table 5.15. The effect of the change in char production atmosphere on char surface area is also outlined in Table 5.15 which is in agreement with the increased surface areas in CO_2 produced chars. Brix et al. (221) suggested that no significant difference is seen in the surface areas of chars produced in N_2 and CO_2 atmospheres and that the differences seen in Table 5.15 are the result of heating rates, coal compositions, residence times and final temperatures. The residence times and final temperatures are especially important factors if the CO_2 gasification reaction contributes to the increase in surface area (229). In the case of the PEL, ELC and PIT chars produced at ballistic heating rates the

residence time at elevated temperatures (>700°C) is one minute (due to both the heating and cooling) significantly longer than those experiments seen in Table 5.15 allowing for the char-CO_2 gasification reaction and the resulting increase in surface area.

Table 5.15: Surface area measurements of coal chars produced in N_2 and CO_2 environments by N_2 - BET

Coal	Char Atmosphere		Pyrolysis Method	Pyrolysis Temperature	Residence Time	Surface Area ($m^2 g^{-1}$)		
	N_2	CO_2				N_2	CO_2	
BIT	✓	✓	EFR	1673 K	0.15 s	270	280	(221)
HVB	✓	✓	DTR	1573 K	0.3 s	2	15	(156)
LVB	✓	✓				5	60	
MVB	✓	✓				170.4	187.1	
MVB	✓	✓	DTR	1673 K	0.62 s	170.6	214.1	(218)
HVB	✓	✓				182.8	261.4	
HVB	✓	✓				211.6	276.2	
MVB	✓	✓	DTR	1573 K	1 s	6.4	64.8	(230)
MVB	✓		DTR	1573 K	0.4 s	1.6	-	(207)
MVB	✓		HTF	1373 K	150°C min^{-1}	17.3	-	

NOTE: BIT – Bituminous, HVB – High Volatile Bituminous, MVB – Medium Volatile Bituminous, LVB – Low Volatile Bituminous, EFR – Entrained flow reactor, DTR – Drop tube reactor, HTF – Horizontal tube furnace

A selection of biomass char surface areas can be seen in Table 5.16. There is a wide variety of reported surface areas with chars produced in N_2 having surface areas of 1.7 – 296 $m^2 g^{-1}$. The method of char production also varies with some chars prepared at high heating rates and temperatures using drop tube reactors and wire mesh reactors and some at much lower heating rates. The lower heating rate chars also tend to have high residence times at the maximum temperatures which increase volatile yield (127, 231) and has been shown to effect the surface area with either an increase or decrease which is dependent on fuel properties and pyrolysis conditions (232). The surface areas of chars produced at high heating rates in CO_2 atmospheres also seem to be dependent on fuel and pyrolysis conditions with some surface areas increasing and some decreasing when N_2 is replaced with CO_2. As a result it was decided that the intrinsic reactivity of the biomass samples could not be determined by assuming a surface area derived from literature.

Table 5.16: Surface area measurements of biomass chars produced in N_2 and CO_2 environments by N_2-BET

Biomass	Char Atmosphere		Pyrolysis Method	Pyrolysis Temperature	Residence Time	Surface Area ($m^2 g^{-1}$)		
	N_2	CO_2				N_2	CO_2	
Rice Husk	✓	✓				254	208	
Wood Chip	✓	✓	DTR	1223 K	0.3 s	277	331	(223)
Forrest residue	✓	✓				225	158	
Sawdust	✓	✓	DTR	1373 K	105 K s^{-1}	2	9	(182)
Pinewood	✓	✓				6	12	
Wheat Straw	✓	-					-	
			FBR	1073 K	20 K min^{-1}	8.16		(233)
Rice Husk	✓	-				12.28	-	
Wheat Straw	✓	-			Not		-	(233)
			FBR	1073 K	Reported	23.17		
Rice Husk	✓	-				19.32	-	
Wheat Straw	✓	-	TR	773 K	12 ^oC min^{-1}	9.8	-	(234)
Willow	✓	-				57	-	
Willow A	✓	-				26.7	-	
Eucalyptus	✓	-	DTR	1373 K	10^{4-5} K s^{-1}	94	-	(208)
Eucalyptus A	✓	-				66	-	
Sugar Cane Bagasse	✓	-	Proximate Oven	1173 K	Not Reported	410	-	(145)
Beech	✓	-				11	-	
Oil Palm Shell	✓	-	VTF	1173 K	3 K min^{-1}	7	-	(235)
Pine	✓	-	TR	1223 K	20 K s^{-1}	57	-	(236)
	✓	-	WMR	1223 K	500 K s^{-1}	296	-	
Japanese				623 K		1.7	-	
Hardwood	✓	-	FBR		5 K min^{-1}			
(AQB)				1123 K		2.1	-	(237)
Japanese				623 K		2.5	-	
Hardwood	✓	-	FBR		5 K min^{-1}			
(AA)				1123 K		100	-	
Walnut Shell	✓	-				280	-	
Almond Tree	✓	-			Not	204	-	(238)
Almond Shell	✓	-	TR	873 K	Reported	42	-	
Olive Stone	✓	-				53	-	

Note: DTR – Drop tube reactor, FBR – Fixed bed reactor, TR – Tubular furnace, VTF- Vertical tube furnace, WMR – Wire mesh reactor, Willow A and Eucalyptus A - torrefied at 290^{o}C for 30 minutes

5.7 Scanning electron microscopy

The morphology of char is an important characteristic when trying to understand the combustion behaviour of chars. Several methods of char morphological analysis exist such as oil immersion microscopy, scanning electron microscopy and manual or semi-automated image analysis techniques (239). Image analysis techniques have been developed by several authors (240-243) to clarify coal char analysis and are based on common characteristics; shape, wall thickness, fused and unfused structures, porosity and voidage (241). The international committee for coal and organic petrology developed a char atlas with the aim of producing a clearer methodology for char classification based on the above common characteristics (244). The author of this work was unable to determine the above characteristics due to time and equipment limitations and instead SEM was used to image the external surfaces of the chars to give some understanding of the final temperature, heating rates and pyrolysis atmosphere effect the devolatilisation process. The images for the PEL and PWWP raw fuels and chars produced using the TGA in N_2 and CO_2 and the DTR in N_2 can be seen in Figure 5.7 and Figure 5.8.

The change in morphology between the raw fuels and chars is seen easily in the SEM images. The PEL raw fuel has a regular form with angular and sharp edges while the chars produced using the TGA (PEL N_2 and PEL CO_2) have irregular shapes. In general the char particles have become rounded but have a corroded like surface with irregular sharp edged micro particles attached to the surface. During the TGA production of char, the fuel sits statically on top of a pan causing the char particles produced to agglomerate into a biscuit like material. The PEL DTR char has a much more rounded appearance and is much more porous (cenosphere type char) than the TGA chars due to the increased devolatilisation rates and particle size.

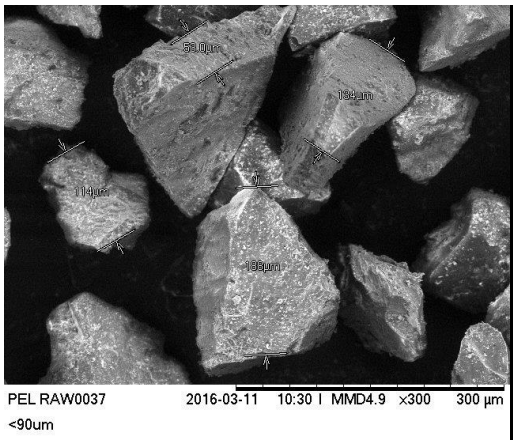

(a)

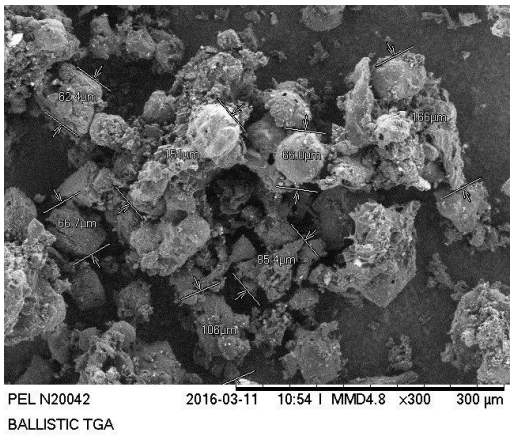

(b)

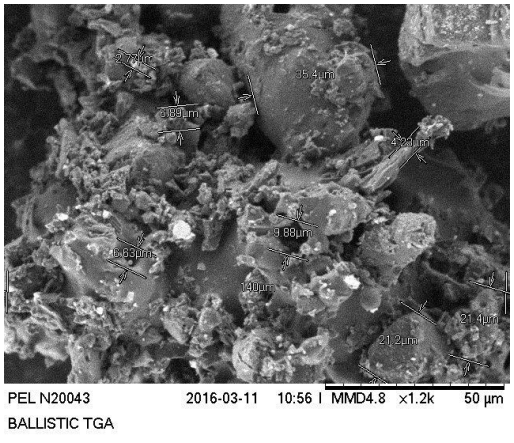

(c)

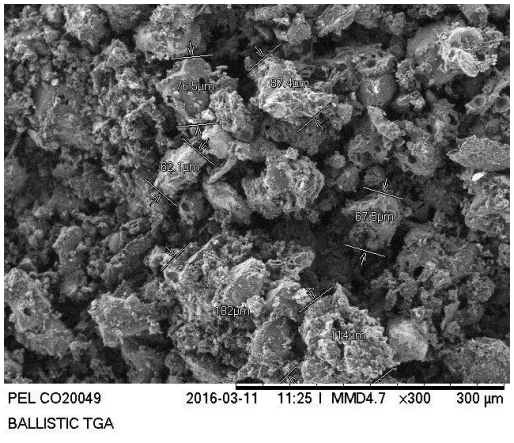

(d)

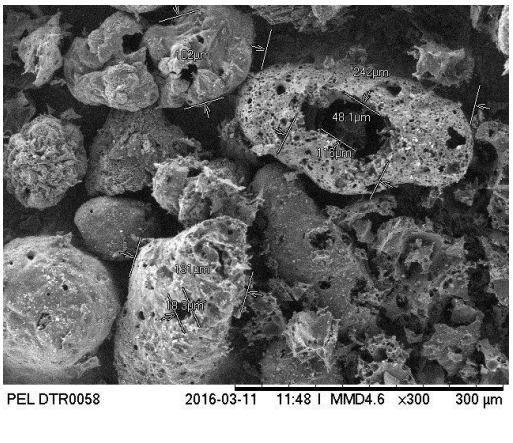

(e)

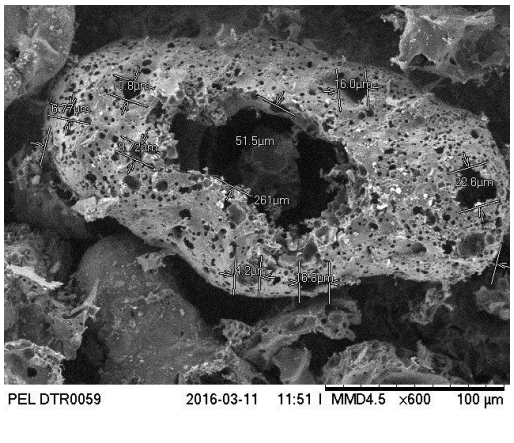

(f)

Figure 5.7: SEM imaging of PEL fuel and chars PEL raw fuel (a), PEL N_2 (b and c), PEL CO_2 (d) and PEL DTR (e and f)

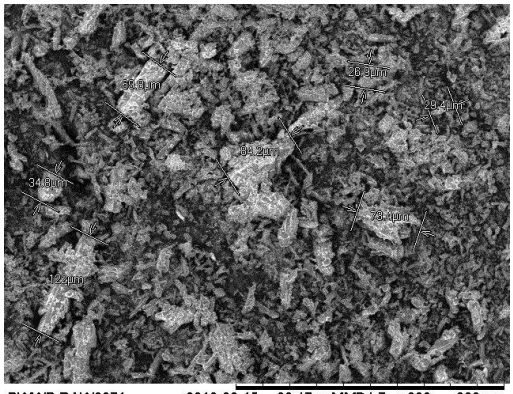

(a)

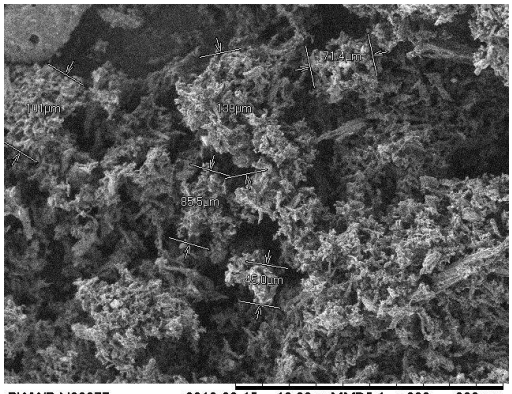

(b)

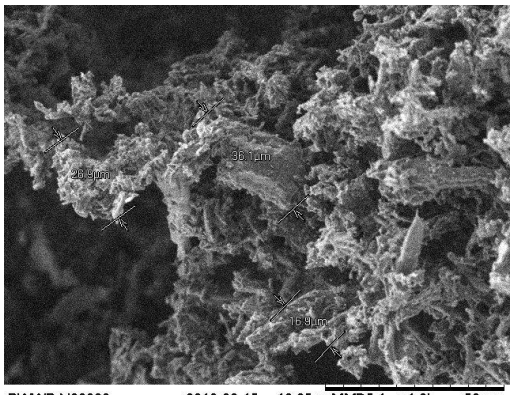

(c)

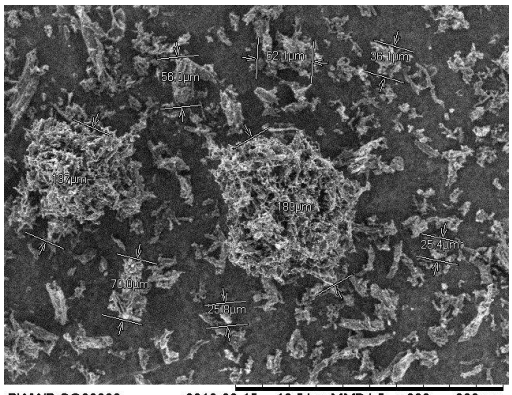

(d)

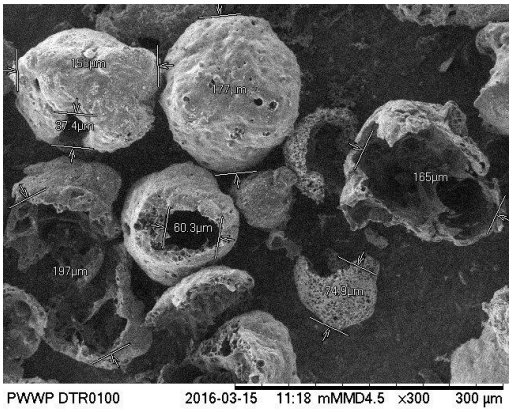

(e)

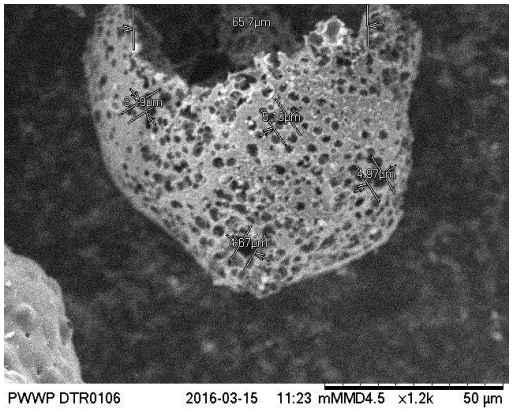

(f)

Figure 5.8: SEM imaging of PWWP fuels and chars PWWP raw fuel (a), PWWP N_2 (b and c), PWWP CO_2 (d) and PWWP DTR (e and f)

The PWWP (Figure 5.8) raw fuel sample is irregular and fibrous while the TGA chars are similar to those seen in the coal with a corroded sharp edged irregular surface. The DTR chars are more rounded and porous than the TGA chars with some particles having walls blown out due to the higher volatile content, up to 85wt% in the PWWP raw fuel.

The difference in morphology of the chars is due to the different heating rates in the two char production methods. During the devolatilisation stage a fluid layer is formed on the outside of the char particle and can reduce the porosity. The thickness of this liquid layer is reduced as the heating rate is increased due to the faster release of volatiles and allows for the formation of larger pores as seen in Figure 5.7 and Figure 5.8 (207). At high heating rates such as those seen in the DTR the speed of the devolatilisation process is much faster causing the porosity seen in Figure 5.7. The difference in TGA char and DTR char was also seen in work by Le Manquis et al (207) where TGA heating rates of 150^{o}C min^{-1} and final temperature of 1300^{o}C produced chars similar to the parent fuel and rounded porous chars from the DTR.

5.8 Modified HGI and particle size distribution of the torrefied spruce

The modified HGI index and the particle size distribution experiments were performed on the TSP sample to get a better understanding of the unknown torrefaction conditions. The particle size distribution and the HGI_{Eq} determined using the methodology outlined in section 4.3.5 can be seen in Figure 5.9. The particle size distributions for the calibration coals (HGI 32, 49, 66 and 92) along with two willow samples taken from Bridgeman et al (197) are also shown. The Willow A was torrefied at high temperatures and long residence time (290^{o}C, 60 minutes) and Willow B lower temperatures at the same residence time (240, 60 minutes). Figure 5.9 suggests that the torrefaction conditions may not have been very severe when comparison is made with Willow B (low temperature and residence time) however the author is unable to say for definite.

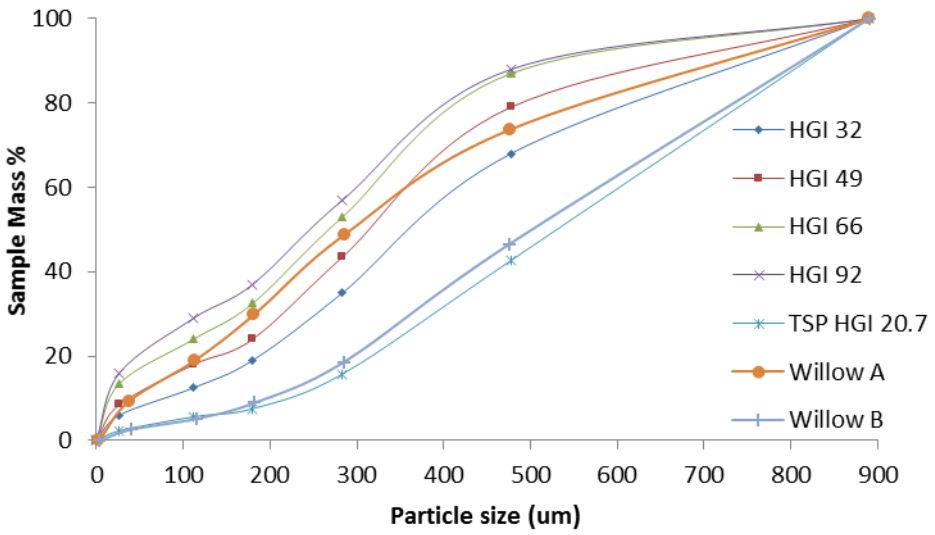

Figure 5.9: Particle size distribution and HGI_{Eq} curves for four standard reference coals (197) and TSP

5.9 General discussion

Proximate and ultimate analysis of the fuels highlights the difference between the coal and biomass fuels with the coals contain larger amounts of carbon and much less volatile contents. Ballistic heating rate chars were produced to closer replicate the process of devolatilisation in a pulverised fuel burner and the differences in characteristic properties of the fuels results in fuel dependent pyrolysis behaviour. The higher volatile content of the biomass and TSP fuels results in smaller char yields than seen in the coals. The difference in char production atmospheres also effect the fuels differently. Coal chars are less effected by the switch to CO_2 atmospheres with char yields, volatile contents and fixed carbon contents similar in the two atmospheres. The largest difference in coal chars is seen in the measurements of the surface areas where CO_2 chars are 2-7 times larger. These trends however are not universal to all coals as has been shown in the discussion of each section. The biomass fuels are more effected by the switch to CO_2 with lower char yields, similar volatile contents and a large decrease in fixed carbon content due to the char – CO_2 gasification reaction. The TSP fuel falls in between the coal and biomass fuels in terms of fuel composition and this trend is also seen in its chars and the effect the environments have on char properties. This would be expected as the purpose of the torrefaction process is to convert biomass into a more coal like fuel.

Pyrolysis in the DTR results in lower char yields than the TGA but the chars contain higher levels of volatiles but lower amounts of fixed carbon. This is due to the higher heating rates, higher final temperatures and lower residence times in the DTR.

The work in this chapter is used to help understand the overall combustion behaviour, the devolatilisation, char combustion behaviour and reactivity in a range of combustion environments in the following chapters.

5.10 Conclusions

- Fundamental characterisation of the fuels and their chars, produced using a TGA (N_2 and CO_2) atmosphere and DTR (N_2 atmosphere) were performed to determine the effect of pyrolysis atmosphere, heating rate, heating temperature and particle size on the resulting chars characteristics.
- The coal fuels have similar characteristics in terms of proximate and ultimate analysis and are significantly different to the biomass fuels.
- Char yields in all atmospheres and char production methods are significantly lower in the biomass samples due to the higher volatile content present.
- The theoretical char yield in the coal samples is similar to the measured char yield when using the TGA in both N_2 and CO_2 atmospheres.
- The theoretical char yield of the biomass chars is again similar to the theoretical when using the TGA in N_2. However when CO_2 is used the char yield is significantly reduced due to the char – CO_2 gasification reaction.
- The char yields are significantly lower than the theoretical yield when chars are produced using the DTR due to the presence of oxygen in the reactor and the increased reactivity of the fuels at the higher heating rates and final temperature achieved in the DTR.
- The different char atmospheres and production methodologies result in a change in the char properties.
- The change from N_2 to a CO_2 char production atmosphere in the TGA was shown to have a similar effect on the three coal samples. In each coal the relative fixed carbon content in the chars is similar in both atmospheres. The relative volatile content of the chars is higher in the coal chars produced in CO_2 thought to be the result of enhanced crosslinking (due to the CO_2 atmosphere) preventing devolatilisation.

- The char production atmosphere has a greater effect on the biomass chars with the PWWP and WWP chars produced in the CO_2 atmosphere retaining lower levels of the volatiles and fixed carbon.
- The TSP char contain similar levels of volatiles but a decrease in the levels of fixed carbon when produced in CO_2.
- The PEL and PWWP chars produced using the DTR retained more of the original volatile content and less of the fixed carbon content of the original fuel than the chars produced using the TGA in an N_2 atmosphere. The increase in volatile content can be attributed to the increase in particle size and decrease in residence time and the decrease in fixed carbon attributed to the presence of oxygen, the higher final temperatures and higher heating rates seen in the DTR.
- Ultimate analysis of the chars showed that the carbon content of the coal chars is similar in N_2 and CO_2 atmospheres.
- The biomass and TSP char samples retain less of the carbon than the coals due to the increased reactivity of the fuels and when chars are produced in CO_2 the yield is further reduced as a result of the char gasification reaction.
- Ultimate analysis also provided information of the nitrogen partitioning as a result of the change in atmosphere and production method.
- The PEL fuel retained the majority of the fuel bound nitrogen in its char when chars are produced using the TGA. All remaining chars the majority of the nitrogen is released during the devolatilisation stage.
- The biomass chars retain significantly less of the fuel bound nitrogen than the coal samples.
- The change to a CO_2 atmosphere in the TGA results in greater retention of nitrogen in the ELC and PIT chars. The PEL, PWWP, WWP and TSP chars show a reversed trend with less nitrogen retained in the chars when chars are produced in CO_2. This is attributed to the degree of devolatilisation seen in each of the fuels under each condition.
- The surface area of the coal chars was determined and it was found that CO_2 chars resulted in a higher surface area as a result of the char gasification reaction.
- It was also found that the PEL char produced in the DTR has a greater surface area than the PEL N_2 char produced using the TGA. This is the result of the increased heating rates and associated devolatilisation rate.
- SEM analysis is used to indicate the effect of production atmosphere and methodology. The use of the DTR char results in a very different char than that seen

when using the TGA. The DTR chars are much more rounded and more porous than the comparable TGA char.

- Comparison of the TSP fuel to coals and other torrefied biomass fuels suggests that the torrefaction conditions of the original Spruce biomass are not very severe.

6 Overall combustion and pyrolysis behaviour of fuels and the associated devolatilisation kinetics

6.1 Introduction

This chapter focuses on the overall combustion characteristics of the fuels in air and oxy-fuel environments and the devolatilisation behaviour during both combustion and pyrolysis. The chapter starts with the overall combustion behaviour of the raw fuels in the full range of combustion environments (air and 5-30% O_2/CO_2) using the TGA, and the identification of key temperatures and rates of mass loss. In addition the degree of low temperature oxygen chemisorption and an estimation of the active surface area of the coals in the full range of combustion environments is determined. Following the combustion behaviour is the pyrolysis behaviour of the fuels in N_2 and CO_2 environments, also using the TGA. The apparent first order devolatilisation kinetics are determined from the non-isothermal mass loss profiles produced during the overall combustion and pyrolysis sections. Finally a fuel specific model is developed allowing for the determination of the kinetic parameters (A, E_a and k) as a function of oxygen concentration present in the oxy-fuel combustion atmosphere.

6.2 Overall combustion behaviour of the raw fuels in air and oxy-fuel environments

The overall combustion behaviour of the raw fuels in air and oxy-fuel environments (5-30%O_2 in CO_2) can be seen below. All fuels were milled to less than 90 µm and combusted using the TGA at a heating rate of 10^{o}C min^{-1} to 900^{o}C.

In order to evaluate the combustion profiles, the peak temperatures and the maximum rates of mass loss were analysed. In the case of the coal samples the low volatile content results in a single unresolved peak. The temperatures at which the initial rate of mass loss reached 0.016 wt% s^{-1} (1 wt% min^{-1}) (T_{IM}), the maximum rate of mass loss occurred (T_P), the maximum rate of mass loss (dm/dt_P) and the burnout temperature (T_B) are evaluated for the coal samples. In the case of the biomass and TSP samples, two clear peaks are seen which are associated with the volatile and char combustion stages. The temperatures at which the initial mass loss (T_{IM}) and maximum rate of mass loss during devolatilisation was seen (T_V), the rate at this temperature (dm/dt_V), the temperature at which maximum mass loss was

seen during char combustion (T_C), the rate at this temperature (dm/dt_C) and the burnout temperature (T_B) were recorded. The burnout temperature was taken at the point at which the rate of mass loss was 0.016 wt% s^{-1} (1 wt% min^{-1}) immediately before the end of the mass loss to ensure comparable temperature measurements.

6.2.1 Overall combustion behaviour of coals in air and oxy-fuel environments

The overall combustion profiles of the coals can be seen in Figure 6.1-Figure 6.6 and the key temperatures and rates of mass loss extracted from the TGA and DTG plots in Table 6.1.

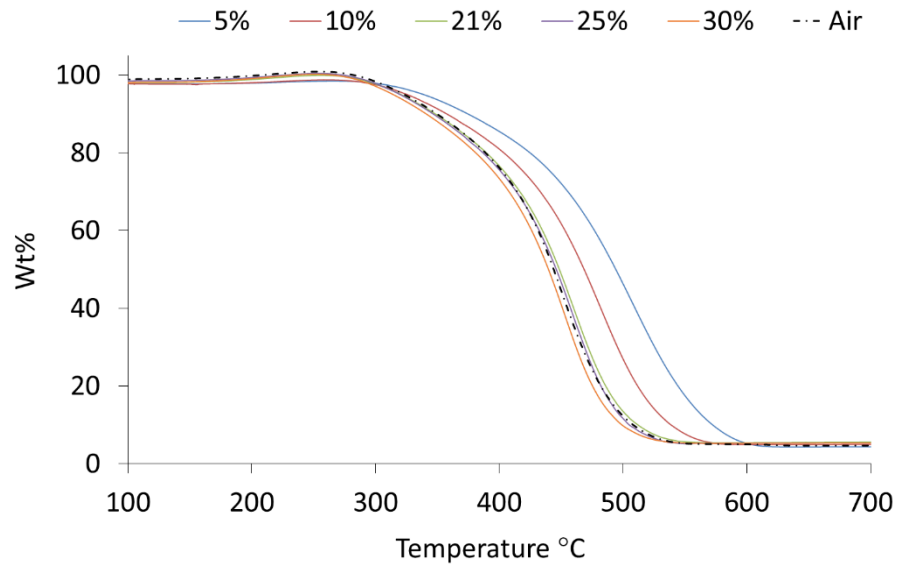

Figure 6.1: Mass loss behaviour of the PEL fuel combusted in air and 5-30%O_2 in CO_2

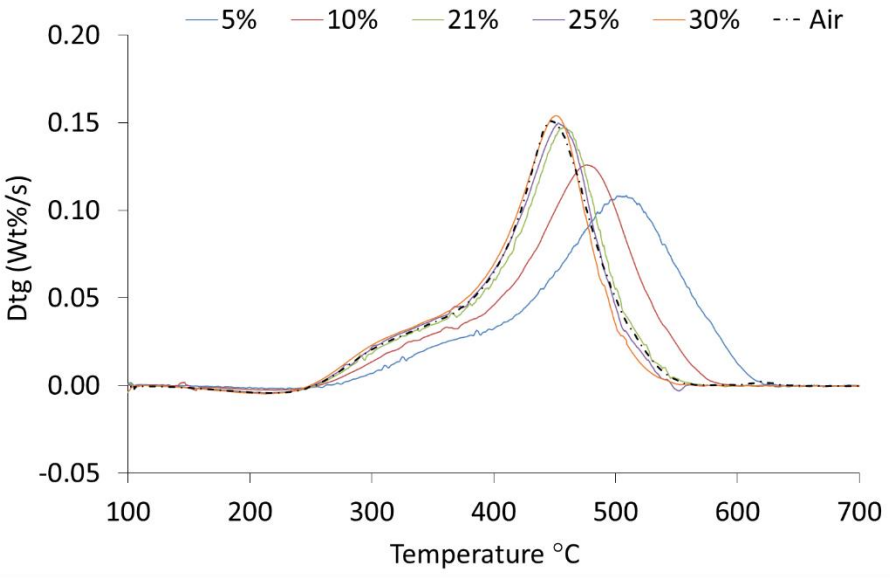

Figure 6.2: DTG behaviour of the PEL fuel combusted in air and 5-30%O_2 in CO_2

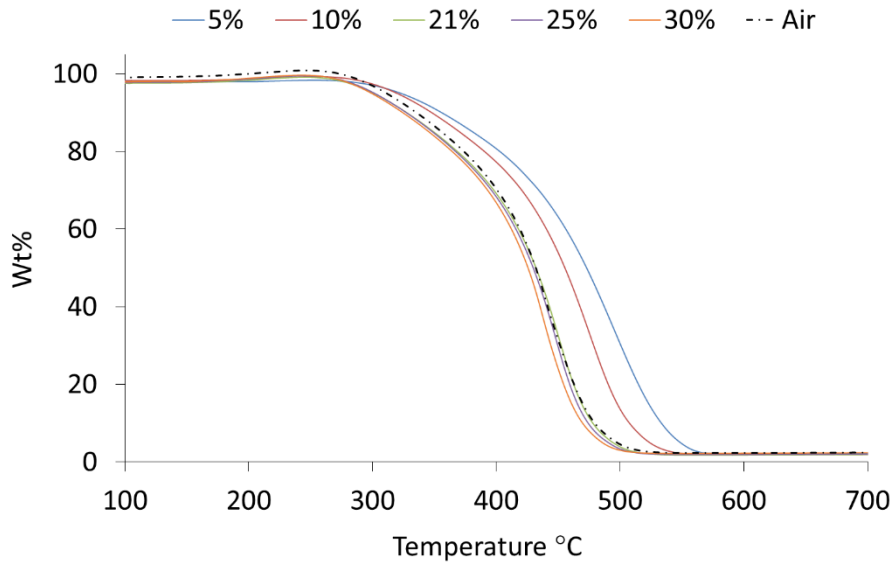

Figure 6.3: Mass loss behaviour of the ELC fuel combusted in air and 5-30%O_2 in CO_2

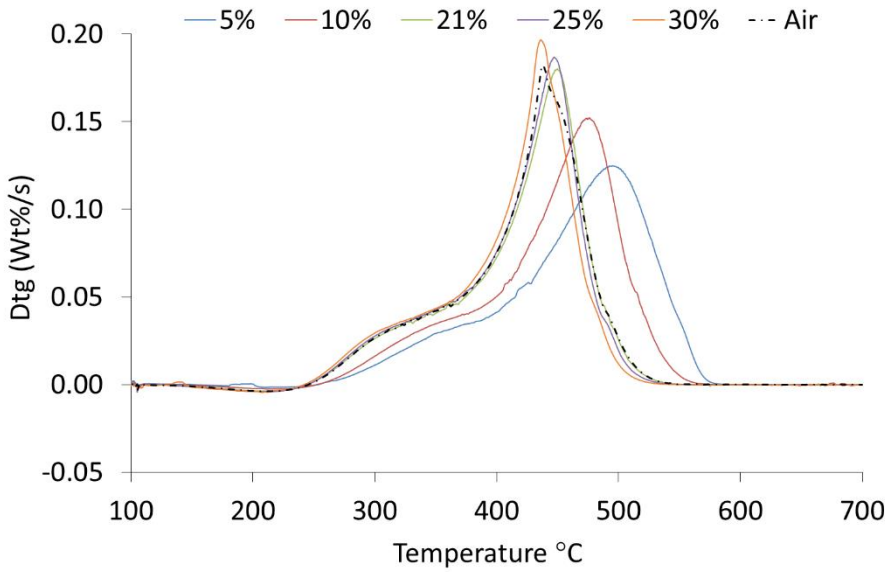

Figure 6.4: DTG behaviour of the ELC fuel combusted in air and 5-30%O_2 in CO_2

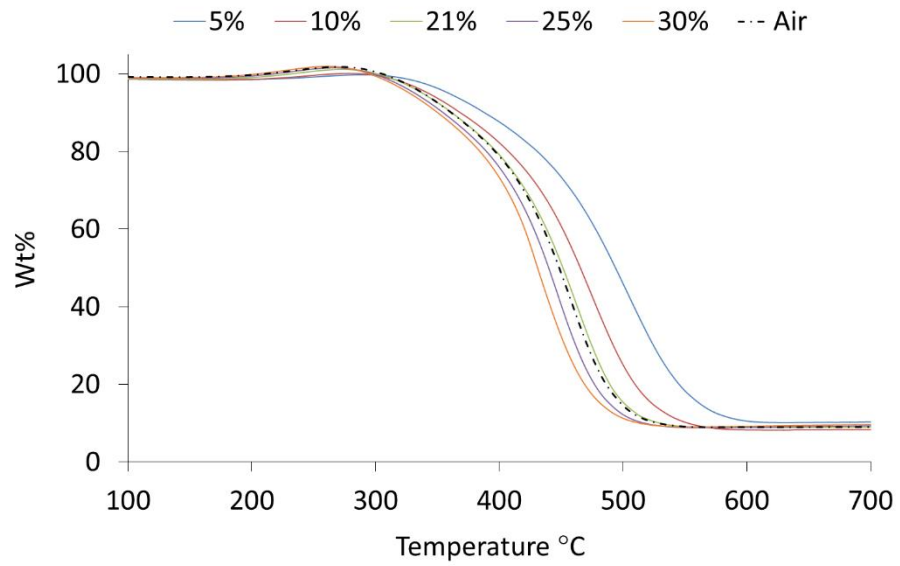

Figure 6.5: Mass loss behaviour of the PIT fuel combusted in air and 5-30%O_2 in CO_2

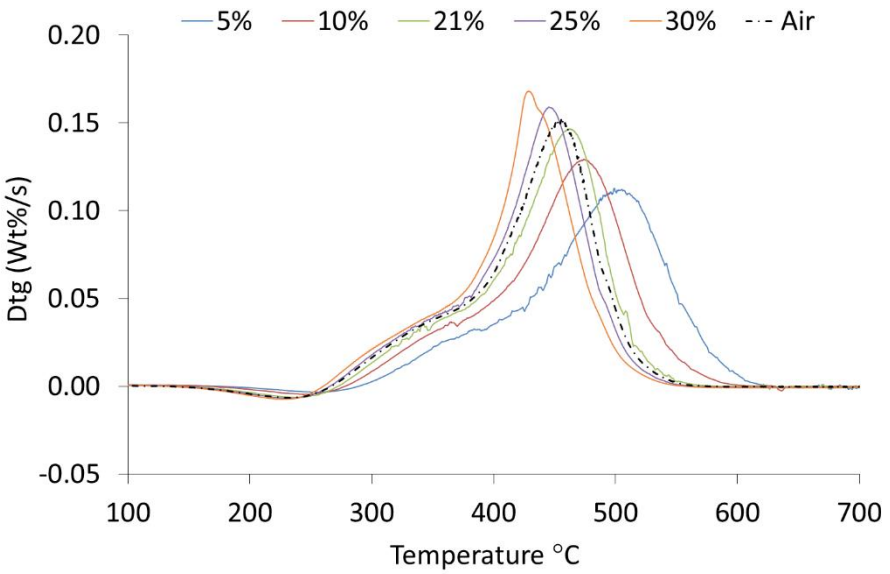

Figure 6.6: DTG behaviour of the PIT fuel combusted in air and 5-30%O_2 in CO_2

Table 6.1: Characteristic temperatures and rates of mass loss observed during combustion of coals in air and oxy-fuel environments

		T_{IM} (°C)	T_P (°C)	dm/dt_P (Wt% s^{-1})	T_B (°C)
PEL	5%	334	508	0.109	597
	10%	314	483	0.127	561
	21%	300	461	0.148	530
	25%	293	458	0.153	527
	30%	288	453	0.155	519
	Air	292	450	0.151	529
ELC	5%	317	496	0.125	561
	10%	301	475	0.152	537
	21%	283	450	0.180	505
	25%	280	448	0.187	502
	30%	277	437	0.197	496
	Air	282	439	0.182	507
PIT	5%	339	501	0.113	583
	10%	318	475	0.129	550
	21%	304	463	0.147	525
	25%	298	447	0.159	512
	30%	289	429	0.168	504
	Air	299	461	0.153	522

In all coals an initial mass loss is seen at temperatures between 100°C and 200°C due to the release of moisture, with similar trends in all fuels and in all combustion environments, suggesting that the moisture release is not effected by the combustion environment. This would be expected as the drying stage is a heat transfer limited process (described by Eq 3.1 in the literature review) influenced by the surrounding gas temperature, which is identical in all environments, and raw fuel properties such as surface area and porosity (114).

In the case of the three coals after the drying stage, a mass increase is observed due to the chemisorption of oxygen onto the particle surface. In order to determine the effect of the combustion atmosphere on the chemisorption behaviour, the temperature at which the maximum mass in the TGA profile is seen (T_{Chem}) and the wt% increase were analysed and can be seen in Table 6.2. In addition the active surface area (ASA) (the active sites during coal combustion) are estimated.

As the amount of oxygen present in the combustion atmosphere increases the degree of oxygen chemisorbed is increased and as a result the active surface area increases (the area of the fuel undergoing reaction). The ASA increases linearly with the increase in oxygen in the combustion atmosphere as can be seen in Figure 6.7. The ASA is increased through the availability of the oxygen at the particle surface rather than any morphological changes to

the fuel structure. In addition the temperature at which the maximum mass in the TGA plots is seen (Figure 6.1 - Figure 6.6) (T_{Chem}) reduces with the increase in O_2 in the combustion atmosphere.

Table 6.2: Characteristic oxygen chemisorption temperatures, wt% gain seen during coal combustion and estimation of the active surface area

O_2	PEL			ELC			PIT		
	T_{Chem} (°C)	Wt%	ASA (m^2g^{-1})	T_{Chem} (°C)	Wt%	ASA (m^2g^{-1})	T_{Chem} (°C)	Wt%	ASA (m^2g^{-1})
5%	262	0.70	21.9	256	0.33	10.2	289	1.24	38.7
10%	262	1.06	33.2	254	1.05	32.7	279	1.67	52.0
21%	257	1.90	59.3	245	1.54	48.2	274	2.55	79.5
25%	253	1.91	59.8	244	1.68	52.6	266	2.70	84.2
30%	252	2.13	66.6	242	1.72	53.8	261	2.89	90.4
Air	257	1.88	58.6	247	1.64	51.1	271	2.56	80.0

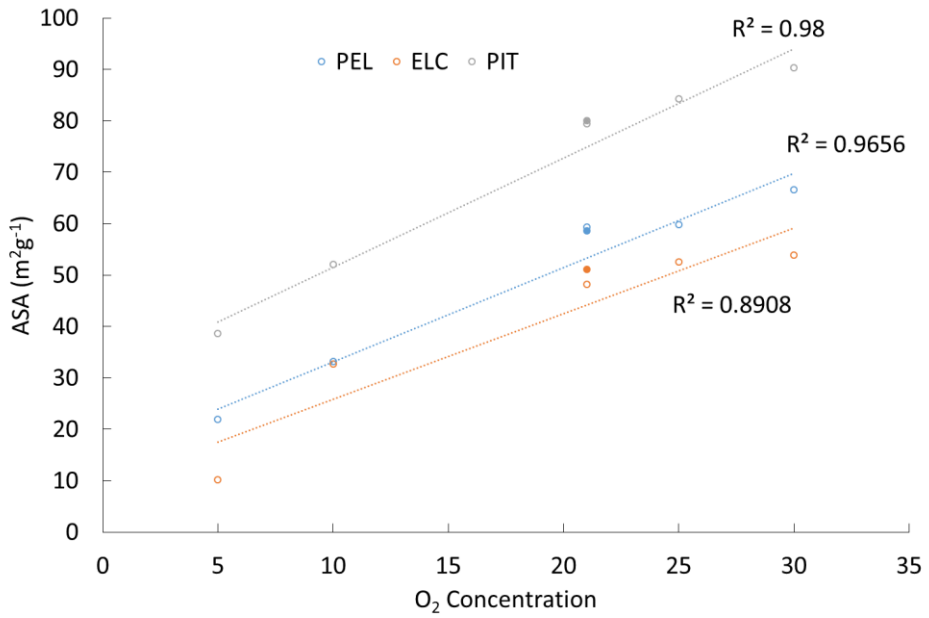

Figure 6.7: Active surface area of coals in the full range of combustion atmospheres (Solid – combustion in air, Empty combustion in oxy-fuel atmospheres)

The increase in ASA results in an oxygen rich surface where at sufficient temperatures heterogeneous ignition takes place increasing the rate of devolatilisation, which can be seen in the TGA plots (Figure 6.1- Figure 6.6). It is also seen that when N_2 is replaced by CO_2 the difference in the degree of chemisorption is negligible and as a result, the estimated ASA of

the fuels is almost identical. From this it is expected that the devolatilisation reaction rates of the coals should be similar when combusted in air and 21% O_2/CO_2 environments, which is determined in section 6.4.1. After the chemisorption stage, the coals start to lose mass due to thermal and oxidative degradation at the T_{Chem} temperatures reported in Table 6.2.

Of the three coals, the ELC fuel has the lowest characteristic temperatures (T_P, T_{IM} and T_B) (Table 6.1) and the highest maximum rates of mass loss (dm/dt_P) in all combustion environments. The decrease in the key temperatures suggests that the ELC sample is the most reactive, followed by the PEL and then the PIT sample. The reactivity of the fuels is investigated in section 6.4.

In order to determine the effect of the change from N_2 to CO_2 based atmospheres, combustion experiments were performed in 21% O_2/CO_2 and results compared to combustion in air. The TGA plots (Figure 6.1 - Figure 6.6) look quite similar in terms of the change in combustion environment at the same oxygen conditions but identification of the key temperatures and rates of mass loss Table 6.1 suggest that a delay is seen in the 21% O_2/CO_2 atmosphere relative to air. The initial mass loss temperature (T_{IM}) is 1°C higher in the ELC sample, 8°C higher in the PEL sample and 5°C higher in the PIT sample, suggesting that the initial stages of combustion are slightly delayed in the CO_2 based environments. The difference between the two atmospheres is small at temperatures below 400°C, after this the difference between the two environments is more easily identified through the peak temperature T_P and the maximum rate of mass loss dm/dt_P. The dm/dt_P is reduced by as much as 4% in the PIT sample (1-2% in the PEL and ELC) and the T_P is increased (11°C in the PEL and ELC and 2°C in the PIT sample) when combusted in CO_2 based environment.

The combustion in the full range of oxy-fuel environments allows for the analysis of the effect of increased oxygen on the overall combustion behaviour. When the coals are combusted in low oxygen environments (5-10%) the TGA and DTG profiles shift to higher temperatures relative to combustion in 21% O_2/CO_2. As the oxygen levels are increased T_P and T_B shift to lower temperatures and dm/dt_P is increased (Table 6.1). The change in oxygen levels within the combustion environment were shown to have a large effect on the combustion profiles, the extent of which is fuel dependent.

When the PEL fuel was combusted in 5% O_2/CO_2, the T_P was 508°C, this was 55°C higher than that seen when combusted in 30% O_2/CO_2 (Table 6.1). The dm/dt_P is increased when combusted in 30% O_2, with a 42% increase relative to that seen in the 5% O_2 experiment. The T_B is also reduced as oxygen concentration is increased, from 597°C at 5% O_2 and 519°C

at 30% O_2. The change in key temperatures and rates of mass loss with oxygen concentration is not linear and the greatest difference is seen between the 5% and 10% O_2 atmospheres. At higher oxygen concentrations >21% O_2/CO_2 the difference between the identified temperatures and rates of mass loss become smaller. It has been suggested that in oxy-fuel environments an increase in oxygen concentrations >21% is required to match conditions in air combustion (51, 148), the same is true in relation to the combustion behaviour. The TGA and DTG profile of the PEL, when combusted in air, are most similar to the 25% and 30% O_2/CO_2 profiles; the maximum rate of mass loss and burnout temperature are most similar to the 25% O_2 which itself has characteristic temperatures similar to the 30% case.

The ELC fuel showed similar trends to the PEL fuel (Table 6.1), with T_P and T_B decreasing and dm/dt_P increasing as the oxygen levels were increased. The difference in the T_P and T_B temperatures, as the oxygen levels were increased, were also similar to the PEL fuel, with T_P decreasing by 59°C from 496°C in 5% O_2 to 437°C at 30% O_2, and T_B decreasing from 561°C to 496°C, a difference of 65°C. The maximum rate of mass loss in 30% O_2 shows a 57% increase compared to combustion in 5% O_2. Again at higher oxygen concentrations, >21% O_2/CO_2, the difference between the atmospheres is small (the difference in T_P is 13°C and that for T_B is 9°C between the 21% and 30% O_2 combustion atmospheres). The difference between the 5% O_2 and 21% O_2 is much greater (ΔT_P is 46°C and ΔT_B is 56°C). The ELC, when combusted in air, has a maximum rate of mass loss and burnout temperature similar to those seen in 21% O_2 combustion but a peak temperature closer to the 30% O_2 combustion.

The increase in oxygen concentration has the greatest effect on the PIT fuel with a decrease in T_P of 72°C and T_B of 79°C when combusted in 30% O_2 (429°C) relative to 5% O_2 (501°C). The maximum rate of mass loss seen in the 30% O_2 combustion environment is also increased by 50% relative to combustion in 5% O_2. The effect of the change in oxygen levels above 21% O_2 are more pronounced in the PIT fuel then the PEL and ELC fuels. The PIT sample when combusted in air is most similar to the 21% O_2 in terms of peak temperature and burnout temperature but has a maximum mass loss rate between those seen in the 21% and 25% O_2 experiments.

6.2.1.1 Discussion

At the temperatures at which the maximum rate of mass loss is seen (T_P), the majority of the volatiles component of the coals are already released, and a carbon rich char is likely to have formed. Evidence of this can be seen from the pyrolysis of the fuels in Figure 6.14. According to the three zone char combustion theory at the temperatures seen in Table 6.1 the

combustion rate is chemically controlled (Regime I, Figure 3.9) and the lower diffusivity of O_2/CO_2 compared to N_2 should be negligible in relation to its effect on the combustion rate. The oxygen consumption rate is compared to the mass transfer rate of oxygen to the particle surface in section 6.2.3. The slight delay seen in the 21% O_2/CO_2 atmosphere relative to air, identified through the increase in T_P and decrease in dm/dt_P, are believed to be the result of the competition for active sites between the CO_2 and O_2 present in the combustion atmosphere (122).

In addition it has been suggested that the increased thermal sink (ρ.Cp) of the CO_2 based atmosphere compared to N_2 may reduce the particle temperature by adsorbing more of the chemically released heat from the particle and therefore decreasing the combustion rates compared to air (148, 154, 245, 246) (ρ.Cp ratio CO_2/N_2 is 1.6 $kJ/m^3.K$ at 700 K (224, 247)). In the TGA system the thermocouple is not in direct contact with the fuel surface so the exact temperature and the effect of the atmosphere on the surface temperature of the char are unknown. It is expected that the effect of this is more dominant in high heating rate experiments were the residence time of the particle is small and the heat is not able to penetrate the particle. The delays in mass loss due to the switch to a 21% O_2/CO_2 atmosphere are believed to be driven by the competition for active sites between CO_2 and O_2.

Work has been performed by several research groups using TGA to investigate the difference between N_2 and CO_2 based combustion atmospheres at elevated oxygen concentrations. Li et al. (219) investigated the combustion behaviour of a pulverised coal in air and oxy-fuel environments with oxygen concentrations from 21% to 80%. The results shown are similar to those seen in this work with the mass loss curves of the two combustion environments similar at temperatures below ~450°C. At higher temperatures a delay is seen in the CO_2 based environment with a reduction in dm/dt_P and an increase in T_P and T_B. The authors attribute the delay to the difference in thermo-physical properties in the combustion atmospheres but do not go any further.

Yuzbasi et al (245) investigated the combustion behaviour of a high ash containing lignite sample in N_2 and CO_2 based atmospheres with oxygen concentrations of 21 and 30%. The lignite sample used produced a singular peak when combusted in air but when combusted in 21% O_2/CO_2, a distinction can be made between the devolatilisation and char combustion steps. This resulted in a large decrease in T_P when combusted in O_2/CO_2 atmospheres relative to air due to the formation of an initial devolatilisation peak. However when the lignite was combusted in 30% O_2 in both N_2 and CO_2 based environment a slight delay was seen in the

CO_2 case with a 3°C increase in T_P and T_B and a decrease in dm/dt_P of ~8%. This was attributed to the higher heat capacity of the CO_2.

The delay has also been investigated at higher heating rates. Shaddix et al (246) investigated the ignition and devolatilisation behaviour of single particles of high volatile bituminous coals in 12-36 volume % O_2 in both N_2 and CO_2 using a combustion driven laminar flow reactor. It was found that at all oxygen levels the presence of CO_2 retards particle ignition and causes a small increase in volatile combustion duration. The delay in ignition of the single particle was attributed to the higher molar specific heat of CO_2 at the experimental temperatures acting as a heat sink and reducing the temperature of the local fuel air mixture. The experiments performed by Shaddix et al. were at higher temperatures (1700K) than those seen during the devolatilisation stage of the coal combustion (250-450°C). At temperatures of 325°C the ratio of the specific heat capacity of CO_2/N_2 is 1 (247) but the higher density of CO_2 (224) results in a higher value of the thermal sink, ρ.Cp (kJ/m^3.K) with a ratio of 1.57 . This suggests that the CO_2 based atmospheres are able to adsorb more of the chemical energy released during the combustion of the volatiles thus reducing the particle temperature and reducing the combustion rate. The measure of the thermal sink increases with temperature and the effect may be more pronounced, depending on the effect of residence time, at the flame temperatures seen in a pulverised fuel furnace. Once ignited the increase in devolatilisation duration was attributed to the decrease in the fuel vapour diffusivity in CO_2 compared to N_2, that is the ability of the volatile species released to diffuse into the local combustion atmosphere.

Work by Molina et al (148) investigating the ignition behaviour of coals also noted the delay in ignition in CO_2 environments and again attributed the delay to the higher specific heat and density of CO_2. It was also noted that under the experimental conditions that the change to CO_2 based combustion had negligible effect on the consumption rates of the evolved volatile species.

Meng et al. (248) investigated combustion behaviour at elevated oxygen environments (21, 30 and 40% O_2) in both N_2 and CO_2 based environments using a DTR. They found that when the coal was combusted at the same oxygen levels that the combustion performance is always better in the N_2 based environments, due to the lower diffusivity of O_2 in CO_2 which affects the transport of O_2 to the particle surface thus reducing combustion rates.

The effect of increasing the oxygen concentration in an oxy-fuel atmosphere have also been investigated using a TGA. Li et al (219) investigated the effect of the increase in oxygen

concentration from 21% - 80% O_2 in CO_2 using a TGA and found that as the oxygen levels are increased the characteristic temperatures decrease and maximum rates of mass loss are increased. It was also found that as the oxygen concentration increased the increase in key temperatures and rates of mass loss decreased, as seen in this work. The improved combustion characteristics in enriched oxygen atmospheres is seen in all work regardless of heating rates and temperatures. The improved combustion performance is due to the increase in local mixture reactivity, the increase in diffusivity of the volatile species in enriched oxygen combustion compared to diffusion in CO_2 (148, 151, 218, 219, 245, 246, 248, 249) .

The experimental work here is performed at identical gas temperatures in all environments, in reality if 21% O_2/CO_2 was used in a conventional pulverised fuel system a reduction in flame temperature, a delay in flame ignition and flame stability would be impacted. In order to produce flame temperatures, ignition times, and heat transfer similar to those seen in air combustion an increase in oxygen levels in the combustion environment is required (25-30%) (51, 122, 148, 210, 218, 246).

6.2.2 Overall combustion behaviour of biomass and torrefied biomass in air and oxy-fuel environments

The overall combustion profiles (10°C min^{-1} heating rate) of the biomass and TSP fuels can be seen in Figure 6.8 - Figure 6.13 and the key temperatures and rates of mass loss extracted from the TGA and DTG plots in Table 6.3.

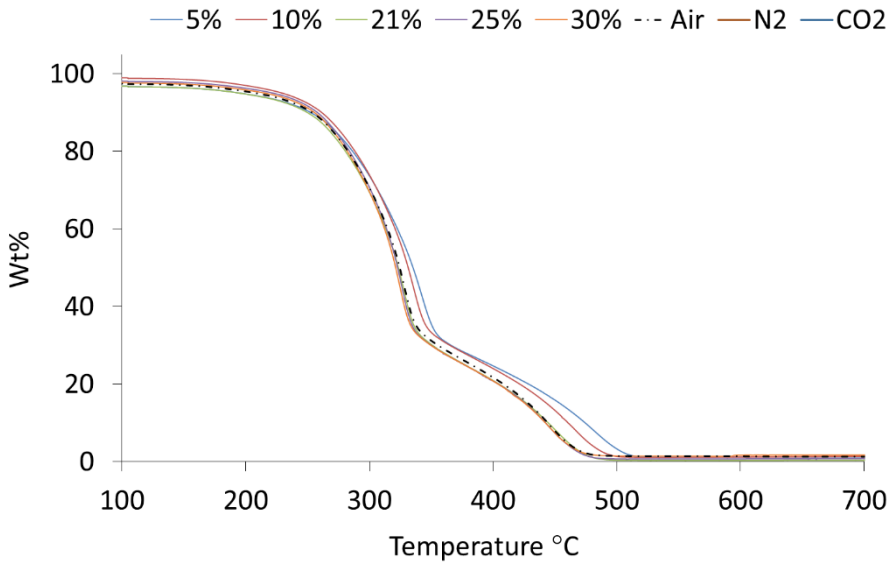

Figure 6.8: Mass loss behaviour of the PWWP fuel combusted in air and 5-30%O_2 in CO_2

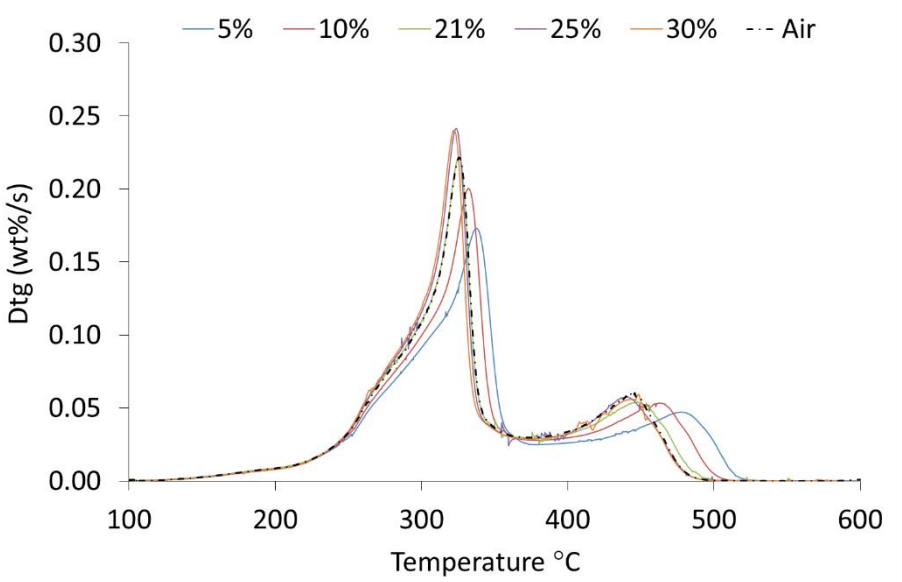

Figure 6.9: DTG behaviour of the PWWP fuel combusted in air and 5-30%O_2 in CO_2

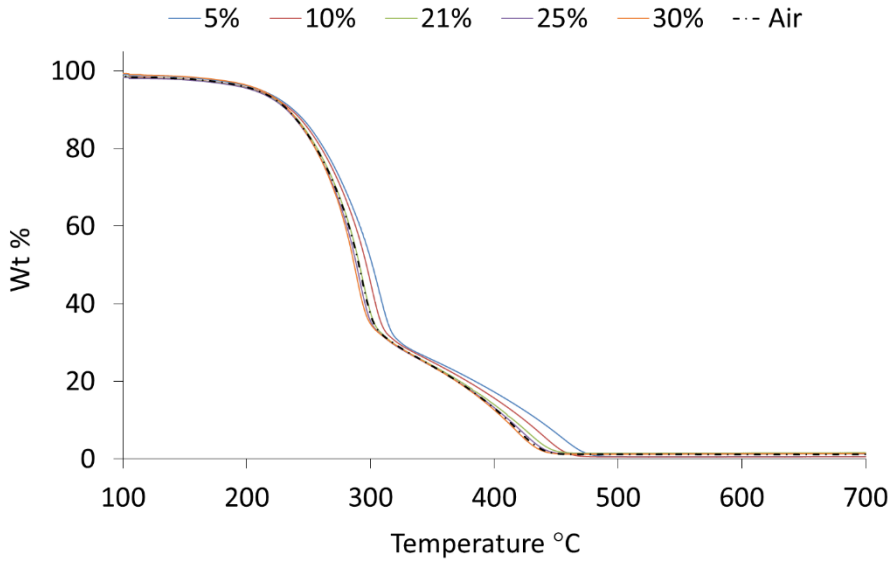

Figure 6.10: Mass loss behaviour of the WWP fuel combusted in air and 5-30%O_2 in CO_2

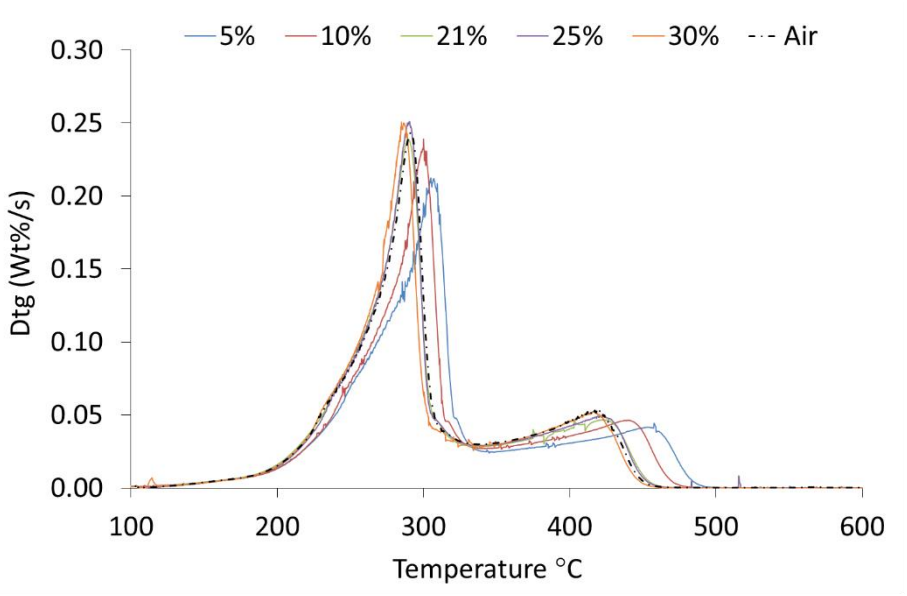

Figure 6.11: DTG behaviour of the WWP fuel combusted in air and 5-30%O_2 in CO_2

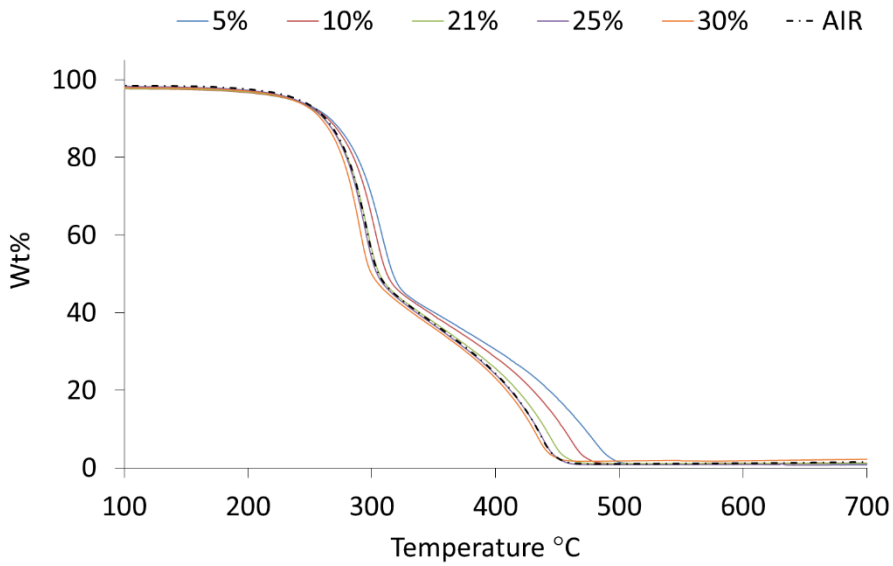

Figure 6.12: Mass loss behaviour of the TSP fuel combusted in air and 5-30%O_2 in CO_2

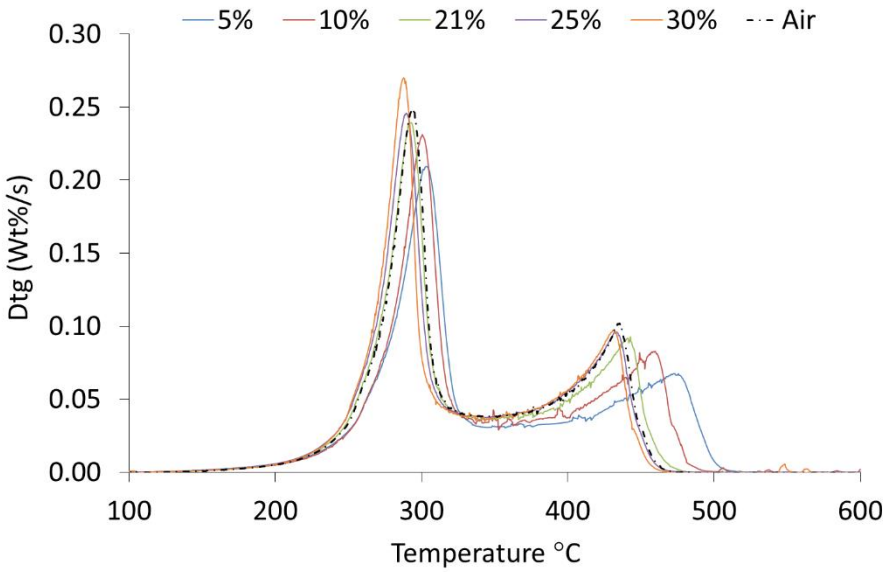

Figure 6.13: DTG behaviour of the TSP fuel combusted in air and 5-30%O_2 in CO_2

Table 6.3: Characteristic temperatures and rates of mass loss observed during combustion of biomass and torrefied biomass in air and oxy-fuel environments

		T_{IM} (°C)	T_V (°C)	dm/dt_V (Wt% s^{-1})	T_C (°C)	dm/dt_C (Wt% s^{-1})	T_B (°C)
PWWP	5%	228	342	0.177	481	0.048	510
	10%	228	336	0.205	467	0.052	494
	21%	227	327	0.225	449	0.055	479
	25%	228	326	0.245	446	0.064	476
	30%	228	324	0.243	447	0.067	473
	Air	228	328	0.225	450	0.062	474
WWP	5%	203	307	0.212	454	0.044	476
	10%	202	300	0.239	441	0.046	461
	21%	200	293	0.246	427	0.047	449
	25%	202	291	0.251	423	0.050	445
	30%	201	288	0.268	418	0.056	440
	Air	201	293	0.244	422	0.055	443
TSP	5%	234	308	0.221	481	0.065	499
	10%	234	302	0.233	460	0.084	480
	21%	231	296	0.253	444	0.100	463
	25%	229	295	0.256	439	0.108	457
	30%	229	290	0.278	434	0.099	452
	Air	232	295	0.250	437	0.104	457

There is a clear difference between the coals and the biomass and TSP fuels with the coals having one unresolved peak compared to the two clear peaks seen in the biomass and TSP. This is due to the higher volatile contents and higher reactivity of the raw biomass and TSP fuels as seen in Table 5.2.

The biomass and TSP fuels combust at lower temperatures than the coals, with TGA and DTG profiles shifting to lower temperatures as a result of the increased reactivity of the fuels as outlined in the following sections. The PWWP and WWP fuels, although both white wood pellets, have a significant difference in the identified key temperatures and mass loss rates. When combusted in air, the PWWP fuel has a lower maximum rate (dm/dt_V) of mass loss during the devolatilisation stage but a higher maximum rate of mass loss during the char combustion stage (dm/dt_C) (Table 6.3). The proximate analysis shows that the PWWP fuel contains slightly higher fixed carbon than the WWP fuel, which is mirrored in the ultimate analysis in terms of the carbon content (Table 5.1 and Table 5.3). The key temperatures identified, T_{IM}, T_V, T_C and T_B are also higher in the PWWP sample relative to the WWP sample. This is an indication in variability of the combustion behaviour seen in white wood pellets that must be managed when large amounts are utilised in large scale electricity production.

The initial mass loss temperature (T_{IM}), for the TSP fuel is seen at the highest temperature of the biomass fuels, but the characteristics identified during the devolatilisation stage are similar to those seen in the WWP sample. During the char combustion stage the TSP fuel has the highest maximum rates of mass loss due to the higher fixed carbon, carbon, and as a result larger char yield as can be seen in Table 5.5.The WWP sample has the lowest characteristic temperatures of the three biomass fuels and is expected to be the most reactive, which is investigated in the following sections.

The initial mass loss seen in the TGA plots is due to the release of moisture, and is again identical in all combustion environments, as seen in the coals. The temperature at which the initial mass loss (T_{IM}) is seen is lower than that seen in the coals (~60^{o}C less in air) due to the increased reactivity, investigated in the following sections and the increased volatile content in the biomass fuels, as described in chapter 5.

It can be clearly seen that the change due to oxy-fuel combustion and the increase in oxygen concentrations are less prominent for the biomass and TSP fuels than seen for the coals. Comparison of the combustion profiles, key temperatures and rates of mass loss in air and 21% O_2/CO_2 show that the initial devolatilisation stage is similar in all fuels, with T_{IM} and T_V within 1^{o}C (Table 6.3). The dm/dt_V is identical in the PWWP and WWP and ~ 1% higher in the CO_2 environment in the TSP sample. The differences in the two atmospheres at higher temperatures, associated with the char combustion, is more evident with a small increase in T_C in the WWP and TSP fuels and decrease in dm/dt_C for all fuels. The PWWP and WWP char combustion rate (dm/dt_C) is decreased by 12% and 15% respectively and the TSP by

only 4% in the CO_2 atmosphere, similar to the levels seen in the coals. The burnout temperature (T_B) is 5-6°C higher in the biomass fuels, slightly higher than in the coals.

Increasing the oxygen levels during oxy-fuel combustion has less of an effect on the biomass samples than seen in the coals. The variation in T_{IM} due to the increase in oxygen concentration is negligible in the two biomass fuels and changes by only ~5°C between 5-30% O_2 in the TSP fuel; this is much smaller than those seen in the coals (~40°C).

The increase in oxygen has a larger effect on the key temperatures and rates of mass loss associated with the devolatilisation step than during the initial mass loss stages. The temperature at which the maximum rate of mass loss is seen (T_V) in the PWWP, WWP and TSP fuel increases by 18-19°C when the oxygen levels are increased from 5-30% O_2. An increase in the rate of mass loss (dm/dt_V) is also seen with the increase in oxygen (5-30% O_2) with the PWWP increasing by 37%, the WWP by 23% and the TSP by 25%. As seen in the coals, the greatest change in temperature and rates of mass loss was seen at the lower oxygen concentrations, between the 5% - 21% O_2 environments.

The effect of the increase in the oxygen levels is most prominent during the char combustion step where the difference in T_C and dm/dt_C in 5-30% O_2 levels is greatest. The PWWP and WWP sample showed a difference in T_C of 34°C and 36°C respectively and the TSP sample a difference 47°C. The maximum rate of mass loss during the char combustion is also increased when combusted in 30% O_2 (by 39% in the PWWP, 21% in WWP and 52% in the TSP) relative to the 5% combustion atmospheres. The effect of the increase in oxygen during the char combustion stage was not as severe as seen in the coals.

Comparison of the key temperatures and rates of mass loss with the oxy-fuel environment again shows that in order to replicate air combustion the oxygen levels in an oxy-fuel environment must be increased. The PWWP fuel reached the maximum rate of weight loss at temperatures similar to that seen in the 21% O_2/CO_2 experiment, but the maximum mass loss rate associated with char combustion, (dm/dt_C) closer to that seen in the 25% O_2/CO_2 experiment. The WWP fuel combusted in 21% O_2/CO_2 was similar to the air combustion during the devolatilisation stage and 25-30% O_2 stage during char combustion. The TSP fuel produced maximum mass loss rates in air closer to those seen in the 30% O_2/CO_2 experiment but at a temperature closer to the 25% O_2 in CO_2 experiment. During devolatilisation the TSP fuel combusted in 21% O_2/CO_2 was the closest to air combustion and 25-30% O_2 during char combustion.

The burnout temperature of the biomass and TSP samples were lower than those seen in the coal samples; PWWP reached burnout at temperatures of 510°C – 473°C (5-30%O_2) and T_B for combustion in air of 474°C. The WWP reached burnout temperatures lower than the PWWP, at 476°C - 440°C, and in air at 443°C. Finally the TSP sample reached burnout temperatures of 499°C - 452°C and 457°C in air.

6.2.2.1 Discussion

The change in combustion atmospheres is not as severe in the biomass and TSP fuels as is seen in the coals. The effect of the change to CO_2 based environments and the increase in oxygen levels is more prominent as combustion proceeds. At the initial mass loss temperatures (T_{IM}) only a small change in temperature is seen in all biomass fuels. Work by Jones et al (250) investigated the ignition behaviour of several biomass fuels and found that, at the same heating rates used in this work, Pine (a source of white wood pellet production) ignited at 271°C. At the T_{IM} temperatures seen it is expected that the volatile gases are yet to be ignited and that the mass loss is caused by the release of the volatile species due to thermal degradation, which is a heat transfer limited process. As the temperature and heating rates are identical in all environments the particle is heated at the same rate in all environments so the devolatilisation step (before ignition) is expected to be similar regardless of the combustion atmosphere.

The similarity in the devolatilisation stage, in all environments, is believed to be due to the availability of oxygen present in the biomass fuels (Table 5.3) providing enough oxygen at the surface of the particle for homogeneous ignition and combustion of the evolving volatile components. Shaddix, Molina and Meng (148, 246, 248) attributed the delay in the initial stages of coal combustion in CO_2 in part to the decrease in volatile diffusivity in CO_2 atmospheres. The higher levels of inherent oxygen present in the biomass fuels reduces the amount of oxygen required from the combustion atmosphere, and so reduces the effect of the lower diffusivity and therefore minimises the effects of the switch from air to an oxy-fuel environment (249). It was also shown in the pyrolysis experiments in section 6.3 that when pyrolysis is performed in N_2 and CO_2 environments that the devolatilisation behaviour of the fuels is very similar.

The change in combustion environment has the largest effect during the char combustion in the biomass and TSP fuels. Again, at these temperatures the three zone char combustion theory can be applied, and at these temperatures the reaction is chemically controlled as is shown in section 6.2.3. The delay when combusted in 21% O_2/CO_2 relative to air can again

be attributed to the competition for active sites and the adsorption of CO_2 on to the char surface. The small changes in the char combustion behaviour can again be attributed to the higher oxygen concentration present in the chars (Table 5.6) which is readily available for reaction with the carbon.

In general all of the fuels used in this work show the same trends, that is a slight delay is seen when combustion is performed in 21% O_2/CO_2 relative to air and as the oxygen levels are increased the mass loss profiles move to lower temperatures with higher rates of peak mass loss. The extent of the effects is fuel dependent but in general the change in atmosphere has a greater effect on the coals than is seen in the biomass and TSP fuels. This is believed to be due to the higher volatile content, higher oxygen levels and increased reactivity of the biomass fuels.

In order to achieve combustion profiles similar to those seen when the samples are combusted in air it was found that the higher oxygen levels were required. The amount of oxygen required varied between samples but in general the coals would require oxygen concentrations between 21% and 25% O_2/CO_2 and biomass and TSP samples 25% - 30% O_2/CO_2 to produce TGA and DTG plots similar to those seen in air under these conditions. This is mainly due to the slower char combustion step in CO_2 atmospheres.

6.2.3 Determination of mass transfer rates during combustion experiments

As discussed in section 6.2.1.1 and 6.2.2.1 the rates of combustion are assumed to be chemically controlled and are not limited by the mass transfer of oxygen from the combustion atmosphere to the particle surface. The rate of mass transfer can be described by Eq 6.1.

$$ro_2 = A_s\, k_g([O_2]_g - [O_2]_p) \quad \text{Eq 6.1}$$

ro_2 – rate of oxygen mass transfer (mol s^{-1})

A_s – surface area (m^2)

k_g – mass transfer coefficient in gas phase (m s^{-1})

$[O_2]_g$ – oxygen concentration in the gas phase (mol m^{-3})

$[O_2]_p$ – oxygen concentration at the particle surface (mol m^{-3})

The mass transfer coefficient (k_g) can be estimated from Eq 6.2 with the assumption that the Sherwood number is equal to two, due to the low Reynolds number in the TGA (7.43×10^{-3}) (251) as determined in section 5.5.1.

$$k_g = \frac{Sh.\ D_g}{d} \qquad \text{Eq 6.2}$$

Sh – Sherwood number

D_g – Diffusivity coefficient for O_2 in CO_2 or N_2 ($m^2\ s^{-1}$)

d – particle diameter (m)

The mass transfer rates were determined for both a single PEL fuel particle and for 5 mg mass of PEL fuel on a TGA pan in 5 and 30%O_2/CO_2 combustion atmospheres. The mass transfer rates were determined at the maximum rate of mass loss seen in the PEL fuel combustion experiments as reported in Table 6.3.

The diffusivity coefficient (D_g) of O_2 in CO_2, at the temperature of maximum rate of mass loss (T_p), were estimated using coefficients taken from (224) and are reported in Table 6.4 along with the maximum rates of mass loss (dm/dt_p) and temperatures at which they occur (T_p).

Table 6.4: Maximum rate of mass loss and diffusivity coefficients of O_2 in CO_2 at the temperature at which the maximum rates are seen

	dm/dt_p (wt% s^{-1})	**T_p (°C)**	**D_g ($m^2\ s^{-1}$)**
PEL 5% O_2/CO_2	0.109	597	1.17×10^{-4}
PEL 30% O_2/CO_2	0.155	453	8.44×10^{-5}

The mass transfer coefficients (k_g) were then determined for a single particle of diameter 90 µm and for a sample placed on a TGA pan. In the case of the TGA pan it is assume that the sample forms a cylinder and the diameter is assumed to be the depth of a cylinder with a radius of 5 mm and mass of 5 mg (the mass used in the combustion experiments. Determination of the volume of a cylinder with a radius of 5 mm and mass of 5 mg and density of 1080 kg m^{-3} resulted in a depth of 0.06 mm. The determination of the mass transfer rate (ro_2) were then determined assuming that the oxygen concentration at the particle surface ($[O_2]_p$) is 99% of that in the gas phase ensuring that the minimum rate of mass diffusion were obtained. In the case of the fuel sitting on a TGA pan, not all of the sample is readily available for the oxygen present in the combustion atmosphere to attack the surface. In this case it was assumed the readily available surface area was only the top

of the cylinder (radius 5 mm). This is expected to underestimate the surface area of the fuel on a sample pan as it does not take into account the increased surface area of a number of particles compared to a single surface. The rates of mass transfer (ro_2),determined using Eq 6.1 and the values of k_g, determined using Eq 6.2 for a single particle and sample on a TGA pan in 5 and 30% O_2/CO_2 can be seen in Table 6.5.

Table 6.5: Mass transfer coefficients, oxygen concentration at the particle surface and in the gas phase and rates of oxygen mass transfer to a single particle and TGA pan

	PEL 5% O_2/CO_2		**PEL 30% O_2/CO_2**	
	Single Particle (90 µm)	**Sample on TGA pan**	**Single Particle (90 µm)**	**Sample on TGA pan**
k_g (m s^{-1})	2.60	3.96	1.88	2.86
$[O_2]_g$ (mol m^{-3})	0.84	0.84	5.04	5.04
$[O_2]_p$ (mol m^{-3})	0.83	0.83	4.99	4.99
ro_2 (mol s^{1})	5.45 x 10^{-10}	2.61 x 10^{-6}	2.40 x 10^{-9}	1.12 x 10^{-5}

The rates of oxygen consumption at the maximum rate of mass loss for 5 mg of PEL fuel combusted in 5% O_2/CO_2, assuming the mass loss is attributed to carbon conversion to CO_2 were determined in section 5.4. The oxygen demand was found to be 0.327 mg min^{-1} which is equal to 4.54 x 10^{-7} mol s^{-1}. The oxygen demand of a single particle was determined assuming that the same maximum rate of mass loss occurs as reported in Table 6.4 and found to be 3.74 x 10^{-11} mol s^{-1}. The oxygen requirements for the single particle and TGA sample pan in the 30% O_2 atmosphere were determined assuming the maximum rate of mass loss reported in Table 6.4 (0.155 wt% s^{-1}) and found that the oxygen demands were 5.32 x 10^{-11} mol s^{-1} and 6.46 x 10^{-7} mol s^{-1} respectively, again assuming carbon conversion to CO_2. The oxygen consumption rates determined are 5 – 45 times that of the mass transfer rates determined giving evidence that the combustion process is not mass transfer controlled and that the reaction rates reported in section 6.2 are chemically controlled. The calculated values of ro_2 are expected to be underestimates and the values of $[O_2]_p$ and the area of a sample on a TGA pan were chosen in order to represent a worst case scenario. In reality it is expected that the mass transfer rates are much higher than those reported here.

6.3 Devolatilisation behaviour during pyrolysis in N_2 and CO_2 environments

Pyrolysis experiments were performed on the fuels in N_2 and CO_2 atmospheres to determine the change in devolatilisation behaviour as a result of the pyrolysis atmosphere. The same size fraction (<90µm) and heating rates (10°C min^{-1}) were used as in the overall combustion experiments (section 6.2), but the final temperature is increased from 900°C to 1000°C to ensure complete pyrolysis in the CO_2 based atmospheres.

6.3.1 Pyrolysis of coal in N_2 and CO_2 atmospheres

The results of the pyrolysis in N_2 and CO_2 for the three coals can be seen in Figure 6.14-Figure 6.15 and characteristic temperatures and rates of mass loss in Table 6.6. The nomenclature used in the pyrolysis experiments is the same as seen in the biomass combustion as the single peak identified in the N_2 and CO_2 atmospheres is associated with the releases of the volatiles and the second peak in CO_2 atmosphere associated with the char – CO_2 gasification reaction.

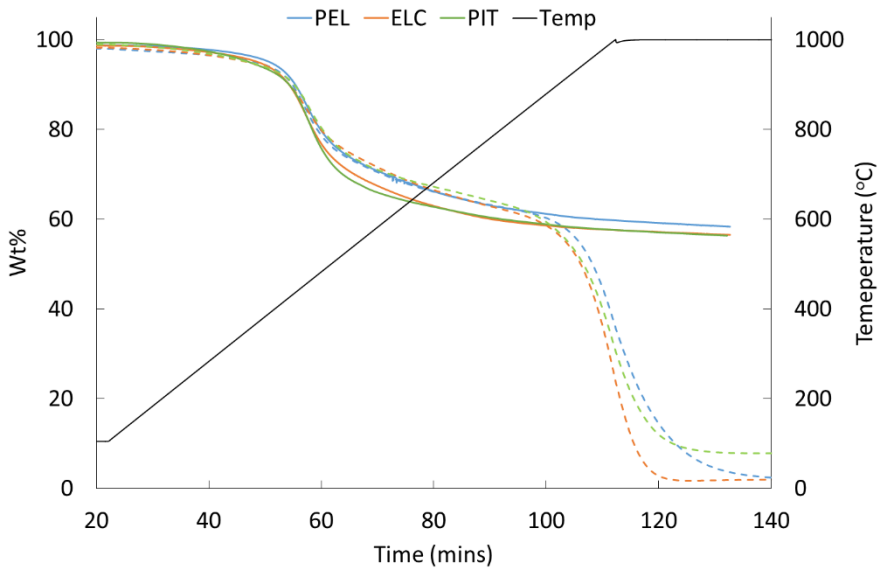

Figure 6.14: TGA profiles during pyrolysis behaviour of coals in N_2 (solid) and CO_2 (dashed) atmospheres

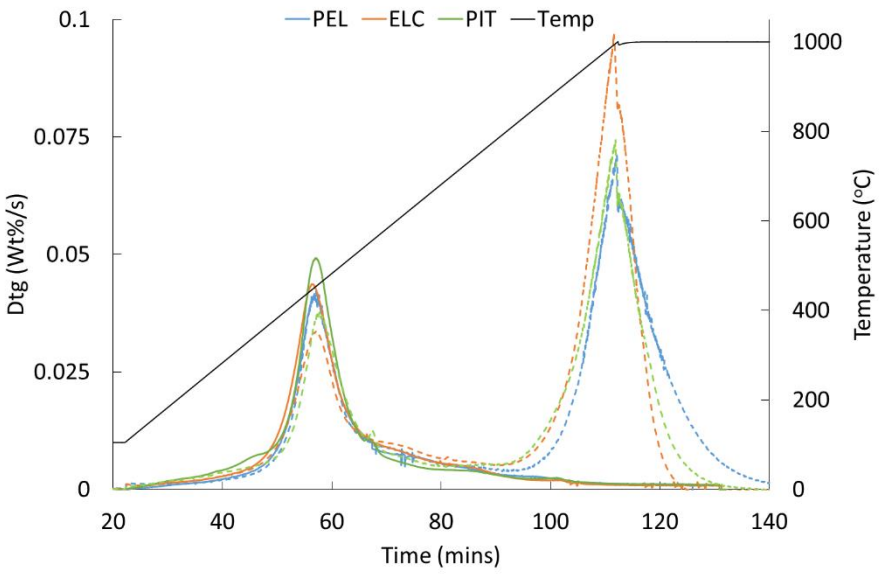

Figure 6.15: DTG profiles during pyrolysis behaviour of coals in N_2 (solid) and CO_2 (dashed) atmospheres

Table 6.6: Key temperatures and rates of mass loss identified during the pyrolysis of the coals in N_2 and CO_2 environments

		T_{IM} (°C)	T_V (°C)	dm/dt_V (Wt% s^{-1})	T_C (°C)	dm/dt_C (Wt% s^{-1})	Final Mass (Wt%)
PEL	N_2	408	449	0.048	-	-	55.54
	CO_2	413	454	0.041	1000	0.070	2.04
ELC	N_2	405	447	0.043	-	-	54.79
	CO_2	414	457	0.034	997	0.094	2.01
PIT	N_2	413	459	0.049	-	-	56.11
	CO_2	424	462	0.038	1000	0.073	7.83

It is clear that from Figure 6.14, Figure 6.15 and Table 6.6 that during the pyrolysis of the coals in CO_2 there is a delay in the devolatilisation behaviour relative to N_2. In addition a second peak, associated with the char – CO_2 gasification reaction, is visible in all coals.

During the initial stage of devolatilisation (<200°C) the TGA and DTG profiles are similar in both pyrolysis atmospheres indicating that CO_2 behaves as an inert gas during coal pyrolysis at low temperatures. In addition no mass gain is seen in either N_2 or CO_2 environments at low temperatures; this confirms that the mass gain seen during combustion is the result of low temperature oxygen chemisorption (section 6.2.1). The TGA and DTG profiles of the ELC and PIT coals start to separate at temperatures ~300°C while in the PEL coal the separation is seen at ~400°C. This is echoed in the temperature of initial mass loss with a small delay in

CO_2 atmospheres (3-10^oC) compared to N_2 pyrolysis. The maximum rate of mass loss in the three coals occurs at lower temperatures than those seen during combustion, but note that the single unresolved peak during combustion is the result of char combustion rather than the lower temperature devolatilisation seen during pyrolysis. The T_V are also increased in CO_2 atmospheres by similar levels seen in the T_{IM} temperatures, except for in the PIT coal where the difference in temperature increased to 11^oC; this suggests that as the temperature is increased the CO_2 has a greater effect. The maximum rate of mass loss (dm/dt_V) is decreased in the CO_2 atmosphere with rates reaching 77-85% of those seen in N_2 environments.

A second peak is present in all of the coals and is associated with the char – CO_2 gasification reaction. The maximum rates of mass loss associated with the char are larger than those seen during the devolatilisation stage due to the low levels of volatiles present in the coals. The temperatures at which dm/dt_C is detected, are all at the maximum temperature (1000^oC) and so the rates are essentially isothermal.

The final mass of the fuels pyrolysed in CO_2 are similar to the levels of ash found in the fuel (Table 5.5). The char yields seen in the N_2 environments are slightly lower than those seen during ballistic heating with the PEL and ELC ~1.9 wt% lower and the PIT ~3 wt% lower (Ad basis). This could be as a result of the increased residence times seen during the pyrolysis experiments compared to the ballistic heating rates (10^oC min $^{-1}$ compared to 1000^oC min^{-1}). The final mass determined during combustion in CO_2 is closer to the ash content levels determined by proximate analysis using the TGA as described in section 5.2.1, which is the result of high char conversion of char in the CO_2 atmospheres.

The decrease in the initial rate of devolatilisation (dm/dt_V) in the CO_2 atmosphere can be attributed to the crosslinking of CO_2 on the particle surface. As pyrolysis in both N_2 and CO_2 are endothermic processes (and no chemical heat is released due to the combustion of the volatiles species) the effect of the CO_2 as a heat sink is not relevant during pyrolysis. Work by Deshpande (134) and Solomon (135) identified crosslinking of CO_2 in coals at similar temperatures to the T_V seen and found that crosslinking was enhanced at lower heating rates as used in this work.

Duan et al (252) investigated the pyrolysis behaviour of a bituminous coal at similar size fractions and heating rates as used in this work and found that at low temperatures, the pyrolysis atmosphere had no effect on the fuel pyrolysis behaviour. As the temperature increased, the CO_2 atmosphere enhanced volatile release with a slight increase in dm/dt_V,

no change in T_P, and a second peak was seen at 900°C due to the char gasification reaction. In work by Rathnam et al (218) no difference in pyrolysis behaviour was seen for an Australian coal at low temperatures, <750°C, after which the char gasification reaction could clearly be seen. Zhou et al (220) investigated three different coals in N_2 and CO_2 using a TGA and found that the pyrolysis behaviour is dependent on the coal type. Two bituminous coals were investigated, the first showed similar trends in mass loss behaviour up to 450°C at which point the CO_2 atmosphere resulted in a higher rate of mass loss. The second bituminous coal showed similar pyrolysis behaviour at temperatures up to ~800°C. Finally pyrolysis of a sub-bituminous coal in CO_2 resulted in a delay in the mass loss profiles from the start. They determined that the difference in pyrolysis behaviour is a result of the coal rank.

6.3.2 Pyrolysis of biomass in N_2 and CO_2 atmospheres

The results of the pyrolysis in N_2 and CO_2 for the biomass and torrefied biomass can be seen in Figure 6.16 - Figure 6.17 and characteristic temperatures and rates of mass loss in Table 6.7. The biomass samples were heated to 900°C rather than 1000°C as the char gasification reaction occurs at lower temperatures.

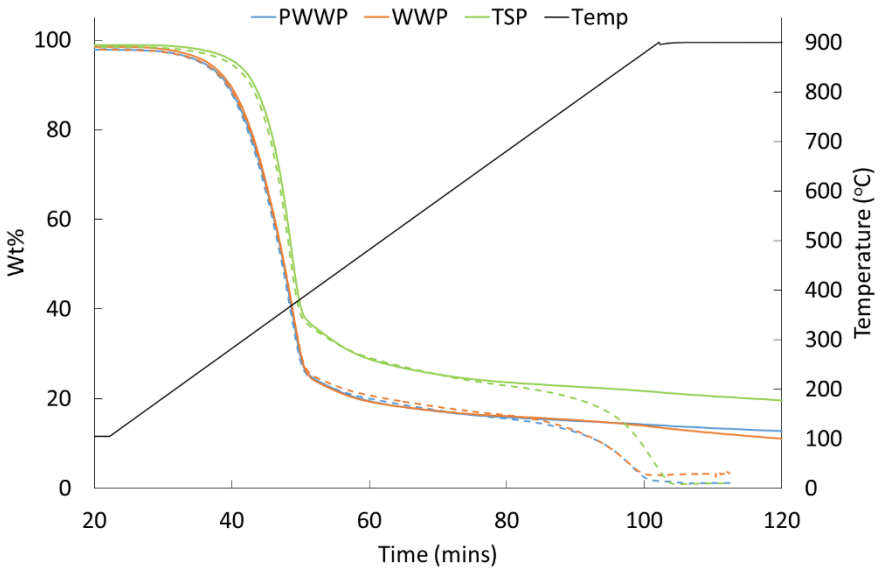

Figure 6.16: TGA profiles during pyrolysis behaviour of biomass and TSP fuels in N_2 (solid) and CO_2 (dashed) atmospheres

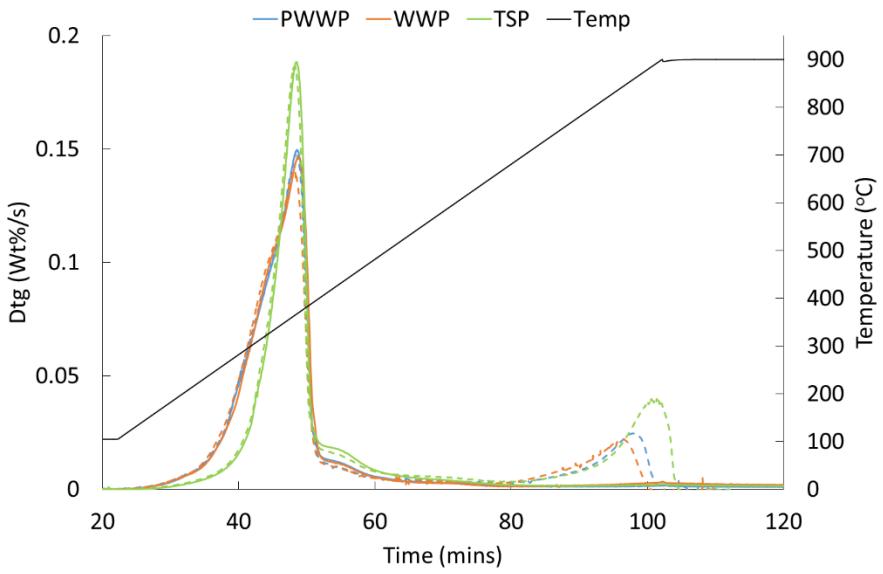

Figure 6.17: DTG profiles during pyrolysis behaviour of biomass and TSP fuels in N_2 (solid) and CO_2 (dashed) atmospheres

Table 6.7: Key temperatures and rates of mass loss identified during the pyrolysis of the biomass and torrefied biomass in N_2 and CO_2 environments

		T_{IM} (°C)	T_V (°C)	dm/dt_V (Wt% s^{-1})	T_C (°C)	dm/dt_C (Wt% s^{-1})	Yield (Wt%)
PWWP	N_2	243	367	0.144	-	-	10.75
	CO_2	247	368	0.143	860	0.024	1.13
WWP	N_2	246	367	0.149	-	-	9.99
	CO_2	248	371	0.140	854	0.023	2.13
TSP	N_2	282	368	0.186	-	-	18.50
	CO_2	285	368	0.184	897	0.039	1.00

The biomass and torrefied biomass fuels show much more similar behaviour during pyrolysis in N_2 and CO_2 atmospheres than the coals. The temperature of initial mass loss (T_{IM}) is slightly delayed in the three biomass fuels when pyrolysed in CO_2 .The T_V and dm/dt_V are similar in the PWWP and TSP fuels in both environments while in the WWP fuel a slight delay of 4°C and decrease in dm/dt_V is seen. The coals have a slightly larger difference in T_{IM}, T_V and dm/dt_V than the biomass and TSP fuels. The smaller influence of atmosphere for biomass is because of the increased reactivity and the volatile content of the biomass and TSP fuels.

Two peaks are well defined and in the DTG curves there is again a clear secondary mass loss peak (char gasification) in the CO_2 atmospheres. Peak heights are consistent with the high volatile content and low char content found in the biomass samples (Table 5.1 and Table 5.5). The char yields determined from pyrolysis in N_2 are similar to those seen when chars

are produced at ballistic heating rates using the TGA (Table 5.5) and yields in CO_2 are similar to the ash contents determined in by proximate analysis (Table 5.2).

Yuzbasi et al (245) investigated pyrolysis behaviour of an olive residue in a CO_2 atmosphere compared to N_2. As in the present work, only small differences were observed; T_{IM} was slightly lower in the CO_2 atmosphere, T_V was reached at temperatures within 1^oC and the dm/dt_v was almost identical in the olive residue sample.

At these temperatures and heating rates in both the coals and the biomass samples, the change in pyrolysis behaviour in N_2 to CO_2 atmospheres may result in a small change in key temperatures and rates of mass loss during the devolatilisation stage. The extent of difference is believed to be the result of fuel properties but further work is needed on a wider range of fuels to investigate it further.

6.4 Devolatilisation kinetics

The non-isothermal mass loss profiles seen in the overall combustion and pyrolysis sections were then used to determine the reactivity and the kinetic parameters of the devolatilisation step outlined in this section. The devolatilisation step dictates both char yield and char properties, and is therefore a key step in the combustion of coal and biomass. The rates of devolatilisation can influence both NO_X and char burnout. Thus the devolatilisation kinetics were determined in different atmospheres using the reaction rate constant method as outlined in section 4.7.1.

6.4.1 Devolatilisation kinetics derived from the combustion and pyrolysis of coals

The apparent rate constants determined from the pyrolysis (100% N_2 and 100% CO_2) and combustion experiments (5-30% O_2 in CO_2 and air) at temperatures of 280-400^oC can be seen in Figure 6.18- Figure 6.20. The apparent first order kinetic parameters extracted (Ln A and Ea) can be seen in Table 6.8.The trends in the kinetic parameters obtained as a function of oxygen concentration in the devolatilisation atmosphere can be seen in Figure 6.21 and Figure 6.22. Please note that in the following plots the data labels, 5-30% refer to 5-30% O_2/CO_2 atmospheres.

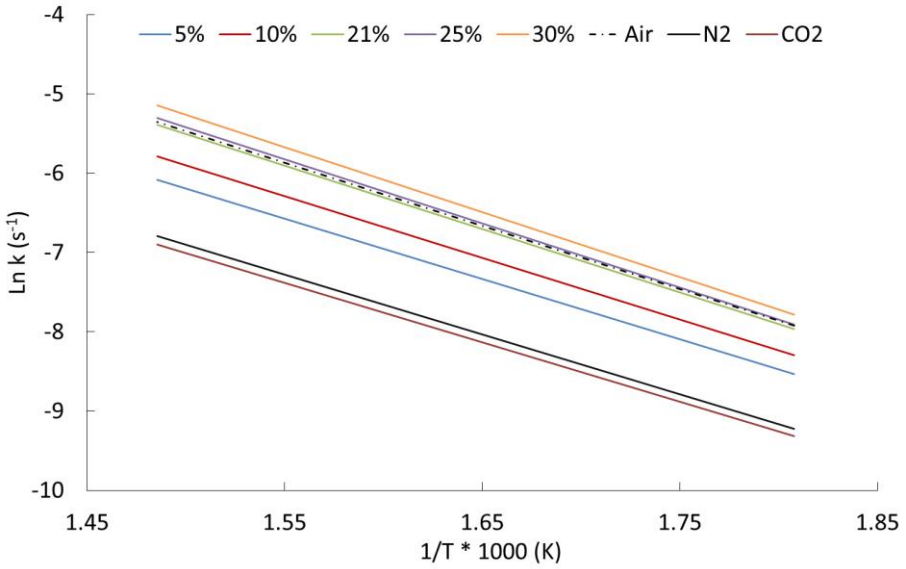

Figure 6.18: PEL devolatilisation reactivity in all combustion and pyrolysis environments

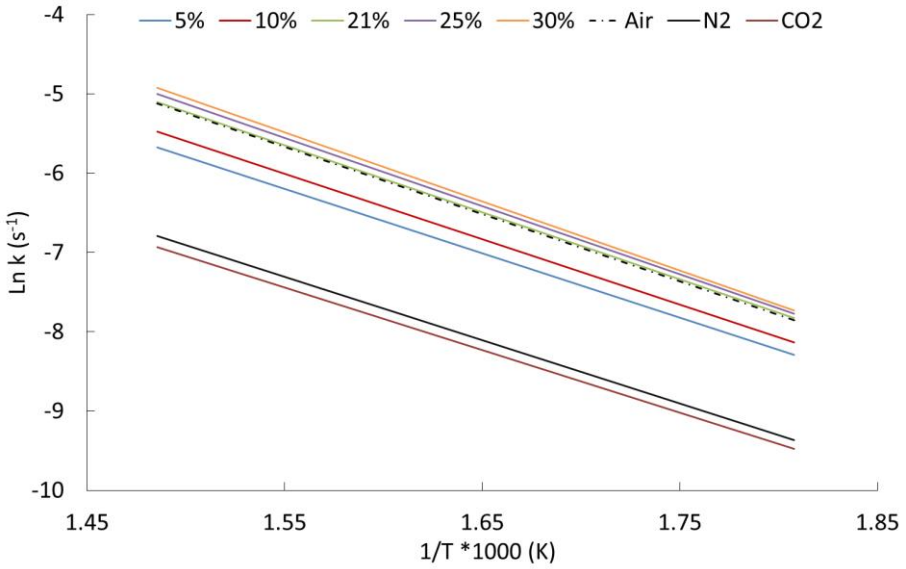

Figure 6.19: ELC devolatilisation reactivity in all combustion and pyrolysis environments

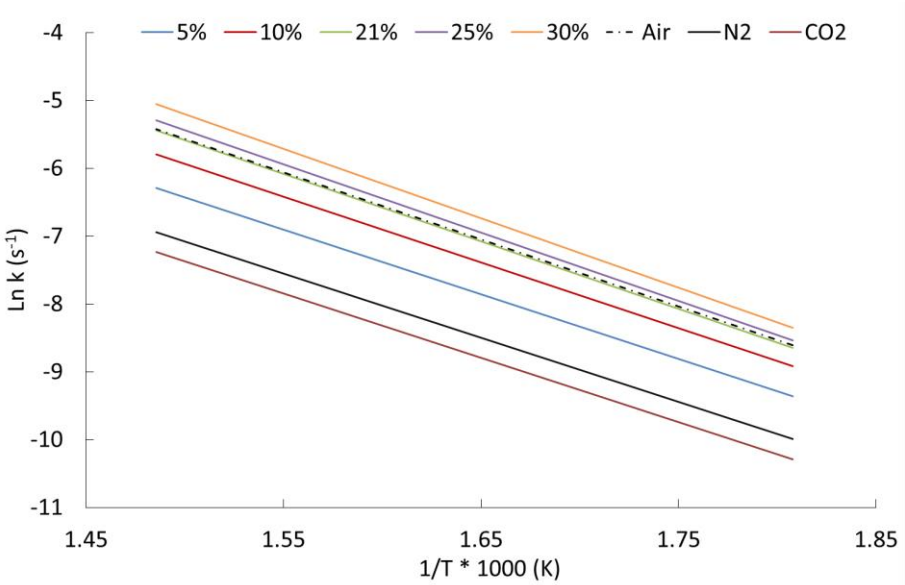

Figure 6.20: PIT devolatilisation reactivity in all combustion and pyrolysis environments

The kinetic rates are clearly affected by the devolatilisation atmosphere; in all coals the kinetic rate of the devolatilisation stage in 100% CO_2 is the slowest followed by the N_2 atmosphere as would be expected from the key temperatures identified in Table 6.1 and Table 6.6. As the oxygen content is increased the apparent kinetic rate constant is also increased, the extent of which is fuel dependent, as seen again in the identification of the key temperatures and rates of mass loss identified in Table 6.1.

The above figures (Figure 6.18 - Figure 6.20) also allow for the easy comparison of air combustion and oxy-fuel combustion in 21% O_2/CO_2. In all of the coals, the rates in 21% O_2/CO_2 are slightly slower than in an air atmosphere where the rates fall in between those seen in 21% and 25% O_2/CO_2, again as suggested by the key characteristics identified. The grouping of the rate constants at oxygen concentrations >21% O_2 highlight the decreasing effect of the oxygen concentration as seen in the TGA and DTG plots in section 6.2.1.

The kinetic parameters derived from the mass loss curves, the temperature region of which the kinetic parameters are applicable and the R^2 parameter, the correlation coefficients of the actual mass loss vs the predicted mass loss as explained in section 4.7.1 can be seen in Table 6.8.

The kinetic parameters derived in each of the pyrolysis atmospheres (N_2 and CO_2) are similar in all of the coals, highlighting the similarity in devolatilisation behaviour. The kinetic parameters determined from combustion in air are similar to those seen in 21% O_2/CO_2

again highlighting the similarity in devolatilisation behaviour, which is expected from the TGA, DTG and key temperatures identified.

Table 6.8: Devolatilisation Arrhenius parameters derived from combustion and pyrolysis experiments of coal

Fuel	Atmosphere	Ln A (s^{-1})	Ea (kJ mol^{-1})	R^2	Temperature region (^oC)
	N_2	4.4	62.7	0.984	200-485
	CO_2	4.2	62.3	0.984	200-485
	5%	5.2	63.2	0.987	265-455
PEL	10%	5.8	64.7	0.998	265-440
	21%	6.5	66.4	0.997	260-426
	25%	6.7	67.2	0.996	255-425
	30%	7.0	68.1	0.996	255-416
	Air	6.5	66.3	0.997	257-430
	N_2	5.1	66.4	0.988	200-490
	CO_2	4.8	65.6	0.993	200-490
	5%	6.4	67.5	0.996	257-440
ELC	10%	6.8	68.6	0.997	255-435
	21%	7.5	70.3	0.993	245-425
	25%	7.8	71.5	0.992	245-420
	30%	8.0	72.5	0.994	245-420
	Air	7.5	70.5	0.995	250-425
	N_2	7.1	78.7	0.985	200-490
	CO_2	6.9	78.8	0.982	200-500
	5%	7.9	79.2	0.996	290-475
PIT	10%	8.6	80.6	0.995	280-455
	21%	9.3	82.7	0.994	275-440
	25%	9.7	83.7	0.995	265-440
	30%	10.2	85.1	0.994	260-430
	Air	9.3	82.2	0.995	270-445

The increase in the oxygen concentration in the oxy-fuel environments has the same effect on each of the coals kinetic parameters. As the oxygen concentration is increased the E_a increases linearly, as shown in Figure 6.21, and A increases exponentially due to a kinetic compensation effect (KCE). The KCE is a widely reported phenomenon but there is no general explanation and there is some controversy over whether it has a mathematical or a physical origin (253, 254). The KCE may be present due to the change in combustion rate due to the change in experimental parameters (physical) in this case the change in oxygen concentrations or may be the result of a simple model being used to describe a complicated reaction process and the mutual dependence of A and E_a within the Arrhenius model (mathematical). The development of the understanding of the KCE is beyond the scope of this work and it is accepted that it exists and that it can be used to predict kinetic parameters if the experimental data is incomplete or for comparison with other experimental work (255, 256).

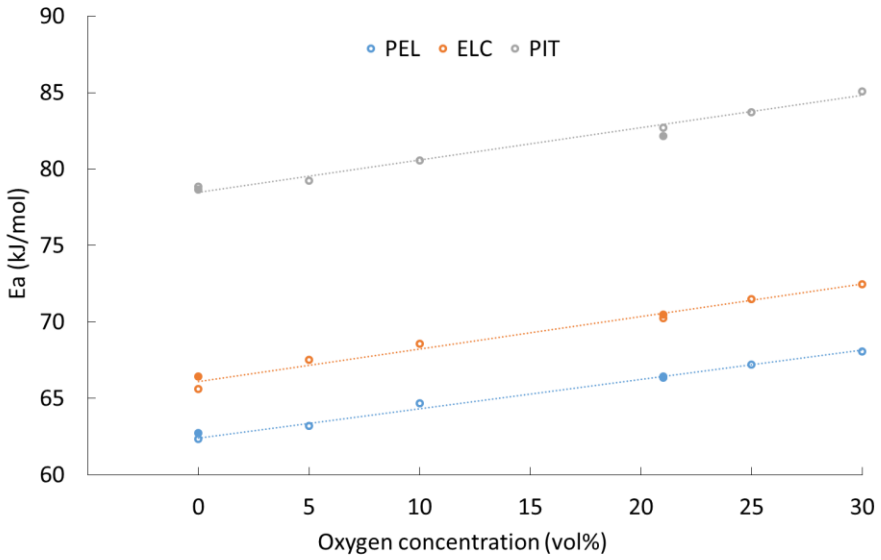

Figure 6.21: Increase in the apparent activation energy with oxygen concentration seen in the coals during devolatilisation (Solid - oxygen concentration in N_2, empty - oxygen in CO_2)

The linear relationships between the activation energy and the oxygen concentration with the correlation coefficient (R^2) are listed below:

PEL $E_a = 0.188 \times O_2 + 62.503$, R^2 0.9903

ELC $E_a = 0.194 \times O_2 + 66.532$, R^2 0.9907

PIT $E_a = 0.2265 \times O_2 + 78.134$, R^2 0.9958

The KCE can be seen in Figure 6.22 where the E_a and Ln A determined during the combustion of coals in 5-30% O_2 in CO_2 are plotted. When the E_a and Ln A values for pyrolysis in CO_2 are added to Figure 6.22 the correlation coefficients are reduced to ~0.96 and deemed too poor a correlation to predict the Arrhenius parameters at unknown oxygen concentrations.

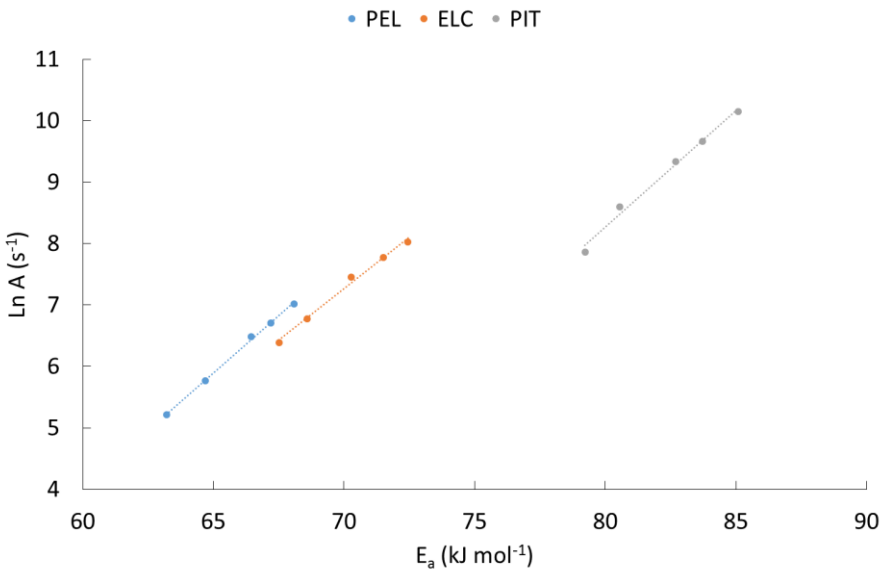

Figure 6.22: Kinetic compensation effect seen in devolatilisation of coals (Combustion in 5-30% O_2 in CO_2 atmospheres

The KCE is governed by the following linear relationship:

$\ln A = aE_a + b$

Where a and b are the compensation coefficients determined from Figure 6.22 which are listed below with the correlation coefficients (R^2).

PEL $\ln A = 0.3734 \times E_a - 18.381$, R^2 0.9984

ELC $\ln A = 0.3353 \times E_a - 16.211$, R^2 0.9917

PIT $\ln A = 0.379 \times E_a - 22.054$, R^2 0.9907

The combination of the linear relationships determined from Figure 6.21 and Figure 6.22 give devolatilisation rate parameters and rate constant (k) as a function of the oxygen levels during oxy-fuel combustion. This is extremely useful in modelling and can be used to predict the devolatilisation rate at the wide range of oxygen concentrations seen throughout a pulverised fuel flame. The equations for the determination of the rate constant (k) based on the oxygen content for each of the coals are outlined in Eq 6.3 – 6.5.

PEL $k = \{\exp(0.374 \text{ x } [(0.188 \text{ x } O_2) + 62.503] - 18.381\} \text{ x } \exp^{\frac{[(0.188 \text{ x } O_2)+62.503}{RT}}$

Eq 6.3

ELC $k = \{\exp(0.3353 \text{ x } [(0.194 \text{ x } O_2) + 67.502] - 16.211\} \text{ x } \exp^{\frac{[(0.194 \text{ x } O_2)+67.502}{RT}}$

Eq 6.4

PIT $k = \{\exp(0.379 \text{ x } [(0.2265 \text{ x } O_2) + 78.134] - 22.054\} \text{ x } \exp^{\frac{[(0.2265 \text{ x } O_2)+78.134}{RT}}$

Eq 6.5

The predicted rate constants (k) determined using Eq 6.3 – 6.5 compared to the rate constants determined experimentally are shown in Figure 6.23 - Figure 6.25 and the predicted results are in good agreement with the rate constants determined from experimental data.

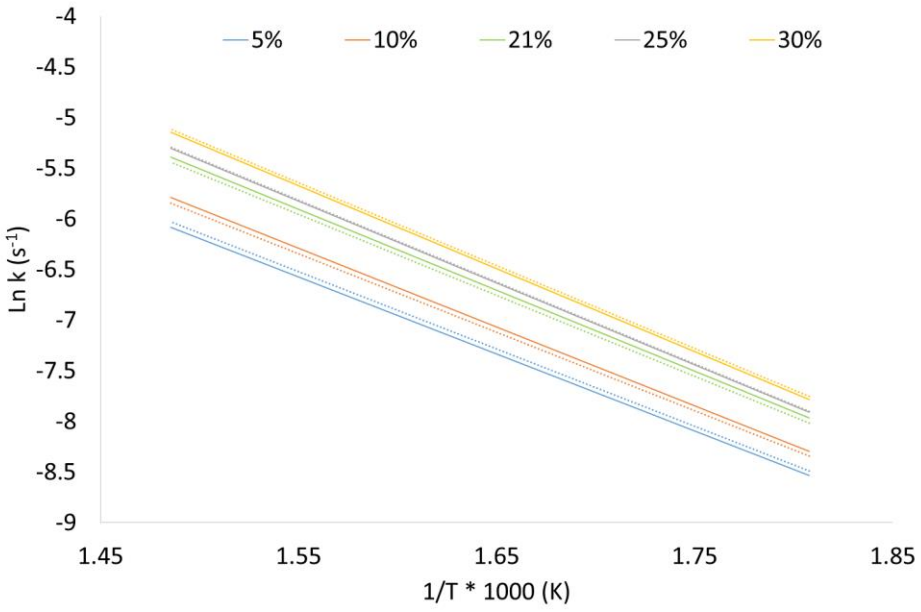

Figure 6.23: PEL devolatilisation rate constants in oxy-fuel environments determined experimentally (Solid lines) and predicted using Eq 6.1 (Dashed lines)

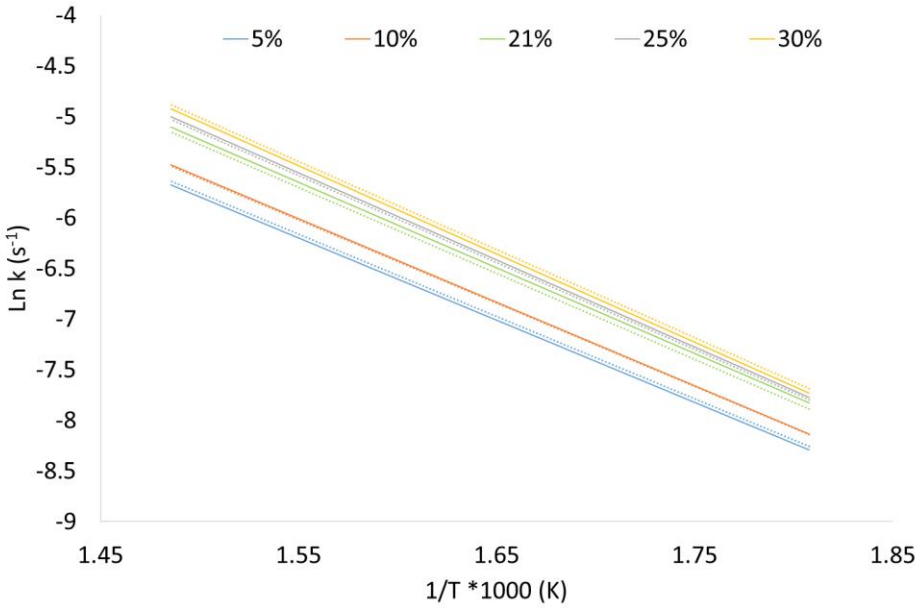

Figure 6.24: ELC devolatilisation rate constants in oxy-fuel environments determined experimentally (Solid lines) and predicted using Eq 6.2 (Dashed lines)

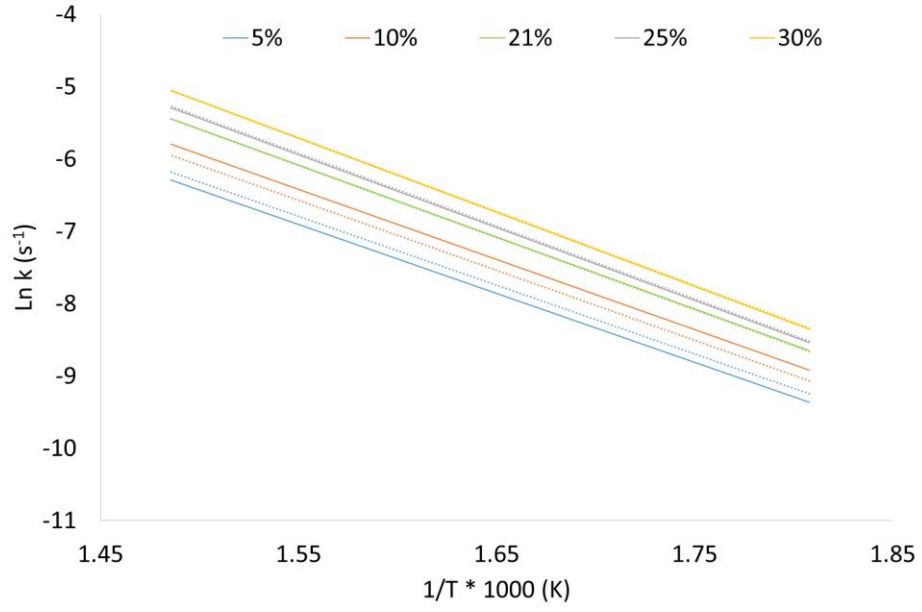

Figure 6.25: PIT devolatilisation rate constants in oxy-fuel environments determined experimentally (Solid lines) and predicted using Eq 6.3 (Dashed lines)

The same trends in kinetic parameters and evidence of the KCE was seen in work by Wang et al. (210) who investigated the pyrolysis and combustion behaviour of two high ash coals in increased oxygen (10-40% O_2) atmospheres both in N_2 and CO_2. The kinetic parameters E_a and Ln A increased linearly regardless of the presence of N_2 or CO_2 meaning that they are solely dependent on the oxygen levels in the combustion atmosphere. Although the same trend was seen, the increase in E_a and Ln A with oxygen concentration were much higher than those seen in this work, with E_a increasing from 58-137 kJ mol^{-1} and Ln A from 7-22 (s^{-1}) as the oxygen concentration is increased from 10-40%. This highlights that the degree of change is fuel specific which in some cases may be quite severe.

The compensation effect is also seen by Zou et al (257) who again combusted two high ash coals using a TGA in increased oxygen in N_2 atmospheres (20-80% O_2). Although the initial values of E_a and Ln A are significantly higher than those reported here (E_a 130-180 kJ mol^{-1} and Ln A 18-28 s^{-1}) the change in kinetic parameters is similar to those seen as those reported in Table 6.8, with E_a increasing by ~10 kJ mol^{-1} and Ln A by 1 at comparable increases in oxygen concentration. Again the compensation effect was shown to follow a linear relationship.

In the work by Wang (210) and Zhou (220) the KCE is present over wider oxygen concentrations than used in the work in this thesis. It is suggested that the kinetic parameters determined in this work could be used to determine the devolatilisation reaction rates at higher oxygen concentrations. This may be important if >30% O_2 is required for comparable flame temperatures to air combustion.

Comparison of the apparent rate constants determined from the pyrolysis of the coals in N_2 and their combustion in air can be seen in Figure 6.26. In addition a summary of a review of coal pyrolysis devolatilisation rate constants performed by Saddawi et al (164) can be seen. The wide range of data in the Saddawi paper indicates the wide range in kinetic parameters available in literature. The black lines indicate low activation energies, and the grey high activation energies derived from pyrolysis of coals. The apparent rate constants derived for the pyrolysis of the PEL, ELC and PIT coals fall between the upper and lower limits of the kinetic rates determined by Saddawi et al. giving confidence in the parameters derived.

The reaction order of the coals can also be determined from Figure 6.26. In the case of pyrolysis in N_2 the apparent rate constants determined for PEL and ELC fuels are identical and are both larger than the PIT fuel (more reactive) at lower temperatures. As the temperatures are increased the apparent rate constants converge (i.e the rates converge)

and at 673 K, the rates become very similar. When combusted in air, the same trends are seen with the ELC and PEL fuels having a similar reactivity and the rates of all three coals converge at higher temperatures.

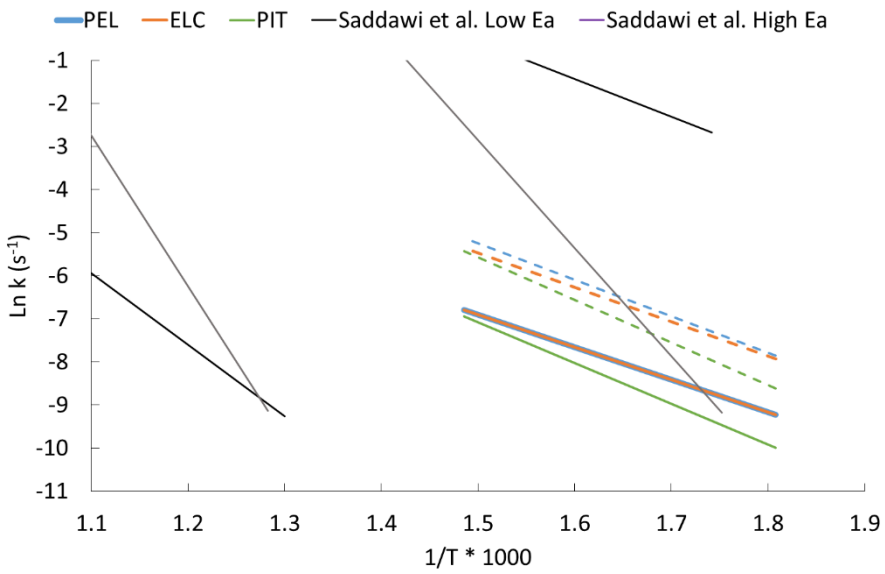

Figure 6.26: Comparison of the devolatilisation rate constants of the coals from pyrolysis in N_2 (solid lines), combustion in air (dashed lines) and comparison with literature values of coal pyrolysis taken from (164)

6.4.2 Devolatilisation kinetics derived from the combustion and pyrolysis of the biomass fuels

The apparent rate constants determined from the pyrolysis (100% N_2 and 100% CO_2) and combustion experiments (5-30% O_2 in CO_2 and air) of the biomass fuels at temperatures of 250-300°C can be seen in Figure 6.27 - Figure 6.29. The apparent first order kinetic parameters extracted can be seen in Table 6.9. The trends in the kinetic parameters obtained as a function of oxygen concentration in the devolatilisation atmosphere can be seen in Figure 6.30 and Figure 6.31. Please note that in the following plots the data labels, 5-30% refer to 5-30% O_2/CO_2 atmospheres.

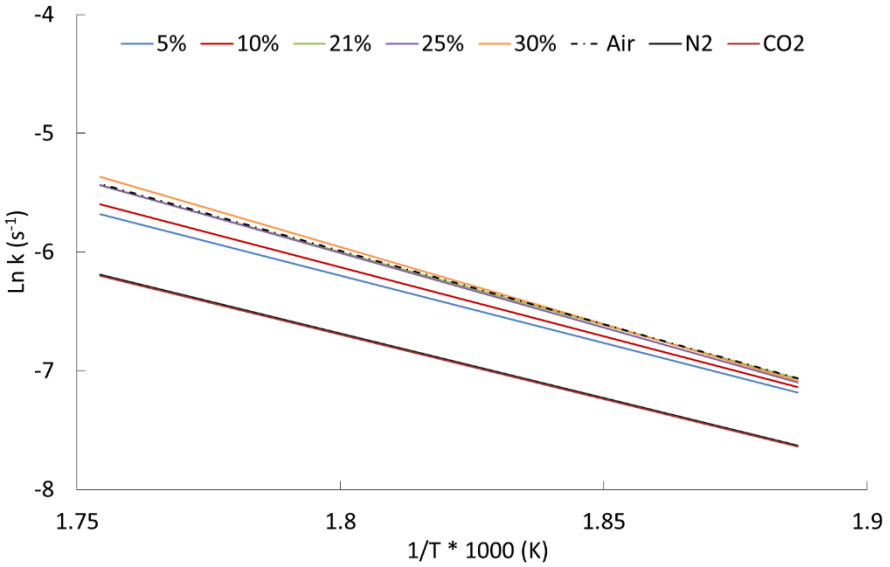

Figure 6.27: PWWP devolatilisation reactivity in all combustion and pyrolysis environments

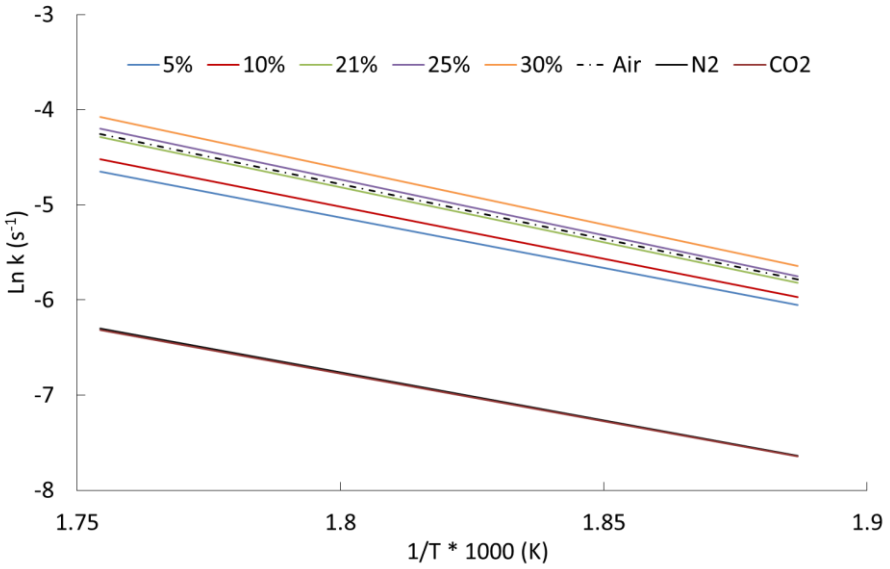

Figure 6.28: WWP devolatilisation reactivity in all combustion and pyrolysis environments

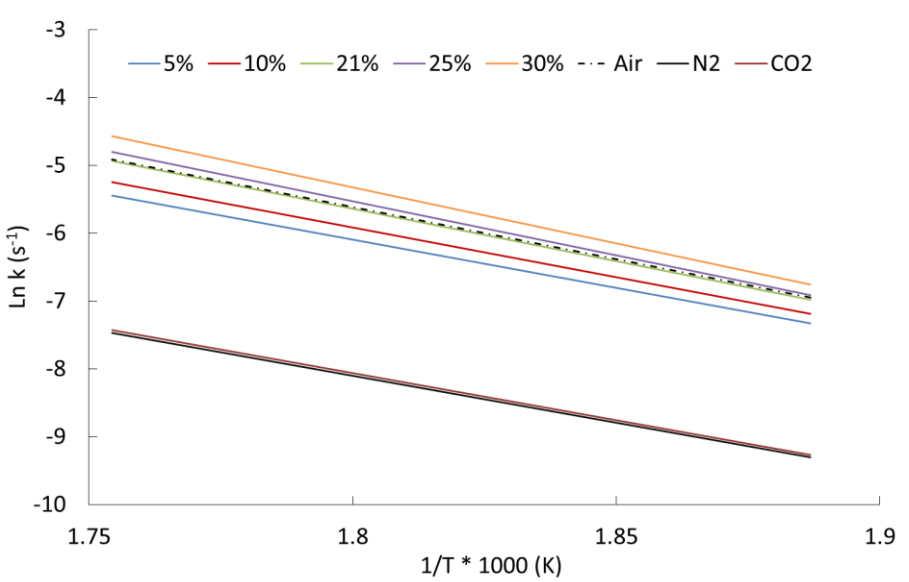

Figure 6.29: TSP devolatilisation reactivity in all combustion and pyrolysis environments

In the biomass and torrefied biomass samples the devolatilisation kinetic rates determined during pyrolysis in N_2 and CO_2 are again the slowest and are almost identical as expected from the pyrolysis TGA and DTG plots seen in section 6.3.2. As the oxygen concentration is increased the apparent rate constants increase (reaction rate increase), as was seen in the coals.

At oxygen concentrations of 21% and above the reaction rates are similar as would be expected when comparing to the TGA and DTG profiles. The reasoning for this is believed to be the availability of inherent oxygen in the fuel providing enough oxygen for localised reactions, that is, an excess of O_2 within the local combustion atmosphere. Again the above reaction rate constant plots are in agreement with the key temperatures identified in Table 6.7 with respect to the effect of increased O_2 on the reaction parameters.

The Arrhenius parameters extracted from Figure 6.27 - Figure 6.29 can be seen in Table 6.9 and these parameters again increase with O_2 concentration (Figure 6.30) with the presence of the KCE (Figure 6.31). The extent of the change in E_a and Ln A is greater in the biomass and TSP samples than the coals, with E_a increasing by 10-19 kJ mol^{-1} and Ln A by 2.8-3.9 s^{-1} when the O_2 is increased from 5-30%; this is around twice the increase seen in the coal samples. The values of Ea and Ln A are also significantly higher than those seen in the coals with Ea ranging from 84 – 137 kJ mol^{-1} in the biomass samples and 62 – 85 kJ mol^{-1} in the coals.

Table 6.9: Devolatilisation Arrhenius parameters derived from combustion and pyrolysis experiments of biomass and torrefied biomass

Fuel	Atmosphere	Ln A (s^{-1})	Ea (kJ mol^{-1})	R^2	Temperature region (°C)
	N_2	12.9	90.4	0.998	150-375
	CO_2	12.9	90.3	0.995	150-365
	5%	14.2	94.3	0.993	150-355
PWWP	10%	14.8	96.7	0.994	150-345
	21%	16.1	102.2	0.993	150-335
	25%	16.6	104.4	0.995	150-335
	30%	17.4	107.9	0.994	150-335
	Air	16.3	102.8	0.993	150-335
	N_2	11.4	84.0	0.998	150-385
	CO_2	11.3	83.4	0.997	150-385
	5%	13.9	88.0	0.998	150-320
WWP	10%	14.7	91.0	0.999	150-310
	21%	16.0	96.2	0.999	150-305
	25%	16.4	97.5	0.999	150-300
	30%	16.7	98.4	0.999	150-300
	Air	16.0	96.1	0.998	150-305
	N_2	16.8	115.1	0.998	150-375
	CO_2	16.9	115.5	0.995	150-380
	5%	19.5	118.6	0.998	150-315
TSP	10%	20.5	121.9	0.998	150-315
	21%	22.2	128.5	0.998	150-300
	25%	23.1	132.6	0.997	150-300
	30%	24.4	137.3	0.996	150-290
	Air	22.1	127.9	0.998	150-300

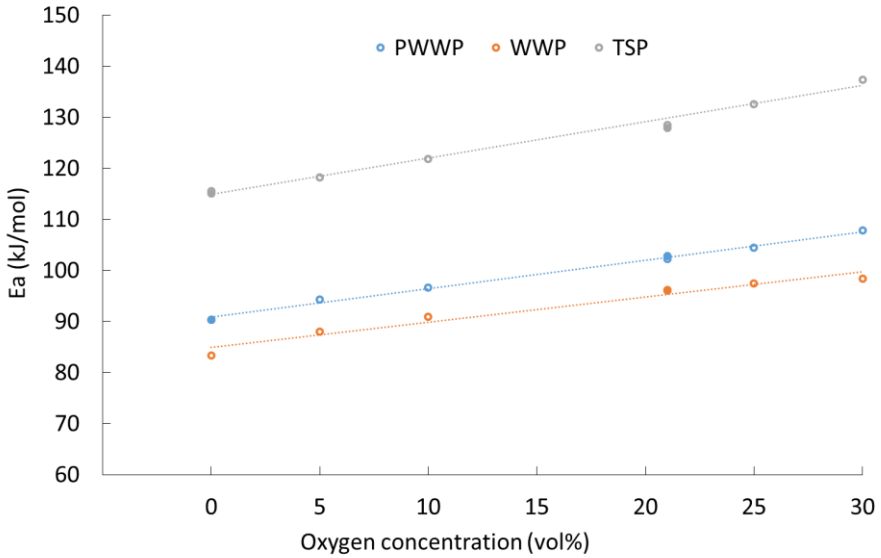

Figure 6.30: Increase in the apparent activation energy with oxygen concentration seen in the biomass samples during devolatilisation (Solid - oxygen concentration in N_2, empty - oxygen in CO_2)

The linear relationships between the activation energy and the oxygen concentration (Figure 6.30) with the correlation coefficient (R^2) are listed below:

PWWP E_a = 0.5333 x O_2 + 91.398, R^2 0.9956

WWP E_a = 0.4252 x O_2 + 86.482, R^2 0.9767

TSP E_a 0.7395 x O_2 + 114.24, R^2 0.9891

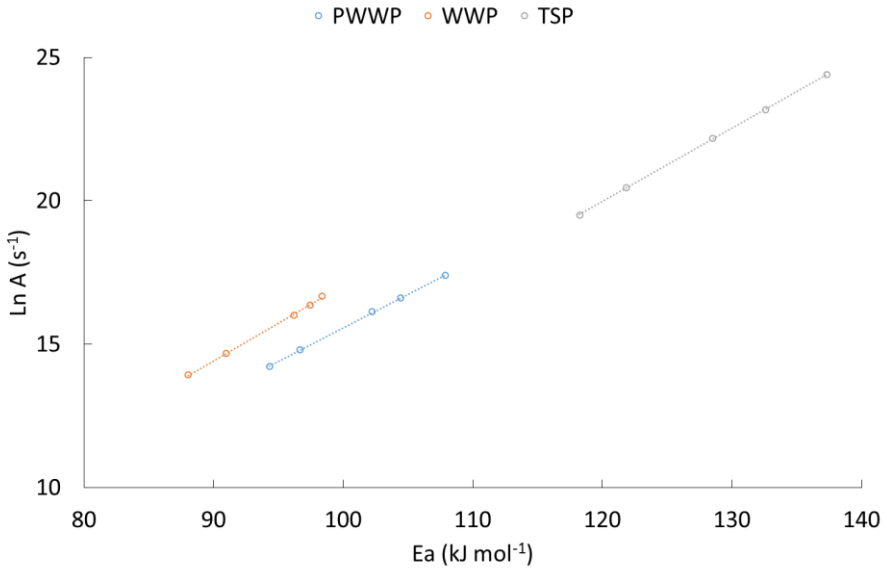

Figure 6.31: Kinetic compensation effect seen in devolatilisation of the biomass samples (Combustion in 5-30% O_2/CO_2 atmospheres)

The KCE (Figure 6.31) is again governed by the same linear relationship and the compensation coefficients as seen in the coals. The linear relationships and the correlation coefficients can be seen below:

PWWP Ln A = 0.234E_a – 7.8298, R^2 0.9996

WWP Ln A = 0.2628E_a – 9.2218, R^2 0.999

TSP Ln A = 0.256E_a – 10.744, R^2 0.9999

The linear relationships outlined above can again be combined in order to produce an equation to determine the devolatilisation reaction rate constant (k) as a function of oxygen concentration for the biomass fuels:

PWWP $k = \{\exp(0.234 \text{ x } [(0.533 \text{ x } O_2) + 91.398] - 7.8298\} \text{ x } \exp^{\frac{[(0.533 \text{ x } O_2)+91.398}{RT}}$ Eq 6.6

WWP $k = \{\exp(0.2628 \text{ x } [(0.452 \text{ x } O_2) + 86.482] - 9.2218\} \text{ x } \exp^{\frac{[(0.452 \text{ x } O_2)+86.482}{RT}}$ Eq 6.7

TSP $k = \{\exp(0.256 \text{ x } [(0.7395\text{x } O_2) + 114.24] - 10.744\} \text{ x } \exp^{\frac{[(0.7395 \text{ x } O_2)+114.24}{RT}}$ Eq 6.8

Figure 6.32 - Figure 6.34 show the predicted rate constants (k) determined using Eq 6.6- 6.8 compared to the devolatilisation rate constants determined experimentally as shown in Figure 6.27 - Figure 6.29. The predicted rate constants are again in good agreement with the rate constants determined experimentally.

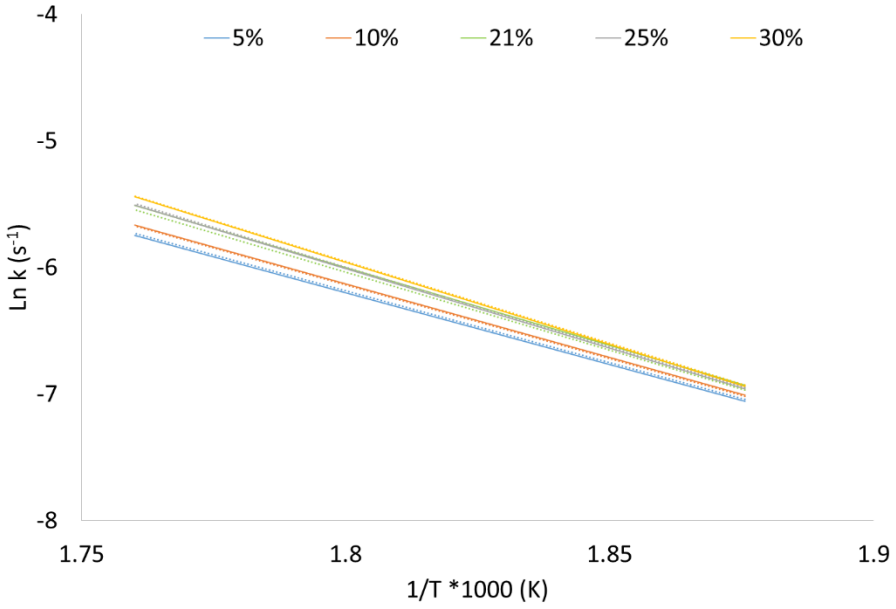

Figure 6.32: PWWP devolatilisation rate constants in oxy-fuel environments determined experimentally (Solid lines) and predicted using Eq 6.4 (Dashed lines)

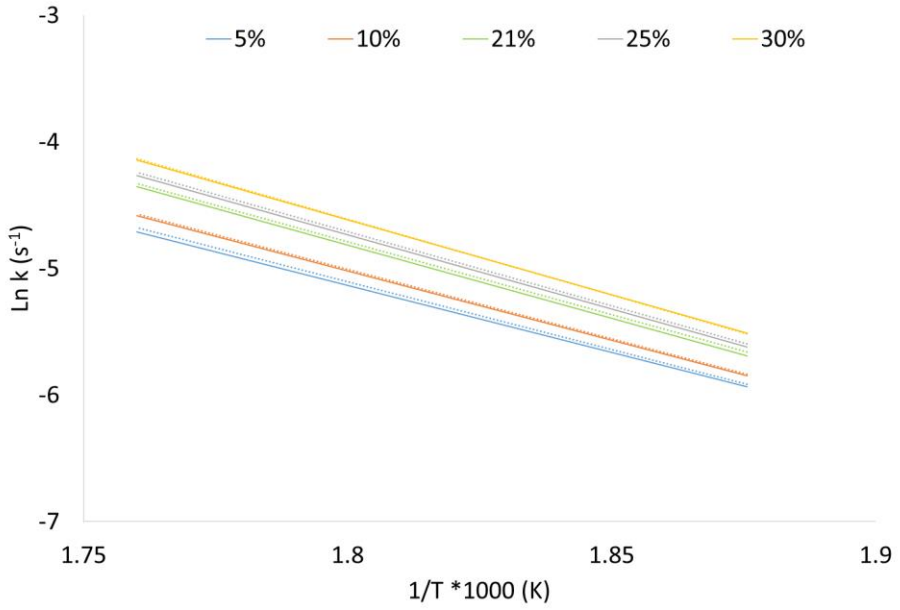

Figure 6.33: WWP devolatilisation rate constants in oxy-fuel environments determined experimentally (Solid lines) and predicted using Eq 6.5 (Dashed lines)

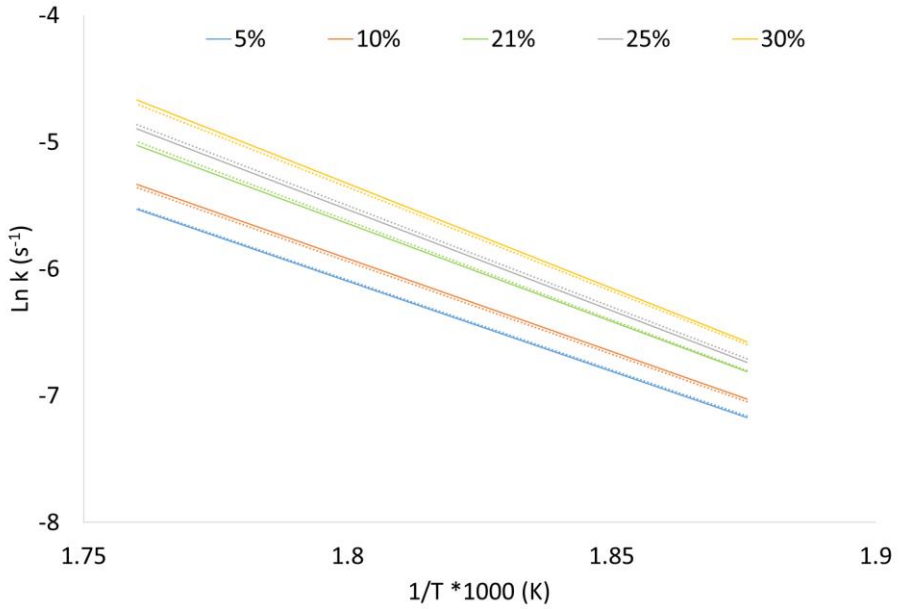

Figure 6.34: TSP devolatilisation rate constants in oxy-fuel environments determined experimentally (Solid lines) and predicted using Eq 6.6 (Dashed lines)

Saddawi et al. (164) also reviewed rates of pyrolysis in N_2 for woody biomass fuels and a general trend was seen as given in Figure 6.35. The same figure also compares the pyrolysis in N_2 and the combustion rate constants of the biomass and TSP fuels along with the rate constant for the pyrolysis in N_2 of the PEL fuel. The biomass fuels are all more reactive than the coals during pyrolysis in N_2, and the torrefied fuel falling between the raw biomass and coal fuels. The PWWP and WWP fuels show similar levels of reactivity during pyrolysis which would be expected from the behaviour seen in Figure 6.16 and Figure 6.17. When combusted in air the WWP fuel is the most reactive of all of the fuels followed by the TSP and then the PWWP. The PWWP and WWP rate constants fall within the region of low activation energy kinetic rates as described by Saddawi et al with activation energies and pre-exponential constants similar to those seen in that work.

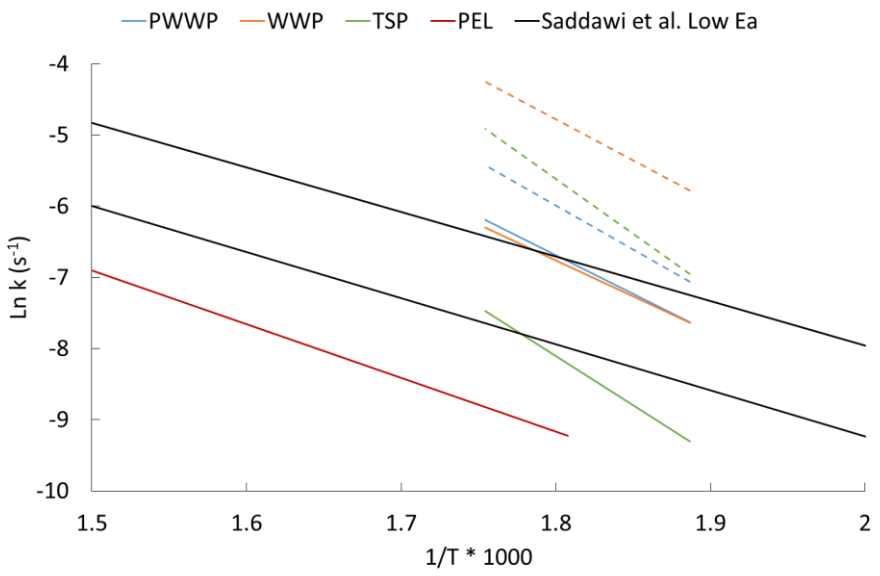

Figure 6.35: Comparison of pyrolysis in N_2 and combustion in air of the biomass reaction rates with literature values taken from Saddawi et al. (164) (Solid pyrolysis in N_2, dashed combustion in air)

These comparisons further demonstrate the differences in the combustion and devolatilisation behaviour between fuels and the need for empirical measurements in determining the devolatilisation behaviour in oxy-fuel environments. This work shows that a small number of experiments can be performed to determine empirical equations that suitably predict the devolatilisation behaviour over a range of oxygen environments, which is particularly useful for CFD modelling of combustion systems.

6.5 Conclusions

6.5.1 Overall Combustion

- Combustion experiments were performed in air and oxy-fuel environments to determine the effect of the change in atmosphere on the coal and biomass fuels.
- The change in oxy-fuel environments and the increase in oxygen concentration has a larger effect on the coals than the biomass and TSP fuels in terms of the change in key indicators.
- The first stage of combustion, the drying of the fuel, is almost identical in all combustion environments in all fuels, as this is a heat transfer phenomenon.
- A delay is seen when the fuels are combusted in 21% O_2/CO_2 atmospheres relative to air. The delay is greater in the coals and is attributed to the adsorption of CO_2 on the particle surface preventing the oxygen from consuming the carbon.
- The delay seen in the biomass and TSP fuels is more pronounced as combustion proceeds. The devolatilisation stage of biomass combustion is almost identical due to the availability of oxygen in the fuel to sustain homogeneous ignition and combustion of the evolving volatile species. During char combustion the change from air to CO_2 based atmosphere is more pronounced again attributed to the competition between CO_2 and O_2 for the active sites available.
- The increase in oxygen concentration in the oxy-fuel environments results in a decrease in key temperatures and increase in the peak rates of mass loss identified in all fuels. The effect of this is again greater in the coals than the biomass fuels.
- Oxygen chemisorption is seen in the coal fuels and its extent is increased as the oxygen levels are increased in the combustion atmosphere. The results in a linear increase in active surface area.
- Examination of the char combustion stage showed that biomass char is more sensitive to oxygen than the devolatilisation stage, with larger differences in key temperatures and maximum rates of mass loss identified. As in the coals this is believed to be the result of competition for the active sites present in the char between O_2 and CO_2.
- The effect of the increase in oxygen concentration is greatest at <21% O_2. At higher oxygen concentrations the difference in the key temperatures and rates of mass loss decreased.

- In order to produce mass loss curves similar to those seen during combustion in air, an increase in the concentration of oxygen in the oxy-fuel environment required. This differs for different fuels as follows:

  PEL – 21-25% O_2/CO_2

  ELC - 21-25% O_2/CO_2

  PIT - 21-30% O_2/CO_2

  PWWP – 21-25% O_2/CO_2

  WWP – 25-30% O_2/CO_2

  TSP– 25-30% O_2/CO_2
- The combustion experiments were found to be chemically controlled

6.5.2 Pyrolysis in N_2 and CO_2

- Pyrolysis experiments were performed in N_2 and CO_2 environments.
- Pyrolysis of coal and biomass in CO_2 results in a second, clearly identifiable peak at high temperatures, associated with the char – CO_2 gasification reaction.
- When the coals are pyrolysed in CO_2 the rate of mass loss is significantly smaller than in N_2. This is attributed to the enhanced crosslinking in CO_2 environments.
- The maximum rate of mass loss of the char – CO_2 gasification peak in the pyrolysis of coal in CO_2 is larger than the primary devolatilisation peak due to the relatively large char content of the fuels.
- In the biomass and TSP fuels the char gasification peak is much smaller than the primary peak due to the relatively low char contents of the fuels.

6.5.3 Devolatilisation kinetics

- Apparent reaction rate constants and kinetic parameters were determined for the full range of combustion and pyrolysis environments derived from TGA data.
- The apparent rate constants highlight the differences in reactivity of the fuels in all pyrolysis and combustion environments.
- Reaction rates during combustion in 21% O_2/CO_2 are slightly lower than the respective rate seen in combustion in air for all fuels as would be expected from the overall combustion analysis.
- As the oxygen concentration is increased the activation energy increase linearly and a kinetic compensation effect is seen between the activation energy and the pre-exponential factor. These linear trends allowed for the development of fuel specific empirical equations to determine the rate constant from the oxygen concentration

present in an oxy-fuel environment. The apparent kinetic parameters, A and E_a, are summarised in the Table 6.10 and the empirical equations in Table 6.11.

- The devolatilisation reaction order of the fuels when combusted in air were determined. The raw biomass fuels are the most reactive followed by the TSP, the PEL and ELC and finally the PIT fuel.

Table 6.10: Summary of fuel devolatilisation kinetic parameters

Fuel	Atmosphere	Ln A (s^{-1})	Ea (kJ mol^{-1})	Fuel	Atmosphere	Ln A (s^{-1})	Ea (kJ mol^{-1})
	N_2	4.4	62.7		N_2	12.9	90.4
	CO_2	4.2	62.3		CO_2	12.9	90.3
	5%	5.2	63.2		5%	14.2	94.3
PEL	10%	5.8	64.7	**PWWP**	10%	14.8	96.7
	21%	6.5	66.4		21%	16.1	102.2
	25%	6.7	67.2		25%	16.6	104.4
	30%	7.0	68.1		30%	17.4	107.9
	Air	6.5	66.3		Air	16.3	102.8
	N_2	5.1	66.4		N_2	11.4	84.0
	CO_2	4.8	65.6		CO_2	11.3	83.4
	5%	6.4	67.5		5%	13.9	88.0
ELC	10%	6.8	68.6	**WWP**	10%	14.7	91.0
	21%	7.5	70.3		21%	16.0	96.2
	25%	7.8	71.5		25%	16.4	97.5
	30%	8.0	72.5		30%	16.7	98.4
	Air	7.5	70.5		Air	16.0	96.1
	N_2	7.1	78.7		N_2	16.8	115.1
	CO_2	6.9	78.8		CO_2	16.9	115.5
	5%	7.9	79.2		5%	19.5	118.6
PIT	10%	8.6	80.6	**TSP**	10%	20.5	121.9
	21%	9.3	82.7		21%	22.2	128.5
	25%	9.7	83.7		25%	23.1	132.6
	30%	10.2	85.1		30%	24.4	137.3
	Air	9.3	82.2		Air	22.1	127.9

Table 6.11: Fuel specific empirical equations used to describe devolatilisation in oxy-fuel environments

Fuel	Empirical equation to determine the rate constant (s^{-1})
PEL	$k = \{\exp(0.374\ x\ [(0.188\ x\ O_2) + 62.503] - 18.381\}\ x\ exp^{\frac{[(0.188\ x\ O_2)+62.503}{RT}}$
ELC	$k = \{\exp(0.3353\ x\ [(0.194\ x\ O_2) + 67.502] - 16.211\}\ x\ exp^{\frac{[(0.194\ x\ O_2)+67.502}{RT}}$
PIT	$k = \{\exp(0.379\ x\ [(0.2265\ x\ O_2) + 78.134] - 22.054\}\ x\ exp^{\frac{[(0.2265\ x\ O_2)+78.134}{RT}}$
PWWP	$k = \{\exp(0.234\ x\ [(0.533\ x\ O_2) + 91.398] - 7.8298\}\ x\ exp^{\frac{[(0.533\ x\ O_2)+91.398}{RT}}$
WWP	$k = \{\exp(0.2628\ x\ [(0.452\ x\ O_2) + 86.482] - 9.2218\}\ x\ exp^{\frac{[(0.452\ x\ O_2)+86.482}{RT}}$
TSP	$k = \{\exp(0.256\ x\ [(0.7395x\ O_2) + 114.24] - 10.744\}\ x\ exp^{\frac{[(0.7395\ x\ O_2)+114.24}{RT}}$

7 Char combustion in air and oxy-fuel environments and the associated kinetics

7.1 Introduction

The rate of devolatilsation can have a profound effect on the char yield and combustion rates, and both heating rate and temperature of devolatilisation are known to be important parameters. This section compares the chars produced in the TGA at ballistic heating rates (1000 K min^{-1}) in two different atmospheres (N_2 and CO_2) described in section 4.5.2. The chars produced are combusted non-isothermally in air and the full range of oxy-fuel environments and kinetics determined from the mass loss profiles. The chapter starts with the presentation of the TGA profiles and the identification of key temperatures and rates of mass loss seen during char combustion. The apparent rate constants and kinetic parameters for all of the chars in all combustion atmospheres are determined using an m^{th} order kinetic model. An n^{th} order kinetic model is then developed for the chars produced in CO_2 and combusted in oxy-fuel environments which accounts for the change reactivity through the introduction of a partial pressure of oxygen term. Finally the intrinsic reactivity of the coal chars is determined with knowledge of the surface areas determined in section 5.6. The comparison of the char production method (TGA vs DTR) is discussed in Chapter 8.

7.2 Char combustion behaviour

The chars produced using the TGA at ballistic heating rates in N_2 and CO_2 were combusted in air (N_2 char) and the full range of oxy-fuel environments (CO_2 char) non-isothermally in order to investigate the effect of the environment on char combustion behaviour. The fundamental characterisation of the chars including proximate, elemental analysis and char yields can be found in Chapter 5. Briefly, the ballistic coal chars produced in N_2 and CO_2 were shown to have similar properties in terms of yields, proximate and ultimate analysis (Table 5.5 - Table 5.7). The only measured significant difference was seen in the surface areas with the chars produced in CO_2 being 2.5-7.7 times higher than those produced in N_2 (Table 5.14). The biomass chars however show enhanced devolatilisation when the chars are produced in CO_2 atmospheres due to the consumption of fixed carbon via the char gasification reaction.

7.2.1 Non-isothermal combustion behaviour of coal chars produced using the TGA

The coal char combustion TGA and DTG profiles can be seen in Figure 7.1 - Figure 7.6 and key temperatures and rates of mass loss in Table 7.1. The coal chars were combusted non-isothermally with a heating rate of 10°C min^{-1} to 900°C. In order to evaluate the combustion profiles, the peak temperatures and the maximum rates of mass loss were analysed. The temperatures at which the initial rate of mass loss reached 0.016 wt% s^{-1} (1 wt% min^{-1}) (T_{IM}), the temperature at which the maximum rate mass loss occurred (T_C), the maximum rate of mass loss (dm/dt_C) and the burnout temperature (T_B) are evaluated for the char samples. Please note that in the following plots the data labels 5-30% refer to chars produced in CO_2 and combusted in oxy-fuel environments and air refers to chars produced in N_2 and combusted in air.

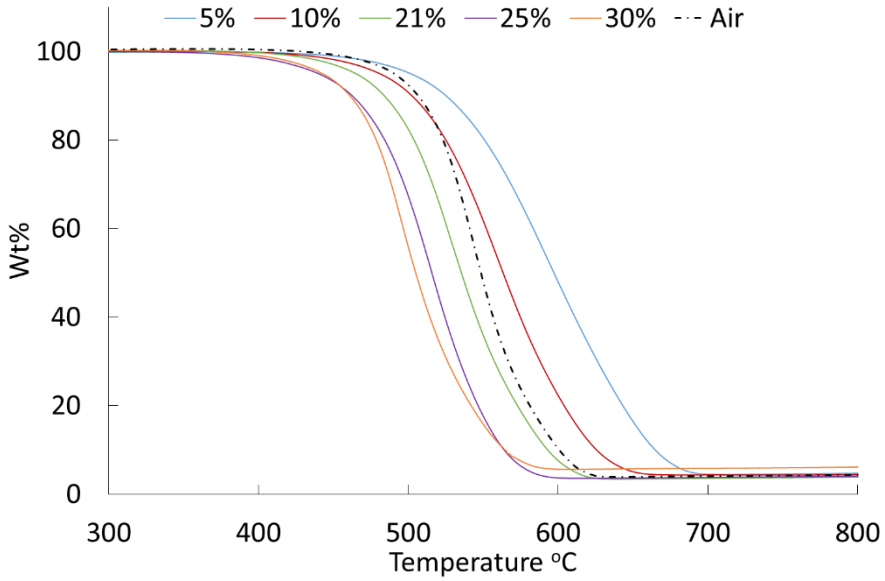

Figure 7.1: TGA non isothermal combustion in air and oxy-fuel of PEL ballistic chars produced in N_2 and CO_2

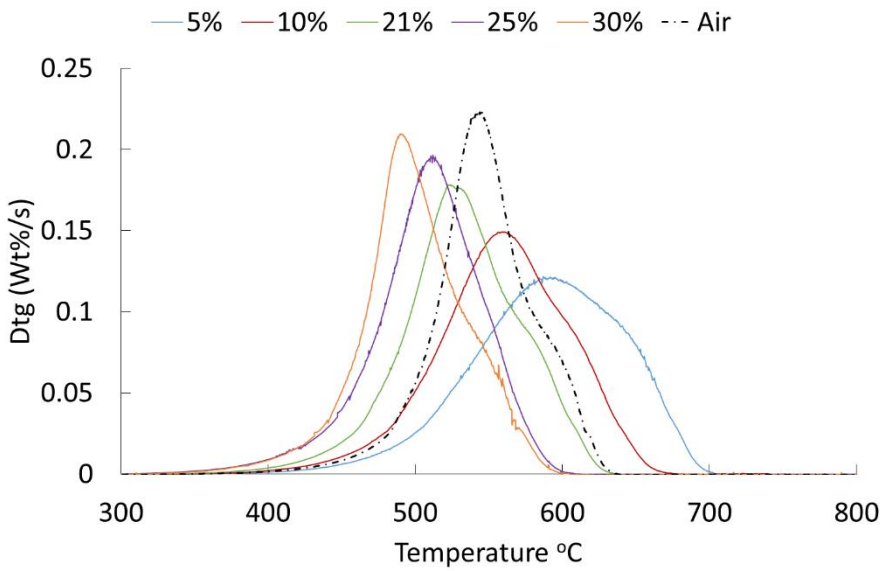

Figure 7.2: DTG non isothermal combustion in air and oxy-fuel of PEL ballistic chars produced in N_2 and CO_2

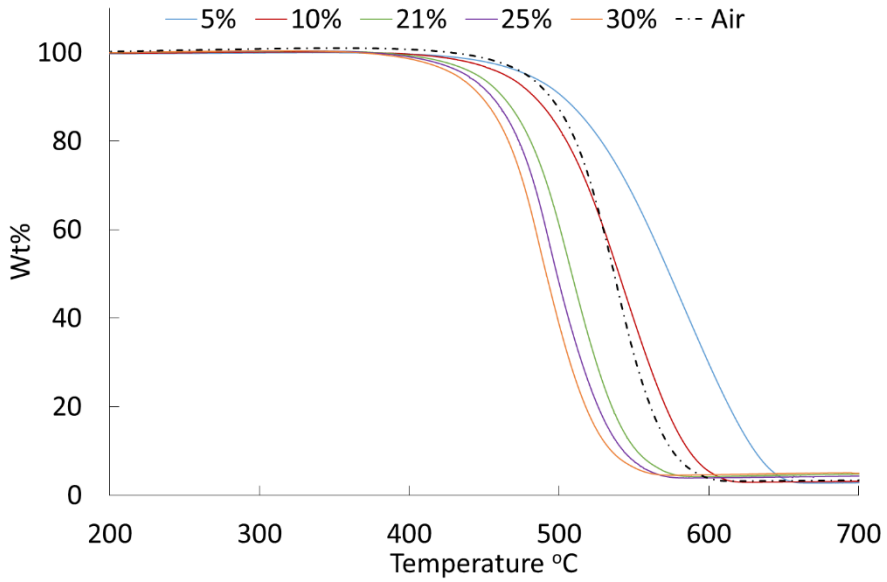

Figure 7.3: TGA non isothermal combustion in air and oxy-fuel of ELC ballistic chars produced in N_2 and CO_2

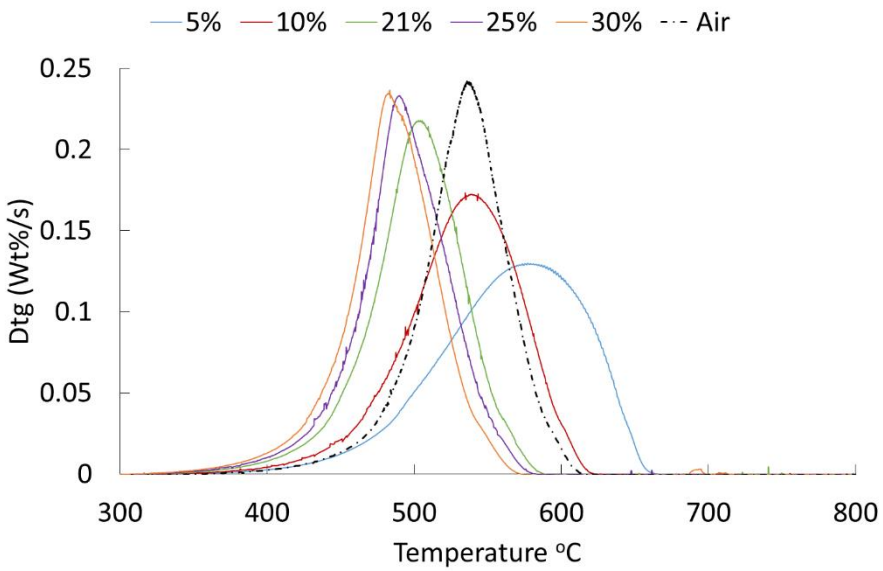

Figure 7.4: DTG non isothermal combustion in air and oxy-fuel of ELC ballistic chars produced in N_2 and CO_2

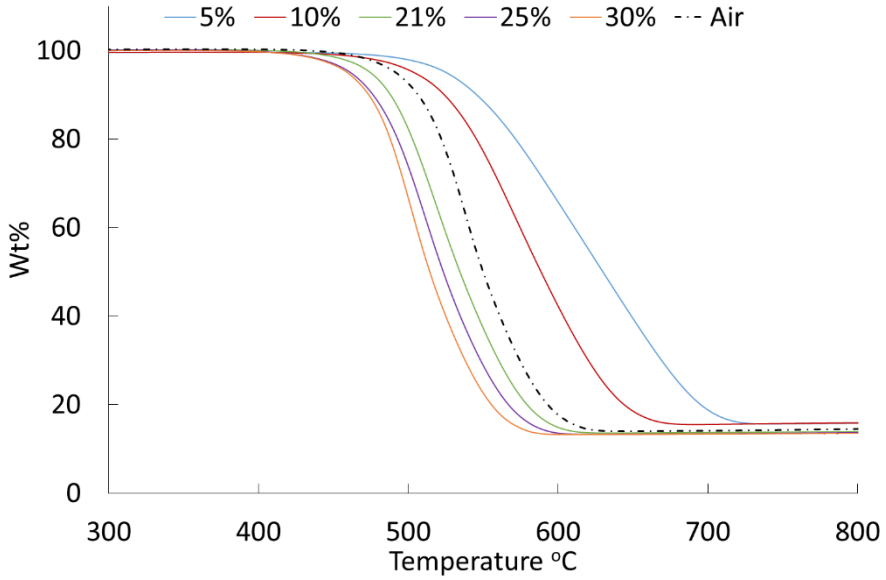

Figure 7.5: TGA non isothermal combustion in air and oxy-fuel of PIT ballistic chars produced in N_2 and CO_2

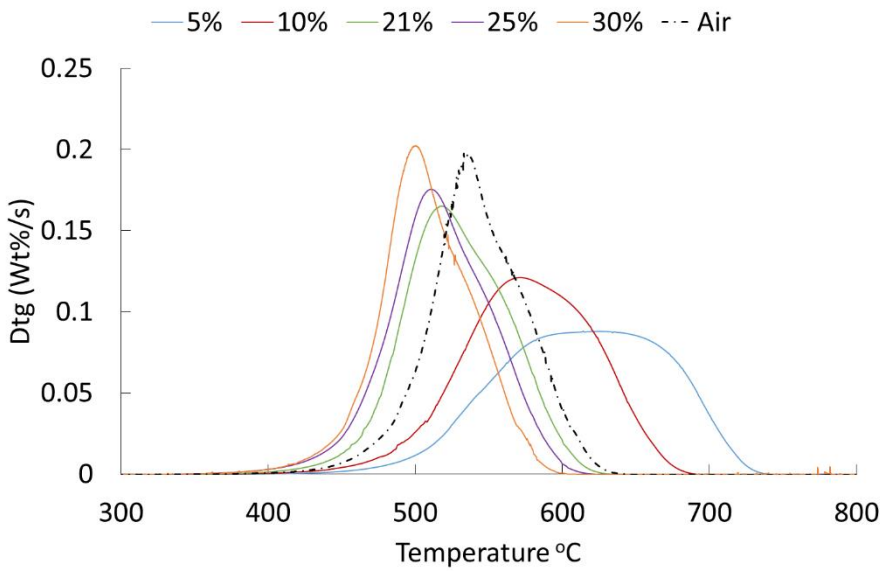

Figure 7.6: DTG non isothermal combustion in air and oxy-fuel of PIT ballistic chars produced in N_2 and CO_2

Table 7.1: Characteristic temperatures and rates of mass loss observed during non-isothermal combustion of coal chars in air and oxy-fuel environments produced in N_2 and CO_2 at ballistic heating rates

			T_{IM} (°C)	T_C (°C)	dm/dt_C (Wt% s^{-1})	T_B (°C)
		5%	483	594	0.127	684
		10%	463	560	0.149	648
PEL	**CO_2**	21%	443	526	0.182	615
		25%	419	514	0.204	583
		30%	419	495	0.212	579
	N_2	Air	470	544	0.223	621
		5%	459	584	0.133	650
		10%	441	541	0.187	608
ELC	**CO_2**	21%	421	506	0.221	571
		25%	414	490	0.239	564
		30%	407	481	0.241	554
	N_2	Air	455	537	0.243	600
		5%	509	623	0.111	714
		10%	487	572	0.123	664
PIT	**CO_2**	21%	455	518	0.165	603
		25%	442	510	0.175	592
		30%	438	502	0.203	579
	N_2	Air	468	533	0.202	615

As shown in Table 7.1, at any given oxygen concentration the initial mass loss temperature (T_{IM}), the temperature at which the maximum rate of mass loss is seen (T_C) and the burnout temperature (T_B) are lowest in the ELC char followed by the PEL char and finally the PIT char. However the maximum rate of mass loss (dm/dt_C) is lowest in the PIT char followed by the PEL then ELC chars. This suggests that the ELC char is the most reactive which is determined in section 7.3.

The differences in the combustion behaviour of the N_2 chars combusted in air and the CO_2 chars combusted in 21% O_2/CO_2 are more pronounced here than was seen in the overall combustion of the raw fuels (section 6.2). The maximum rates of mass loss (dm/dt_C) is reduced by 10% in the ELC char and 19% in the PEL and PIT CO_2 chars when combusted in 21% O_2/CO_2 relative to air. However the temperature at which this is seen (T_C) is decreased in the CO_2 chars, 15°C in the PIT, 31°C in the ELC and 18°C in the PEL CO_2 chars. The burnout temperatures are also significantly reduced in the CO_2 atmosphere. In the three coals the key temperatures identified during combustion of the N_2 char in air fall between the 10-21% oxy-fuel case and peak rates of mass loss are comparable to those seen in the CO_2 char combusted in 30% O_2/CO_2.

In order to determine the reason for the differences in the combustion behaviour of the N_2 and CO_2 chars, the PEL CO_2 char was combusted in air (Figure 7.7 and Figure 7.8). This method allows for the removal of the difference in char characteristics (as a result of production atmosphere) and any differences in the combustion profiles can be directly attributed to the combustion atmosphere. It can be seen in when PEL CO_2 is combusted in air, the mass loss profile is almost identical to when it is combusted in 21% O_2/CO_2 which indicates at these temperatures the char – CO_2 gasification does not take place.

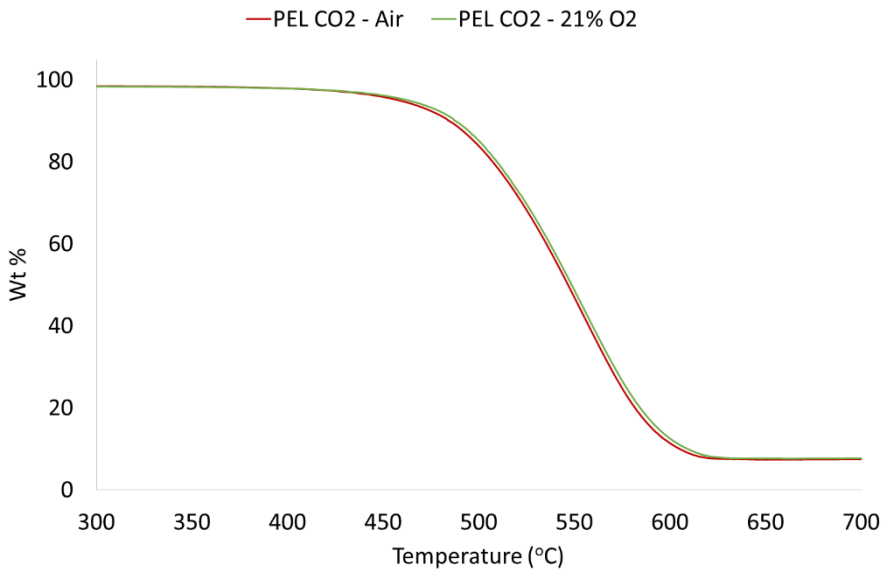

Figure 7.7: TGA profiles of PEL CO_2 char combusted using the TGA in 21% O_2/CO_2 and in air

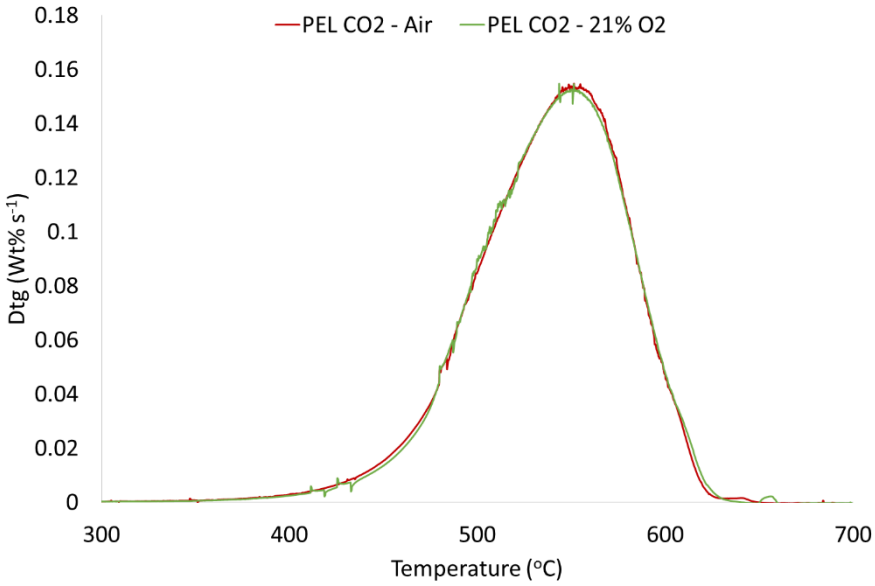

Figure 7.8: DTG profiles of PEL CO_2 char combusted using the TGA in 21% O_2/CO_2 and in air

In order to determine the temperatures at which the char – CO_2 gasification reaction occurs the PEL CO_2 char was gasified in a CO_2 atmosphere at (10°C min^{-1}) to 1000°C (Figure 7.9). The temperature at which the PEL CO_2 char starts to gasify begins at ~680°C and the peak rate of mass loss is seen at 1000°C.

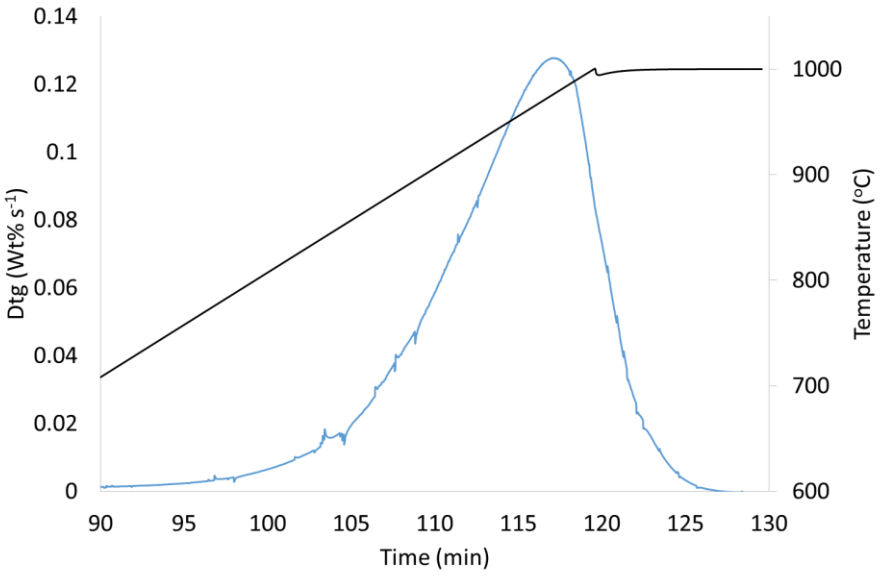

Figure 7.9: PEL CO_2 char gasification in CO_2 DTG plot ($10^oC\ min^{-1}$)

The effect of the increase in oxygen in the oxy-fuel atmospheres is clearly seen in all of the coal chars with peak temperatures decreasing and maximum rates of mass loss increasing. The increase in the key parameters identified are more severe than is seen in the overall combustion profiles (section 6.2.1) in relation to both the devolatilisation and char combustion stages. The effect of the increase in O_2 varies between chars: PEL displays a decrease in T_C of 99°C and an increase in dm/dt_C of 40% when O_2 is increased from 5-30%, ELC shows a similar shift in T_C with a decrease of 103°C but a higher increase in dm/dt_C of 45%; The increase in O_2 levels from 5-30% in the char combustion atmosphere has the largest effect on the PIT char with a decrease in T_C of 121°C and increase in dm/dt of 45%.

7.2.1.1 Discussion

The results of the gasification of the PEL CO_2 char indicate that the temperatures at which the mass loss is seen in Figure 7.1 - Figure 7.6 are too low for the char – CO_2 gasification reaction to occur and that the mass loss is the result of reaction with oxygen. Although in a boiler the flame temperatures are high enough for this reaction to occur, the reaction between the char and oxygen is still the dominant reaction.

Work by Roberts et al (258) investigated the gasification reaction rates of chars produced from Australian coals in O_2, CO_2 and steam. The gasification reactions were performed under Regime I conditions (low temperature combustion) with the gasification performed in CO_2 at 900°C and O_2 at 500°C. The intrinsic reaction rates determined were extrapolated to higher temperatures (Regime III) using the effectiveness factor (η), based on measurements

of pore diameters and surface areas. They found that the O_2 reaction is dominant at both the lower and high temperature regions (coal flame temperature ~1600 ^oC), as can be seen in Figure 7.10.

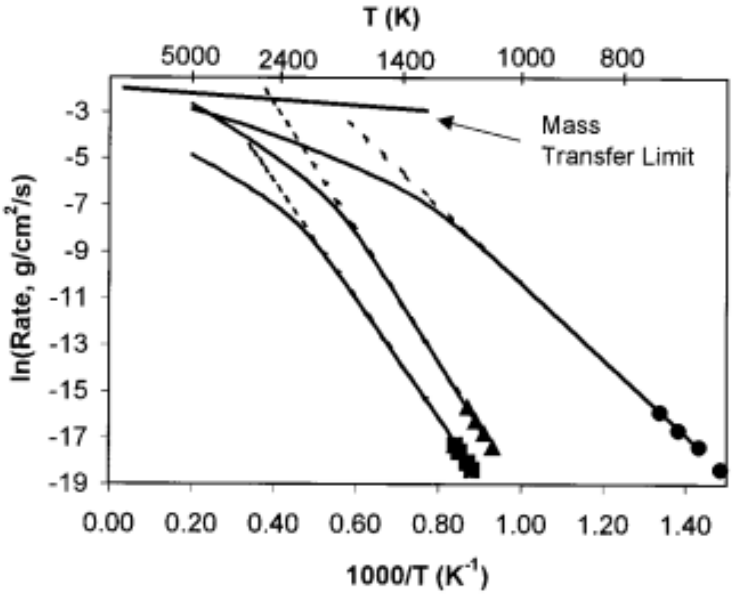

Figure 7.10: High temperature reactivity of coal char gasified in O_2 and CO_2 (symbols- low temperature reactivity determined from experimental data, solid lines higher temperature reactivity)(circles – O_2, triangles – CO_2, squares – steam)

There has also been several studies to investigate coal oxy-fuel combustion at higher temperatures using drop tube reactors and entrained flow reactors (150, 158, 218, 221, 259, 260) and the differences in combustion behaviour between air and oxy-fuel environments have been determined by the derivation of kinetic parameters by measuring the ratio of CO/CO_2 released during the experiment. The DTR and EFR are utilised to try and closer replicate the high heating rates seen in a pf boiler and result in char combustion taking place under diffusional control (Regime II and III) (60). Under these conditions, the reaction rate is controlled by mass and heat transfer which would reflect the hydrodynamics of the laboratory equipment used instead of the true reaction rate (261). In addition there is some uncertainty in true yields of CO and CO_2 from char combustion. The CO released during char combustion (R 3.1 – 3.3) may react with oxygen present in the gas layer surrounding the particle making the determination of the CO/CO_2 ratio difficult (127). Several research groups have utilised low temperature TGA experiments in order to investigate raw fuel and char oxy-fuel combustion behaviour (144, 212, 218, 220, 222, 245, 262-265).

Although in the work in this thesis, the combustion of the chars occurs at temperatures too low for the char – CO_2 gasification reaction to take place, the elevated temperatures experienced during char production (1000^oC) allow for the influence of the CO_2 during devolatilisation. This step is known to have a profound effect on char combustion rates.

The differences in the combustion behaviour in the N_2 chars and CO_2 chars combusted in the same oxygen levels, as seen in Figure 7.1 - Figure 7.6 are therefore not the result of the char – CO_2 gasification reaction. Instead it is thought that the char production atmosphere and the resulting change in char properties, particularly surface area, are the reason for the differences in combustion behaviour seen. The CO_2 chars from all coals were found to have an increased surface area (Table 5.14) and therefore an increase in the number of active sites relative to the N_2 chars. It is well known that active sites play a key role in the combustion of chars (section 3.5.3) and the increase in active sites in the CO_2 chars results in more sites for both the O_2 and CO_2 present in the combustion atmosphere to attack. It is thought that the increase in availability of the active sites increases the reactivity through attack by oxygen therefore reduces the temperatures at which the maximum rates of mass loss (T_C) are seen. In addition the CO_2 may, compete with the oxygen for the active sites or crosslink into the char structure resulting in the decrease in dm/dt_C relative to the N_2 char combusted in air. The intrinsic reactivity can be determined to provide greater understanding of the reactivity of the active sites and is discussed in section 7.3.3.

The effect of the increase in oxygen in the oxy-fuel environments was found to be more pronounced in the dedicated char combustion stage than was seen in the overall combustion of the fuels (section 6.2.1). In that case the chars remaining at the end of the combustion process are the result of low heating rate combustion experiments in oxygen containing atmospheres (10$^oC\ min^{-1}$) rather than high heating rate non oxygen containing atmospheres. At the slow heating rates both homogeneous and heterogeneous combustion can take place at the same time resulting in a small char yield. In comparison, the ballistic heating rate chars produce a larger char yields containing higher levels of unburnt carbon. It is also expected that the ballistic chars would have a larger surface area due to the increased devolatilisation rates. The chars produced at ballistic heating rates undergo physical and chemical changes more comparable to what would be expected in a pulverised fuel burner, that is fast devolatilisation rates in a pyrolysis atmosphere (121). The increased sensitivity of the chars relative to the devolatilisation stage of combustion is due to the increased carbon contents, surface areas and the nature of heterogeneous O_2 – carbon reaction.

7.2.2 Non isothermal combustion behaviour of biomass chars produced using the TGA

The biomass char combustion TGA and DTG profiles can be seen Figure 7.11 - Figure 7.16 and key temperatures and rates of mass loss in Table 7.2. The PWWP and WWP chars were combusted at a heating rate of 5°C min^{-1} as the higher heating rate did not produce well defined mass loss profiles making the extraction of the kinetic data unreliable. Please note that in the following plots the data labels 5-30% refer to chars produced in CO_2 and combusted in oxy-fuel environments and air refers to chars produced in N_2 and combusted in air.

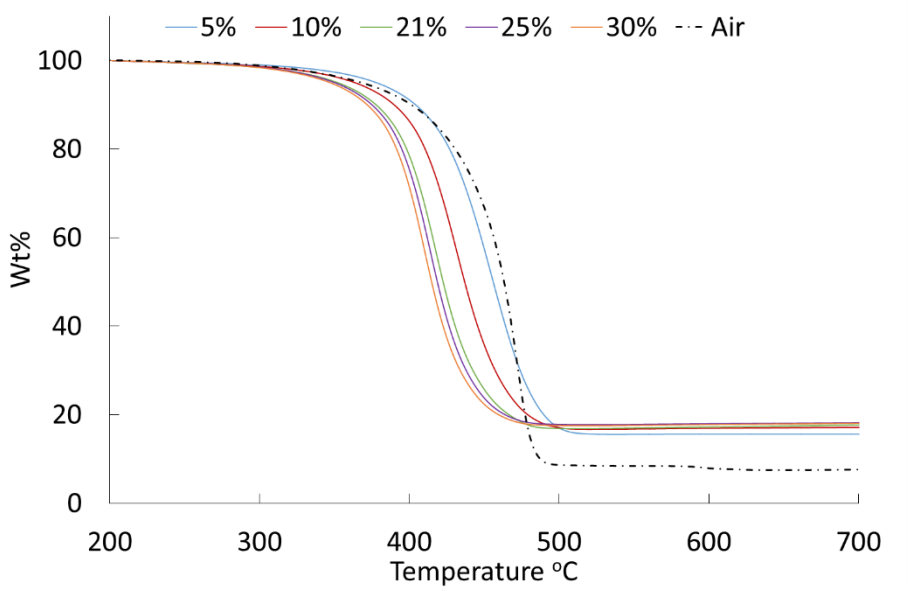

Figure 7.11: TGA non isothermal combustion in air and oxy-fuel of PWWP ballistic chars produced in N_2 and CO_2 (5°C min^{-1})

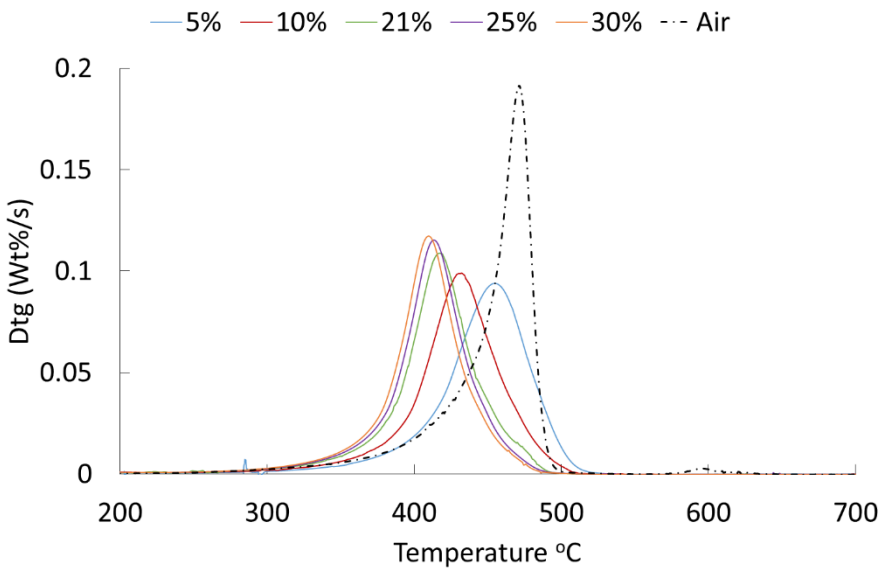

Figure 7.12: DTG non isothermal combustion in air and oxy-fuel of PWWP ballistic chars produced in N_2 and CO_2 (5°C min^{-1})

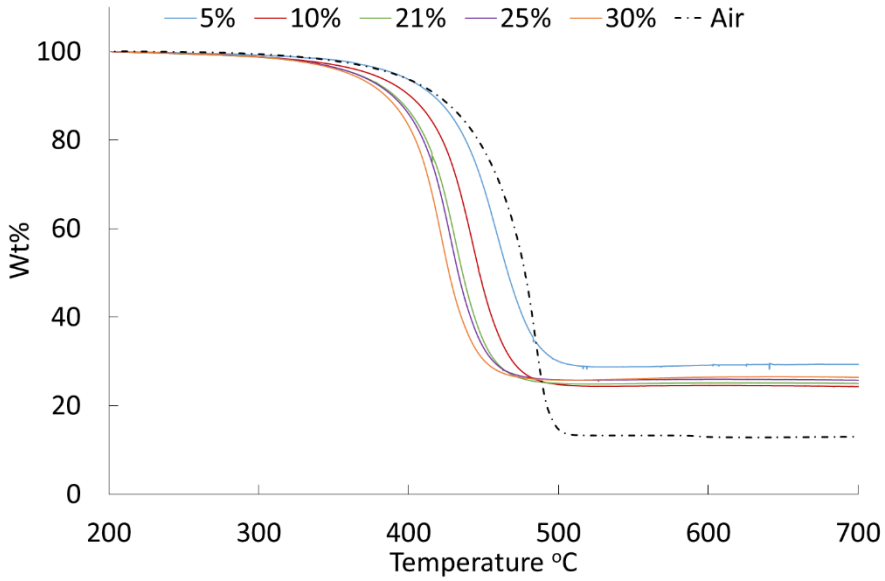

Figure 7.13: TGA non isothermal combustion in air and oxy-fuel of WWP ballistic chars produced in N_2 and CO_2 (5°C min^{-1})

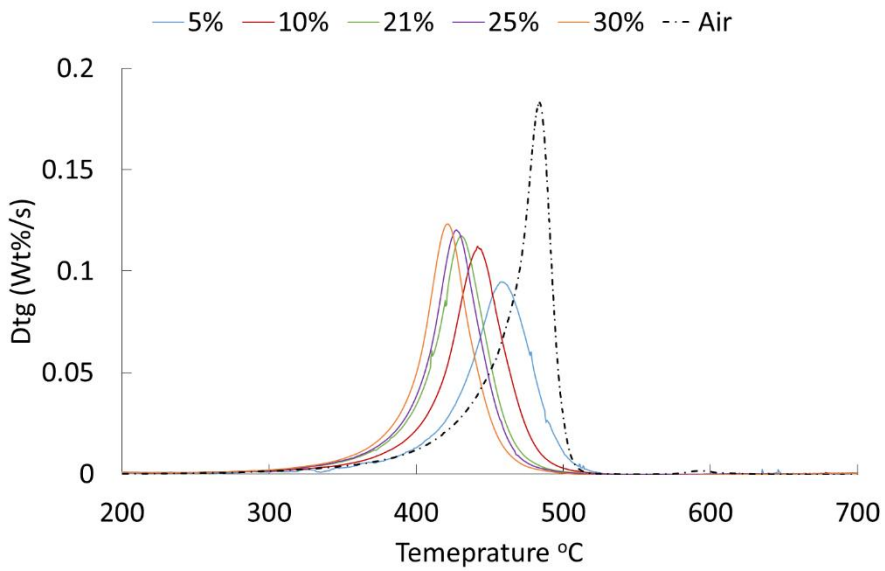

Figure 7.14: DTG non isothermal combustion in air and oxy-fuel of WWP ballistic chars produced in N_2 and CO_2 (5°C min^{-1})

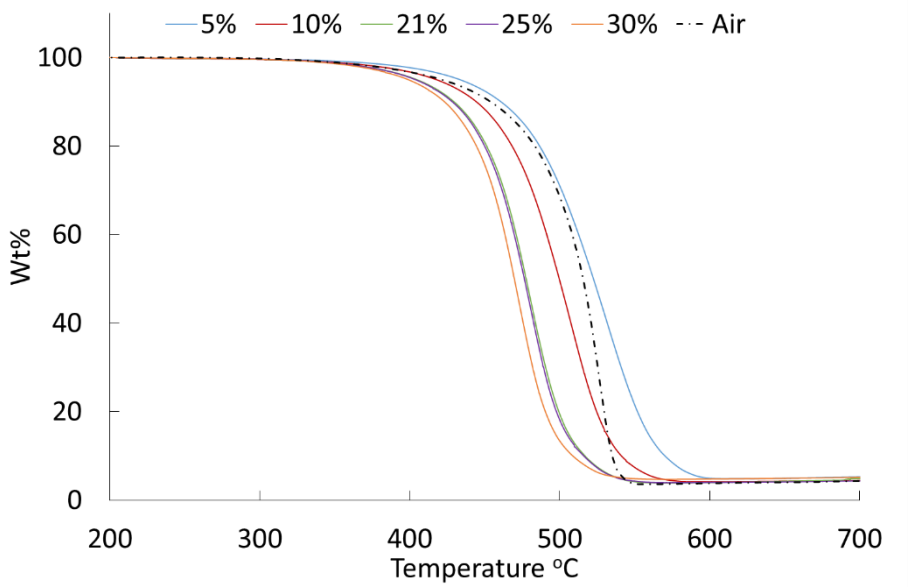

Figure 7.15: TGA non isothermal combustion in air and oxy-fuel of TSP ballistic chars produced in N_2 and CO_2 (10°C min^{-1})

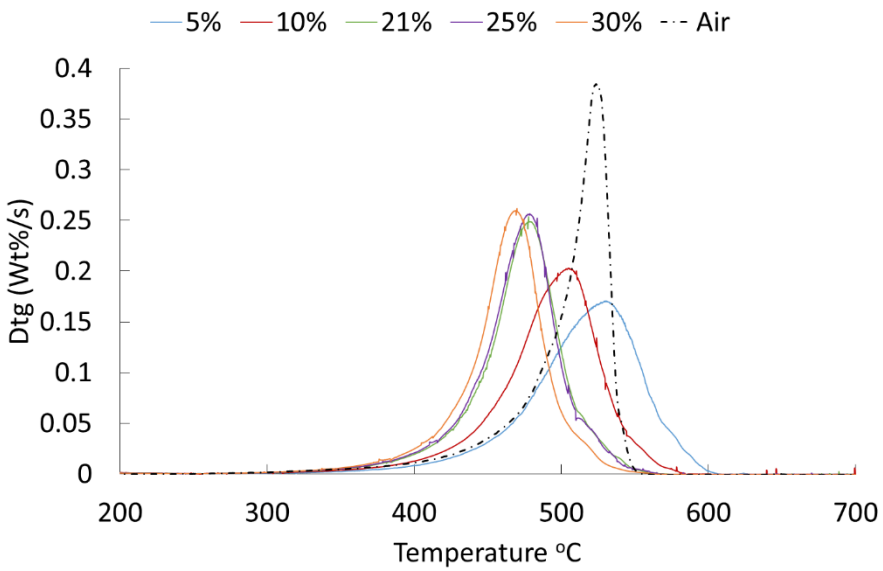

Figure 7.16: DTG non isothermal combustion in air and oxy-fuel of TSP ballistic chars produced in N_2 and CO_2 ($10^oC\ min^{-1}$)

Table 7.2: Characteristic temperatures and rates of mass loss observed during non-isothermal combustion of biomass chars in air and oxy-fuel environments produced in N_2 and CO_2 at ballistic heating rates

			T_{IM} (°C)	T_C (°C)	dm/dt_C (Wt% s^{-1})	T_B (°C)
PWWP	**CO_2**	5%	399	455	0.087	497
		10%	380	432	0.091	482
		21%	373	417	0.098	465
		25%	369	413	0.105	458
		30%	366	410	0.107	454
	N_2	Air	397	467	0.192	489
WWP	**CO_2**	5%	405	458	0.095	496
		10%	392	442	0.112	479
		21%	381	431	0.117	466
		25%	378	427	0.120	463
		30%	373	422	0.123	457
	N_2	Air	411	484	0.183	502
TSP	**CO_2**	5%	425	533	0.168	589
		10%	408	510	0.199	561
		21%	393	483	0.243	539
		25%	391	482	0.244	537
		30%	386	471	0.259	525
	N_2	Air	418	526	0.383	546

Biomass chars are much more reactive than coal chars as can be seen from the key indicators seen in Table 7.2 in comparison to Table 7.1. The PWWP chars have the lowest T_{IM} and T_C temperatures of the three biomass chars followed by the WWP and then the TSP chars. The T_B temperature is similar between the PWWP and WWP chars but significantly higher in the TSP char. The PWWP char also has the lowest maximum rate of mass loss, followed by the WWP then the TSP char.

The difference in the combustion behaviour of the N_2 and CO_2 chars is more severe in the biomass and TSP chars than is seen in the coal chars. The T_C is reduced again reduced in the CO_2 chars but not to the same extent as seen in the coals (ΔT_C 100-121°C). The T_C is again reduced in the CO_2 chars relative to the N_2 chars with the PWWP and WWP chars reduced by ~50°C and 43°C in the TSP char. The peak maximum rate of mass loss (dm/dt_C) are also significantly reduced in the CO_2 chars, a 48% reduction in the PWWP and 36% reduction in the WWP and TSP chars relative to the N_2 char combusted in air.

Again by combusting the PWWP CO_2 char in air and comparing it to the PWWP CO_2 char combusted in 21% O_2/CO_2 the direct effects of the combustion atmosphere can be determined (Figure 7.17 and Figure 7.18). In contrast to the PEL char, when the PWWP CO_2 char is combusted in air, the mass loss profile shifts to a lower temperature and the maximum rate of mass loss is increased relative to combustion in 21% O_2/CO_2 indicating that the CO_2 present in the oxy-fuel atmosphere is inhibiting combustion.

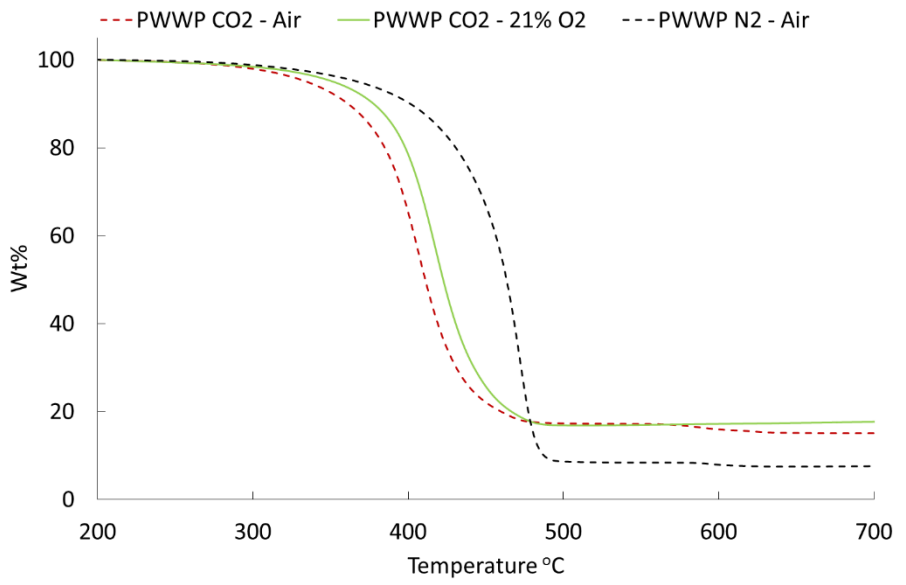

Figure 7.17: TGA profiles of PWWP char produced in CO_2 atmosphere using the TGA combusted in 21% O_2/CO_2 and in air and PEL char produced in N_2 combusted in air

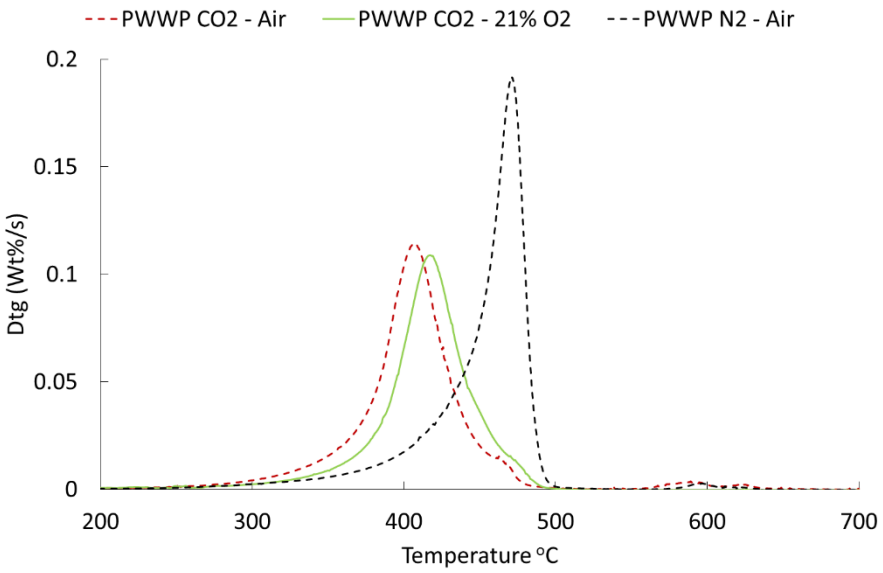

Figure 7.18: DTG profiles of PWWP char produced in CO_2 atmosphere using the TGA combusted in 21% O_2/CO_2 and in air and PEL char produced in N_2 combusted in air

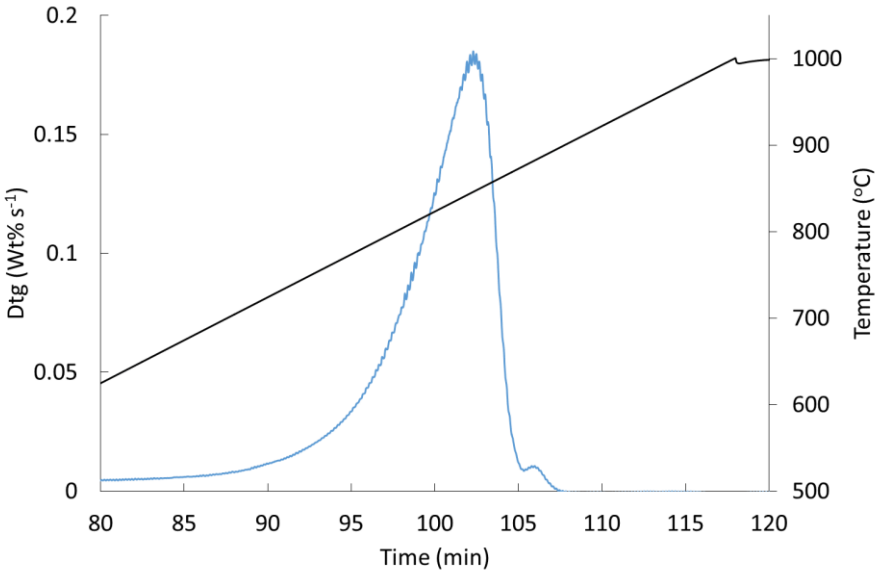

Figure 7.19: PWWP CO_2 char gasification in CO_2 DTG plot ($10^oC\ min^{-1}$)

The PWWP CO_2 char was gasified in CO_2 to determine the temperatures at which the char – CO_2 reaction occurs (Figure 7.19). It can be clearly seen that the char gasification reaction does not take place until temperatures ~700°C. There is evidence of a slight mass loss at lower temperatures but this is the result of the remaining volatiles being released due to pyrolysis rather than true gasification. As in the coals, the char – CO_2 reaction does not affect the overall combustion rates of the biomass chars used in this work.

The effects of the increase in oxygen concentration are not as significant in the biomass and TSP chars as seen in the coals, and the observed decrease in dm/dt_C are 19% in the PWWP, 23% in the WWP and 35% in the TSP chars when the oxygen level is decreased from 30-5 %. The key temperature difference is also lower with T_{IM} decreasing by ~ 33°C in the PWWP and WWP chars and 39°C the TSP char. The T_C is reduced by 45°C in the PWWP, 36°C in the WWP and 62°C in the TSP sample. The T_B is reduced by ~41°C in the PWWP and WWP and 64°C in the TSP char. The TSP sample falls between the biomass and coals samples in terms of change to T_{IM}, T_C, T_B and dm/dt_c.

7.2.2.1 Discussion

There is a clear difference between the biomass chars produced in N_2 and combusted in air compared to those chars produced in CO_2 and combusted in oxy-fuel environments. In the biomass and TSP samples the char yields are significantly higher when chars are produced in N_2 atmospheres, with PWWP and WWP char yields in CO_2 half and TSP three quarters of those seen in N_2 (Table 5.14). The composition of the chars also differ in terms of proximate and ultimate analysis. The relative volatile and fixed carbon contents are determined in section 5.3.2, and show that the volatile content is similar regardless of the char production atmosphere and the decrease in char yield is the result of the significant reduction of fixed carbon in CO_2 chars. The ash contents of the chars produced in CO_2 are significantly higher than the N_2 chars and the inorganic content is known to play a role in the rates of char combustion (119, 122). The change in char morphology due to char production atmosphere is unknown as the surface areas was not measured. The result of the above differences in char characteristics is that the CO_2 chars are more reactive than the N_2 chars as can be seen from Figure 6.8 - Figure 6.13.

However the differences in mass loss behaviour are not only attributed to the char characteristics as in the coals. Figure 7.17 and Figure 7.18 indicate that when the same char (PWWP CO_2) is combusted in air and oxy-fuel atmospheres at the same oxygen levels a delay is seen in the oxy-fuel case. This is thought to be the result of CO_2 chemisorption onto the

char surface reducing the number of active sites for O_2 in the combustion atmosphere to attack, thereby reducing the overall burning rate (122, 154).

Work by several authors (266, 267) investigated the CO_2 chemisorption behaviour of coal chars and found that two types of chemisorption of CO_2 exist at low temperatures. The first, strong chemisorption, is the chemisorption of CO_2 onto the metals present on the char surface, and secondly, weak chemisorption, which is associated with the organic structure of the char (266). The chemisorption experiment involved producing a coal char in a nitrogen atmosphere, then heating in argon to temperatures of 800-850^{o}C to remove any oxygen that may have been adsorbed during the char preparation stage. The temperature was then lowered to 300^{o}C and atmosphere switched to CO_2 and held for 30 minutes. The atmosphere was then switched to argon and temperature raised to 850^{o}C to remove any weakly chemisorbed CO_2. The mass of the char was monitored throughout and the amount of weakly and strongly chemisorbed CO_2 determined (266, 267). Molina et al (266) found that the majority of the chemisorbed CO_2 on a coal char was weakly bonded and that by dosing the coal with potassium the trend is reversed and that strongly chemisorbed CO_2 is prominent. In addition the coal was also doped with iron and it was found that this favoured weakly chemisorbed CO_2.

It is known that biomass contain larger amounts of potassium and significantly less iron than coals. Mason et al (183) found that, for similar types of biomass used in this work, the majority of potassium is retained in the chars after devolatilisation. The increase in potassium content of biomass fuels compared to coals and the expected increase in potassium content of the biomass chars, due to higher ash content in their chars relative to the coals (Table 5.5) may enhance the amount of strongly chemisorbed CO_2.

It is suggested that the increase in combustion rate in the CO_2 produced chars relative to the N_2 chars, particularly in the case of the PWWP and WWP fuels would be greater if not for the chemisorption of CO_2 which slightly delays combustion.

The effect of the increase in oxygen in the oxy-fuel environments is less severe in the biomass chars than the coals. This is the result of the increased reactivity of biomass and the higher oxygen contents of the chars (after devolatilisation (Table 5.6)) readily available for reaction with active sites.

7.3 Char combustion kinetics

The non-isothermal mass loss profiles seen in the previous section were used to determine the char apparent reactivities using an m^{th} order kinetic model as described in section 4.7.2.1. The kinetic parameters determined were then used to develop an n^{th} order reaction model that relates the change in reactivity to the partial pressure of oxygen present in the oxy-fuel combustion atmospheres (section 4.7.2.2). Finally the n^{th} order kinetic models were used to determine the intrinsic reactivity of the coal chars (section 4.7.2.3) using the surface areas reported in Table 5.14. The intrinsic reactivity of the biomass and TSP chars could not be determined due to the lack of surface area measurements.

7.3.1 Char apparent reactivity (m^{th} order)

7.3.1.1 Coal char apparent reactivity

The coal char apparent rate constants determined from the non-isothermal coal char combustion experiments are shown in Figure 7.20 to Figure 7.22. The apparent kinetic parameters extracted and the reaction order with respect to carbon conversion (^{m}) can be seen in Table 7.3. The trends in the kinetic parameters, as a function of oxygen concentration, can be seen in Figure 7.23 and Figure 7.24. Please note that in the following plots the data labels 5-30% refer to chars produced in CO_2 and combusted in oxy-fuel environments and air refers to chars produced in N_2 and combusted in air.

The lines in Figure 7.20 - Figure 7.22 are different lengths since the comparison of reactivity is based on a conversion range (0.05-0.85) rather than a temperature range to allow for the comparison of multiple fuels.

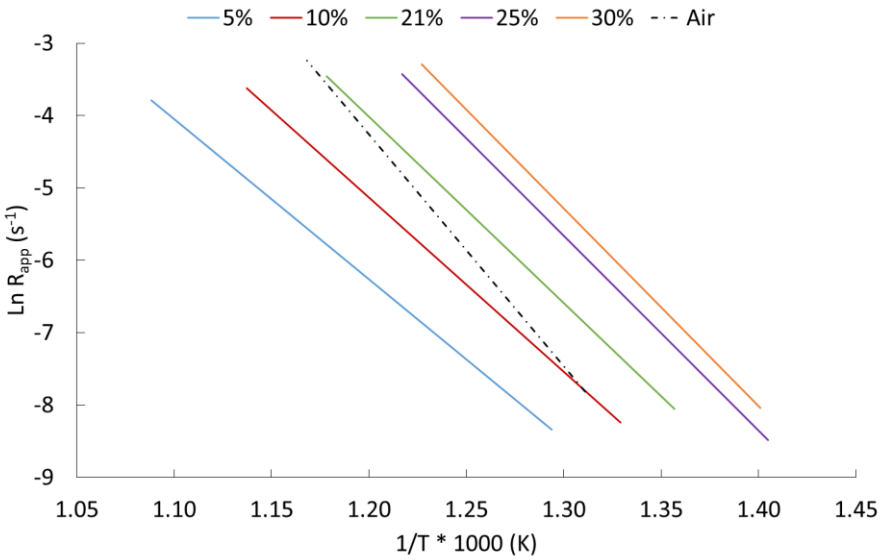

Figure 7.20: Apparent reactivity of the PEL chars combusted in air and oxy-fuel environments

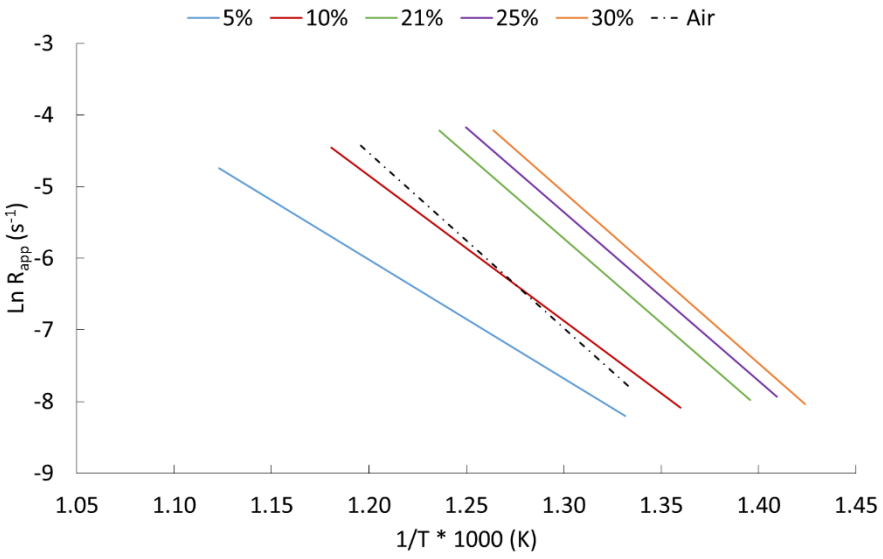

Figure 7.21: Apparent reactivity of the ELC chars combusted in air and oxy-fuel environments

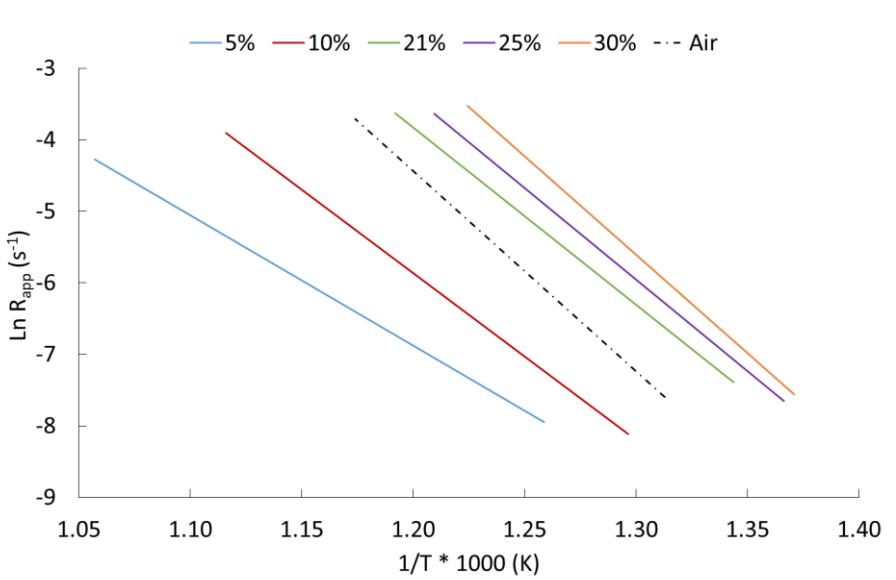

Figure 7.22: Apparent reactivity of the PIT chars combusted in air and oxy-fuel environments

Table 7.3: Apparent kinetic parameters and reaction order with respect to coal char conversion determined by combustion of coal chars (Conversion range 0.05-0.85)

Char	Atmosphere	Ln A_{app} (s^{-1})	Ea_{app} (kJ mol^{-1})	m	R^2	Temperature region (°C)
	5%	20.3	184.0	1.9	0.999	500-646
	10%	23.8	200.1		0.999	479-606
PEL CO_2	21%	26.9	214.0		0.996	464-576
	25%	29.3	223.8		0.990	440-549
	30%	30.2	227.0		0.988	441-542
PEL N_2	Air	34.2	266.5	1.9	0.996	490-583
	5%	13.9	137.9	1.2	0.997	478-617
ELC CO_2	10%	19.5	168.4		0.997	462-574
	21%	24.9	196.0		0.998	443-536
	25%	25.3	195.8		0.981	436-527
	30%	26.0	198.6		0.994	429-518
ELC N_2	Air	24.8	203.1	1	0.991	477-563
	5%	15.0	151.5	1.7	0.983	521-673
PIT CO_2	10%	22.1	194.0		0.993	498-623
	21%	25.9	206.0		0.993	471-566
	25%	27.3	212.9		0.996	459-554
	30%	30.2	228.9		0.993	456-544
PIT N_2	Air	29.1	232.5	1.6	0.991	489-579

NOTE: The R^2 value is a measure of the linearity of the Ln R_{app} vs 1/T over the conversion range of 0.05 – 0.85

The apparent kinetic parameters seen in Table 7.3 were used to predict the conversion of the coal chars and compared to the actual conversion determined experimentally. The predicted and experimental conversion plots and the deviation between the two (Eq 4.36 and 4.37) can be seen in the appendix section 12.3 (Figure 12.2 - Figure 12.4). The predicted conversion is in good agreement with the experimental conversion. In addition the position of the reaction rate constant lines in Figure 7.20 - Figure 7.22 are in good agreement with what would be expected from the mass loss profiles seen in section 7.2.1.

The difference in the reactivity of the CO_2 char combusted in 21% O_2/CO_2 and the N_2 chars combusted in air are again highlighted in Figure 7.20 - Figure 7.22. As mentioned earlier, this is due to the difference in char properties as a result of the pyrolysis atmosphere rather than the change in the combustion atmosphere (Figure 7.9). As a result of the differences in the apparent reactivity, the kinetic parameters differ in the two atmospheres, with Ea_{app} and LnA_{app} both larger in the N_2 produced chars.

The values of the reaction orders (m) with respect to char conversion are similar in each of the chars despite the change in atmosphere, and all fall into the expected range (0.4-2) suggested by Di Blasi et al. (127). The large value of m for the PEL and PIT chars are the result of the change in reactivity of the chars at conversion levels of ~0.75 which can be clearly seen by the slight change in slope of the mass loss curves (Figure 7.1) (25 Wt%), particularly at higher oxygen concentrations in the PEL sample.

The increase in oxygen concentration in the oxy-fuel combustion atmospheres has a greater effect on the kinetic parameters associated with the char combustion stage than is seen during the devolatilisation stage. The Ea_{app} determined for the chars increase by 43 kJ mol^{-1} in the PEL char, 61 kJ mol^{-1} in the ELC char and 77 kJ mol^{-1} in the PIT sample (during the devolatilisation stage the Ea values only increased by ~7 kJ mol^{-1}). The pre-exponential factors also increase more than is seen in the devolatilisation stage with an increase of 10-15 s^{-1} in the chars and only 2-3 s^{-1} during devolatilisation.

The change in Ea_{app} with the change in oxygen concentration is not linear in the chars as is seen in the devolatilisation step (Figure 7.23). Oxygen has a larger effect on Ea_{app} at low concentrations. At oxygen concentrations of >21% the effect of oxygen on the Ea_{app} is reduced. However, as seen in the devolatilisation step there is evidence of the kinetic compensation effect (KCE) which can be seen in Figure 7.24.

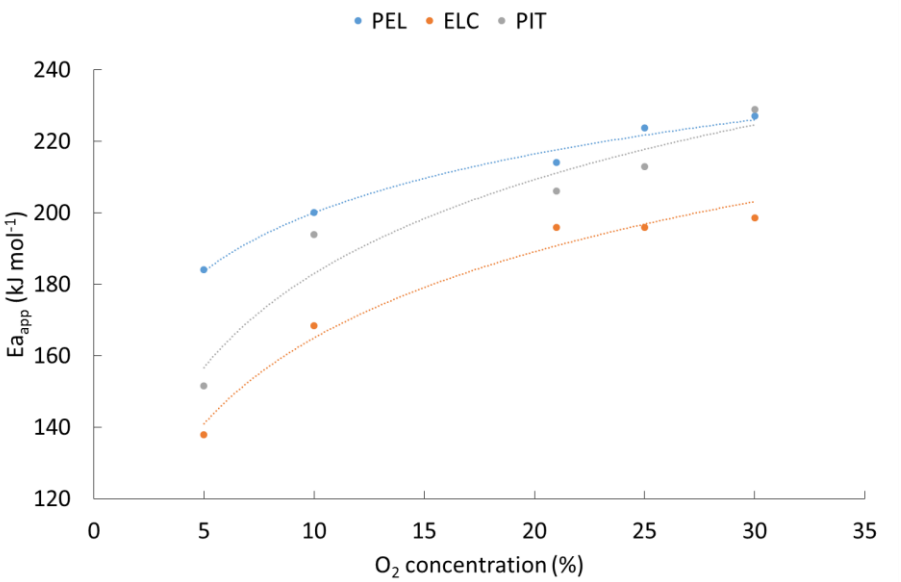

Figure 7.23: Increase in the apparent activation energy with oxygen concentration seen in the coals during char combustion

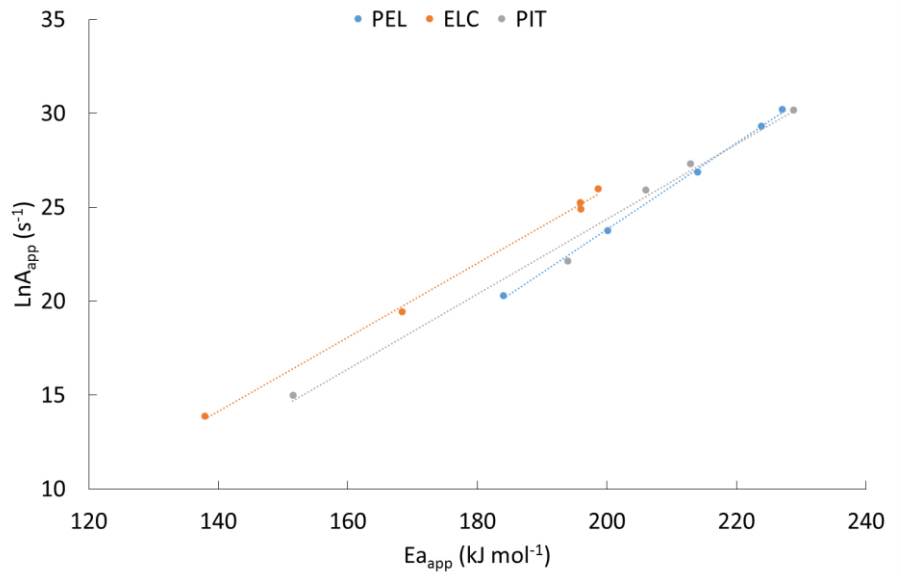

Figure 7.24: Kinetic compensation effect seen in the combustion of coal chars (Combustion in 5-30% O_2/CO_2 atmospheres)

The linear equations relating to the KCE and the correlation coefficients (R^2) are outlined below:

PEL Ln A = $0.229Ea_{app} - 22.147$, R^2 0.9986

ELC Ln A = $0.197Ea_{app} - 13.437$, R^2 0.9976

PIT Ln A = $0.1997Ea_{app} - 15.557$, R^2 0.9896

7.3.1.1.1 Discussion

Gil et al. (212) determined apparent activation energies of coals chars combusted in 30% O_2/CO_2 atmospheres and reported values of 116-171 kJ mol^{-1}. They also performed a small literature review an determined that coal char activation energies ranged from 109 – 248 kJ mol^{-1} (chars combusted in 10% - 30% O_2/CO_2). The wide range of activation values reported is due to both the differences in fuel (and resulting char properties) and the experimental procedures from which kinetic parameters were determined. The results in this work fall in the range of Ea_{app} reported by Gil et al.

The trend in Ea_{app} with the increase in oxygen concentration, seen in the work in this thesis, was also reported in work performed by Janse et al. (261). Janse et al. investigated pine char combustion in increased oxygen and nitrogen environments (2.25 - 36 % O_2) and reported that at higher oxygen concentrations (>18% O_2) the activation energy became constant. They argued that the change in Ea_{app} could be caused by a change in reaction mechanism, where the adsorption of the oxygen (R 3.6) is less important than the desorption of the products at high oxygen concentrations (R 3.8 and R 3.9 in section 3.5.3 (142, 261). Essentially this means that at higher oxygen concentrations (21% O_2) there is sufficient oxygen for the char reaction and the rate is controlled by the speed of the desorption of the products from the char surface.

The trends in the kinetic parameters seen during devolatilisation (section 6.4) were linear and fuel specific kinetic models based solely on oxygen concentration were developed (Table 6.11). The development of a char kinetic model based on the partial pressure of oxygen (n^{th} order model) is derived in section 7.3.2.

7.3.1.2 Biomass char apparent reactivity

The apparent rate constants determined from the non-isothermal biomass and TSP char combustion experiments are shown in Figure 7.25 - Figure 7.27. The apparent kinetic parameters extracted and the reaction order with respect to carbon conversion can be seen in Table 7.4. The trends in the kinetic parameters with respect to oxygen concentration are shown in Figure 7.29. Please note that in the following plots the data labels 5-30% refer to chars produced in CO_2 and combusted in oxy-fuel environments and air refers to chars produced in N_2 and combusted in air.

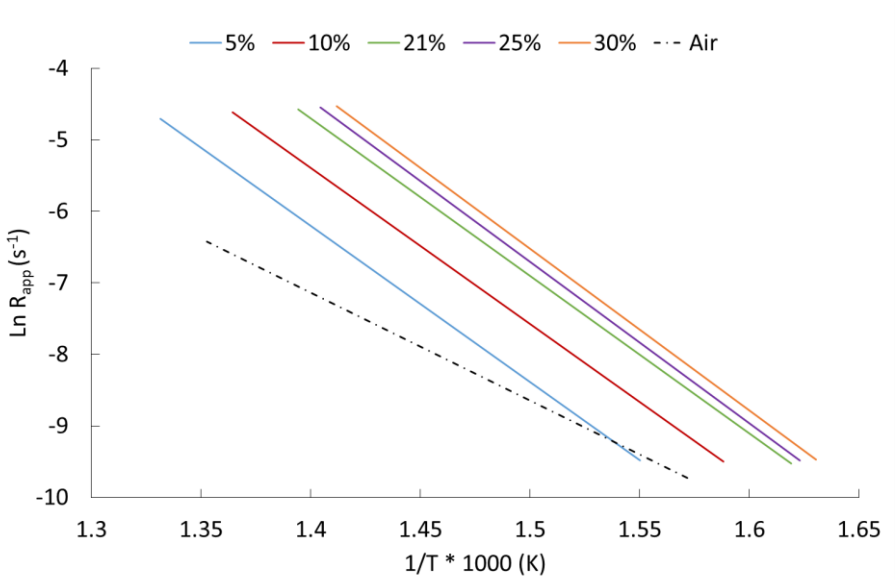

Figure 7.25: Apparent reactivity of the PWWP chars combusted in air and oxy-fuel environments (Chars produced at 1000 K min^{-1} heating rate, at 1000 K)

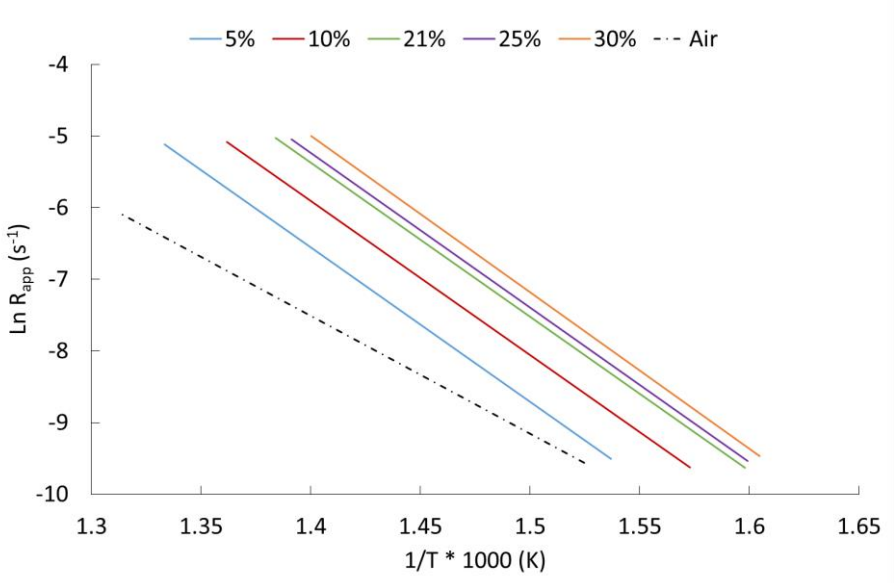

Figure 7.26: Apparent reactivity of the WWP chars combusted in air and oxy-fuel environments

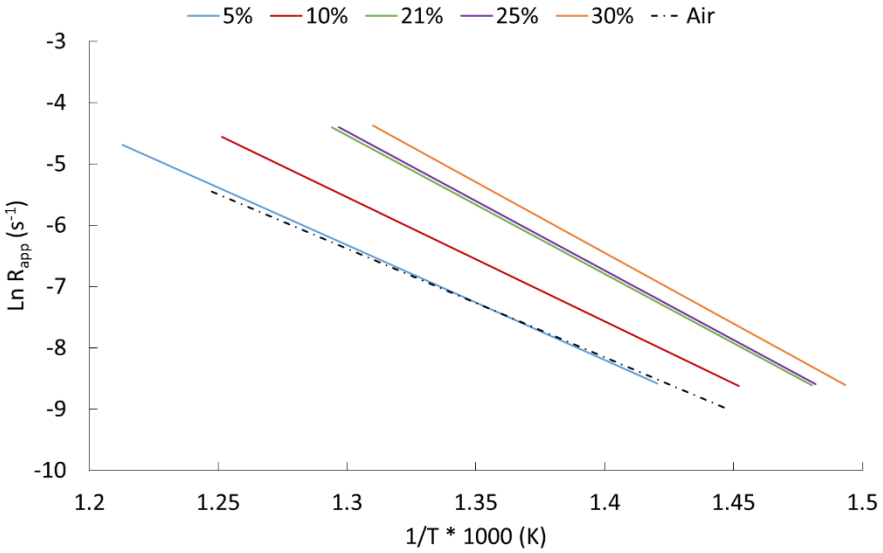

Figure 7.27: Apparent reactivity of the TSP chars combusted in air and oxy-fuel environments

Table 7.4: Apparent kinetic parameters and reaction order with respect to biomass char conversion determined by combustion of coal chars (Conversion range 0.05-0.85)

Char	Atmosphere	Ln A_{app} (s^{-1})	Ea_{app} (kJ mol^{-1})	m	R^2	Temperature region (°C)
	5%	24.4	181.6	1.4	0.999	372-586
	10%	25.2	181.4		0.999	357-460
PWWP CO_2	21%	26.1	183.1		0.996	344-444
	25%	27.2	187.1		0.990	343-439
	30%	27.4	188.0		0.988	340-435
PWWP N_2	Air	14.0	125.3	0.2	0.976	363-476
	5%	23.6	179.2	1	0.982	377-477
WWP CO_2	10%	24.2	178.9		0.982	363-461
	21%	24.7	178.9		0.912	353-449
	25%	25.0	179.5		0.983	352-446
	30%	25.6	181.7		0.988	350-441
WWP N_2	Air	15.6	137.0	0.2	0.973	383-488
	5%	18.1	155.9	1	0.998	431-551
TSP CO_2	10%	20.8	168.4		0.997	416-526
	21%	24.8	187.8		0.977	402-500
	25%	25.0	188.4		0.998	402-498
	30%	25.9	192.0		0.989	396-490
TSP N_2	Air	18.1	155.9	0.4	0.979	418-530

The apparent kinetic parameters seen in Table 7.4 were again used to predict the conversion of the biomass and TSP chars and compared to the actual conversion determined experimentally. The predicted and experimental conversion plots and the deviation between the two (Eq 4.36 and 4.37) can be seen in the appendix section 12.3 (Figure 12.5 -

Figure 12.7). The predicted and experimental conversion are in good agreement and the rate constant parameters shown in Figure 7.25 - Figure 7.27 are in good agreement with the mass loss profiles seen in section 7.2.2.

The difference in the reactivity of the biomass N_2 and CO_2 chars are highlighted in Figure 7.25 - Figure 7.27 where it is easily seen that the CO_2 chars are more reactive. In fact for PWWP and WWP chars, the rate in air, for the N_2 chars are slower than the rates in 5% O_2/CO_2 of the CO_2 chars. The TSP N_2 char combusted in air has a similar rate to the TSP CO_2 char combusted in 5%O_2/CO_2 atmosphere. This is in good agreement with the char combustion profiles seen in section 7.2.2. The values of the kinetic parameters Ea_{app} and Ln A_{app} as a result of the char production atmosphere (N_2 vs CO_2) show the reverse of the trend seen in the coal chars, with Ea_{app} and LnA_{app} being smaller in the biomass and TSP N_2 chars.

The effect of the increase in oxygen concentration in the oxy-fuel environments (Figure 7.28) on the kinetic parameters is less severe in the biomass and TSP chars than seen in the coals. A linear trend is seen in the small changes in Ea_{app} in the biomass chars while a logarithmic trend is seen in the TSP chars, as was seen in the coal chars (Figure 7.23). The Ea_{app} increase by 6 kJ mol^{-1} in the PWWP char, 2 kJ mol^{-1} in the WWP char and 7 kJ mol^{-1} in the TSP char compared to 40-77 kJ mol^{-1} in the coal char when oxygen levels are increased from 5-30%. The same is seen in the values of LnA_{app} where the PWWP and WWP increase by ~3 s^{-1} and TSP 7 s^{-1} compared to 10-15 s^{-1} increase in the coal chars.

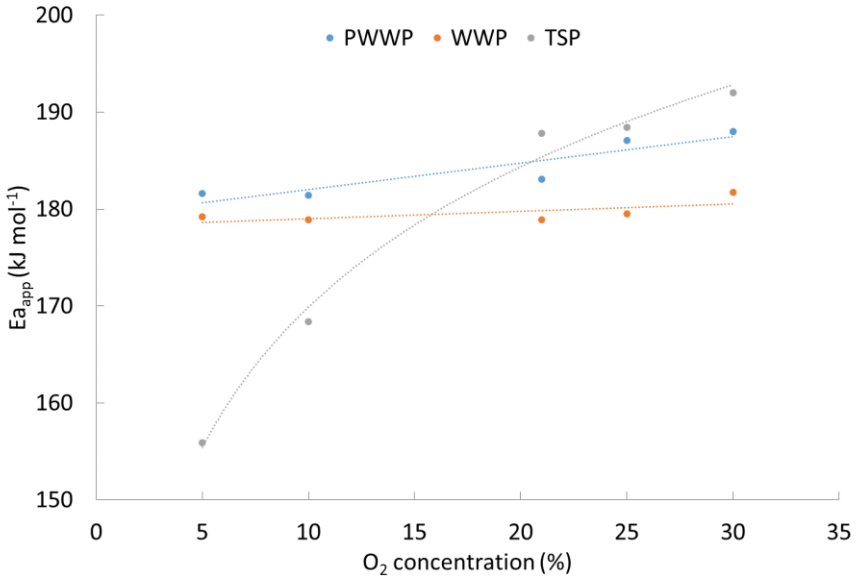

Figure 7.28: Increase in the apparent activation energy with oxygen concentration seen in the biomass and TSP during char combustion

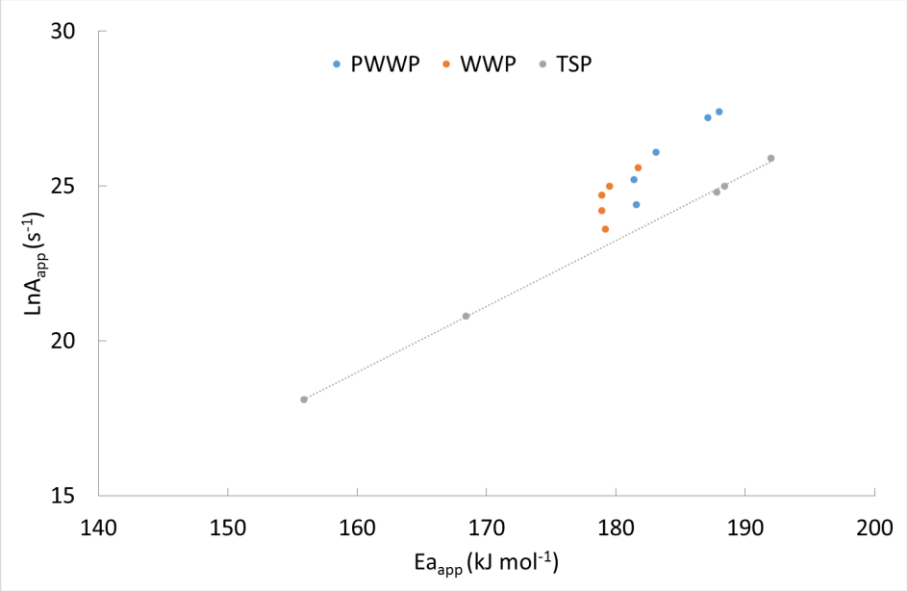

Figure 7.29: Kinetic compensation effect seen in the combustion of biomass chars (Combustion in 5-30% O_2/CO_2 atmospheres)

The linear KCE is not present in the biomass chars but is seen in the TSP chars (also seen in the coals) (Figure 7.29) and is outlined below:

TSP Ln A = 0.2141.Ea_{app} – 15.312, R^2 0.9997

A comparison of the reaction rate constants of the CO_2 chars produced from each fuel and combusted in 21% O_2/CO_2 and the reaction order of the fuels can be seen in Figure 7.30. The order of reactivity of the chars is PWWP, WWP, TSP, ELC, PEL and finally the PIT.

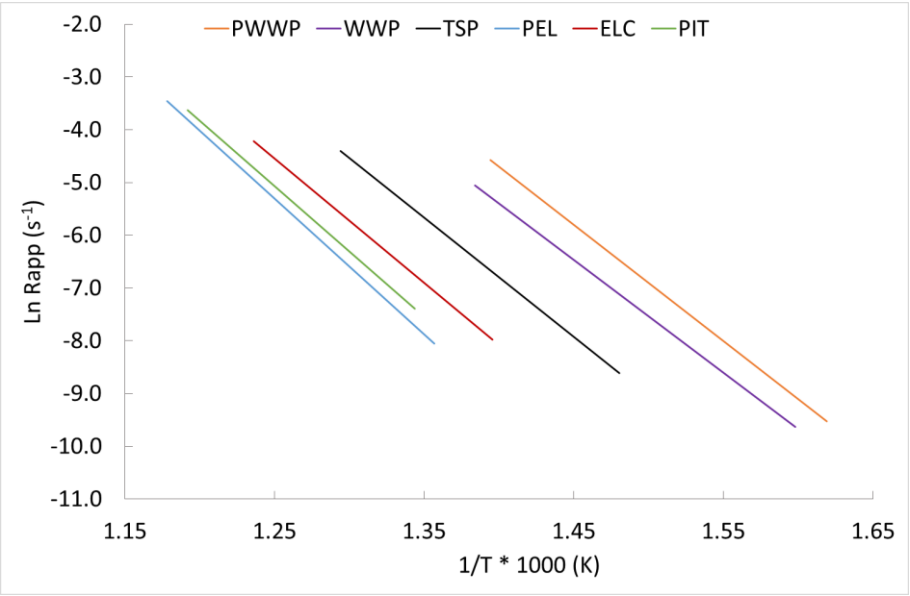

Figure 7.30: Apparent reaction rate constants of the chars produced in CO_2 and combusted in 21% O_2/CO_2

7.3.1.2.1 Discussion

Several researchers have investigated the kinetics of biomass char combustion in air and the values of the activation energies and pre-exponential factors vary of a wide range. Activation energies derived from experiments performed using a TGA at similar heating rates to those used in the work in this thesis range from 79 – 208 kJ mol^{-1} and the natural log of the pre-exponential factors from ~14-29 (268-271). The results in this work are in the expected ranges outlined in the literature.

The differences in the reactivities of the biomass and TSP chars as a result of the char production atmosphere are more pronounced, with a greater change in the kinetic parameters derived seen in the coals. This can be attributed to the higher sensitivity of the biomass to fuels to the change in pyrolysis environment.

The impact of increasing oxygen concentrations in the oxy-fuel atmospheres on the kinetic parameters is less pronounced in biomass char combustion than in the devolatilisation stage; the opposite was seen for the coal chars. The increase in Ea_{app} was 7 kJ mol^{-1} (5-30% O_2) during char combustion and E_a changed by 17.5 kJ mol^{-1} during devolatilisation. The same trend is seen in the WWP CO_2 char but the trend in the TSP CO_2 is reversed and behaves more like a coal. This suggests that the kinetic parameters derived for the biomass chars are less sensitive to the change in oxygen than the change in pyrolysis atmosphere and the reverse is true in the coals and TSP fuels.

7.3.2 Global n^{th} order reaction model

7.3.2.1 Coal char n^{th} order reaction model

The global n^{th} order reaction model was applied to the coal chars produced in CO_2 and combusted in oxy-fuel environments to produce a single fuel specific simple kinetic model. The model uses a single value of A_n and Ea_n and the change in reactivity is determined by knowledge of the partial pressure of oxygen and the reaction order n. The methodology is outlined in section 4.7.2.2 and the parameters determined for each of the coal chars can be seen in Table 7.5. The reaction rate (dx/dt) is described by the following equation:

$$\frac{dx}{dt} = A_n \exp^{-Ea_n/RT} P_{O2}^{n} (1-x)^{m} \quad \text{Eq 7.1}$$

Table 7.5: Coal char oxidation in oxy-fuel environments n^{th} order reaction model parameters

Char	n^{th} order reaction model parameters (dx/dt s^{-1})
PEL CO_2	$dx/dt = 9.0 \times 10^8 . \exp^{(-209.8/RT).} P_{O2}^2 . (1-x)^{1.9}$ (Ln A = 28.6)
ELC CO_2	$dx/dt = 3.2 \times 10^7 . \exp^{(-179.4/RT).} P_{O2}^{1.7} . (1-x)^{1.2}$ (Ln A = 17.3)
PIT CO_2	$dx/dt = 6.3 \times 10^7 . \exp^{(-198.7/RT).} P_{O2}^{2.2} . (1-x)^{1.7}$ (Ln A = 18.0)

Note: Ea (kJ/mol), A (s^{-1} KPa^{-1})

The n^{th} order reaction models seen in Table 7.5 were then used to predict the mass loss and derivative mass loss behaviour of the chars. The predicted conversion and the experimental conversion of the coal chars can be seen in Figure 7.31 - Figure 7.33 and the deviation between the predicted and experimental TGA and DTG profiles, as determined by Eq 4.36 and 4.37, can be seen in Table 7.6.

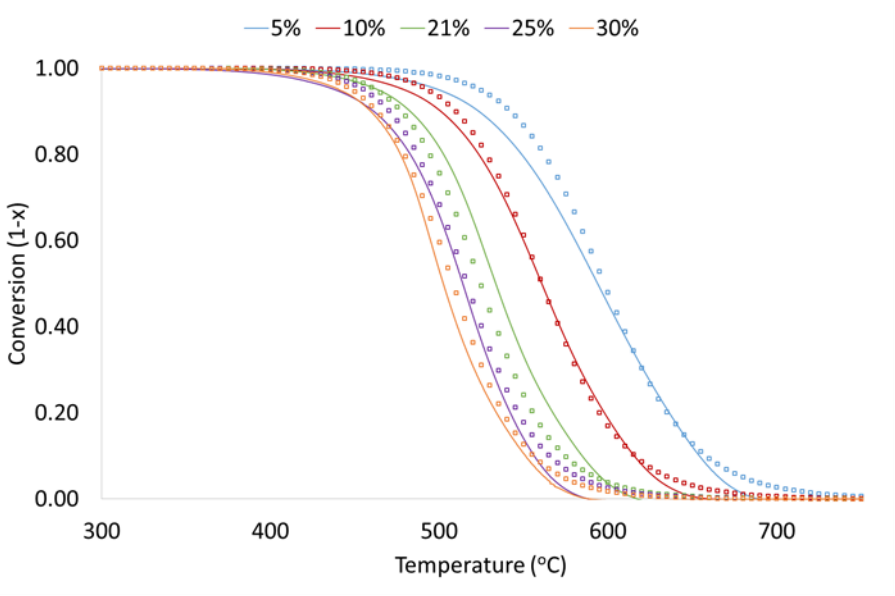

Figure 7.31: Conversion of the PEL CO_2 char in the full range of oxy-fuel conditions and the predicted conversion using the n^{th} order reaction model (line – experimental, squares – predicted)

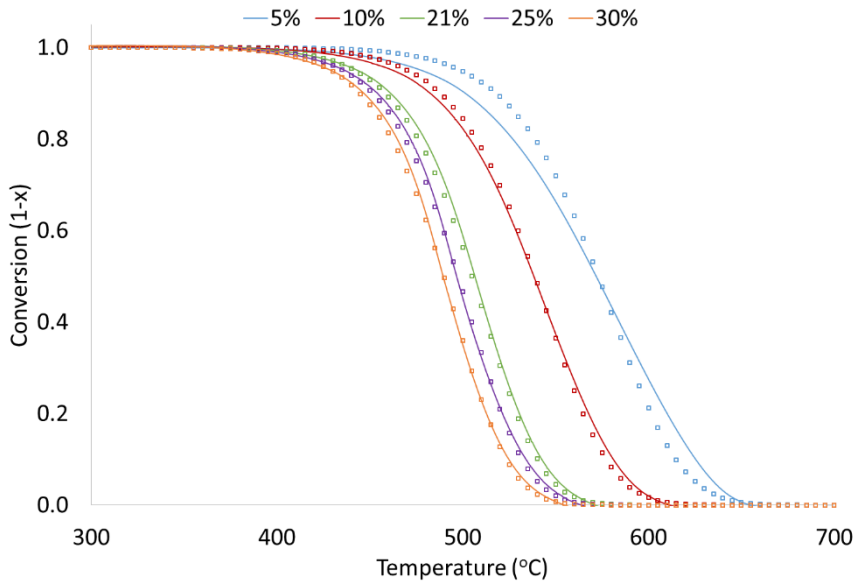

Figure 7.32: Conversion of the ELC CO_2 char in the full range of oxy-fuel conditions and the predicted conversion using the n^{th} order reaction model (line – experimental, squares – predicted)

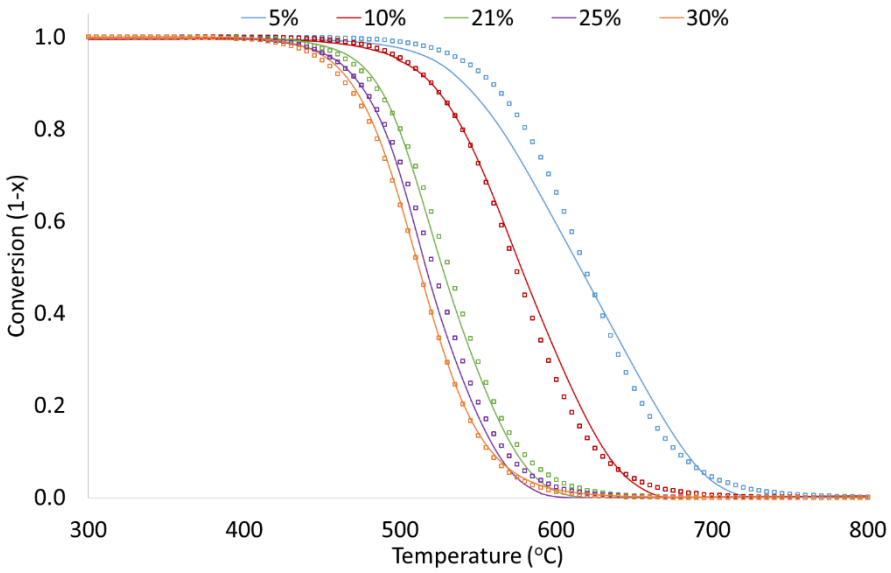

Figure 7.33: Conversion of the PIT CO_2 char in the full range of oxy-fuel conditions and the predicted conversion using the n^{th} order reaction model (line – experimental, squares – predicted)

Table 7.6: Deviation between the experimental coal char conversion in oxy-fuel and predicted char conversion using the n^{th} order reaction model

	Combustion atmosphere	Dev (1-x) (%)	Dev (dx/dt) (%)
PEL CO_2	5%	2.08	6.04
	10%	0.98	3.48
	21%	3.04	6.34
	25%	1.70	2.61
	30%	1.51	4.52
ELC CO_2	5%	2.09	8.71
	10%	0.67	2.09
	21%	1.23	2.20
	25%	0.92	2.66
	30%	0.94	2.48
PIT CO_2	5%	2.22	8.33
	10%	1.50	5.62
	21%	1.31	3.24
	25%	1.29	2.64
	30%	0.97	4.15

In the n^{th} order kinetic model a constant value of Ea_n and A_n are required for the full range of oxygen environments, and the change in the reactivity (dx/dt) is determined by the partial pressure of O_2 and the reaction order with respect to oxygen n. The mean of the apparent activation energies (Table 7.3) for each of the chars seen in the previous sections was chosen and used in this model as suggested by Cozzani (214). The work by Cozzani focused on

biomass fuels and found that the range in apparent activation energies was small (± 5%) as seen in the biomass fuels here. Murphy et al (150) investigated coal char combustion rates and found that two separate values of Ea and A were better fitted to the experimental data than a single value. The two sets of kinetic parameters were determined for high (24-36%) and low (6-12%) oxygen concentrations. However in the work by Murphy et al., the value of n was assumed, which required the fitting of the data through the change in the kinetic parameters E_a and A.

In this thesis the determination of the average value of Ea_{app} allowed for the determination of A' at each oxygen concentration. The term A' that incorporates both A and P_{O2}^n was then determined by minimising the value of DEV(1-x) between the experimental data and the predicted model. The reaction order (n) could then be determined using Eq 4.39 and as can be seen in Table 7.5 they fall in the range of 1.7 – 2.2. The PIT char has the largest n^{th} order term followed by the PEL and finally the ELC chars. The differences in the reaction order in each of the chars can be related to the differences in the mass loss behaviour and the key indicators measured in (section 7.2.1, Table 7.1) or the conversion plots seen here (Figure 7.31 - Figure 7.33). The PIT char has the largest degree of change in characteristics due to the change in oxygen concentration from 5-30%, followed by the PEL and the ELC chars. According to literature the expected range of n is 0 - 1 widely reported in literature (142, 150, 272-274) and the reaction order is assumed to be constant, which in reality is not.

Janse et al. (261) investigated the reactivity of Pine chars using isothermal thermogravimetric analysis in increased oxygen - N_2 atmospheres. The reaction rate order (n) was determined at a range of conversions and temperatures and it was found that the as the temperature increased the order increased, and as the conversion increased the order decreased. The authors explained that at lower temperatures the rate limiting mechanisms in char conversion is the desorption of CO and CO_2 (R 3.8 and 3.9 in the literature review section 3.5.3). At the lower temperatures the reaction order with respect to oxygen is expected to be 0. At increased temperatures the rate limiting mechanism is the adsorption of oxygen on to the char surface (R 3.6) and when this is the rate limiting step the reaction order with respect to oxygen is equal to 1. It was also noted that as conversion increased the reaction order decreased implying that the adsorption of oxygen (R 3.6) is less important than the desorption of CO and CO_2 (R 3.8 and 3.9). In the work by Janse the experiments were determined isothermally, so the derivation of n at the different temperatures is easily performed.

In the work in this thesis the value of n is the averaged over a wide range of temperatures at conversion levels of 0.05 – 0.85 through the term A' seen in Eq 4.39. From the TGA and DTG conversion plots seen in section 7.2.1 it is clear that the difference between the conversion rates, in the different combustion atmospheres, changes throughout the combustion profile. This change in rates and the derivation of a single term for E_a and A result in the higher than expected value of n. However it can be seen from Figure 7.31 - Figure 7.33 that the n^{th} order models adequately predict the conversion behaviour of the coal chars in the full range of oxy-fuel atmospheres.

7.3.2.2 Biomass char n^{th} order reaction model

The global n^{th} order reaction model was applied to the biomass chars produced in CO_2 and combusted in oxy-fuel environments to produce a simple model that takes into account the partial pressure of oxygen in the combustion system. The methodology is outlined in section 4.7.2.2 and the parameters determined for each of the biomass chars can be seen Table 7.7

Table 7.7: Biomass and TSP char oxidation in oxy-fuel environments n^{th} order reaction model parameters

Char	n^{th} order reaction model parameters (dx/dt s^{-1})
PWWP CO_2	$dx/dt = 1.2 \times 10^{10} . \exp^{(-184.4/RT).} P_{O2}^{1} . (1-x)^{1.4}$ (Ln A = 23.2)
WWP CO_2	$dx/dt = 1.6 \times 10^{10} . \exp^{(-190.7/RT).} P_{O2}^{0.9} . (1-x)^{1}$ (Ln A = 23.5)
TSP CO_2	$dx/dt = 2.9 \times 10^{8} . \exp^{(-178.5/RT).} P_{O2}^{1.2} . (1-x)^{1}$ (Ln A = 19.5)

Note: Ea (kJ/mol), A (s^{-1} KPa^{-1})

The n^{th} order reaction models seen in Table 7.7 were used to predict the mass loss and derivative mass loss behaviour of the chars. The predicted conversion and the experimental conversion of the biomass and TSP chars can be seen in Figure 7.34 - Figure 7.36 and the deviation between the predicted and experimental TGA and DTG profiles, as determined by Eq 4.36 and 4.37, can be seen in Table 7.8.

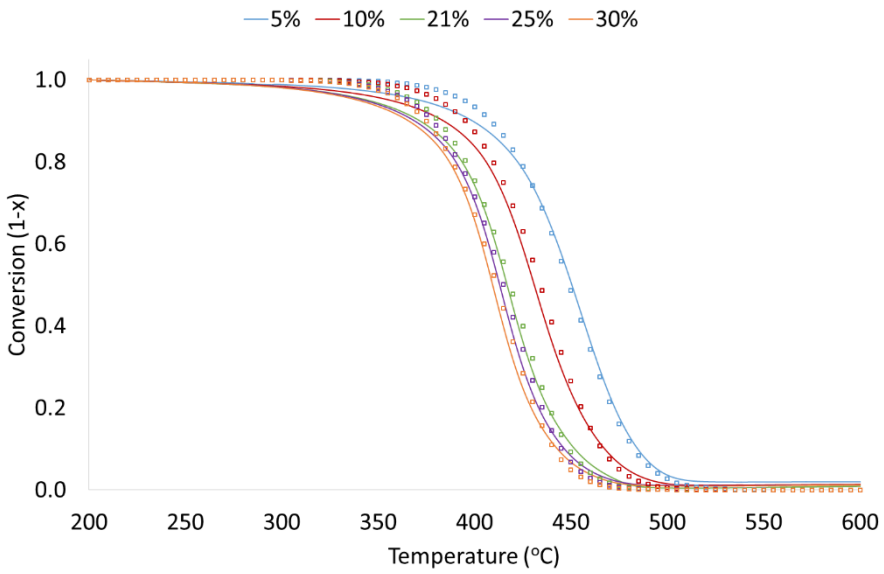

Figure 7.34: Conversion of the PWWP CO_2 char in the full range of oxy-fuel conditions and the predicted conversion using the n^{th} order reaction model (line – experimental, squares – predicted)

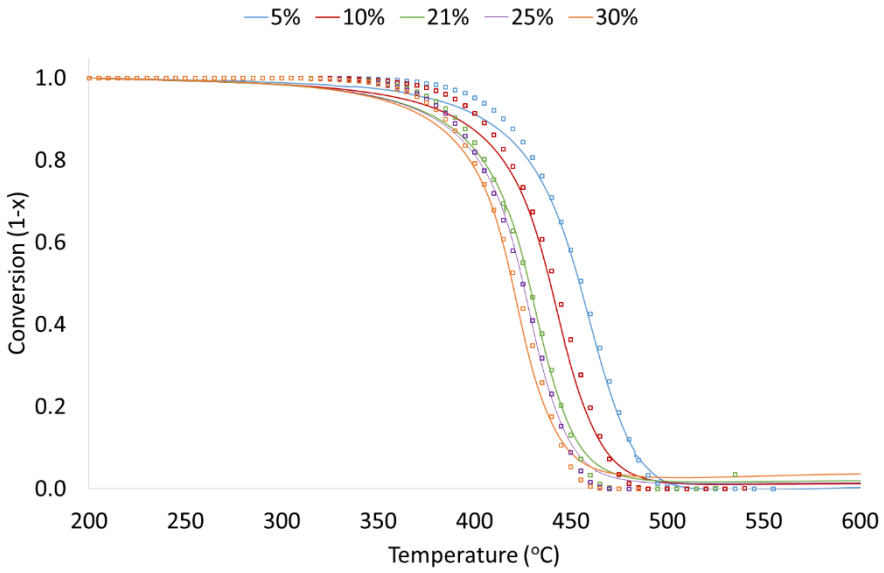

Figure 7.35: Conversion of the WWP CO_2 char in the full range of oxy-fuel conditions and the predicted conversion using the n^{th} order reaction model (line – experimental, squares – predicted)

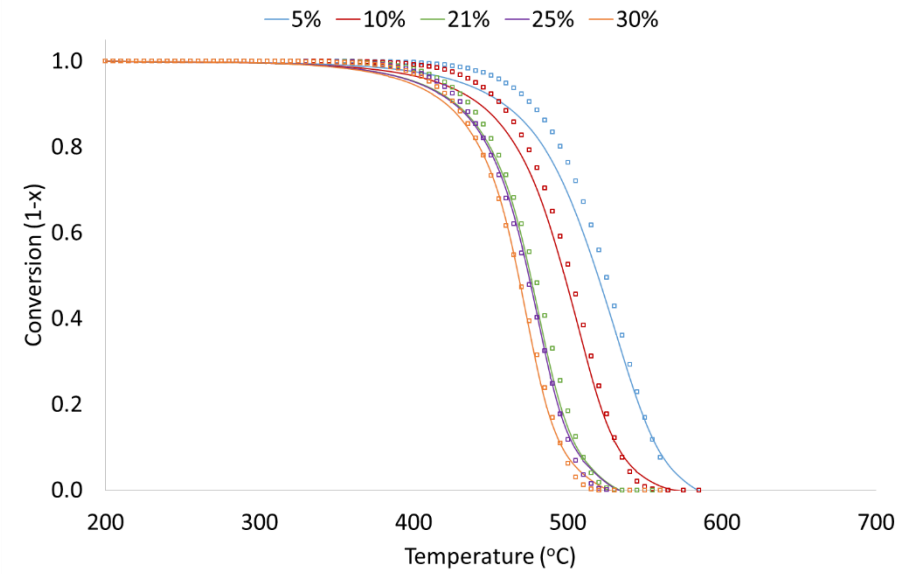

Figure 7.36: Conversion of the WWP CO_2 char in the full range of oxy-fuel conditions and the predicted conversion using the n^{th} order reaction model (line – experimental, squares – predicted)

Table 7.8: Deviation between the experimental biomass char conversion in oxy-fuel and predicted char conversion using the n^{th} order reaction model

	Combustion atmosphere	Dev (1-x) (%)	Dev (dx/dt) (%)
PWWP CO_2	5%	1.68	3.23
	10%	1.54	2.61
	21%	1.34	3.18
	25%	2.15	4.17
	30%	1.39	3.31
WWP CO_2	5%	1.27	4.10
	10%	1.60	3.63
	21%	1.84	4.31
	25%	1.60	3.74
	30%	2.57	4.30
TSP CO_2	5%	2.02	3.54
	10%	1.47	3.11
	21%	1.35	3.81
	25%	1.41	3.11
	30%	1.11	3.54

It can be seen from the comparison of error between the experimental conversion and the predicted conversion seen in Table 7.6 and Table 7.8 that the n^{th} order models determined for the biomass and TSP chars are more accurate than those for the coal chars. The reason for this is that the biomass and TSP conversion are less effected by the increase in oxygen than the coal chars which resulted in a small change in the Ea_{app} over the full range of

combustion environments (PWWP CO_2 ΔEa_{app} = 6.4 compared to PEL CO_2 ΔEa_{app} = 43). When the average of the Ea_{app} was determined for the n^{th} order reaction model, the error in A' is reduced and therefore the estimation of the reaction rate and conversion is more accurate.

Again the value of n was determined to fit the whole conversion range and not determined at any specific temperatures or degrees of conversion. The reaction order of the biomass and TSP chars is half of that seen in the coal chars and ranges from 0.9-1.2, more similar to the values that would be expected from literature. The lower value of n can be attributed to the lesser effect the combustion atmosphere and the increase in oxygen concentration has on the biomass and TSP chars compared the coal chars.

The development of the n^{th} order model with the use of a single value of E_a, A and n is useful for modellers in determining the reactivity of the fuels in the full range of oxy-fuel environments and has been shown to adequately predict the conversion of all chars under the char combustion conditions used in this work.

7.3.3 Intrinsic reactivity of coal chars

In this section only the intrinsic reactivities of the coals are determined as the surface areas of the biomass chars are unknown. The intrinsic reactivities, the reactivity per unit area, were determined using the global n^{th} order models (Table 7.5) for the CO_2 produced chars. In the case of the N_2 produced chars, where no n^{th} order model was determined the apparent reactivities are utilised (Table 7.3). The surface areas are reported in (Table 5.14) and methodology described in section 4.7.2.3. The intrinsic reaction rate constants R_i determined for the coal chars produced in N_2 and combusted in air and the chars produced in CO_2 and combusted in the full range of oxy-fuel environments can be seen in Figure 7.37 - Figure 7.39. In addition the intrinsic rate constants of a Pittsburgh coal char produced using a DTR (275) and the correlation line for the intrinsic reactivity of 32 coal chars determined by Smith (276), both of which are combusted in air, are added for comparison.

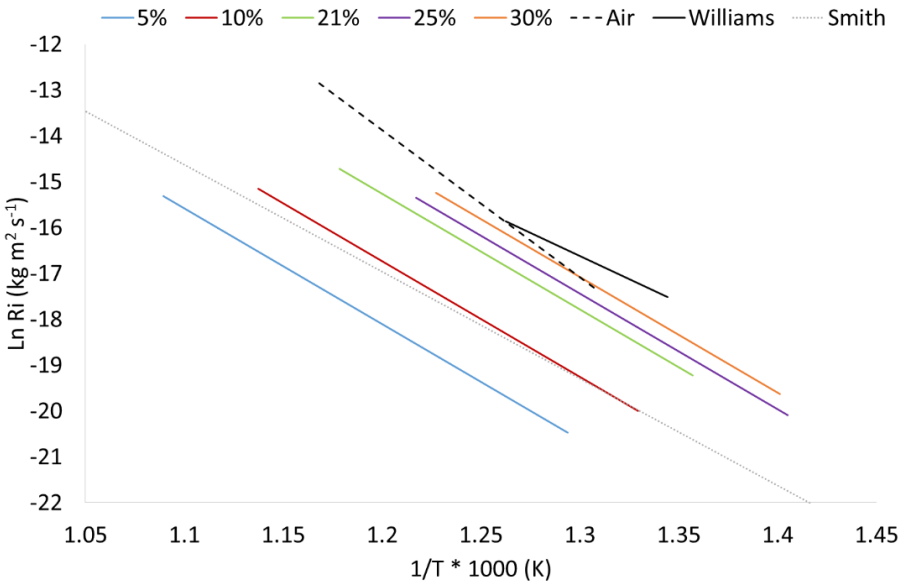

Figure 7.37: Intrinsic rate constants of the PEL chars produced in N_2 and combusted in air and chars produced in CO_2 and combusted in the full range of oxy-fuel environments

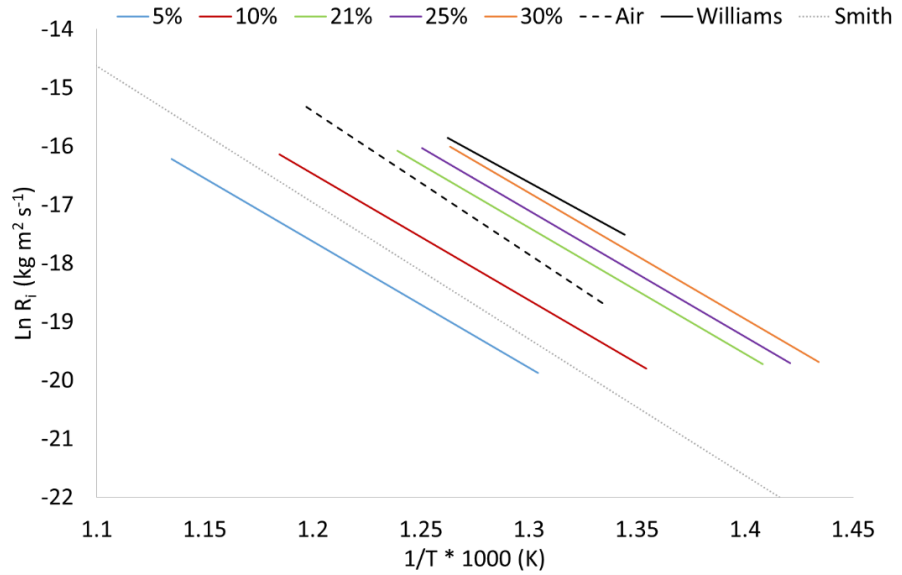

Figure 7.38: Intrinsic rate constants of the ELC chars produced in N_2 and combusted in air and chars produced in CO_2 and combusted in the full range of oxy-fuel environments

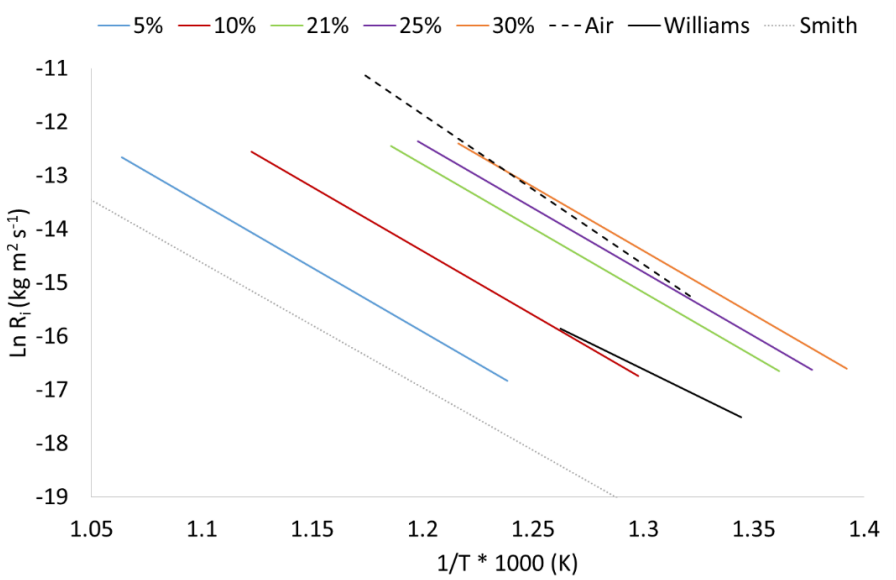

Figure 7.39: Intrinsic rate constants of the PIT chars produced in N_2 and combusted in air and chars produced in CO_2 and combusted in the full range of oxy-fuel environments

It can be seen that the intrinsic reaction rates determined are in the same regions as the work produced by Williams (275) and Smith (276) and give some confidence in the determined intrinsic reaction rates.

Comparison with the apparent reactivity measurements of the coal chars seen in section 7.3.1.1 and the intrinsic rates seen in Figure 7.37 - Figure 7.39 highlight that the reactivity of the N_2 chars is higher when determined on an intrinsic basis, the extent of which is fuel dependent. The intrinsic reactivity gives a measure of the rate of reaction per unit area and it can be seen from Figure 7.37 and Figure 7.39 that the PEL N_2 and PIT N_2 chars are more reactive than the PEL CO_2 and PIT CO_2 chars combusted in 21%O_2/CO_2. In fact the reactivity of both chars is similar to the CO_2 produced chars combusted in 30% O_2/CO_2. The ELC char does not show the same trend with the intrinsic reactivity of the N_2 char less reactive than the CO_2 char combusted in 21% O_2/CO_2. The PEL and ELC fuels, although from the same coal field do not have the same composition as can be seen from Table 5.5 and Table 5.6; the resulting difference in char properties may explain the difference in the intrinsic reactivity trends discussed above.

It is thought that the CO_2 produced chars may undergo a degree of crosslinking (135, 248, 277) at the char surface, due to CO_2 present during char production and during char combustion in oxy-fuel environments (156). The increase in crosslinking results in a more ordered and less reactive carbon remaining in chars produced in N_2 where the degree of crosslinking is expected to be less (in the case of the PEL and PIT coals).

It was shown in section 5.3 that the char yields and the composition of the coal chars is almost identical regardless of the char production atmosphere. The only significant difference in char properties between the two atmospheres is the char surface area (Table 5.14). The measurement of char surface area is known to be difficult due to the porous nature and structural integrity of the pore network. In addition the for microporous carbons, nitrogen adsorption can be limited by the slow rates of diffusion of nitrogen molecules throughout the porous network leading to errors in the determination of surface areas (208, 278). The difficulty in the determination of the char surface area may result in the lack of trends (in terms of intrinsic reactivity) seen in this work. Further work is required to fully understand the influence of the char production atmosphere on the char intrinsic reactivity.

7.4 Conclusions

7.4.1 Char combustion

- Chars were produced from the fuels using a TGA at ballistic heating rates of 1000 K min^{-1} in N_2 and CO_2 atmospheres and the remaining chars combusted in air and the full range of oxy-fuel environments.
- The extent of the difference in the combustion behaviour of N_2 chars and CO_2 chars is greater in the biomass fuels than in the coals.
- Chars produced in N_2 and combusted in air are less reactive than chars produced in CO_2 and combusted at the same oxygen concentrations in oxy-fuel conditions. The increase in reactivity of the coal CO_2 chars can be attributed the differences in char characteristics, as a result of char production atmosphere. The biomass CO_2 chars, although still much more reactive than the biomass N_2 chars due to char characteristics also exhibit a degree of CO_2 chemisorption which reduces the overall combustion rate.
- All chars exhibit the same trends when the oxygen levels are increased in oxy-fuel environments. As the oxygen levels increase the key temperatures identified are decreased and the peak rates of mass loss are increased.
- The increase in oxygen concentration has a greater effect on the coal chars than the biomass chars due the increased inherent oxygen levels present in the biomass chars.

7.4.2 Char combustion kinetics

7.4.2.1 Char apparent reactivity

- Apparent kinetic parameters were determined from the char combustion experiments in the full range of combustion atmospheres.
- In all chars the apparent rate constants determined were in good agreement with the char combustion profiles reported in section 7.2.
- The predicted conversion determined using the extracted kinetic parameters produce conversion plots in good agreement with the experimentally derived conversion.
- The differences in the combustion behaviour of the N_2 and CO_2 chars results in a change in the kinetic parameters derived. In the coals the Ea_{app} and LnA_{app} are larger in the N_2 char, the reverse is seen in the biomass and TSP chars.
- The increase in the oxygen concentrations in the oxy-fuel environments increases the reactivity of the chars and the derived kinetic parameters (to a greater extent in the coals). The increase in Ea_{app} with the increase in oxygen is linear in the biomass chars and a logarithmic trend is seen in the coals and TSP chars.
- The increase in oxygen concentration has more of an effect on the coal and TSP char kinetic parameters than in the devolatilisation stage; both Ea_{app} and A_{app} increasing significantly when chars are combusted in oxy-fuel environments. In the biomass chars the reverse is true.
- The KCE is present in the TSP and coal chars but is not present in the biomass chars.
- The change in pyrolysis atmosphere and its effect on the resulting char combustion behaviour has more of an effect on the biomass char combustion behaviour than the change in oxygen concentrations during oxy-fuel combustion. The opposite is true of the coals.
- The order of fuel reactivity was determined for the CO_2 chars combusted in 21% O_2/CO_2 and was found to be PWWP, WWP, TSP, ELC, PEL and finally the PIT.

7.4.2.2 n^{th} order

- The char combustion profiles were used to determine the apparent reactivity of the chars from which an n^{th} order reaction model was determined providing a simple model to adequately describe char combustion in oxy-fuel environments. The n^{th} order models are summarised in Table 7.9.

Table 7.9: Summary of n^{th} order char combustion models.

Char	n^{th} order reaction model parameters (dx/dt s^{-1})
PEL CO_2	$dx/dt = 9.0 \times 10^8 . \exp^{(-209.8/RT).} P_{O2}^{2}. (1-x)^{1.9}$ (Ln A = 28.6)
ELC CO_2	$dx/dt = 3.2 \times 10^7 . \exp^{(-179.4/RT).} P_{O2}^{1.7}. (1-x)^{1.2}$ (Ln A = 17.3)
PIT CO_2	$dx/dt = 6.3 \times 10^7 . \exp^{(-198.7/RT).} P_{O2}^{2.2} . (1-x)^{1.7}$ (Ln A = 18.0)
PWWP CO_2	$dx/dt = 1.2 \times 10^{10} . \exp^{(-184.4/RT).} P_{O2}^{1} . (1-x)^{1.4}$ (Ln A = 23.2)
WWP CO_2	$dx/dt = 1.6 \times 10^{10} . \exp^{(-190.7/RT).} P_{O2}^{0.9} . (1-x)^{1}$ (Ln A = 23.5)
TSP CO_2	$dx/dt = 2.9 \times 10^8 . \exp^{(-178.5/RT).} P_{O2}^{1.2} . (1-x)^{1}$ (Ln A = 19.5)

Note: Ea (kJ/mol), A (s^{-1})

- The n^{th} order model was able to predict the biomass and TSP char conversion better than the coals due to the smaller range in Ea_{app} determined and as a result the decrease in error between the experimentally measured conversion and the predicted conversion.
- The reaction order (n) is larger in the coals than in the biomass and TSP chars. This is attributed to the lesser effect of the change in oxygen concentration has on the conversion of the biomass and TSP chars relative to coal.

7.4.2.3 Intrinsic reactivity

- The measurement of the intrinsic reactivity suggest that cross-linking due to the presence of CO_2 in the char production atmosphere may be occurring (particularly in the PEL CO_2 and PIT CO_2 chars).
- As a result it was found that the PEL N_2 and PIT N_2 chars are more reactive than the chars produced in CO_2 at the same oxygen concentrations.

8 TGA ballistic heating rate char vs DTR char

8.1 Introduction

This chapter compares the PEL and PWWP chars produced at ballistic heating rates in nitrogen using the TGA (referenced as PEL N_2 and PWWP N_2) and chars produced using the drop tube reactor (referenced as PEL DTR and PWWP DTR), also in a nitrogen atmosphere (1% O_2). The chapter starts with the comparison of the combustion behaviour of the chars produced in the DTR compared to that of the TGA chars determined in the previous section. The non-isothermal combustion behaviour is then used to determine the apparent kinetics of the DTR chars using the same methodology as in the previous section. The intrinsic kinetics are then determined from the apparent kinetics and the surface areas reported in Table 5.14.

8.2 Combustion behaviour of chars produced using the TGA and DTR

The PEL and PWWP chars produced using the DTR (in nitrogen) were combusted in the TGA (in air) non-isothermally to determine the combustion behaviour. The mass loss and derivative mass loss curves of the DTR chars compared to the TGA chars can be seen in Figure 8.1 and Figure 8.2 and the key indicators identified can be seen in Table 8.1.

Table 8.1: Key temperatures identified in the combustion of chars produced using the TGA and DTR

		T_{IM} (°C)	T_{Vol} (°C)	dm/dt_{vol} (Wt%/s)	T_C (°C)	dm/dt_C (Wt%/s)	T_B (°C)
PEL	DTR	446	-	-	536	0.158	605
	TGA	470	-	-	544	0.223	621
PWWP	DTR	306	341	0.102	424	0.133	539
	TGA	397	-	-	467	0.192	489

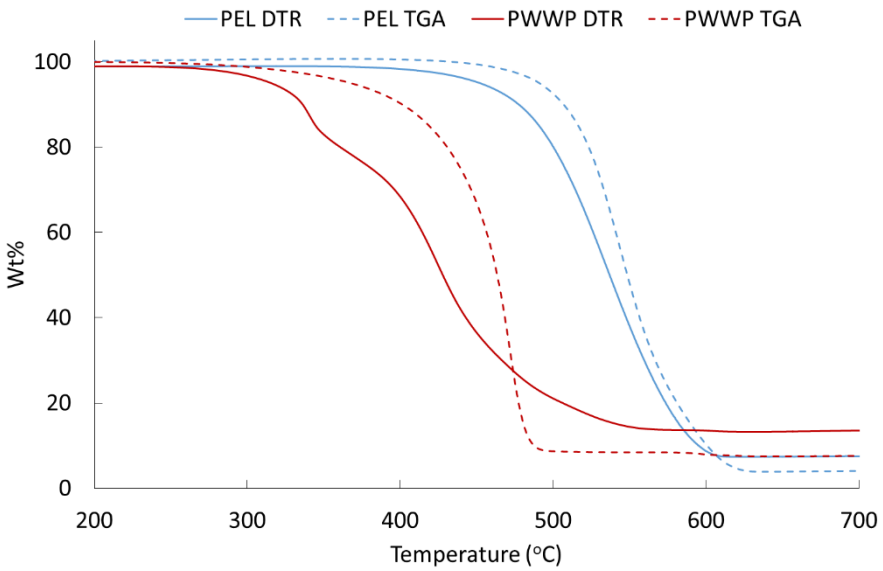

Figure 8.1: Mass loss profiles of the PEL and PWWP chars produced in the TGA and DTR in a nitrogen atmosphere and combusted in the TGA non-isothermally in air

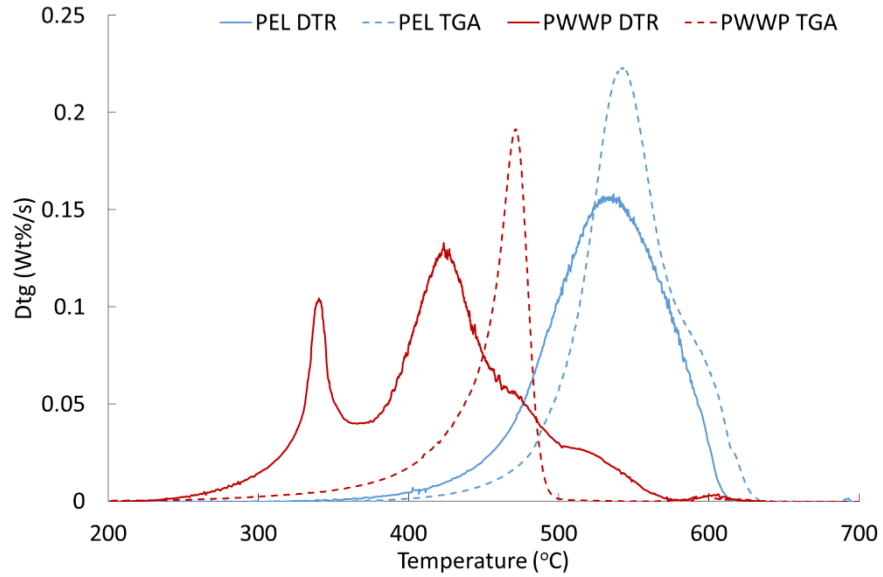

Figure 8.2: DTG profiles of the PEL and PWWP chars produced in the TGA and DTR in a nitrogen atmosphere and combusted in the TGA non-isothermally in air

There is a clear difference in the combustion behaviour of the chars produced in the DTR and TGA. In both the PEL and PWWP chars the combustion profiles shift to lower temperatures and peak rates of mass loss are decreased in DTR produced chars.

The PEL DTR starts to combust at a lower temperature than the PEL TGA char with the temperature of initial combustion (T_{IM}) ~24°C lower and T_C at 536°C, 12°C lower than the PEL TGA char. The maximum rate of mass loss (dm/dt_C) is also reduced, ~70% of that seen in the PEL TGA and the complete combustion is seen at 605°C, 16°C lower than the PEL TGA char. The change in mass loss profiles can be explained by the difference in the char properties as a result of production method as seen in section 5.3. The char yield is significantly lower in the DTR than the TGA, 43% and 58.5% respectively, and the composition in terms of volatile and fixed carbon content also differ. Although the char yield is lower in the DTR char, the amount of the relative volatile content (that is the percentage of the volatiles present in the fuel remaining in the char) is larger and the relative fixed carbon content is lower (section 5.3.2). The higher proportion of volatiles present in the DTR char results in the DTR char starting to combust at lower temperatures and the lower maximum rate of mass loss than the PEL TGA char.

The change in char production method has a greater effect on the PWWP char and its resulting combustion behaviour. Two distinct peaks can be seen in the PWWP DTR char, the first is associated with the volatile release and the second the combustion of the carbon rich char. The mass loss in the PWWP DTR char starts at 306°C, 91°C lower than the TGA char due to the higher volatile content. The second peak seen in the PWWP DTR char (associated with the carbon rich char) is seen at 424°C, 43°C lower than the TGA char. The maximum rate of mass loss is again ~70% of that seen in the TGA char but the burnout temperature (T_B) is ~50°C higher in the DTR char. Again comparison of the char yields and the relative volatile and fixed carbon content, as determined in section 5.3 can explain the difference in the above plots. The char yield in the DTR is around half of that seen in the TGA while the volatiles remaining is around twice and fixed carbon around one third of that seen in the TGA produced char. The higher volatile content results in the initial peak and the lower fixed carbon content results in the smaller maximum rates of mass loss seen in the DTR chars. (Figure 5.2 and Figure 5.3).

Production of chars using the DTR results in a decrease in key temperatures and rates of mass loss seen in both fuels due to the change in composition and morphology as a result of char production method. The change in char properties is attributed to the higher heating

rates, shorter residence times and larger particle sizes (to prevent complete burnout) used in the DTR as discussed in section 5.3.

8.3 Comparison of apparent kinetics in chars produced using the TGA and DTR

In this section the apparent kinetic parameters of the PEL and PWWP chars produced using the TGA in nitrogen and determined in section 7.3.1 are compared to the apparent kinetic parameters of the chars produced using the DTR. The DTR chars were prepared as outlined in section 4.5.3.1, combusted non-isothermally and the apparent kinetics determined using the apparent m^{th} order model as outlined in section 4.7.2.1.

The apparent reaction rate constants, the plots of conversion and the predicted conversion, determined as outlined in section 4.7.2, can be seen in Figure 8.3 and Figure 8.4. The apparent kinetic parameters and the error in the fit between the predicted conversion and the actual conversion can be seen in Table 8.2 and Table 8.3.

It should be noted that the apparent m^{th} order model used for the determination of the kinetic parameters does not allow for the multistep mass loss curve as seen in the PWWP DTR char. However the single step model was used in order to directly compare the two PWWP chars and the % error between the predicted and actual conversion (1-x) is deemed acceptable.

The apparent reactivity of the chars can be seen in Figure 8.3. The PEL DTR char is more reactive at lower temperatures, as would be expected from the TGA plots (Figure 8.1). As conversion and the temperature increase, the PEL TGA rate constant increases until the two rates converge. The PWWP chars are more reactive than the PEL chars with the PWWP DTR char significantly more reactive than the PWWP N_2 char produced in the TGA. It is shown in section 5.3 that the difference in the PWWP chars as a result of the char production method is greater than that seen in the PEL chars in terms of changes to composition (the surface area and morphology is not determined) which results in the greater difference in the apparent rate constant (R_{app}) seen here.

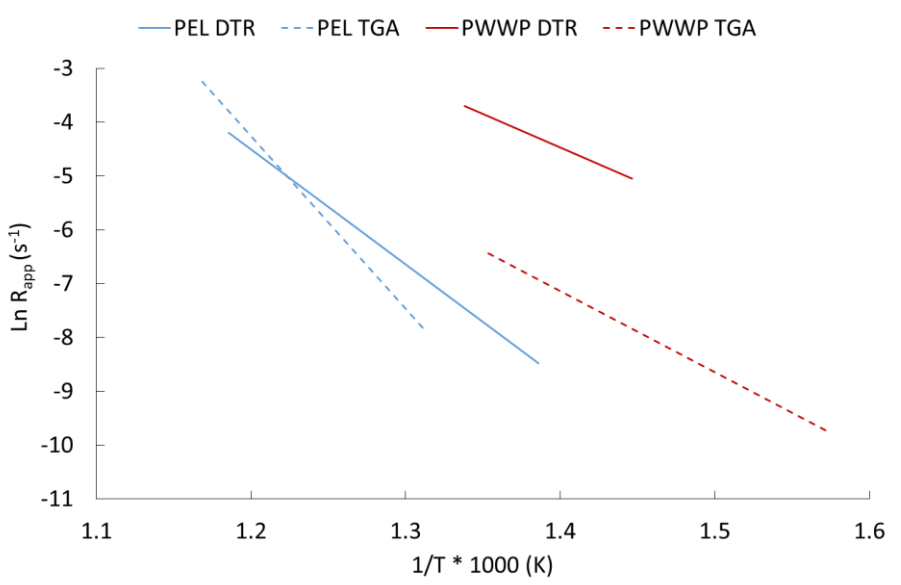

Figure 8.3: Apparent Reaction rate constants of the chars produced in the TGA and DTR

The apparent kinetic parameters determined, the value of the constant m, the temperature range at which the conversion from 0.05-0.85 was seen and kinetic parameters derived from can be seen in Table 8.2. The PEL DTR char has a significantly lower activation energy and pre-exponential factor than the PEL TGA char, this is in part due to the reduction in the conversion factor m. The change in the value of m in the PWWP DTR char is significantly larger than in the PEL chars but results in activation energies and pre-exponential factors more similar to the PWWP TGA char. As would be expected from the TGA plots the temperature region at which conversion from 0.05-0.85 is seen is at lower temperatures in the DTR chars.

Table 8.2: Apparent kinetic parameters and reaction order with respect to coal char conversion determined by combustion of chars produced using the DTR and TGA (Conversion range 0.05-0.85)

Char	Ln A_{app} (s^{-1})	Ea_{app} (kJ mol^{-1})	m	R^2	Temperature region (°C)
PEL DTR	21.1	177.7	1.4	0.999	448-570
PEL N_2	34.2	266.5	1.9	0.996	490-583
PWWP DTR	13.0	103.6	2.0	0.982	310-474
PWWP N_2	14.0	125.3	0.2	0.976	363-476

The predicted conversion derived from the apparent kinetic parameters and the error between that and the experimental conversion can be seen in Figure 8.4 and Table 8.3. The predicted conversion is in good agreement with the experimental conversion except in the case of the PWWP DTR char where two clear stages of conversion are seen. However, in order to directly compare the DTR and TGA chars the same modelling methodology is used. The deviation of the predicted conversion is in good agreement in terms of conversion and rate of conversion and is similar to that seen in other work (212). The good agreement between the predicted and experimental conversion gives confidence in the apparent kinetic parameters determined.

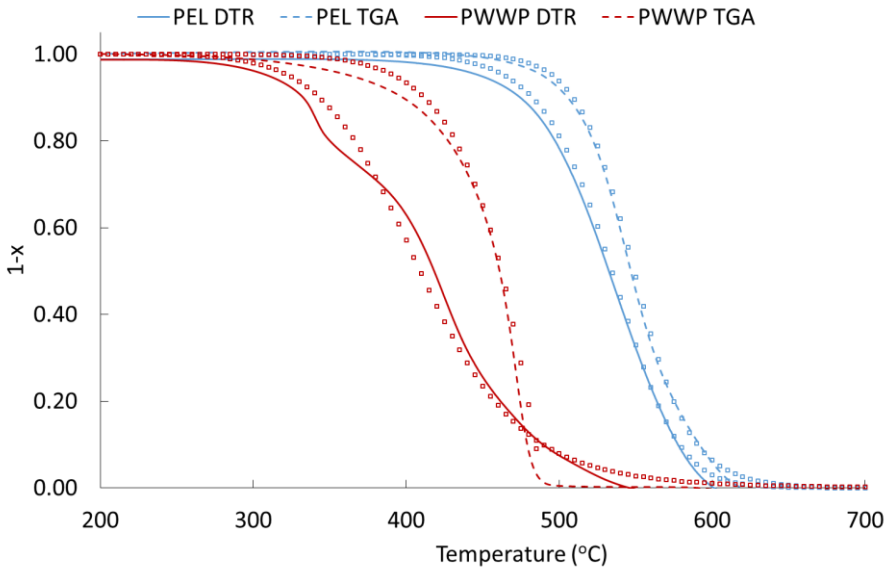

Figure 8.4: Conversion determined using the apparent kinetic parameters of the PEL and PWWP TGA and DTR chars (line – experimental, squares – predicted)

Table 8.3: Deviation between the predicted conversion and the experimental conversion in the chars determined from the apparent kinetic parameters

Char and production method	Dev (1-x) (%)	Dev (dx/dt) (%)
PEL DTR	1.16	2.22
PEL N_2	0.83	2.58
PWWP DTR	2.19	8.68
PWWP N_2	1.97	7.54

8.4 Intrinsic kinetics of the PEL TGA and DTR chars

The intrinsic reactivity (R_i) of the PEL TGA and DTR chars determined as outlined in section 4.7.2.3 and using the surface areas reported in Table 5.14 can be seen in Figure 8.5 alongside the intrinsic kinetics of a Pittsburgh coal (275) (Williams) and the averaged intrinsic reactivities of thirty-two samples taken from work by Smith (160). It can be seen that the intrinsic reactivities of the PEL TGA and DTR chars fit quite well with the intrinsic reactivities determined in the compared work. The intrinsic reactivities of the PWWP chars could not be determined due to the lack of surface area measurements.

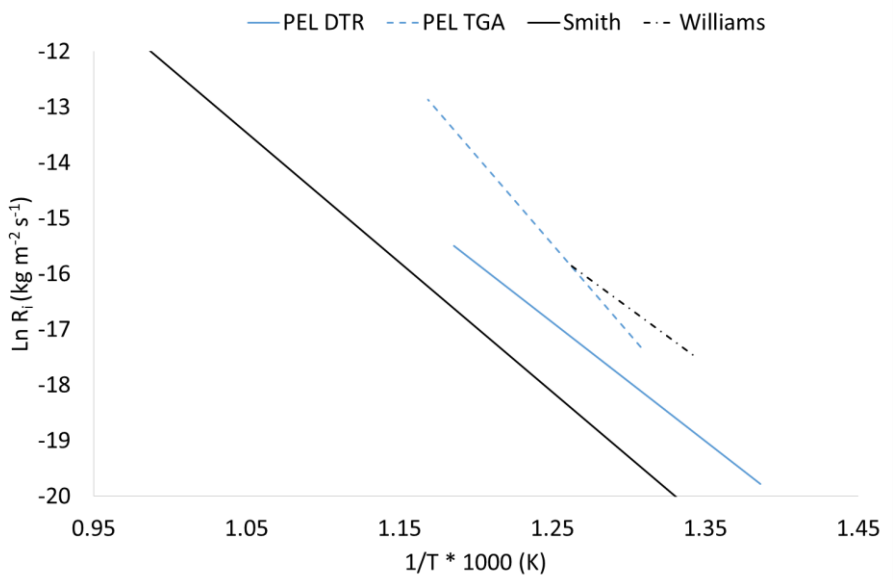

Figure 8.5: Intrinsic reactivity of PEL DTR and PEL N_2 TGA chars and comparison to intrinsic reactivity of chars from literature

The intrinsic reactivity of the chars, that is the reaction rate per unit area, reverse the order of reactivity of the DTR and TGA chars compared to the apparent reactivity determined seen in Figure 8.3, with the TGA char being the most reactive on an intrinsic basis. The surface area of the DTR char is significantly larger than the TGA chars (80 and 15 $m^2 g^{-1}$ respectively) suggesting a greater number of active sites available on the char surface. The increase in surface areas in chars produced using a DTR compared to a TGA are seen in work done by La Manquais (207). However the intrinsic reactivity of the PEL TGA chars is greater suggesting that the active sites of the PEL TGA chars are more reactive. This may be the result of thermal annealing in the DTR chars.

8.5 Discussion of combustion behaviour and apparent kinetics of TGA and DTR produced chars

As is shown throughout this chapter, the two char production techniques have a significant impact on the resulting char combustion behaviour and as a result the kinetic parameters determined.

The reactivity of a char is dependent on the chemical composition, the inorganic constituents and the morphological structure, which is especially influenced by the pyrolysis conditions, (107, 125, 127, 142, 158, 166, 167, 212, 213, 226, 270, 275, 279) as discussed in the literature review (section 3.5.3).

There are several differences in the techniques of char production used in this work. The particle size of the raw fuel used in the DTR is larger than that used in the TGA (PEL 75-180 µm and PWWP 212-355 µm in the DTR and <90 µm in the TGA) in order to prevent burnout and to provide sufficient char yield. The heating profiles of the two pieces of equipment also differ with the DTR temperature set to 1100^{o}C with a heating rate of 10^4 – 10^5 ^{o}C s^{-1}, compared to a maximum temperature of 1000^{o}C and heating rate of 16.6 ^{o}C s^{-1} in the TGA. This is due to the limitations of the TGA. As a result of the different particle heating rates (as described in section 5.5.2) and final temperatures, the particle residence times are much shorter in the DTR, ~0.5 seconds compared to ~1 minute in the TGA. In addition the DTR also contains ~1% O_2 to prevent the char from sticking to the inside of the DTR which provides readily available oxygen to react with the devolatilising particle.

The difference in the above char production techniques results in the difference in char characteristics highlighted in section 5.3. Chars produced using the DTR have a lower mass yield than the TGA chars of the same fuels, due to the higher heating rates and final temperature (125). However the DTR chars retain a larger portion of the volatiles whilst retaining less of the fixed carbon present in the raw fuel. This is believed to be the result of the oxygen present in the DTR pyrolysis gas (1 % O_2) reacting with the fuel surface enhancing carbon burnout and the low residence time (~0.5 s^{-1}) inhibiting complete devolatilisation.

There is also a significant change in the morphological structure of the DTR chars relative to the TGA chars, shown by the increase in surface area in the PEL DTR char. Additionally the SEM analysis of the PEL and PWWP chars, as seen in sections 5.6 and 5.7, provides further insight. The chars produced using the TGA exhibit an irregular shape but have become more rounded than the original fuels with irregular sharp edged particles attached to the surface. In contrast the DTR produced chars are well rounded and show a more developed porous

structure due to the greater rates at which devolatilisation proceeds. The higher volatile contents, relative inorganic content and enhanced morphological changes in the DTR chars results in a more reactive char as can be seen in Figure 8.3. However the difference in reactivity between the TGA and DTR chars is greatest in the PWWP fuel, due to the increased volatile content of the raw fuel and reactivity of the PWWP fuel during pyrolysis. Although the surface areas of the biomass samples were not determined, it is expected that the PWWP chars have a higher surface area than the PEL char. It is also thought that the difference between the TGA and DTR chars is also larger than in the PEL chars leading to the greater difference in the apparent reactivties of the PWWP chars.

The difference in porosity (as shown by the SEM, Figure 5.7 - Figure 5.8) and increase in surface area is believed to increase reactivity through the availability and accessibility of active sites and the enhanced rate of diffusion through the more porous structure (280). At the temperatures seen in the combustion experiments, Figure 8.2, the conversion range analysed (0.05-0.85) occurs at low temperatures, 300-500^{o}C in the PWWP chars and 400-600^{o}C in the PEL chars. As a result it is expected that the availability of active sites is more important than the diffusion rates in determining the reaction rates of the chars as combustion occurs under Regime I conditions (162). However the rate of diffusion in the smaller particles used in the TGA may be partially rate determining particularly at higher temperatures seen at the latter stages of conversion (>85% conversion) (207).

The result of the change in char production techniques and the differences in char characteristics result in the differences in char reactivity. Although the apparent reactivity of the DTR char indicates that it is more reactive than the TGA char (Figure 8.3), the intrinsic reactivity allows for the determination of the reactivity of the of the char material. It is well known that the surface area of a char changes during combustion (276, 281) but determination of this process is difficult. The use of the mth order model in determining the apparent reaction kinetics aims to represent the change in relative available surface area with conversion, but does not have any physical meaning (261). The inclusion of the surface area at the start of the conversion helps to give a better understanding of the reactivity of the char structure without having to measure changes to surface area during conversion.

The determination of the intrinsic reactivity results in the reversal of the char order of reactivity with the PEL TGA char more reactive than the PEL DTR char. This is thought to be due to the difference in the crystalline structure of the chars as a result of the degree of thermal annealing achieved during the two char preparation methods. It is expected that thermal annealing occurs during the char preparation step rather than the combustion step

where combustion is completed at relatively low temperatures (Combustion completed by 600^{o}C).

Thermal annealing is the restructuring of the turbostratically arranged carbon chains present in the parent fuel by loss of active sites, edges and defects on the surface of the particle. The process involves a broad range of solid state transformations to the carbon structure, the type of which is temperature dependent. In coals at low temperatures (<1000^{o}C) carbon hybridization and aromatization is preferred, at moderate temperatures (1000-1200^{o}C) stacking and re-ordering of the graphene layers is seen and at higher temperatures (>1400^{o}C) lateral growth of crystalline structures is seen (282, 283). The reduction of active sites hinders the oxygen accessibility which prevents the formation of surface oxides. Although the relationship between the crystalline order of a carbon and its reactivity is complex, in general, the reactivity of a carbon decreases as the crystalline structural order is increased as a result of thermal annealing (280-282, 284, 285).

From the above it is expected that the PEL DTR char undergoes thermal annealing to a greater degree than the PEL TGA char due to the higher temperatures seen in the DTR (1100^{o}C compared to 1000^{o}C in the TGA). The greater level of thermal annealing would result in a more stable less reactive char, which is seen in this work (Figure 8.5).However, oxygen present in the char production atmosphere (1% O_2 in the DTR) is known to inhibit the degree of thermal annealing through the formation of thermally stable surface oxides (282). In the work performed by Senneca et al (282) chars were produced in a nitrogen based atmosphere with small injections of oxygen throughout the 30 minute residence time to determine the effect of oxygen on the degree of thermal annealing. By pulsing the oxygen into the system the authors prevented carbon burnout. The PEL DTR char produced in this work using the DTR experienced higher oxygen levels than those seen in (282) which resulted in a large degree of carbon burnout, highlighted in Figure 5.3, where ~40 wt% of the original fixed carbon in the fuel is lost during char production. This suggests that rather than the mitigation of thermal annealing through stabilisation of the char surface through the formation of surface oxides, that carbon burnout occurred. As a result it is expected that the levels of oxygen present does not inhibit thermal annealing to a great extent. In addition the larger surface area measured in the PEL DTR char would suggest that the availability of active sites is increased relative to the TGA char and as a result reactivity would be increased. However it is shown that the intrinsic reactivity is greater in the TGA char suggesting that a higher degree of thermal annealing is seen in the DTR.

The aim of using the ballistic heating rates in the TGA was to produce chars that exhibit characteristics more comparable to those seen in pulverised fuel systems. The DTR has been widely used for this purpose but due to operational issues this can be difficult. The comparison of the ballistic heating rates in the TGA to the DTR gives a better understanding of the limitations of both char production methods.

Work has been done previously to analyse the two char production methods, La Manquais et al. (207) investigated the difference using a coal. The coal was devolatilised using a range of coal sizes, heating rates and final temperatures in the TGA. The resulting chars were combusted and isothermal mass loss profiles compared to those of DTR chars. It was found that a coal char prepared in a DTR at 1300^{o}C with a residence time of 0.4 s is comparable, in terms of combustion profile, to a char produced on a TGA at 1100^{o}C with a heating rate of 150^{o}C min^{-1}. Once the TGA final temperature was determined the heating rate was increased from 150^{o}C min^{-1} to 1800^{o}C min^{-1} to closer replicate conditions in the DTR. It was found that the increase in heating rate (150-1800^{o}C min^{-1}) produced a char with more comparable burnout profile than that produced at a lower heating rate. The authors reported that the devolatilisation temperature has a greater effect on the char reactivity than the heating rate (207). The authors also reported an increase in surface area and porosity in DTR chars compared to chars heated at 150^{o}C min^{-1} in the TGA, ranging from 3-95 times the surface area. This was attributed to the higher heating rates and the activation of the char from the oxygen present in the DTR (207), the same is seen in the work presented in this thesis.

Once a comparable char was produced on the TGA, the first order apparent kinetics were determined for a range of particle sizes in both the TGA and DTR. At larger particle size (>75 um) the reaction rate constant of the TGA chars is ~75% (at 525^{o}C) of those seen in the TGA chars (207). At the same temperature the apparent rate constant of the PEL char in the work in this thesis is decreased by 72% in TGA chars relative to DTR chars. The reaction rate of the PWWP TGA char at a comparable conversion level as the PEL char (x = 0.5) is ~6% of that seen in the PWWP DTR char, due to the higher reactivity of the PWWP fuel compared to PEL fuel. In general, the work done by La Manquais is in agreement with the work done here, that is, chars produced in a DTR are more reactive due to the enhanced morphological changes seen in a DTR. This is the result of the increase in heating rate, the higher temperatures used and the use of small concentrations of oxygen in the DTR.

As a result of the differences in char reactivity and morphology identified, La Manquis et al. concluded that a TGA could not be used to realistically imitate chars made using a DTR due to the lack of sufficient heating rate (207). However some of the char investigations

performed in that work, such as surface area and char morphology were performed on chars produced in a high heating rate furnace at a heating rate of 150°C min^{-1} (to produce the large amount of chars required) rather than the 1800°C min^{-1} used on the TGA to determine the apparent reactivity. It is well understood that both the residence time and heating rates used in char production can greatly impact the resulting char morphological characteristics (117, 118, 121, 127, 128). The resulting char surface area and char morphology determined for the heating rate of 150°C min^{-1} are expected to be different than if determined for the 1800°C min^{-1} char.

However, the TGA system does have some benefits. Chars produced on a TGA have been shown to be more uniformed in terms of properties, yields and the reactivity over a number of repeated experiments. La Manquais et al (207) reported the distribution in the reactivity of DTR chars is up to ten times that seen in the TGA due to variations and fluctuations in the operating conditions. The TGA provides a reliable, repeatable heating rate in a true pyrolysis atmosphere therefore mitigating the effect of char activation due to the oxygen that is present in a DTR. The amount of pyrolysis gas required in the TGA is also significantly lower in the TGA and as a large number of samples in both nitrogen and carbon dioxide are used in this work the TGA method was preferred (16 L min^{-1} in the DTR compared to 50 mL min^{1} in the TGA). The flexibility of the TGA in terms of the ability to control the gas atmospheres is also beneficial, the chars produced in the TGA are directly combusted at the end of the pyrolysis process and are not exposed to any outside influence as the DTR chars are during transfer to the TGA. Finally pyrolysis in a TGA, even at high heating rates, allows for a better understanding of the behaviour of the fuel during pyrolysis through the analysis of mass loss data and an accurate measurement of the char yield rather than determination by the ash tracer method.

The work in this thesis utilised the higher heating rates available in the TGA as the majority of the work is comparing both air combustion to oxy-fuel combustion and the comparison of a number of different fuels. The variation in char properties seen by La Manquis et al., as a result if the operating conditions does not lend itself to the analysis of a wide range of fuels or combustion environments. Although the work performed on the TGA is at much lower temperatures and heating rates than those seen in pulverised fuel combustion systems (10^{5-6} K s^{-1} (286) and flame temperatures of ~1600°C (62)) the results provide a useful insight into the kinetics of char combustion (282) and the difference in char production methods.

8.6 Conclusions

- The chars produced from PEL and PWWP fuels using ballistic heating rates in a TGA and high heating rates in a DTR (both in nitrogen atmospheres) were compared in terms of combustion behaviour (in air), apparent kinetics and the PEL chars in terms of intrinsic reactivity.
- The PWWP chars are more reactive than the PEL chars in both char preparation methods.
- The chars produced using the TGA, resulted in an increase in the key temperatures and rates of mass loss identified relative to the DTR chars.
- The apparent reactivity of the DTR chars is higher than the TGA chars, especially in the case of the PWWP fuel. The PEL DTR chars becomes less reactive at higher temperatures where it converges with the TGA char.
- The change in char production method has a greater effect on the combustion behaviour in the PWWP char compared to the PEL char.
- The intrinsic reactivity of the PEL chars was determined and it was found that the reactivity of PEL TGA char is greater than the PEL DTR char. This indicates that the active sites of the PEL TGA chars are more reactive than the PEL DTR chars.
- There is evidence of enhanced thermal annealing in the PEL DTR char when compared to the PEL TGA char.
- There is a significant difference between the DTR and TGA produced chars in terms of the combustion kinetics as a result of the differences in chemical composition and char morphology as outlined in section 5.
- Using the TGA as a char production method at high heating rates offers some benefits over the DTR such as repeatability, true pyrolysis environments and continued monitoring of the devolatilisation steps during devolatilisation.

9 Response to the aims and objectives of the thesis

This section answers the main research questions outlined in chapter 2.

1. **How does the change in combustion atmosphere effect the overall combustion behaviour of the fuels?**

To answer this question the fuels were combusted in a TGA in air and oxy-fuel environments and is reported in Chapter 6. In general the change from air to oxy-fuel combustion at 21% O_2/CO_2 has a small effect on the overall combustion behaviour of the fuels at the heating rates and temperatures used in this work ($10^oC\ min^{-1}$, 900^oC) . The initial stage of combustion, drying, shows no difference in mass loss behaviour. The second stage of combustion, devolatilisation, and the effect of the change in atmosphere is more easily identified in the biomass and TSP fuels due to the larger volatile content and associated peaks seen in the mass loss profiles. The key indicators identified show that the devolatilisation stage is almost identical in the two atmospheres at the slower heating rates used. As combustion proceeds and the temperature increases the difference between the two atmospheres is more pronounced and the greatest difference in the key indicators is seen during the char combustion in all fuels. At this stage of combustion a carbon rich char is present which undergoes heterogeneous combustion, the rate of which is partially controlled by the surface areas and the availability and reactivity of the active sites. The competition for the active sites between the O_2 and CO_2 present in the oxy-fuel environment results in a delay in the oxy-fuel atmosphere. The differences between combustion in air and oxy-fuel combustion are more pronounced in the coals, this is due to the higher reactivity of the biomass fuels. The changes in the key indicators reported for the torrefied spruce fuel fall between the coal and raw biomass samples, as would be expected as torrefaction is the process of upgrading biomass to have properties more comparable to coals.

The oxygen concentrations in the oxy-fuel environment were varied from 5-30% O_2/CO_2 to determine how the fuels may combust a the varying oxygen levels found in a pulverised fuel boiler. The increase in oxygen concentration results in the increased rate of combustion with the mass loss profiles shifting to lower temperatures and the peak rates of mass loss increasing in all fuels, but is again more pronounced in the coals. At low oxygen concentrations (5-10% O_2/CO_2) the difference in mass loss behaviour is at its greatest and as the oxygen concentration is increased (>21%) the differences in the overall combustion behaviour is decreased. At the higher oxygen concentrations (>21%) the biomass fuels show only a small difference in combustion behaviour, while the differences are larger in the coals

with the TSP fuel again falling between the two. This is due to the higher reactivity of the biomass fuel and the readily available oxygen inherent in the fuel, sustaining combustion.

In order to produce combustion profiles similar to those seen in air, in terms of comparable key indicators, it is suggested that the oxygen concentration needs to be increased in the oxy-fuel atmospheres to 21-30% O_2/CO_2.

In general the change from air to oxy-fuel combustion and the increase in oxygen concentration in oxy-fuel environments has more of an effect on the coals than the biomass fuels at the low heating rates and temperatures used in chapter 6.

2. **How is the devolatilisation process affected by the change in combustion atmosphere and does this differ between biomass and coal samples?**

The effects of the change in combustion atmosphere on the devolatilisation process at low heating rates were determined through the derivation of apparent first order kinetics and their associated kinetic parameters (Chapter 6). The kinetic parameters were derived using the overall combustion mass loss profiles determined at low heating rates ($10^oC\ min^{-1}$). Comparison of the kinetic parameters derived from combustion in air and 21% O_2/CO_2 atmospheres highlights the similarity in devolatilisation behaviour with the kinetic parameters almost identical in all of the fuels.

The increase in oxygen concentration in the oxy-fuel environments results in the linear increase in the kinetic parameters with evidence of the kinetic compensation effect. The linear trends determined allowed for the derivation of fuel specific empirical equations that relate the devolatilisation rate constant to the oxygen content present in the combustion atmosphere. The greatest change in kinetic parameters is seen in the biomass fuels due to the increased volatile content present in the parent fuels, although the larger change in kinetic parameters did not equate to a greater degree of change in the reactivity. The development of an empirical model is useful for modelling where in a flame, particles may experience a wide range of oxygen conditions throughout the combustion process. When comparing the kinetic parameters determined for devolatilisation in air and in 21% O_2/CO_2 no significant difference is seen in all of the fuels.

In general no significant difference is seen in the devolatilisation behaviour of the fuels when low heating rates are utilised and fuels are combusted in air and 21% O_2/CO_2. The change in oxygen concentrations in the oxy-fuel environments has a greater effect on the biomass

fuels than the coals, which was identified through the derivation of kinetic parameters and key indicators. The devolatilisation process can be successfully described by fuel specific empirical equations based on the oxygen concentration present in the combustion atmosphere (Table 6.11). This is useful for CFD modelling and process optimisation.

3. **What effect does the devolatilisation atmosphere have on the resulting char properties?**

In order to investigate the differences in devolatilisation behaviour chars were produced at ballistic heating rates and increased final temperatures (1000 ^{o}C min^{-1}, 1000^{o}C) in N_2 and CO_2 atmospheres (chapter 5). The ballistic heating rates and N_2 and CO_2 atmospheres were used to better replicate the pyrolysis conditions experienced by a fuel particle seen in a pulverised fuel burner. It was found that when the coals are pyrolysed at ballistic heating rates the char yield is similar to the theoretical char yield in both the N_2 and CO_2 environments (char yields within 1 wt%). In addition to the analysis of the char yields proximate and ultimate analysis were performed to further understand the ballistic devolatilisation process. The differences in relative volatile and fixed carbon yield (that is the percentage of volatiles present in the fuel remaining in the char) indicate that the change in the char production atmosphere does not affect the composition of the chars. However the coal chars produced in the CO_2 atmosphere have higher surface areas than the N_2 produced chars indicating that the char – CO_2 gasification reaction is occurring at the particle surface. The biomass and torrefied spruce fuels show evidence of enhanced devolatilisation in the CO_2 atmosphere relative to the N_2 atmosphere, which was not seen in the coals. The char yield of the biomass is half and the torrefied spruce two-thirds when produced in CO_2 of that seen in the N_2 atmospheres. The decrease in char yield is the result of the loss of fixed carbon which is evidence of the char – CO_2 gasification reaction, identified through the comparison of relative volatile and fixed carbon content. The differences between the coals, the biomass and the torrefied biomass are due to the increased reactivity of the biomass fuels.

4. **How is the char combustion process affected by the change in combustion atmosphere and does this differ between biomass and coal samples?**

In order to investigate char combustion behaviour chars were produced at ballistic heating rates using the TGA and combusted in the full range of combustion atmospheres (chapter 7). The mass loss profiles were analysed and key indicators identified for comparison. In

addition, the apparent kinetics were determined which were then used to develop fuel specific n^{th} order reactivity models based on the partial pressure of oxygen in the combustion atmosphere. In addition the intrinsic reactivity of the coal chars were determined to give a better understanding of the reactivity of the carbon present in the char.

The difference in combustion behaviour between the air and oxy-fuel combustion environment (chars produce in N_2 combusted in air and CO_2 combusted in 21% O_2/CO_2) is most evident in the biomass and TSP chars. The lower char yields and differences in the composition resulted in very different mass loss combustion profiles. The biomass and TSP CO_2 chars combusted at lower temperatures with the peak rates of mass loss seen 40 - 50^oC lower than the N_2 char. However the maximum rate of mass loss is much larger in the N_2 chars. In order to determine if the differences could be attributed to the combustion atmosphere only the same char (PWWP CO_2) was combusted in air and 21% O_2/CO_2. When combusted in 21% O_2/CO_2 a delay is seen relative to the same biomass char combusted in air, suggesting that the overall differences in the combustion behaviour of the N_2 and CO_2 char could not be the result of the combustion atmosphere only. It is suggested by Molina (266) that potassium present in the fuel enhances the chemisorption of CO_2. The high levels of potassium present in the biomass fuel enhance chemisorption of CO_2 and result in a delay when the identical char is combusted in the oxy-fuel atmosphere. The difference in the combustion profiles of the biomass chars produced in N_2 and CO_2 is therefore the result of both the char preparation atmosphere and the combustion atmosphere. The char production atmosphere and as a result the change in char characteristics is shown to have more of an effect than the combustion atmosphere.

The difference between air and 21% O_2/CO_2 is less severe in the coals due to the similarities in the chars produced. The combustion profile of the N_2 produced coal chars is shifted to higher temperatures indicating a delay in combustion behaviour relative to the CO_2 char combusted in 21% O_2/CO_2. Again an identical char (PEL CO_2) was combusted in air and 21% O_2/CO_2 and in the case of coals no difference in mass loss behaviour is seen, meaning that the differences in combustion environment does not char combustion stage and the differences seen are due to char production atmosphere. The CO_2 chars exhibit larger surface areas, which increase reactivity through the availability of active sites.

The increase in oxygen concentrations in the oxy-fuel environments has a greater effect on the coal chars than the biomass chars with the largest change in key temperatures and rates of mass loss determined. This is due to the increased inherent oxygen content of the biomass chars providing readily available oxygen for the char – O_2 reaction.

The apparent reactivity of the chars (section 7.3.1) were determined from the char combustion profiles mentioned above. The apparent kinetic parameters of the coals and torrefied spruce chars show evidence of the kinetic compensation effect as seen in the devolatilisation step, however the change in activation energy as a function of oxygen concentration is not linear. The biomass chars did not show evidence of a linear kinetic compensation effect. The change in kinetic parameters is more pronounced in the coal chars and the change is greater than that seen during the devolatilisation stage. This is due to the higher char content of the fuels. The change in kinetic parameters is smaller in the biomass chars than was seen in the devolatilisation stage, due to the lower char yields.

The apparent kinetic parameters were utilised in determining fuel specific char reactivity n^{th} order models (section 7.3.2) which can be used to highlight the differences in the fuels. The coal chars have a reaction order almost double that found in the biomass and torrefied spruce chars again highlighting the increased sensitivity of the coal chars to the increase in oxygen concentration. The n^{th} order models derived were found to suitably predict char conversion behaviour of all fuels in the full range of oxy-fuel combustion atmospheres.

The intrinsic reactivity of the coal chars were determined and the reactivity order of the chars is reversed compared to the apparent reactivity, that is that the N_2 chars are more reactive than the CO_2 chars combusted in 21% O_2/CO_2. This suggests that the carbon of the N_2 chars is more reactive and indicates that the CO_2 present in the char production atmosphere may enhance crosslinking during char production stabilising the char structure and reducing reactivity.

In general the mass loss profiles move to lower temperatures when chars are combusted in 21% O_2/CO_2 relative to combustion in air. This is the result of the changes in the devolatilisation behaviour rather than the differences in combustion atmosphere. These changes are reflected in the apparent reactivity kinetic parameters determined. The increase in oxygen in the oxy-fuel environments has a greater effect on the coals due to the higher char content which is again reflected in the n^{th} order kinetic parameters determined. Although the apparent reactivity of the N_2 produced char is higher than the CO_2 char the trend is reversed on an intrinsic basis, suggesting that CO_2 may enhance crosslinking of the CO_2 chars during char production and hence reducing the reactivity of the char matrix.

5. **Are there any differences in the combustion behaviours of coal, biomass and torrefied biomass and are there any lessons that can be learnt by industry?**

There are significant differences in how the types of fuel behave during combustion, which are highlighted in chapters 5, 6 and 7. The biomass and torrefied biomass fuels are overall more reactive than the coals, particularly during the initial stages of combustion. The biomass fuels have been shown to be more sensitive to the devolatilisation atmosphere (at ballistic heating rates). The coal chars although comparable in terms of yield and composition due show morphological changes as a result of char production atmosphere. The above results in chars with different properties that effect the char combustion process. The differences in the combustion behaviour of the chars is greatest in the biomass fuels when comparing the char production atmosphere, but the coal chars are most sensitive to the change in oxygen conditions in the oxy-fuel atmosphere. These differences suggest that an increase in oxygen is required in oxy-fuel atmospheres to match the conditions seen in conventional air to produce comparable mass loss profiles. It is expected that 21-25% O_2/CO_2 is sufficient for the biomass and 25-30% O_2/CO_2 is required for the coals. The derivation of Empirical models for both the devolatilisation and char combustion stages can be useful to determine the fuel specific oxygen requirements through use in CFD modelling. The increase in oxygen requirement is expected to have economic implications for the development of CCS plants, through sizing and operation of the ASU and also the mitigation of potential safety issues associated with the high levels of oxygen required for coal CCS. However the combustion behaviour is only a small part of the process, heat transfer properties due to gas volumes are a particular concern especially if existing plants are to be retrofitted to oxy-fuel combustion.

6. **Can chars produced using a TGA replicate chars produced using a drop tube reactor and is this a reliable method for the investigation of char oxy-fuel combustion?**

A coal and biomass char were produced using both the TGA and DTR in a nitrogen atmosphere (chapter 8). It was found that a TGA will not produce chars with the same properties seen when produced with a DTR. The larger particle size, higher heating rates and higher final temperature seen in the DTR produced chars result in a smaller yield due to the carbon burnout due to the low levels of oxygen present in the DTR system. The resulting DTR chars contained a higher volatile content and lower fixed carbon content. The DTR chars were found to be more reactive than the TGA chars thought to be due to the higher volatile

content and the increased surface areas as a result of the increased devolatilisation rates. The determination of the intrinsic reactivity of the PEL TGA and DTR indicates that thermal annealing may be taking place in the DTR, due to the higher temperatures and heating rates. Although it was not possible to produce chars using the TGA that replicate DTR chars, the TGA is able to provide a true pyrolysis atmosphere and was found to be highly repeatable. This repeatability was key in order to produce a significant amount of char needed in this study.

10 Future work

In this work a small range of fuels have been investigated and the devolatilisation and char combustion behaviour and associated kinetics derived. In order to better understand the fuels used in this work it is suggested that several additional experiments could be performed to enhance the knowledge gained here.

Firstly in the experiments using the TGA the particles are assumed to be independent of each other, well dispersed and are not exchanging heat. Variation of the mass sample in the TGA pan under the same operating conditions would result in the same rates of mass loss if the particles are independent. This would also give further evidence that the TGA experiments are not mass transfer limited.

Secondly the determination of the biomass char surface areas and determination of the pore structures in all chars is suggested, helping to give a better understanding of both the char production and char combustion stages. It is suggested that longer sample tubes which would allow for a larger mass of sample should be used in the NOVA 2200E which may make surface area and porosity measurements more accurate. However, if the difficulty in determining the char surface areas of biomass char still arises determination of surface area and porosity may require a different methodology than the gas adsorption method used for the coals. In addition char image analysis could be performed and the results including knowledge of the porosity may be used to relate the work in this thesis to the char classification scheme developed by the international committee for coal and organic petrology (244). This would also give a better understanding of the differences between char production in a TGA vs DTR.

It is also suggested that the kinetic parameters determined from the char combustion should be extrapolated to higher temperatures (with the greater understanding of the surface area). This would enable a better understanding of how reactive a fuel is at flame temperatures.

The same fuels may also be investigated using experimental equipment that operate at higher temperatures such as an entrained flow reactor or DTR (with oxy-fuel environments) to determine the reactivity of the fuels and chars at temperatures high enough for the char – CO_2 gasification occur. The reactivity and kinetic parameters are determined from knowledge of the CO/CO_2 ratio measured during combustion, an experiment we are unable to perform at the current time.

Additionally some interesting points have been identified in this work that require further investigation. The propensity for CO_2 chemisorption during both the char production and char combustion stages should be investigated further and in particular the influence of the inorganic constituents.

The experiments here should be performed on a wider range of fuels particularly no woody energy crops such as miscanthus to determine if any trends are biomass type specific.

The results in this thesis lend themselves to life cycle analysis and could be used to better understand the potential benefits of CCS and in particular the potential negative emissions associated with BECCS. Finally the devolatilisation and combustion kinetic models determined in this work should be applied to CFD models.

11 References

1. IPCC. *Climate Change 2014–Impacts, Adaptation and Vulnerability: Regional Aspects.* Cambridge University Press, 2014.
2. MYHRE, G., D. SHINDELL, F.-M. BRÉON, W. COLLINS, J. FUGLESTVEDT, J. HUANG, D. KOCH, J.-F. LAMARQUE, D. LEE, B. MENDOZA, T. NAKAJIMA, A. ROBOCK, G. STEPHENS, T. TAKEMURA AND H. ZHANG, . *The Physical Science Basis. Contribution of Working Group 1 to the Fifth Assessment Report of the Intergovernmental Panel on Climate Change*. United Kingdom: Intergovernmental Panel on Climate Change, 2013.
3. NATIONS, U. *Paris Agreement.* 2015.
4. UNFCCC. *Paris Agreement - Status of Ratification* [online]. 2016. [Accessed 2/11/2016]. Available from: http://unfccc.int/paris_agreement/items/9444.php.
5. EUROPEAN COMMISSION. Directive 2009/28/EC of the European Parliament and of the Council of 23 April 2009 on the promotion of the use of energy from renewable sources and amending and subsequently repealing Directives 2001/77/EC and 2003/30. *Official Journal of the European Union*, 2009, pp.1-47.
6. CCC. *UK climate action following the Paris agreement.* London, 2016.
7. CCC. *The Fifth Carbon Budget- The next step towards a low carbon economy.* London, 2015.
8. DECC. *Final Statement for the First Carbon Budget Period.* London, 2014.
9. DECC. *Updated Energy and Emissions Projections 2015.* London, 2015.
10. CCC. *Meeting Carbon Budgets - 2016 Progress Report to Parliament.* London, 2016.
11. CCC. *Meeting Carbon Budgets - Implications of Brexit for UK climate policy.* London, 2016.
12. HMG. *Government response to the committee on climate change - Progress on meeting carbon budgets.* 2016.
13. UK GOV. *Energy Act 2013.* London: The Stationary Office, 2013.
14. LCCC. *CfD Register* [online]. 2016. [Accessed 08/11/2016]. Available from: https://lowcarboncontracts.uk/cfds.
15. NATIONAL GRID. *Final Auction Results - T-$ Capacity Market Auction for 2019/20.* 2016.
16. WMO. *Globally Averaged CO2 Levels Reach 400 parts per million in 2015* [online]. 2016. [Accessed 09/11/2016]. Available from: http://public.wmo.int/en/media/press-release/globally-averaged-co2-levels-reach-400-parts-million-2015.
17. IPCC. *Climate Change 2014: Mitigation of Climate Change. Contribution of Working Group III to the Fifth Assessment Report of the Intergovernmental Panel on Climate Change [Edenhofer, O., R. Pichs Madruga, Y. Sokona, E. Farahani, S. Kadner, K. Seyboth, A. Adler, I. Baum, S. Brunner, P. Eickemeier, B. Kriemann, J. Savolainen, S. Schlömer, C. von Stechow, T. Zwickel and J.C. Minx (eds.)].* Cambridge, United Kingdom and New York, NY, USA.: Cambridge University Press, 2014.
18. IEA. *World ENergy Outlook 2016 - Executive Summary.* Paris, 2016.
19. UNEP. *The Emissions Gap Report 2016.* Nairobi, 2016.

20. DECC. *2014 UK Greenhouse Gas Emissions, FInal Figures.* London: Crown 2016.
21. DECC. *2014 UK Greenhouse Gas Emissions: Final Figures - Data Tables* 2014.
22. DECC. *Amber Rudd's speech on direction for UK energy policy.* 2015.
23. BEIS. *Energy Trends September 2016.* London, 2016.
24. ECCC. *2020 renewable heat and transport targets - Second report of session 2016-17.* London, 2016.
25. DECC, DOT and DEFRA. *UK Bioenergy Strategy.* London, 2012.
26. OFGEM. *Renweables Obligation: Sustainability Criteria.* 2016.
27. THEK, G. and OBERNBERGER, I. *The Pellet Handbook: The production and thermal utilisation of biomass pellets.* Earthscan, 2010.
28. DECC. *Consignments and Mass Balance Approaches.* London: Crown, 2014.
29. GREAT BRITAIN. E. UNION. *REGULATION (EU) No 995/2010 OF THE EUROPEAN PARLIAMENT AND OF THE COUNCIL*. (L 295/23). 2010.
30. DECC. *Woodfuel Advice Note.* London Crown, 2014.
31. FORESTRY COMISSION. *The UK Forestry Standard - The Governments approach to sustainavle forestry.* Edinburgh: Crown, 2011.
32. IWPB. *Report No 1 - Proposal for sustainability principles for woody biomass sourcing and trading.* 2012.
33. OFGEM. *Biomass Sustainability.* 2016.
34. OFGEM. Biomass Sustainability Dataset 2014-15. 2016.
35. RÖDER, M., WHITTAKER, C. and THORNLEY, P. How certain are greenhouse gas reductions from bioenergy? Life cycle assessment and uncertainty analysis of wood pellet-to-electricity supply chains from forest residues. *Biomass and bioenergy*, 2015, **79**, pp.50-63.
36. ADAMS, P., BOWS, A., GILBERT, P., HAMMOND, J., HOWARD, D., LEE, R., MCNAMARRA, N., THORNLEY, P., WHITTAKER, C. and WHITAKER, J. Understanding the greenhouse gas balances of bioenergy systems. 2013.
37. ECCC. *Future of carbon capture and storage in the UK - Second Report of Session 2015–16.* London: The Stationary Office, 2016.
38. STYRING, P., JANSEN, D., DE CONINCK, H., REITH, H. and ARMSTRONG, K. *Carbon Capture and Utilisation in the green economy.* Centre for Low Carbon Futures, 2011.
39. IPCC. *IPCC Special Report on Carbon Dioxide Capture and Storage. Prepared by Working Group III of the Intergovernmental Panel on Climate Change [Metz, B., O. Davidson, H. C. de Coninck, M. Loos, and L. A. Meyer (eds.)].* Cambridge, United Kingdom and New York, NY, USA: Cambridge University Press, 2005.
40. GIBBINS, J. and CHALMERS, H. Carbon capture and storage. *Energy Policy*, 2008, **36**(12), pp.4317-4322.
41. TAN, Z. *Air pollution and greenhouse gases: from basic concepts to engineering applications for air emission control.* Springer, 2014.
42. LEUNG, D.Y.C., CARAMANNA, G. and MAROTO-VALER, M.M. An overview of current status of carbon dioxide capture and storage technologies. *Renewable and Sustainable Energy Reviews*, 2014, **39**, pp.426-443.
43. FENNELL, P. 1 - Calcium and chemical looping technology: An introduction. *In: Calcium and Chemical Looping Technology for Power Generation and Carbon Dioxide (CO2) Capture*. Woodhead Publishing, 2015, pp.3-14.

44. BOOT-HANDFORD, M.E., ABANADES, J.C., ANTHONY, E.J., BLUNT, M.J., BRANDANI, S., MAC DOWELL, N., FERNÁNDEZ, J.R., FERRARI, M.-C., GROSS, R. and HALLETT, J.P. Carbon capture and storage update. *Energy & Environmental Science*, 2014, **7**(1), pp.130-189.
45. GLOBAL CCS INSTITUTE. *Advantages and disadvantages of major CO2 capture technologies* [online]. 2016. [Accessed 24/11/2016]. Available from: https://hub.globalccsinstitute.com/publications/technology-options-co2-capture/advantages-and-disadvantages-major-co2-capture.
46. IEA CLEAN COAL CENTRE. *Post-combustion carbon capture from coal fired plants - solvent scrubbing.* UK London: IEA Clean Coal Centre, 2007.
47. LUIS, P. Use of monoethanolamine (MEA) for CO2 capture in a global scenario: Consequences and alternatives. *Desalination*, 2016, **380**, pp.93-99.
48. NIELSEN, C.J., D'ANNA, B., DYE, C., GRAUS, M., KARL, M., KING, S., MAGUTO, M.M., MÜLLER, M., SCHMIDBAUER, N., STENSTRØM, Y., WISTHALER, A. and PEDERSEN, S. Atmospheric chemistry of 2-aminoethanol (MEA). *Energy Procedia*, 2011, **4**, pp.2245-2252.
49. AARON, D. and TSOURIS, C. Separation of CO2 from Flue Gas: A Review. *Separation Science and Technology*, 2005, **40**(1-3), pp.321-348.
50. BUHRE, B.J.P., ELLIOTT, L.K., SHENG, C.D., GUPTA, R.P. and WALL, T.F. Oxy-fuel combustion technology for coal-fired power generation. *Progress in energy and combustion science*, 2005, **31**(4), pp.283-307.
51. TOFTEGAARD, M.B., BRIX, J., JENSEN, P.A., GLARBORG, P. and JENSEN, A.D. Oxy-fuel combustion of solid fuels. *Progress in energy and combustion science*, 2010, **36**(5), pp.581-625.
52. PERRIN, N., DUBETTIER, R., LOCKWOOD, F., TRANIER, J.-P., BOURHY-WEBER, C. and TERRIEN, P. Oxycombustion for coal power plants: Advantages, solutions and projects. *Applied Thermal Engineering*, 2015, **74**, pp.75-82.
53. MARION J L, K.F., LEVASSEUR A A, NSAKALA N Y, GRUBBSTROM J, LEANDRI J-F. Alstom's 15 MW oxy-fuel test programme for tangential firing. *In: 1st oxyfuel combustion conference* Cottbus, Germany. 2009.
54. XU, B., STOBBS, R.A., WHITE, V., WALL, R.A., GIBBONS, J., LIJIMA, M. and MACKENZIE, A. *FUTURE CO2 CAPTURE TECHNOLOGY OPTIONS FOR THE CANADIAN MARKET - Technical Report Report No. COAL R309 BERR/Pub URN 07/1251 Doosan Babcock Energy Limited (March 2007).* 2007.
55. ESCUDERO, A.I., ESPATOLERO, S., ROMEO, L.M., LARA, Y., PAUFIQUE, C., LESORT, A.-L. and LISZKA, M. Minimization of CO2 capture energy penalty in second generation oxy-fuel power plants. *Applied Thermal Engineering*, 2016, **103**, pp.274-281.
56. IEA CLEAN COAL CENTRE. *Developments in oxyfuel combustion of coal.* London: IEA Clean Coal Centre, 2014.
57. DILLON DJ, W.V., ALLAM RJ, WALL RA, GIBBINS J. . *Oxy Combustion Processes for CO2 capture from power plant. Engineering Investigation Report, 2005/9, IEA Greenhouse Gas Research and Development Programme.* 2005.
58. ZANGANEH, K.E. and SHAFEEN, A. A novel process integration, optimization and design approach for large-scale implementation of oxy-fired coal power plants with CO2 capture. *International Journal of Greenhouse Gas Control*, 2007, **1**(1), pp.47-54.

59. TRABADELA, I., CHALMERS, H. and GIBBINS, J. Oxy-biomass Ignition in Air and Relevant Oxy-combustion Atmospheres for Safe Primary Recycle and Oxy-burner Development. *Energy Procedia*, 2014, **63**, pp.403-414.
60. CHEN, L., YONG, S.Z. and GHONIEM, A.F. Oxy-fuel combustion of pulverized coal: Characterization, fundamentals, stabilization and CFD modeling. *Progress in energy and combustion science*, 2012, **38**(2), pp.156-214.
61. BUHRE, B., ELLIOTT, L., SHENG, C., GUPTA, R. and WALL, T. Oxy-fuel combustion technology for coal-fired power generation. *Progress in energy and combustion science*, 2005, **31**(4), pp.283-307.
62. WALL, T., LIU, Y., SPERO, C., ELLIOTT, L., KHARE, S., RATHNAM, R., ZEENATHAL, F., MOGHTADERI, B., BUHRE, B. and SHENG, C. An overview on oxyfuel coal combustion—state of the art research and technology development. *Chemical Engineering Research and Design*, 2009, **87**(8), pp.1003-1016.
63. ZHENG, L. *Oxy-fuel combustion for power generation and carbon dioxide (CO2) capture.* Elsevier, 2011.
64. EC. *Feasibility study for Europe wide CO_2 Infrastructure.* 2010.
65. CHOI, Y.-S., NESIC, S. and YOUNG, D. Effect of impurities on the corrosion behavior of CO2 transmission pipeline steel in supercritical CO2− water environments. *Environmental science & technology*, 2010, **44**(23), pp.9233-9238.
66. POST. *CO_2 Capture, Transport and Storage.* London, 2009.
67. SIGFUSSON, B., GISLASON, S.R., MATTER, J.M., STUTE, M., GUNNLAUGSSON, E., GUNNARSSON, I., ARADOTTIR, E.S., SIGURDARDOTTIR, H., MESFIN, K., ALFREDSSON, H.A., WOLFF-BOENISCH, D., ARNARSSON, M.T. and OELKERS, E.H. Solving the carbon-dioxide buoyancy challenge: The design and field testing of a dissolved CO2 injection system. *International Journal of Greenhouse Gas Control*, 2015, **37**, pp.213-219.
68. MATTER, J.M., STUTE, M., SNÆBJÖRNSDOTTIR, S.Ó., OELKERS, E.H., GISLASON, S.R., ARADOTTIR, E.S., SIGFUSSON, B., GUNNARSSON, I., SIGURDARDOTTIR, H. and GUNNLAUGSSON, E. Rapid carbon mineralization for permanent disposal of anthropogenic carbon dioxide emissions. *Science*, 2016, **352**(6291), pp.1312-1314.
69. ALVARADO, V. and MANRIQUE, E. Enhanced oil recovery: an update review. *Energies*, 2010, **3**(9), pp.1529-1575.
70. EUROPIPE, C. *Towards a transport infrastructure for large scale CCS in Europe.* 2011.
71. KOVSCEK, A. Screening criteria for CO2 storage in oil reservoirs. *Petroleum Science and Technology*, 2002, **20**(7-8), pp.841-866.
72. ZWEIGEL, P., ARTS, R., LOTHE, A.E. and LINDEBERG, E.B. Reservoir geology of the Utsira Formation at the first industrial-scale underground CO2 storage site (Sleipner area, North Sea). *Geological Society, London, Special Publications*, 2004, **233**(1), pp.165-180.
73. SCHILLING, F., BORM, G., WÜRDEMANN, H., MÖLLER, F., KÜHN, M. and GROUP, C.S. Status report on the first European on-shore CO2 storage site at Ketzin (Germany). *Energy Procedia*, 2009, **1**(1), pp.2029-2035.

74. ROMANAK, K.D., BENNETT, P., YANG, C. and HOVORKA, S.D. Process-based approach to CO2 leakage detection by vadose zone gas monitoring at geologic CO2 storage sites. *Geophysical Research Letters*, 2012, **39**(15).
75. WILLIAMS, R.G. and FOLLOWS, M.J. *Ocean dynamics and the carbon cycle: Principles and mechanisms.* Cambridge University Press, 2011.
76. IEA. *20 Years of Carbon Capture and Storage - Accelerating Future Deployment.* Paris, France,, 2016.
77. IEAGHG. *Potential for biomass and carbon dioixde capture and storage.* 2011.
78. GŁADYSZ, P. and ZIĘBIK, A. Environmental analysis of bio-CCS in an integrated oxy-fuel combustion power plant with CO2 transport and storage. *Biomass and bioenergy*, 2016, **85**, pp.109-118.
79. SANZ-PÉREZ, E.S., MURDOCK, C.R., DIDAS, S.A. and JONES, C.W. Direct Capture of CO2 from Ambient Air. *Chemical Reviews*, 2016, **116**(19), pp.11840-11876.
80. THE ROYAL SOCIETY. *Geo-engineering the climate. Science, governance and security.* London: The Royal Society,, 2009.
81. KINDERMANN, G., OBERSTEINER, M., SOHNGEN, B., SATHAYE, J., ANDRASKO, K., RAMETSTEINER, E., SCHLAMADINGER, B., WUNDER, S. and BEACH, R. Global cost estimates of reducing carbon emissions through avoided deforestation. *Proceedings of the National Academy of Sciences*, 2008, **105**(30), pp.10302-10307.
82. STRENGERS, B.J., VAN MINNEN, J.G. and EICKHOUT, B. The role of carbon plantations in mitigating climate change: potentials and costs. *Climatic Change*, 2008, **88**(3), pp.343-366.
83. VAN VUUREN, D.P., DEETMAN, S., VAN VLIET, J., VAN DEN BERG, M., VAN RUIJVEN, B.J. and KOELBL, B. The role of negative CO2 emissions for reaching 2 °C—insights from integrated assessment modelling. *Climatic Change*, 2013, **118**(1), pp.15-27.
84. GLOBAL CCS INSTITUTE. *Large-Scale CCS Projects – Definitions* [online]. 2016. [Accessed 30/11/2016]. Available from: http://www.globalccsinstitute.com/projects/large-scale-ccs-projects-definitions.
85. DECC. *HM Government Statement to Markets Regarding Carbon Capture and Storage Competition.* 2016.
86. OXBURGH. *LOWEST COST DECARBONISATION FOR THE UK: THE CRITICAL ROLE OF CCS - Report to the Secretary of State for Business, Energy and Industrial Strategy from the Parliamentary Advisory Group on Carbon Capture and Storage (CCS)".* 2016.
87. EC. *Climate Action - NER 300 Programme* [online]. 2016. [Accessed 25/11/2016]. Available from: https://ec.europa.eu/clima/policies/lowcarbon/ner300/index_en.htm.
88. ETI. *Reducing the cost of CCS: Developments in capture plant technology.* Loughborough, 2016.
89. ETI. *The evidence for deploying bioenergy with CCS (BECCS) in the UK.* Loughborough, 2016.
90. THE WHITE HOUSE. *U.S.-China Joint Announcement on Climate Change* [online]. 2014. [Accessed 25/11/2016]. Available from:

https://www.whitehouse.gov/the-press-office/2014/11/11/us-china-joint-announcement-climate-change.
91. SMITH, K.L., SMOOT, L.D., FLETCHER, T.H. and PUGMIRE, R.J. *The structure and reaction processes of coal.* Springer Science & Business Media, 1994.
92. IEA. *Coal Medium-Term Market Report 2015*. Paris: International Energy Agency, 2015.
93. MILLER, B.G. CHAPTER 1 - Introduction to Coal. *In: Coal Energy Systems*. Burlington: Academic Press, 2005, pp.1-27.
94. HUGGINS, F.E. Overview of analytical methods for inorganic constituents in coal. *International Journal of Coal Geology*, 2002, **50**(1), pp.169-214.
95. HOLUSZKO, M.E. and MASTALERZ, M.D. Coal macerals chemistry and its implications for selectivity in coal floatability. *International Journal of Coal Preparation and Utilization*, 2015, **35**(2), pp.99-110.
96. BERKOWITZ, N. CHAPTER 1 - ORIGINS AND FORMATION. *In: An Introduction to Coal Technology*. Academic Press, 1979, pp.3-20.
97. TILLMAN, D.A., DUONG, D.N. and HARDING, N.S. *Solid fuel blending: principles, practices, and problems.* Elsevier, 2012.
98. VAN KREVELEN, D.W. *Coal: typology, chemistry, physics, constitution.* Elsevier Publishing Company, 1961.
99. MEYERS, R. *Coal structure.* Elsevier, 2012.
100. DE ABREU, Y., PATIL, P., MARQUEZ, A.I. and BOTTE, G.G. Characterization of electrooxidized Pittsburgh No. 8 Coal. *Fuel*, 2007, **86**(4), pp.573-584.
101. KUBACHI, M.L. *Co-pyrolysis and co=combustion of coal and biomass*. thesis, University of Leeds, 2007.
102. VAN LOO, S. and KOPPEJAN, J. *The handbook of biomass combustion and co-firing.* Earthscan, 2008.
103. SARKANEN, K.V. and TILLMAN, D.A. *Progress in biomass conversion.* Elsevier, 2013.
104. MOHAN, D., PITTMAN, C.U. and STEELE, P.H. Pyrolysis of wood/biomass for bio-oil: a critical review. *Energy & Fuels*, 2006, **20**(3), pp.848-889.
105. SHANKAR TUMULURU, J., SOKHANSANJ, S., HESS, J.R., WRIGHT, C.T. and BOARDMAN, R.D. REVIEW: A review on biomass torrefaction process and product properties for energy applications. *Industrial Biotechnology*, 2011, **7**(5), pp.384-401.
106. SIMONEIT, B.R.T. Biomass burning — a review of organic tracers for smoke from incomplete combustion. *Applied Geochemistry*, 2002, **17**(3), pp.129-162.
107. GLASSMAN, I., YETTER, R.A. and GLUMAC, N.G. *Combustion.* Academic press, 2014.
108. MCNAMEE, P. *Torrefied Biomass for Large Scale Electricity Generation*. thesis, University of Leeds, 2015.
109. OBERNBERGER, I., BIEDERMANN, F., WIDMANN, W. and RIEDL, R. Biomass Quality for Power ProductionConcentrations of inorganic elements in biomass fuels and recovery in the different ash fractions. *Biomass and bioenergy*, 1997, **12**(3), pp.211-224.
110. JOCHEN, B. Introduction and context. *In: Biomass as Energy Source*. CRC Press, 2013, pp.5-33.

111. OBERNBERGER, I. and THEK, G. *The Pellet Handbook: The Production and Thermal Utilization of Biomass Pellets.* Routledge Ltd, 2012.
112. MCNAMEE, P., ADAMS, P.W.R., MCMANUS, M.C., DOOLEY, B., DARVELL, L.I., WILLIAMS, A. and JONES, J.M. An assessment of the torrefaction of North American pine and life cycle greenhouse gas emissions. *Energy Conversion and Management*, 2016, **113**, pp.177-188.
113. SCHIPFER, F., BIENERT, K. and KRANZL, L. Production of Solid Sustainable Energy Carriers from Biomass by Means of Torrefaction.
114. TILLMAN, D. *The combustion of solid fuels and wastes.* Academic Press, 1991.
115. WILLIAMS, A., POURKASHANIAN, M. and JONES, J.M. Combustion of pulverised coal and biomass. *Progress in energy and combustion science*, 2001, **27**(6), pp.587-610.
116. WU, Z. *Understanding fluidised bed combustion.* IEA Coal Research, 2003.
117. UNSWORTH, J.F., BARRATT, D.J. and ROBERTS, P.T. Coal quality and combustion performance: An international perspective. *Coal science and technology*, 1991, **19**, pp.1-609.
118. YAN, J. *Handbook of Clean Energy Systems, 6 Volume Set.* John Wiley & Sons, 2015.
119. JONES, J.M., LEA-LANGTON, A.R., MA, L., POURKASHANIAN, M. and WILLIAMS, A. *Pollutants Generated by the Combustion of Solid Biomass Fuels.* Springer, 2014.
120. WU, Z. Fundamentals of pulverised coal combustion. *IEA Clean Coal Centre Reports*, 2005.
121. MILLER, B.G. and TILLMAN, D. *Combustion engineering issues for solid fuel systems.* Academic Press, 2008.
122. TOPOROV, D. *Combustion of Pulverised Coal in a Mixture of Oxygen and Recycled Flue Gas.* Elsevier, 2014.
123. WILLIAMS, A., JONES, J.M., MA, L. and POURKASHANIAN, M. Pollutants from the combustion of solid biomass fuels. *Progress in energy and combustion science*, 2012, **38**(2), pp.113-137.
124. AFR. *Advanced Fuel Research - Functional-Group, Deplymerization, Vaporization, Cross-linking Model* [online]. 2009. [Accessed 27/07/2016]. Available from: http://www.afrinc.com/products/fgdvc/default.htm#What is FG-DVC.
125. SAXENA, S.C. Devolatilization and combustion characteristics of coal particles. *Progress in energy and combustion science*, 1990, **16**(1), pp.55-94.
126. UMBERTO, D. and FRANCESCO, F. Biomass combustion and chemical looping for carbon capture and storage. *In: Technologies for Converting Biomass to Useful Energy*. CRC Press, 2013, pp.129-173.
127. DI BLASI, C. Combustion and gasification rates of lignocellulosic chars. *Progress in energy and combustion science*, 2009, **35**(2), pp.121-140.
128. CAI, H.Y., GÜELL, A.J., CHATZAKIS, I.N., LIM, J.Y., DUGWELL, D.R. and KANDIYOTI, R. Combustion reactivity and morphological change in coal chars: Effect of pyrolysis temperature, heating rate and pressure. *Fuel*, 1996, **75**(1), pp.15-24.

129. DEMIRBAS, A. Effects of temperature and particle size on bio-char yield from pyrolysis of agricultural residues. *Journal of Analytical and Applied Pyrolysis*, 2004, **72**(2), pp.243-248.
130. MANI, T., MURUGAN, P., ABEDI, J. and MAHINPEY, N. Pyrolysis of wheat straw in a thermogravimetric analyzer: Effect of particle size and heating rate on devolatilization and estimation of global kinetics. *Chemical Engineering Research and Design*, 2010, **88**(8), pp.952-958.
131. SERIO, M.A., HAMBLEN, D.G., MARKHAM, J.R. and SOLOMON, P.R. Kinetics of volatile product evolution in coal pyrolysis: experiment and theory. *Energy & Fuels*, 1987, **1**(2), pp.138-152.
132. SOLOMON, P.R. and FLETCHER, T.H. Twenty-Fifth Symposium (International) on Combustion Impact of coal pyrolysis on combustion. *Symposium (International) on Combustion*, 1994, **25**(1), pp.463-474.
133. SOLOMON, P.R., HAMBLEN, D.G., CARANGELO, R., SERIO, M. and DESHPANDE, G. General model of coal devolatilization. *Energy & Fuels*, 1988, **2**(4), pp.405-422.
134. DESHPANDE, G., SOLOMON, P. and SERIO, M. Cross-linking reactions in coal pyrolysis. *Prepr Am Chem Soc Div Fuel Chem*, 1988, **33**(2), pp.310-321.
135. SOLOMON, P.R., SERIO, M.A., DESPANDE, G.V. and KROO, E. Cross-linking reactions during coal conversion. *Energy & Fuels*, 1990, **4**(1), pp.42-54.
136. SMOOT, L.D. and SMITH, P.J. *Coal combustion and gasification.* Springer Science & Business Media, 1985.
137. QUAAK, P., KNOEF, H. and STASSEN, H.E. *Energy from biomass: a review of combustion and gasification technologies.* World Bank Publications, 1999.
138. YARIN, L.P., HETSRONI, G. and MOSYAK, A. *Combustion of two-phase reactive media.* Springer Science & Business Media, 2013.
139. HUNT, J., FERRARI, A., LITA, A., CROSSWHITE, M., ASHLEY, B. and STIEGMAN, A. Microwave-specific enhancement of the carbon–carbon dioxide (Boudouard) reaction. *The Journal of Physical Chemistry C*, 2013, **117**(51), pp.26871-26880.
140. JONES, J. and GODEFROY, J. Stages in the coalification sequence reflected in oxidation reactivities. *International Journal on Engineering Performance-Based Fire Codes*, 2002, **4**(1), pp.10-12.
141. MARSH, H. and KUO, K. Chapter 4 - Kinetics and Catalysis of Carbon Gasification. *In: Introduction to Carbon Science*. Butterworth-Heinemann, 1989, pp.107-151.
142. LAURENDEAU, N.M. Heterogeneous kinetics of coal char gasification and combustion. *Progress in energy and combustion science*, 1978, **4**(4), pp.221-270.
143. GEIER, M., SHADDIX, C.R. and HOLZLEITHNER, F. A mechanistic char oxidation model consistent with observed CO2/CO production ratios. *Proceedings of the Combustion Institute*, 2013, **34**(2), pp.2411-2418.
144. NUNES, K.G.P., OSÓRIO, E. and MARCÍLIO, N.R. Kinetics of the Oxy-fuel Combustion of High-Ash-Content Coal from the Candiota Mine, Rio Grande do Sul. *Energy & Fuels*, 2016, **30**(3), pp.1958-1964.
145. LUO, M. and STANMORE, B. The combustion characteristics of char from pulverized bagasse. *Fuel*, 1992, **71**(9), pp.1074-1076.

146. WALL, T.F. Combustion processes for carbon capture. *Proceedings of the Combustion Institute*, 2007, **31**(1), pp.31-47.
147. ANDERSSON, K., JOHANSSON, R., JOHNSSON, F. and LECKNER, B. Radiation intensity of propane-fired oxy-fuel flames: implications for soot formation. *Energy & Fuels*, 2008, **22**(3), pp.1535-1541.
148. MOLINA, A. and SHADDIX, C.R. Ignition and devolatilization of pulverized bituminous coal particles during oxygen/carbon dioxide coal combustion. *Proceedings of the Combustion Institute*, 2007, **31**(2), pp.1905-1912.
149. BROWN, A.L., DAYTON, D.C., NIMLOS, M.R. and DAILY, J.W. Design and characterization of an entrained flow reactor for the study of biomass pyrolysis chemistry at high heating rates. *Energy & Fuels*, 2001, **15**(5), pp.1276-1285.
150. MURPHY, J.J. and SHADDIX, C.R. Combustion kinetics of coal chars in oxygen-enriched environments. *Combustion and Flame*, 2006, **144**(4), pp.710-729.
151. RIAZA, J., GIL, M.V., ÁLVAREZ, L., PEVIDA, C., PIS, J.J. and RUBIERA, F. Oxy-fuel combustion of coal and biomass blends. *Energy*, 2012, **41**(1), pp.429-435.
152. RATHNAM, R.K., ELLIOTT, L.K., WALL, T.F., LIU, Y. and MOGHTADERI, B. Differences in reactivity of pulverised coal in air (O2/N2) and oxy-fuel (O2/CO2) conditions. *Fuel processing technology*, 2009, **90**(6), pp.797-802.
153. IRFAN, M.F., ARAMI-NIYA, A., CHAKRABARTI, M.H., WAN DAUD, W.M.A. and USMAN, M.R. Kinetics of gasification of coal, biomass and their blends in air (N2/O2) and different oxy-fuel (O2/CO2) atmospheres. *Energy*, 2012, **37**(1), pp.665-672.
154. SHADDIX, C.R. and MOLINA, A. *Effect of O2 and High CO2 Concentrations on PC Char Burning Rates during Oxy-Fuel Combustion*. Sandia National Laboratories (SNL-CA), Livermore, CA (United States), 2008.
155. DHANESWAR, S.R. and PISUPATI, S.V. Oxy-fuel combustion: The effect of coal rank and the role of char-CO2 reaction. *Fuel processing technology*, 2012, **102**, pp.156-165.
156. BORREGO, A.G. and ALVAREZ, D. Comparison of chars obtained under oxy-fuel and conventional pulverized coal combustion atmospheres. *Energy & Fuels*, 2007, **21**(6), pp.3171-3179.
157. KIM, D., CHOI, S., SHADDIX, C.R. and GEIER, M. Effect of CO 2 gasification reaction on char particle combustion in oxy-fuel conditions. *Fuel*, 2014, **120**, pp.130-140.
158. GEIER, M., SHADDIX, C. and HOLZLEITHNER, F. A mechanistic char oxidation model consistent with observed CO 2/CO production ratios. *Proceedings of the Combustion Institute*, 2013, **34**(2), pp.2411-2418.
159. BEWS, I., HAYHURST, A., RICHARDSON, S. and TAYLOR, S. The order, Arrhenius parameters, and mechanism of the reaction between gaseous oxygen and solid carbon. *Combustion and Flame*, 2001, **124**(1), pp.231-245.
160. SMITH, I.W. The intrinsic reactivity of carbons to oxygen. *Fuel*, 1978, **57**(7), pp.409-414.
161. LIU, H. Combustion of coal chars in O2/CO2 and O2/N2 mixtures: a comparative study with non-isothermal thermogravimetric analyzer (TGA) tests. *Energy & Fuels*, 2009, **23**(9), pp.4278-4285.

162. SIMA-ELLA, E., YUAN, G. and MAYS, T. A simple kinetic analysis to determine the intrinsic reactivity of coal chars. *Fuel*, 2005, **84**(14), pp.1920-1925.
163. KOTZ, J.C., TREICHEL, P.M. and TOWNSEND, J. *Chemistry and chemical reactivity.* Cengage Learning, 2012.
164. SADDAWI, A., JONES, J., WILLIAMS, A. and WOJTOWICZ, M. Kinetics of the thermal decomposition of biomass. *Energy & Fuels*, 2009, **24**(2), pp.1274-1282.
165. HILLIER, J., BEZZANT, T. and FLETCHER, T.H. Improved method for the determination of kinetic parameters from non-isothermal thermogravimetric analysis (TGA) data. *Energy & Fuels*, 2010, **24**(5), pp.2841-2847.
166. DI BLASI, C. Modeling and simulation of combustion processes of charring and non-charring solid fuels. *Progress in energy and combustion science*, 1993, **19**(1), pp.71-104.
167. HURT, R.H. Structure, properties, and reactivity of solid fuels. *Symposium (International) on Combustion*, 1998, **27**(2), pp.2887-2904.
168. CARBERRY, J.J. *Chemical and catalytic reaction engineering.* Courier Corporation, 1976.
169. TREMEL, A. *Reactions Kinetics of Solid Fuels during Entrained Flow Gasification*. thesis, Technische Universität München, 2012.
170. ISHIDA, M. and WEN, C.Y. Comparison of zone-reaction model and unreacted-core shrinking model in solid—gas reactions—I isothermal analysis. *Chemical Engineering Science*, 1971, **26**(7), pp.1031-1041.
171. SZEKELY, J. and EVANS, J.W. A structural model for gas—solid reactions with a moving boundary. *Chemical Engineering Science*, 1970, **25**(6), pp.1091-1107.
172. BHATIA, S.K. and PERLMUTTER, D. A random pore model for fluid-solid reactions: I. Isothermal, kinetic control. *AIChE Journal*, 1980, **26**(3), pp.379-386.
173. GLARBORG, P., JENSEN, A.D. and JOHNSSON, J.E. Fuel nitrogen conversion in solid fuel fired systems. *Progress in energy and combustion science*, 2003, **29**(2), pp.89-113.
174. NORDIN, J.S. and MERRIAM, N.W. *NOx emissions produced with combustion of powder river basin coal in a utility boiler*. Federal Energy Technology Center, Morgantown, WV (US); Federal Energy Technology Center, Pittsburgh, PA (US), 1997.
175. NUSSBAUMER, T. Combustion and co-combustion of biomass: fundamentals, technologies, and primary measures for emission reduction. *Energy & Fuels*, 2003, **17**(6), pp.1510-1521.
176. DARVELL, L.I., BRINDLEY, C., BAXTER, X.C., JONES, J.M. and WILLIAMS, A. Nitrogen in biomass char and its fate during combustion: a model compound approach. *Energy & Fuels*, 2012, **26**(11), pp.6482-6491.
177. DI NOLA, G., DE JONG, W. and SPLIETHOFF, H. The fate of main gaseous and nitrogen species during fast heating rate devolatilization of coal and secondary fuels using a heated wire mesh reactor. *Fuel processing technology*, 2009, **90**(3), pp.388-395.

178. TSUBOUCHI, N., ABE, M., XU, C. and OHTSUKA, Y. Nitrogen release from low rank coals during rapid pyrolysis with a drop tube reactor. *Energy & Fuels*, 2003, **17**(4), pp.940-945.
179. TSUBOUCHI, N. and OHTSUKA, Y. Nitrogen release during high temperature pyrolysis of coals and catalytic role of calcium in N2 formation. *Fuel*, 2002, **81**(18), pp.2335-2342.
180. OKAZAKI, K. and ANDO, T. International Symposium on CO<inf>2</inf> Fixation and Efficient Utilization of EnergyNOx reduction mechanism in coal combustion with recycled CO2. *Energy*, 1997, **22**(2), pp.207-215.
181. SHADDIX, C.R. and MOLINA, A. Fundamental investigation of NOx formation during oxy-fuel combustion of pulverized coal. *Proceedings of the Combustion Institute*, 2011, **33**(2), pp.1723-1730.
182. FARROW, T.S., SUN, C. and SNAPE, C.E. Impact of CO2 on biomass pyrolysis, nitrogen partitioning, and char combustion in a drop tube furnace. *Journal of Analytical and Applied Pyrolysis*, 2015, **113**, pp.323-331.
183. MASON, P. *On the Combustion of solid biomass fuels for large scale power generation*. Doctor of Philosophy thesis, University of Leeds, 2016.
184. C.E.N STANDARD. BS EN 14774-3:2009 Solid biofuels - Determination of moisture content. 2009.
185. C.E.N STANDARD. BS EN 15148:2009 Solid biofuels - Determination of the content of volatile matter. 2009.
186. C.E.N STANDARD. BS EN 14775:2009 Solid biofuels - Determination of ash content. 2009.
187. I.S.O STANDARD. BS ISO 11722:2013 Solid mineral fuels - Hard coal - Determination of moisture in the general analysis test sample by drying in nitrogen. 2013.
188. I.S.O STANDARD. BS ISO 562:2010 Hard coal and coke - Determination of volatile matter. 2010.
189. I.S.O STANDARD. BS ISO 1171:2010 Solid mineral fuels - Determination of ash. 2010.
190. C.E.N STANDARD. BS EN 15296:2011 Solid biofuels- Conversion of analytical results from one basis to another. 2011.
191. I.S.O STANDARD. ISO 17246:2010 Coal - Proximate analysis. 2010.
192. C.E.N STANDARD. BS EN ISO 16948:2015 Solid biofuels - Determination of toal content of carbon, hydrogen and nitrogen. 2015.
193. ŠEVČÍK, J. *Detectors in gas chromatography.* Elsevier Scientific Publishing Company, 1976.
194. C.E.N STANDARD. BS EN 15104:2011 Solid biolfuels - Determination of total content of carbon, hydrogen and nitrogen - Instrumental methods. 2011.
195. BIEHLIG, E. *Nitrogen Determination in the Times of Scarcity of Natural Resources*. Elemental Analysis Feature, 2015.
196. FRIEDL, A., PADOUVAS, E., ROTTER, H. and VARMUZA, K. Prediction of heating values of biomass fuel from elemental composition. *Analytica Chimica Acta*, 2005, **544**(1–2), pp.191-198.
197. BRIDGEMAN, T.G., JONES, J.M., WILLIAMS, A. and WALDRON, D.J. An investigation of the grindability of two torrefied energy crops. *Fuel*, 2010, **89**(12), pp.3911-3918.

198. OAKEY, J.E. *Power plant life management and performance improvement.* Elsevier, 2011.
199. HEIN, K.R.G. and BEMTGEN, J.M. EU clean coal technology—co-combustion of coal and biomass. *Fuel processing technology*, 1998, **54**(1–3), pp.159-169.
200. HARDGROVE, R. Grindability of coal. *Trans. ASME, Fuels and Steam Power*, 1932, **54**, pp.37-46.
201. KLOBES, P. and MUNRO, R.G. Porosity and Specific Surface Area Measurements for Solid Materials. 2006.
202. SING, K.S. Reporting physisorption data for gas/solid systems with special reference to the determination of surface area and porosity (Recommendations 1984). *Pure and applied chemistry*, 1985, **57**(4), pp.603-619.
203. HAYHURST, A.N. The kinetics of the pyrolysis or devolatilisation of sewage sludge and other solid fuels. *Combustion and Flame*, 2013, **160**(1), pp.138-144.
204. MORGAN, P.A., ROBERTSON, S.D. and UNSWORTH, J.F. Combustion studies by thermogravimetric analysis. *Fuel*, 1986, **65**(11), pp.1546-1551.
205. CAUSTON, P. and MCENANEY, B. Determination of active surface areas of coal chars using a temperature-programmed desorption technique. *Fuel*, 1985, **64**(10), pp.1447-1452.
206. CLEMENS, A.H., MATHESON, T.W. and ROGERS, D.E. Low temperature oxidation studies of dried New Zealand coals. *Fuel*, 1991, **70**(2), pp.215-221.
207. LE MANQUAIS, K., SNAPE, C., MCROBBIE, I., BARKER, J. and PELLEGRINI, V. Comparison of the combustion reactivity of TGA and drop tube furnace chars from a bituminous coal. *Energy and Fuels*, 2009, **23**(9).
208. MCNAMEE, P., DARVELL, L.I., JONES, J.M. and WILLIAMS, A. The combustion characteristics of high-heating-rate chars from untreated and torrefied biomass fuels. *Biomass and bioenergy*, 2015, **82**, pp.63-72.
209. SHUANGNING, X., ZHIHE, L., BAOMING, L., WEIMING, Y. and XUEYUAN, B. Devolatilization characteristics of biomass at flash heating rate. *Fuel*, 2006, **85**(5–6), pp.664-670.
210. WANG, C.A., ZHANG, X., LIU, Y. and CHE, D. Pyrolysis and combustion characteristics of coals in oxyfuel combustion. *Applied Energy*, 2012, **97**, pp.264-273.
211. FISHER, E.M., DUPONT, C., DARVELL, L.I., COMMANDRÉ, J.M., SADDAWI, A., JONES, J.M., GRATEAU, M., NOCQUET, T. and SALVADOR, S. Combustion and gasification characteristics of chars from raw and torrefied biomass. *Bioresource Technology*, 2012, **119**, pp.157-165.
212. GIL, M.V., RIAZA, J., ÁLVAREZ, L., PEVIDA, C., PIS, J.J. and RUBIERA, F. Kinetic models for the oxy-fuel combustion of coal and coal/biomass blend chars obtained in N2 and CO2 atmospheres. *Energy*, 2012, **48**(1), pp.510-518.
213. BRANCA, C. and DI BLASI, C. Global kinetics of wood char devolatilization and combustion. *Energy & Fuels*, 2003, **17**(6), pp.1609-1615.
214. COZZANI, V. Reactivity in oxygen and carbon dioxide of char formed in the pyrolysis of refuse-derived fuel. *Industrial & engineering chemistry research*, 2000, **39**(4), pp.864-872.

215. MASON, P.E. *On the combustion of solid biomass fuels for large scale power generation: Investigations on the combustion behaviour of single particles of pulverised biomass fuel*. thesis, University of Leeds, 2016.
216. ECN. *Phyliss 2 Database* [online]. 2016. Available from: https://www.ecn.nl/phyllis2/Browse/Standard/ECN-Phyllis#pine.
217. YAN, B.-H., CAO, C.-X., CHENG, Y., JIN, Y. and CHENG, Y. Experimental investigation on coal devolatilization at high temperatures with different heating rates. *Fuel*, 2014, **117, Part B**, pp.1215-1222.
218. RATHNAM, R.K., ELLIOTT, L.K., WALL, T.F., LIU, Y. and MOGHTADERI, B. Differences in reactivity of pulverised coal in air (O 2/N 2) and oxy-fuel (O 2/CO 2) conditions. *Fuel processing technology*, 2009, **90**(6), pp.797-802.
219. LI, Q., ZHAO, C., CHEN, X., WU, W. and LI, Y. Comparison of pulverized coal combustion in air and in O2/CO2 mixtures by thermo-gravimetric analysis. *Journal of Analytical and Applied Pyrolysis*, 2009, **85**(1–2), pp.521-528.
220. ZHOU, Y., CHU, W., GU, G., XU, Y. and WENDT, J.O. Ignition and combustion characteristics of different rank coals in O2/CO2 environments. *In: Cleaner combustion and sustainable world*. Springer, 2013, pp.1335-1345.
221. BRIX, J., JENSEN, P.A. and JENSEN, A.D. Coal devolatilization and char conversion under suspension fired conditions in O2/N2 and O2/CO2 atmospheres. *Fuel*, 2010, **89**(11), pp.3373-3380.
222. FARROW, T.S. *A fundamental study of biomass oxy-fuel combustion and co-combustion*. PhD thesis, University of Nottingham, 2013.
223. BORREGO, A.G., GARAVAGLIA, L. and KALKREUTH, W.D. Characteristics of high heating rate biomass chars prepared under N2 and CO2 atmospheres. *International Journal of Coal Geology*, 2009, **77**(3–4), pp.409-415.
224. HAYNES, W.M. *CRC handbook of chemistry and physics.* CRC press, 2014.
225. YAWS, C.L. *Chemical properties handbook.* McGraw-Hill, 1999.
226. SUUBERG, E., KULAOTS, I., AARNA, I., CALLEJO, M. and HSU, A. *Study of activation of coal char*. Brown University, 2003.
227. OH, M.S., PETERS, W.A. and HOWARD, J.B. An experimental and modeling study of softening coal pyrolysis. *AIChE Journal*, 1989, **35**(5), pp.775-792.
228. FONG, W.S., KHALIL, Y.F., PETERS, W.A. and HOWARD, J.B. Plastic behaviour of coal under rapid-heating high-temperature conditions. *Fuel*, 1986, **65**(2), pp.195-201.
229. YU, J., LUCAS, J.A. and WALL, T.F. Formation of the structure of chars during devolatilization of pulverized coal and its thermoproperties: A review. *Progress in energy and combustion science*, 2007, **33**(2), pp.135-170.
230. LIU, X., XU, M., YAO, H., GU, Y., SI, J. and XIONG, C. Comparison of Char Structural Characteristics and Reactivity During Conventional Air and Oxy-Fuel Combustion. *In: Cleaner Combustion and Sustainable World*. Springer, 2013, pp.989-998.
231. ZHANG, Y., ZHAI, M., WANG, X., SUN, J., DONG, P., LIU, P. and ZHU, Q. Preparation and characteristics of biomass char. *BioResources*, 2015, **10**(2), pp.3017-3026.
232. NEWALKAR, G., IISA, K., D'AMICO, A.D., SIEVERS, C. and AGRAWAL, P. Effect of temperature, pressure, and residence time on pyrolysis of pine in an entrained flow reactor. *Energy & Fuels*, 2014, **28**(8), pp.5144-5157.

233. SHU, T., LU, F., WANG, Q. and LU, P. Study on Pore Structure Properties of Steam Activated Biomass Chars. *In: Cleaner Combustion and Sustainable World*. Springer, 2013, pp.305-311.
234. MANI, T., MAHINPEY, N. and MURUGAN, P. Reaction kinetics and mass transfer studies of biomass char gasification with CO2. *Chemical Engineering Science*, 2011, **66**(1), pp.36-41.
235. KLOSE, W. and WÖLKI, M. On the intrinsic reaction rate of biomass char gasification with carbon dioxide and steam. *Fuel*, 2005, **84**(7–8), pp.885-892.
236. CETIN, E., GUPTA, R. and MOGHTADERI, B. Effect of pyrolysis pressure and heating rate on radiata pine char structure and apparent gasification reactivity. *Fuel*, 2005, **84**(10), pp.1328-1334.
237. ROCCA, P.A.D., CERRELLA, E.G., BONELLI, P.R. and CUKIERMAN, A.L. Pyrolysis of hardwoods residues: on kinetics and chars characterization. *Biomass and bioenergy*, 1999, **16**(1), pp.79-88.
238. GONZÁLEZ, J.F., ROMÁN, S., ENCINAR, J.M. and MARTÍNEZ, G. Pyrolysis of various biomass residues and char utilization for the production of activated carbons. *Journal of Analytical and Applied Pyrolysis*, 2009, **85**(1–2), pp.134-141.
239. WU, T., LESTER, E. and CLOKE, M. Advanced automated char image analysis techniques. *Energy & Fuels*, 2006, **20**(3), pp.1211-1219.
240. ALVAREZ, D., BORREGO, A.G. and MENÉNDEZ, R. Unbiased methods for the morphological description of char structures. *Fuel*, 1997, **76**(13), pp.1241-1248.
241. LESTER, E., ALVAREZ, D., BORREGO, A.G., VALENTIM, B., FLORES, D., CLIFT, D.A., ROSENBERG, P., KWIECINSKA, B., BARRANCO, R., PETERSEN, H.I., MASTALERZ, M., MILENKOVA, K.S., PANAITESCU, C., MARQUES, M.M., THOMPSON, A., WATTS, D., HANSON, S., PREDEANU, G., MISZ, M. and WU, T. The procedure used to develop a coal char classification—Commission III Combustion Working Group of the International Committee for Coal and Organic Petrology. *International Journal of Coal Geology*, 2010, **81**(4), pp.333-342.
242. BAILEY, J.G., TATE, A., DIESSEL, C.F.K. and WALL, T.F. A char morphology system with applications to coal combustion. *Fuel*, 1990, **69**(2), pp.225-239.
243. BARRANCO, R., CLOKE, M. and LESTER, E. Prediction of the burnout performance of some South American coals using a drop-tube furnace☆. *Fuel*, 2003, **82**(15–17), pp.1893-1899.
244. ICCP. *International Committee for Coal and Organic Petrology: Atlas of Chars, Combustion Working Group* [online]. 2017. [Accessed 16/01/2017]. Available from: http://www.nottingham.ac.uk/~eczehl/charatlas/images/CHAR%20ATLAS.swf.
245. YUZBASI, N.S. and SELÇUK, N. Air and oxy-fuel combustion characteristics of biomass/lignite blends in TGA-FTIR. *Fuel processing technology*, 2011, **92**(5), pp.1101-1108.
246. SHADDIX, C.R. and MOLINA, A. Particle imaging of ignition and devolatilization of pulverized coal during oxy-fuel combustion. *Proceedings of the Combustion Institute*, 2009, **32**(2), pp.2091-2098.

247. CENGEL, Y.A. and BOLES, M.A. Thermodynamics: an engineering approach. *Sea*, 2007, **1000**, p.8862.
248. MENG, F., YU, J., TAHMASEBI, A. and HAN, Y. Pyrolysis and combustion behavior of coal gangue in O2/CO2 and O2/N2 mixtures using thermogravimetric analysis and a drop tube furnace. *Energy & Fuels*, 2013, **27**(6), pp.2923-2932.
249. RIAZA, J., ÁLVAREZ, L., GIL, M.V., PEVIDA, C., PIS, J.J. and RUBIERA, F. Effect of oxy-fuel combustion with steam addition on coal ignition and burnout in an entrained flow reactor. *Energy*, 2011, **36**(8), pp.5314-5319.
250. JONES, J.M., SADDAWI, A., DOOLEY, B., MITCHELL, E.J.S., WERNER, J., WALDRON, D.J., WEATHERSTONE, S. and WILLIAMS, A. Low temperature ignition of biomass. *Fuel processing technology*, 2015, **134**, pp.372-377.
251. FENNELL, P.S. and HAYHURST, A.N. The kinetics of the reduction of NO to N2 by reaction with particles of Fe. *Proceedings of the Combustion Institute*, 2002, **29**(2), pp.2179-2185.
252. DUAN, L., ZHAO, C., ZHOU, W., QU, C. and CHEN, X. Investigation on coal pyrolysis in CO2 atmosphere. *Energy & Fuels*, 2009, **23**(7), pp.3826-3830.
253. BARRIE, P.J., PITTAS, C.A., MITCHELL, M.J. and WILSON, D.I. A critical analysis of the compensation effect and its application to heat exchanger fouling studies. *Heat Transfer Engineering*, 2013, **34**(8-9), pp.744-752.
254. BROWN, M.E. and GALWEY, A.K. The significance of “compensation effects” appearing in data published in “computational aspects of kinetic analysis”: ICTAC project, 2000. *Thermochimica Acta*, 2002, **387**(2), pp.173-183.
255. LIU, N., ZONG, R., SHU, L., ZHOU, J. and FAN, W. Kinetic compensation effect in thermal decomposition of cellulosic materials in air atmosphere. *Journal of applied polymer science*, 2003, **89**(1), pp.135-141.
256. DE CAPRARIIS, B., SANTARELLI, M.L., SCARSELLA, M., HERCE, C., VERDONE, N. and DE FILIPPIS, P. Kinetic analysis of biomass pyrolysis using a double distributed activation energy model. *Journal of Thermal Analysis and Calorimetry*, 2015, **121**(3), pp.1403-1410.
257. ZOU, C., ZHANG, L., CAO, S. and ZHENG, C. A study of combustion characteristics of pulverized coal in O2/H2O atmosphere. *Fuel*, 2014, **115**, pp.312-320.
258. ROBERTS, D. and HARRIS, D. Char gasification with O2, CO2, and H2O: Effects of pressure on intrinsic reaction kinetics. *Energy & Fuels*, 2000, **14**(2), pp.483-489.
259. BEJARANO, P.A. and LEVENDIS, Y.A. Single-coal-particle combustion in O2/N2 and O2/CO2 environments. *Combustion and Flame*, 2008, **153**(1–2), pp.270-287.
260. BRIX, J., JENSEN, P.A. and JENSEN, A.D. Modeling char conversion under suspension fired conditions in O2/N2 and O2/CO2 atmospheres. *Fuel*, 2011, **90**(6), pp.2224-2239.
261. JANSE, A.M., DE JONGE, H.G., PRINS, W. and VAN SWAAIJ, W.P. Combustion kinetics of char obtained by flash pyrolysis of pine wood. *Industrial & engineering chemistry research*, 1998, **37**(10), pp.3909-3918.
262. LI, X., RATHNAM, R.K., YU, J., WANG, Q., WALL, T. and MEESRI, C. Pyrolysis and Combustion Characteristics of an Indonesian Low-Rank Coal under O2/N2 and O2/CO2 Conditions. *Energy & Fuels*, 2009, **24**(1), pp.160-164.

263. SELCUK, N. and YUZBASI, N.S. Combustion behaviour of Turkish lignite in O2/N2 and O2/CO2 mixtures by using TGA–FTIR. *Journal of Analytical and Applied Pyrolysis*, 2011, **90**(2), pp.133-139.
264. AHN, S., CHOI, G. and KIM, D. The effect of wood biomass blending with pulverized coal on combustion characteristics under oxy-fuel condition. *Biomass and bioenergy*, 2014, **71**, pp.144-154.
265. YI, B., ZHANG, L., HUANG, F., XIA, Z., MAO, Z., DING, J. and ZHENG, C. Investigating the combustion characteristic temperature of 28 kinds of Chinese coal in oxy-fuel conditions. *Energy Conversion and Management*, 2015, **103**, pp.439-447.
266. MOLINA, A., MONTOYA, A. and MONDRAGÓN, F. CO2 strong chemisorption as an estimate of coal char gasification reactivity. *Fuel*, 1999, **78**(8), pp.971-977.
267. GOMEZ-BAREA, A., OLLERO, P. and VILLANUEVA, A. Diffusional effects in CO2 gasification experiments with single biomass char particles. 2. Theoretical predictions. *Energy & Fuels*, 2006, **20**(5), pp.2211-2222.
268. DI BLASI, C., BUONANNO, F. and BRANCA, C. Reactivities of some biomass chars in air. *Carbon*, 1999, **37**(8), pp.1227-1238.
269. ADÁNEZ, J., DE DIEGO, L.F., GARCÍA-LABIANO, F., ABAD, A. and ABANADES, J.C. Determination of biomass char combustion reactivities for FBC applications by a combined method. *Industrial & engineering chemistry research*, 2001, **40**(20), pp.4317-4323.
270. BRANCA, C. and DI BLASI, C. Devolatilization and combustion kinetics of wood chars. *Energy Fuels*, 2003, **17**, pp.1609-1615.
271. BRANCA, C., IANNACE, A. and DI BLASI, C. Devolatilization and Combustion Kinetics of Q uercus c erris Bark. *Energy & Fuels*, 2007, **21**(2), pp.1078-1084.
272. HURT, R.H. and CALO, J.M. Semi-global intrinsic kinetics for char combustion modeling. *Combustion and Flame*, 2001, **125**(3), pp.1138-1149.
273. KARLSTRÖM, O., BRINK, A., HUPA, M. and TOGNOTTI, L. Multivariable optimization of reaction order and kinetic parameters for high temperature oxidation of 10 bituminous coal chars. *Combustion and Flame*, 2011, **158**(10), pp.2056-2063.
274. SUUBERG, E.M., WÓJTOWICZ, M. and CALO, J.M. Reaction order for low temperature oxidation of carbons. *Symposium (International) on Combustion*, 1989, **22**(1), pp.79-87.
275. WILLIAMS, A., BACKREEDY, R., HABIB, R., JONES, J.M. and POURKASHANIAN, M. Modelling coal combustion: the current position. *Fuel*, 2002, **81**(5), pp.605-618.
276. SMITH, I. The combustion rates of coal chars: a review. *In: Symposium (International) on Combustion*: Elsevier, 1982, pp.1045-1065.
277. WANG, Q., ZHANG, R., LUO, Z., FANG, M. and CEN, K. Effects of Pyrolysis Atmosphere and Temperature on Coal Char Characteristics and Gasification Reactivity. *Energy Technology*, 2016, **4**(4), pp.543-550.
278. MARSH, H. and WYNNE-JONES, W.F.K. The surface properties of carbon-I the effect of activated diffusion in the determination of surface area. *Carbon*, 1964, **1**(3), pp.269-279.
279. BASU, P. Combustion of coal in circulating fluidized-bed boilers: a review. *Chemical Engineering Science*, 1999, **54**(22), pp.5547-5557.

280. ALONSO, M.J.G., BORREGO, A.G., ÁLVAREZ, D. and MENÉNDEZ, R. A reactivity study of chars obtained at different temperatures in relation to their petrographic characteristics. *Fuel processing technology*, 2001, **69**(3), pp.257-272.
281. DAVIS, K.A., HURT, R.H., YANG, N.Y.C. and HEADLEY, T.J. Evolution of char chemistry, crystallinity, and ultrafine structure during pulverized-coal combustion. *Combustion and Flame*, 1995, **100**(1–2), pp.31-40.
282. SENNECA, O., SALATINO, P. and MASI, S. The influence of char surface oxidation on thermal annealing and loss of combustion reactivity. *Proceedings of the Combustion Institute*, 2005, **30**(2), pp.2223-2230.
283. EMMERICH, F.G. Evolution with heat treatment of crystallinity in carbons. *Carbon*, 1995, **33**(12), pp.1709-1715.
284. SENNECA, O., RUSSO, P., SALATINO, P. and MASI, S. The relevance of thermal annealing to the evolution of coal char gasification reactivity. *Carbon*, 1997, **35**(1), pp.141-151.
285. EMMERICH, F. Evolution with heat treatment of crystallinity in carbons. *Carbon*, 1995, **33**(12), pp.1709-1715.
286. SU, S., POHL, J.H., HOLCOMBE, D. and HART, J.A. Techniques to determine ignition, flame stability and burnout of blended coals in p.f. power station boilers. *Progress in energy and combustion science*, 2001, **27**(1), pp.75-98.
287. C.E.N. BS EN ISO 17225-2:2014 Solid biofuels — Fuel specifications and classes Part:2 Graded wood pellets. 2014.

12 Appendix

12.1 Example calculations

12.1.1 Determination of relative volatile and fixed carbon yield and the associated errors

Proximate analysis was performed on each of the fuels and chars using the TGA method. Below is an example calculation of the volatile content of the PEL N_2 char relative to the volatile content of the PEL raw fuel and the associated errors.

Table 12.1: PEL raw fuel and PEL N_2 data used to determine the relative volatile yield

		Volatile content (wt%) (db)	Absolute error	%Relative error
Raw Fuel	Run 1	39.37		
	Run 2	40.16		
	Avg	39.76	0.39	0.99
Char	Run 1	4.11		
	Run 2	4.08		
	Avg	4.10	0.02	0.43
Char yield (wt%) (db)		58.50	2.47	4.22

Note: Absolute error determined from Eq 4.4 and 4.5 and %RE determined from Eq 4.8

The relative volatile yield was determined using Eq 4.7 in section 4.3.2.3

$$\text{Relative volatile yield (wt\%)} = \frac{100}{39.76 \pm 0.39}.(58.50 \pm 2.47 .\frac{4.10 \pm 0.02}{100})$$

The relative volatile yield in the in the PEL N_2 char is 6.03 wt%.

The absolute error associated with the volatile yield is determined from the %RE in Table 12.1 and Eq 4.9 from section 4.3.2.3.

$$\text{Absolute error} = \frac{\sqrt{0.99^2 + 0.43^2 + 4.22^2}}{100}. 6.03 = 0.26$$

12.2 Char production using the TGA

The chars produced using the TGA provided a good understanding of the char yields through the generation of mass loss curves. An example of the mass loss plots can be seen in Figure 12.1. In this case the PEL coal was added to the TGA and heated at ballistic heating rates 1000°C min^{-1} to 1000°C in either a CO_2 or N_2 atmosphere. Once cooled to ~40°C the atmosphere was switched to the required combustion atmosphere (air or 5-30% O_2/CO_2) and the remaining char combusted non-isothermally to a final temperature of 900°C.

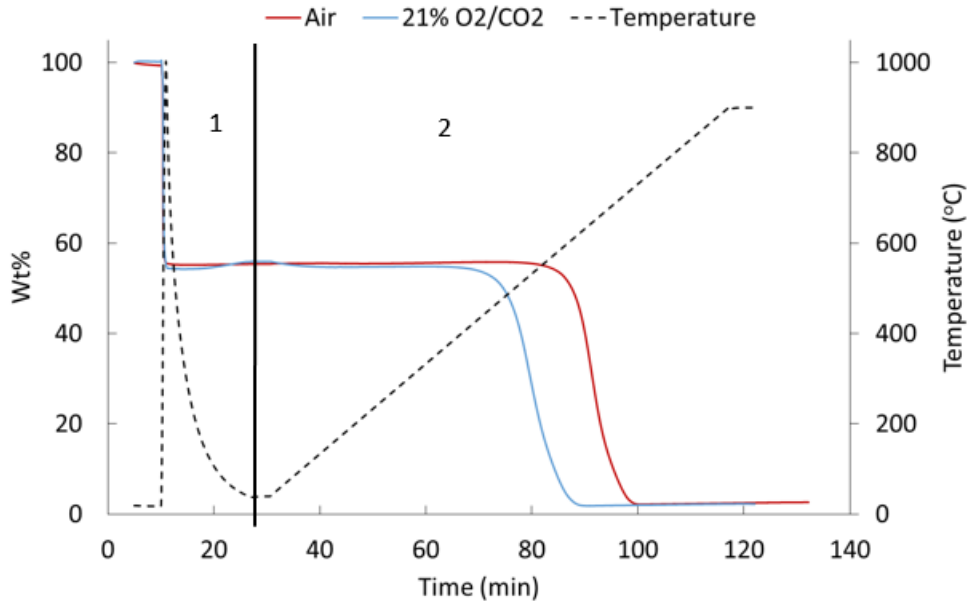

Figure 12.1: TGA plot of ballistic heating rate PEL char production in N_2 and CO_2 and combusted in air and 21% O_2/CO_2

12.3 Char conversion determined using the apparent kinetics

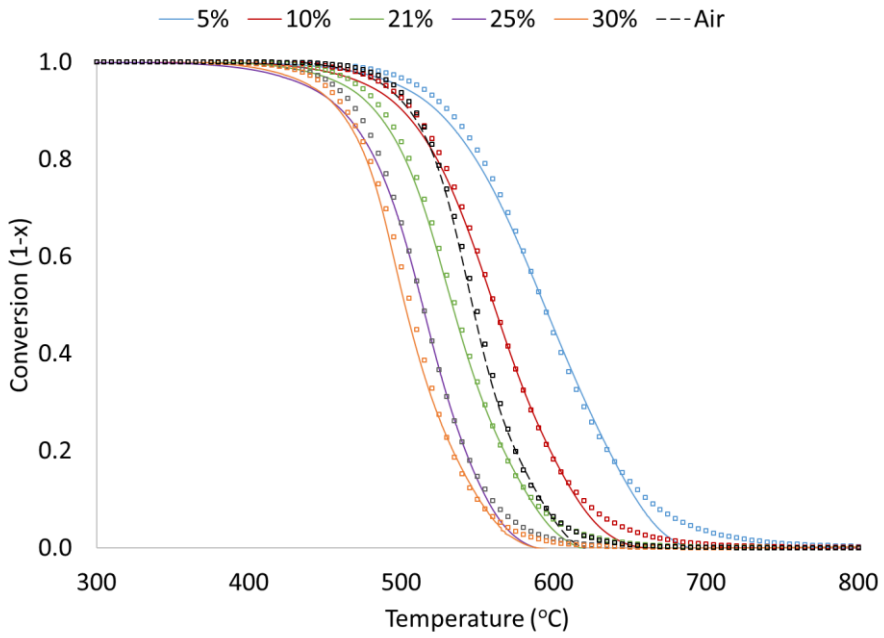

Figure 12.2: Conversion determined using the apparent kinetics of the PEL char combustion (line – experimental, squares – predicted)

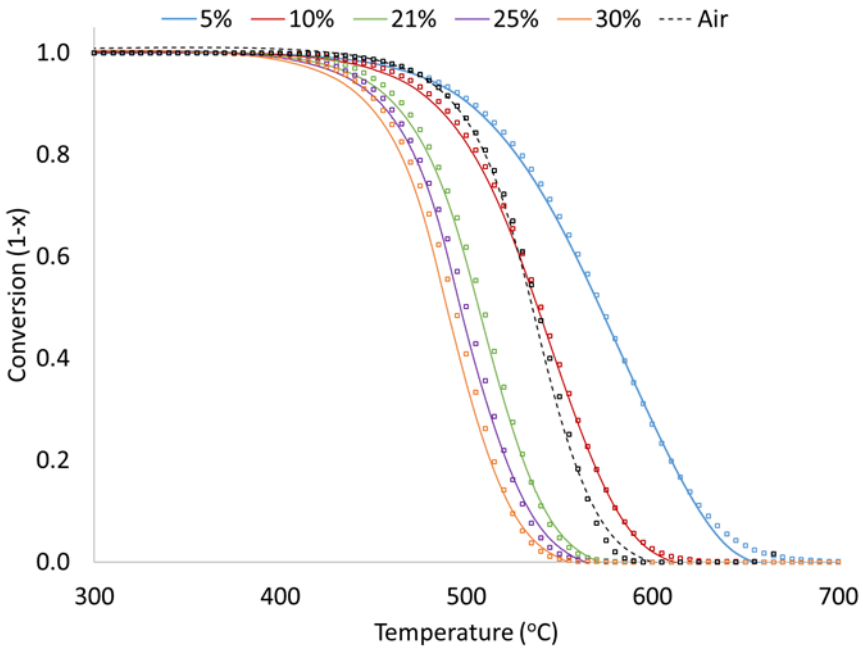

Figure 12.3: Conversion determined using the apparent kinetics of the ELC char combustion (line – experimental, squares – predicted)

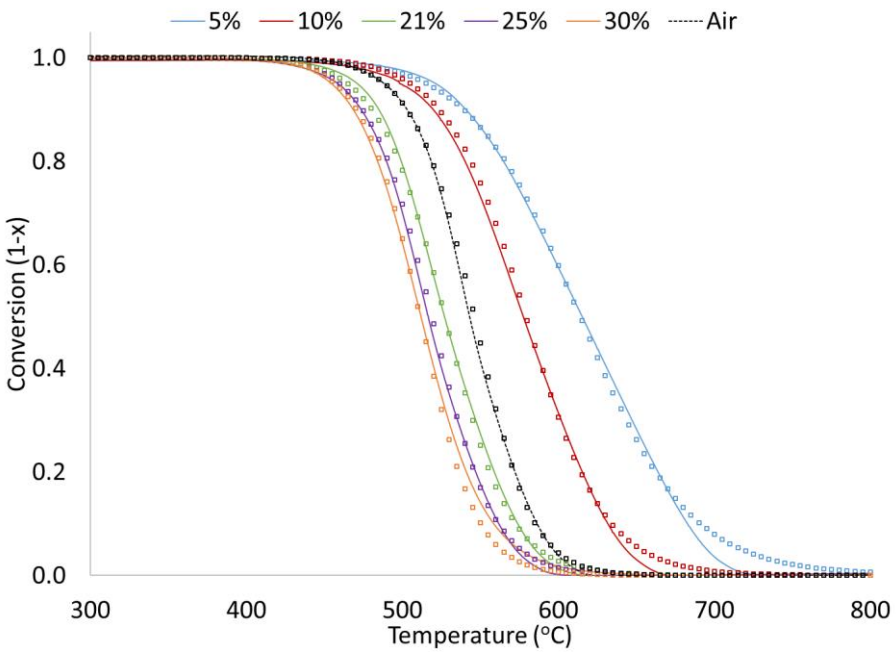

Figure 12.4: Conversion determined using the apparent kinetics of the PIT char combustion (line – experimental, squares – predicted)

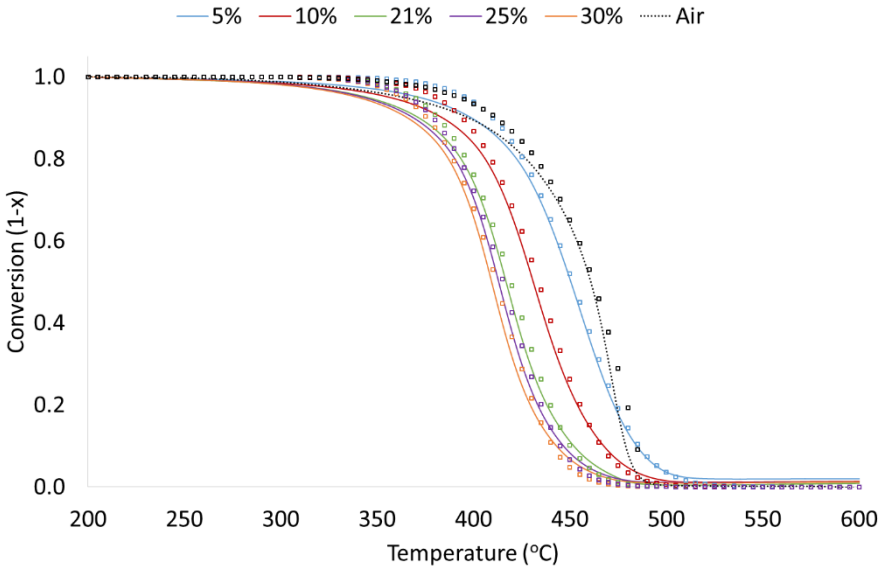

Figure 12.5: Conversion determined using the apparent kinetics of the PWWP char combustion (line – experimental, squares – predicted)

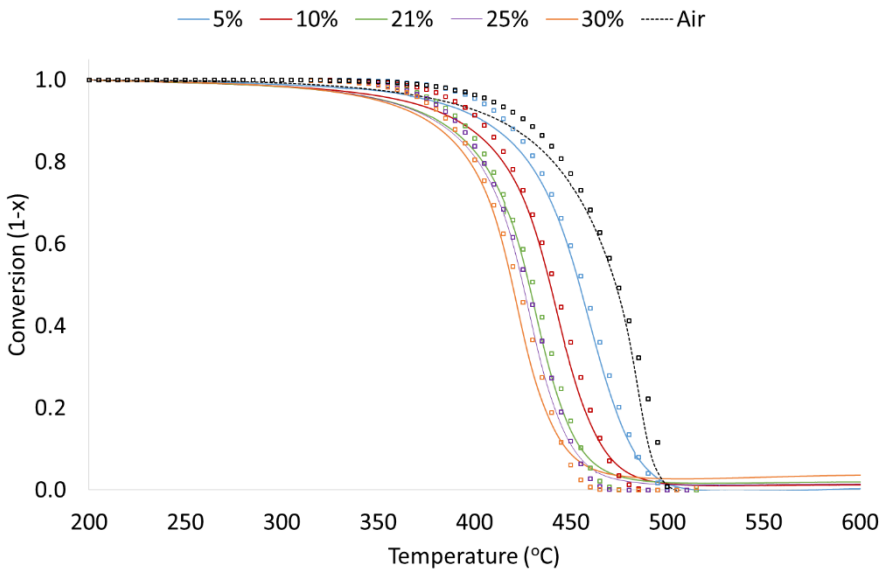

Figure 12.6: Conversion determined using the apparent kinetics of the WWP char combustion (line – experimental, squares – predicted)

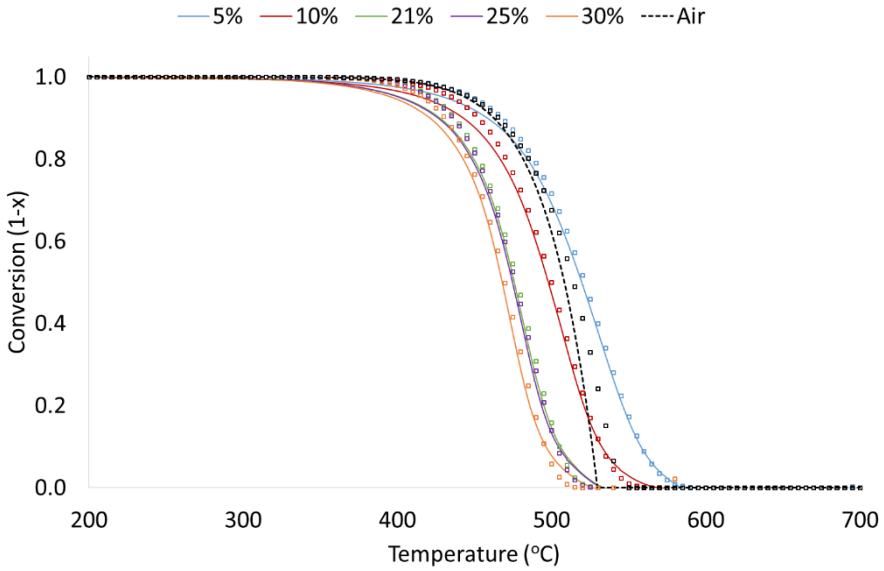

Figure 12.7: Conversion determined using the apparent kinetics of the TSP char combustion (line – experimental, squares – predicted)

Table 12.2: Deviation between the predicted conversion and experimental conversion in the chars determined from the apparent kinetic parameters

	Combustion atmosphere	Dev (1-x) (%)	Dev (dx/dt) (%)
PEL	5%	1.43	4.97
	10%	0.97	2.98
	21%	0.90	2.36
	25%	1.23	2.52
	30%	0.84	3.33
	Air	0.83	2.58
ELC	5%	0.65	3.34
	10%	0.35	1.30
	21%	0.50	1.79
	25%	0.64	2.90
	30%	0.93	2.59
	Air	0.65	2.53
PIT	5%	1.39	4.89
	10%	0.87	4.10
	21%	0.01	2.88
	25%	0.50	2.04
	30%	0.01	3.33
	Air	0.58	2.55
PWWP	5%	1.58	2.57
	10%	1.46	2.62
	21%	1.41	3.30
	25%	1.46	3.15
	30%	1.46	3.23
	Air	1.46	10.67
WWP	5%	1.36	5.19
	10%	1.57	3.03
	21%	1.80	4.36
	25%	1.57	4.62
	30%	2.64	4.34
	Air	1.97	7.54
TSP	5%	1.05	1.50
	10%	0.94	2.47
	21%	1.26	3.23
	25%	1.33	3.00
	30%	1.20	3.47
	Air	3.59	5.12

12.4 Specification of graded wood pellets

Table 12.3: Specifications of graded wood pellets for industrial use (287).

Property class, Analysis method	Unit	I1	I2	I3
Origin and source ISO 17225-1		1.1 Forest, plantation and other virgin wood 1.2.1 Chemically untreated wood residues [a]	1.1 Forest, plantation and other virgin wood 1.2.1 Chemically untreated wood residues [a]	1.1 Forest, plantation and other virgin wood 1.2 By-products and residues from wood processing industry 1.3.1 Chemically untreated used wood
Diameter, D [b] and Length L [c], ISO 17829 According Figure 1		D06, 6 ± 1; 3,15 < L ≤ 40 D08, 8 ± 1; 3,15 < L ≤ 40	D06, 6 ± 1; 3,15 < L ≤ 40 D08, 8 ± 1; 3,15 < L ≤ 40 D10, 10 ± 1; 3,15 < L ≤ 40	D06, 6 ± 1; 3,15 < L ≤ 40 D08, 8 ± 1; 3,15 < L ≤ 40 D10, 10 ± 1; 3,15 < L ≤ 40 D12, 12 ± 1; 3,15 < L ≤ 40
Moisture, M, ISO 18134-1, ISO 18134-2	w-% as received, wet basis	M10 ≤ 10	M10 ≤ 10	M10 ≤ 10
Ash, A, ISO 18122	w-% dry	A1.0 ≤ 1,0	A1.5 ≤ 1,5	A3.0 ≤ 3,0
Mechanical durability, DU, ISO 17831-1	w-% as received	97,5 ≤ DU ≤ 99,0	97,0 ≤ DU ≤ 99,0	96,5 ≤ DU ≤ 99,0
Fines, F [d], ISO 18846	w-% as received	F4.0 ≤ 4,0	F5.0 ≤ 5,0	F6.0 ≤ 6,0
Additives [e]	w-% as received	< 3 Type and amount to be stated	< 3 Type and amount to be stated	< 3 Type and amount to be stated
Net calorific value, Q, ISO 18125	MJ/kg as received	Q16.5 ≥ 16,5	Q16.5 ≥ 16,5	Q16.5 ≥ 16,5
Bulk density, BD [f], ISO 17828	kg/m3	BD600 ≥ 600	BD600 ≥ 600	BD600 ≥ 600
Nitrogen, N, ISO 16948	w-% dry	N0.3 ≤ 0,3	N0.3 ≤ 0,3	N0.6 ≤ 0,6
Particle size distribution of disintegrated pellets, ISO 17830	w-% equilibrated basis	≥ 99 % (<3.15 mm) ≥ 95 % (<2.0 mm) ≥ 60 % (<1.0 mm)	≥ 98 % (<3.15 mm) ≥ 90 % (<2.0 mm) ≥ 50 % (<1.0 mm)	≥ 97 % (<3.15 mm) ≥ 85 % (<2.0 mm) ≥ 40 % (<1.0 mm)
Sulfur, S, ISO 16994	w-% dry	S0.05 ≤ 0,05	S0.05 ≤ 0,05	S0.05 ≤ 0,05
Chlorine, Cl, ISO 16994	w-% dry	Cl0.03 ≤ 0,03	Cl0.05 ≤ 0,05	Cl0.1 ≤ 0,1
Arsenic, As, ISO 16968	mg/kg dry	≤ 2	≤ 2	≤ 2
Cadmium, Cd, ISO 16968	mg/kg dry	≤ 1,0	≤ 1,0	≤ 1,0
Chromium, Cr, ISO 16968	mg/kg dry	≤ 15	≤ 15	≤ 15
Copper, Cu, ISO 16968	mg/kg dry	≤ 20	≤ 20	≤ 20
Lead, Pb, ISO 16968	mg/kg dry	≤ 20	≤ 20	≤ 20
Mercury, Hg, ISO 16968	mg/kg dry	≤ 0,1	≤ 0,1	≤ 0,1
Zinc, Zn, ISO 16968	mg/kg dry	≤ 200	≤ 200	≤ 200
Ash Melting Behaviour [g]	°C	Should be Stated	Should be Stated	Should be Stated

Table 12.1 Continued

a -Negligible levels of glue, grease and other timber production additives used in sawmills during production of timber and timber product from virgin wood are acceptable if all chemical parameters of the pellets are clearly within the limits and/or concentrations are too small to be concerned with.

b -Selected size D06, D08, D10 or D12 of pellets to be stated.

c -Amount of pellets longer than 40 mm can be 1 w-%. Maximum length shall be ≤ 45 mm. Pellets are longer than 3,15 mm, if they stay on a round hole-sieve of 3,15 mm. Amount of pellets shorter than 10 mm, w-% recommended to be stated.

d- At factory gate in bulk transport (at the time of loading) and large sacks (at time of packing or when delivering to end-user).

e -Type of additives to aid production, delivery or combustion (e.g. pressing aids, slagging inhibitors or any other additives like starch, corn flour, potato flour, vegetable oil, lignin).

f- Maximum bulk density is 750 kg/m3.

g- It is recommended that all characteristic temperatures (shrinkage starting temperature (SST), deformation temperature (DT), hemisphere temperature (HT) and flow temperature (FT)) in oxidizing conditions should be stated.